Calculations and experiments
on γ-type Stirling engines

A Thesis submitted to the University of Wales, Cardiff,

for

the Degree of Doctor of Philosophy

by

Andreas Wagner

School of Engineering,

University of Wales, Cardiff

March 2008

UMI Number: U585566

UMI U585566

ProQuest LLC
789 East Eisenhower Parkway
P.O. Box 1346
Ann Arbor, MI 48106-1346

Abstract

This thesis is written to give an overview of the most important types of calculation methods for the analysis of γ-type Stirling engines found in the last 60 years.

Simple methods like the ideal process calculation and the 0th order analysis found by Beale and West are given to describe the process steps and to get a first reference value of performance and efficiency. Higher order calculations like the Schmidt analysis (1st order) and 2nd order methods for the ideal adiabatic and quasi steady flow models are described in detail and optimised for the γ-type Stirling engine. With a generated quasi steady computer program code parameter variation is used to obtain an impression of the dependency of performance and efficiency on varying geometry data and boundary conditions. In addition to these models the heat exchanger sections heater, cooler and regenerator are analysed in depth with the CFD program ANSYS CFX.

To compare the results of the theoretical analysis to measured ones three experimental engines are used. Different process values are determined on a biomass fired CHP Stirling system and on a solar Dish / Stirling system. On a Stirling engine test bench some of the parameter variations of the quasi steady program are repeated in experiments for comparison. These engines are modified in ways to make them run properly and to improve durability.

The behaviour of the γ-type Stirling engine is analysed in detail both in experiments and theoretically: this is felt to be unique. With the modified quasi steady flow model a method is found that is able to predict the process performance with a higher accuracy than it can be done with any other calculation method. This method can easily be modified to fit any other type of Stirling engine.

Acknowledgements

I would like to thank all of the people who contributed their time or support to me during my studies in Cardiff and in Regensburg:

To all the people at Cardiff University and the University of Applied Sciences in Regensburg, especially Prof. Nick Syred and Prof. Dr. Michael Elsner who always helped me with words and deeds.

To Deborah and Harry-Mark Zinsser-Krys and Helmut Pirthauer from the Heidolph company in Kelheim in Germany for their never ending support. Without their help the production of this work would not have been possible.

To Mr. Mauser from the Energiebig company in Austria who gave me needed parts for the measurements for free over a long period.

To Mr. Elsbett who worked at the EPAS company when this work was started and gave me all the needed information about the experimental engines.

To all the students of the University of Applied Sciences in Regensburg who wrote their diploma thesis in the thermodynamics laboratory and supported me to find solutions for different problems of the experimental engines.

To my family, my mother, for her immense and never ending help and support, even in times when she most needed help herself and to my father, who did so much for me, the advice and guidance he gave me were most helpful for the hard times during my work.

A very special thanks to my friends, who encouraged and helped me during this work and showed so much understanding.

I could not mention everybody who helped; to all the people left out: Thank You.

Table of contents

List of figures

List of tables

Nomenclature

A	Free flow area	[m²]
A	Substitution variable (Schmidt analysis)	[-]
Aw	Wetted area	[m²]
B	Substitution variable (Schmidt analysis)	[-]
Be	Beale number	[-]
c	Substitution variable (Schmidt analysis)	[-]
C	Carnot efficiency ratio (0th order calculation)	[-]
C	Concentration proportion (chapter 6)	[-]
Cmr	Heat capacity of the regenerator matrix	[J/K]
Cp	Specific heat capacity at constant pressure	[J/(kg·K)]
Cv	Specific heat capacity at constant specific volume	[J/(kg·K)]
d	Diameter	[m]
Diss	Derivative of the dissipation	[J/°]
dm	Mass derivative	[kg/°]
dp	Pressure derivative	[bar/°]
dQ	Heat derivative	[J/°]
dT	Temperature derivative	[K/°]
dV	Volume derivative	[m³/°]
dW	Work derivative	[J/°]
dz	Angle speed	[°/s]
f	Frequency	[Hz]
F	West factor (0th order calculation)	[-]
fA	Auxiliary ratio (0th order calculation)	[-]
fr	Fanning friction factor	[-]
h	Stoke of the working piston and displacer (Schmidt analysis)	[m]
h	Heat transfer coefficient (adiabatic analysis)	[J/(m²·K)]
Hu	Caloric value	[J/g]
I	Current	[A]
J	Number of the days (0 to 365)	[-]
l	Length	[m]
L	Length	[m]
L	Latitude (in chapter 6)	[°]
M	Torque	[Nm]
m	Mass	[kg]
mdot	Mass flow	[kg/s]
n	Rotational speed	[1/min]
p	Pressure	[N/m²]
P	Performance	[W]
pL	Preload pressure	[N/m²]
Pr	Prandtl number	[-]
Q	Heat	[J]
Qdot	Heat flow	[W]
R	Radius (adiabatic analysis)	[m]
R	Gas constant	[J/(kg·K)]
Re	Reynolds number	[-]
s	Entropy	[J/(kg·K)]
s	Reduced dead space (Schmidt analysis)	[-]
s	Distance (adiabatic analysis)	[-]
S	Solar irradiation	[kWh/m²]

t	Time	[s]
t	Proportion of temperatures (Schmidt analysis)	[-]
T	Temperature	[K]
u	Substitution variable	[m]
U	Internal energy (ideal process)	[J]
U	Thermal conductance	[J/K]
U	Voltage	[V]
v	Specific volume	[m³/kg]
v	Proportion of swept volumes (Schmidt analysis)	[-]
v	Velocity	[m/s]
V	Volume	[m³]
Vdot	Volume flux	[m³/s]
V_0	Displacement of the working piston (0th order calculation)	[cm³]
W	Work	[J]
x	Distance	[m]
X	Substitution variable (Schmidt analysis)	[-]

Indices

a	Air
ap	Auxiliary power
b	Biomass engine
c	Compression space (adiabatic analysis – non sinusoidal)
cef	Combustible energy flow
cg	Combustion gas
chp	Combined heat and power
ck	Compression space - cooler interface
cr	Crankcase
C	Compression space (Ideal process and Schmidt analysis - sinusoidal)
d	Displacer
d	Dead space (adiabatic analysis – non sinusoidal)
D	Dead space (Ideal process and Schmidt analysis - sinusoidal)
D	Direct (irradiation in combination with S)
dc	Dead compression space (adiabatic analysis – non sinusoidal)
DC	Dead compression space (Ideal process and Schmidt analysis - sinusoidal)
de	Dead expansion space (adiabatic analysis – non sinusoidal)
DE	Dead expansion space (Ideal process and Schmidt analysis - sinusoidal)
Diff	Diffuse (irradiation in combination with S)
e	Expansion space (adiabatic analysis – non sinusoidal)
E	Expansion space (Ideal process and Schmidt analysis - sinusoidal)
eff	Effective value
fb	Flow temperature of the cooling water of the hot water boiler
fs	Flow temperature of the cooling water of the Stirling
g	Gas
G	Global
gs	Generator of the Stirling engine
h	Heater (adiabatic analysis)
H	Heater (Schmidt analysis)
he	Heater – expansion space interface
hor	Horizontal

hwb	Hot water boiler
i	In
io	Insulation outside
iso	Insulation
irr	Irradiation
k	Cooler space (adiabatic analysis)
kr	Cooler - regenerator interface
L	Loss
m	Mean
M	Mechanical
MR	Middle of the regenerator (Schmidt analysis)
max	Maximal value
min	Minimum value
N	Normal conditions
o	Out
P	Pump
r	Regenerator (adiabatic analysis)
rh	Regenerator - heater interface
rr	Regenerator - regenerator interface
rw	Return temperature of the cooling water
R	Regenerator (Ideal process and Schmidt analysis)
S	Stirling engine
s	Solar engine
sc	Swept compression space (adiabatic analysis – non sinusoidal)
SC	Swept compression space (Ideal process and Schmidt analysis - sinusoidal)
se	Swept expansion space (adiabatic analysis – non sinusoidal)
SE	Swept expansion space (Ideal process and Schmidt analysis - sinusoidal)
th	Thermal
w	Working piston
w	Wall
wb	Cooling water in the hot water boiler
wc	Combustion chamber wall
wh	Heater wall
wk	Cooler wall
wr	Regenerator wall
ws	Cooling water in the Stirling engine

Abbreviations

2-D	Two dimensional
3-D	Three dimensional
CAD	Computer aided design
CET	Central European time
CFD	Computational fluid dynamics
CHP	Combined heat and power
CPU	Central processing unit
CSV	Coma separated values
FEM	Finite element method
FSI	Fluid structure interaction
GMT	Greenwich mean time

IR	Infra red
PID	Proportional integral differential (control unit)
PLC	Programmable logic controler
RAM	Random access memory
REM	Reflection electron microscope
RMS	Residual mean square
SST	Shear stress transport (turbulence model for CFD)

Greek

α	Crank angle	[°]
α_t	Thermal efficiency for CHP systems	[-]
α_S	Azimuth angle of the sun	[°]
β	Electrical efficiency for CHP systems	[-]
δ	Substitution variable (Schmidt analysis)	[-]
Δ	Difference between two values (used as prefix)	
η	Efficiency	[-]
ε	Volume ratio / compression ratio	[-]
κ	Isentropic exponent	[-]
φ	Phase shift angle	[°]
π	= 3,141592	[-]
ρ	Density	[kg/m³]
Σ	Sum	[-]
λ	Connecting rod ratio (adiabatic analysis)	[-]
λ	Thermal conductivity (adiabatic analysis)	[W/(m·K)]
λ_p	Friction factor (adiabatic analysis)	[-]
μ	Dynamic viscosity	[Pa·s]
υ	Kinematic viscosity	[m²/s²]
ω	Combustible utilization factor	[-]
σ	Current characteristic for CHP systems	[-]
Φ	Angle between the solar irradiation and the vertical of the plain	[°]
γ_S	Elevation	[°]
δ	Declination	[°]
ω	Angular velocity	[°/s]

This work is dedicated to Prof. Dr. Michael Elsner

who advised me and gave me a helping hand for many years.

1 Introduction

This work is written to show how the Stirling process, especially when used with γ-type engines, and renewable energy sources for the generation of electrical power, can be calculated and improved. In the following sections the need for renewable energy sources to cover the energy consumption of our planet in the future without raising the pollution of the environment and the greenhouse effect is extensively discussed. Also a characterisation of the calculation methods needed for the work, the structure of the thesis and its aims are pointed out.

1.1 Total primary energy consumption

For many hundred of years the total primary energy consumption of the world was extremely low. A decisive reason for this fact apart from the low development status of mankind was low population. Since the end of the 19th century total energy consumption has risen continuously. Mineral oil has been developed as today's leading energy source, followed by hard and brown coal. In the last few decades the importance of natural gas has risen rapidly and since about 1970 nuclear energy has become more and more important.
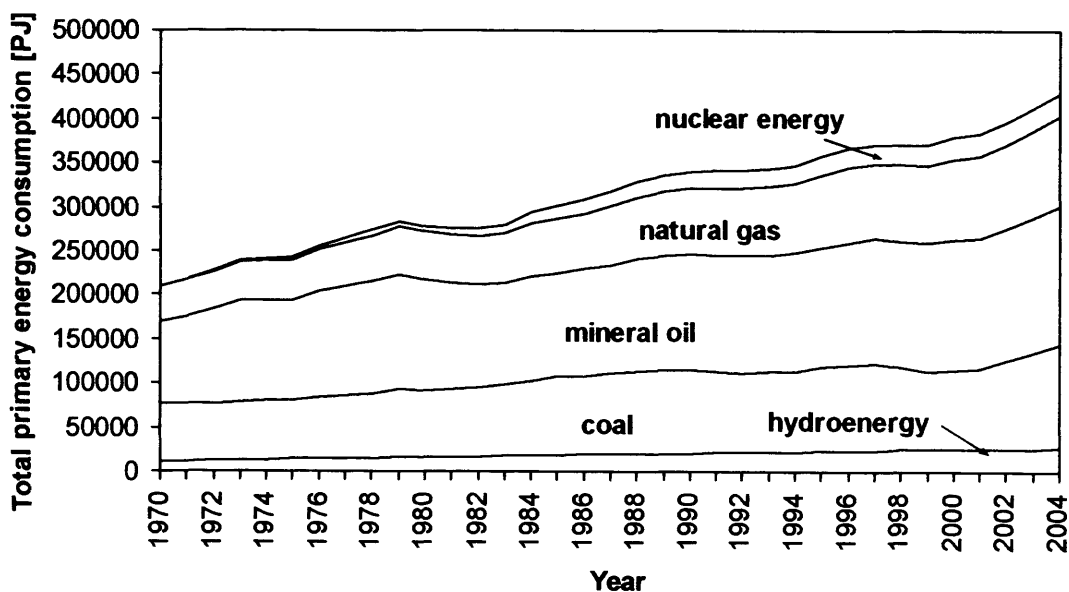
Figure 1-1: Development of the total primary energy supply of the world [1]

The development of the total primary energy consumption of the world can be seen in figure 1-1, where only commercially traded energy sources are considered. It can be clearly seen, that the total primary energy consumption since 1970 has doubled till

today. The real energy consumption is higher than the one shown in figure 1-1, because especially in developing countries energy sources like wood are not traded and can not be included in statistics.

1.2 Energy reserves

The energy reserves to meet the needs of the total primary energy consumption of the world can be divided into two groups: the non renewable energy sources (fossil and nuclear energies) and the renewable energies. Brown coal, hard coal, mineral oil and natural gas are among the fossil energy sources and uranium and thorium among the nuclear ones. For the evaluation of deposits the terms reserve and resource are used. Reserves are that part of the total resources that are measured with high accuracy and can be won with today's technical facilities in a cost effective way. As a consequence the reserves depend on the market prices of the different energy sources. Resources are the part of the total resources, that are either detected, but can not be won technically or in a cost effective way, or are geologically expected and can be demonstrated with exploration. The total resources are the sum of the reserves and the resources. The total potential includes the total resources and the accumulated extraction.

The worldwide detected reserves of non renewable energy sources had in 2004 a value of 37'491 EJ. The distribution on the different sources can be seen in table 1.1.

Energy source	Reserve		Resource	
	[EJ]	[%]	[EJ]	[%]
Conventional mineral oil	6'669	17,8	3'431	1,9
Conventional natural gas	5'599	14,9	6'563	3,6
Non conventional mineral oil	2'761	7,4	10'460	5,7
Non conventional natural gas	63	0,2	48'633	26,7
Hard coal	18'811	50,2	96'110	52,7
Brown coal	1'963	5,2	8'922	4,9
Uranium, Thorium	1'625	4,3	8'230	4,5
Total (non renewable)	**37'491**	**100,0**	**182'349**	**100,0**

Table 1.1: Reserves and resources of non renewable energy sources 2004 [1]

The dominant energy source on the world is coal with 55,4 %, whereof 50,2 % is hard coal and 5,2 % is brown coal. Coal is followed by conventional mineral oil with

17,8 % and conventional natural gas with 14,9 %. On the fourth place non conventional mineral oil (oil shale and oil sand) can be found with a value 7,4 %. Uranium and thorium with 4,3 % stand for the rest of the reserves of the earth.

Additionally to the reserves in 2004 about 182'000 EJ of resources are available. The dominant energy source is coal with more than half of the resources. It is followed by conventional natural gas forming a quarter of the total amount. All the other energy sources are less than 10 % each in this balance.

Comparing the total primary energy consumption in EJ with the reserves and resources a relation of 1 to 100 to 500 can be found. The global reserves of energy sources, except conventional mineral oil which is discussed in the following section, appear to give long-term coverage of the required energy supply.

1.2.1 Mineral oil

Mineral oil with a share of 36,8 % of the total primary energy consumption is the worldwide most important energy source. Forecasts of the development of energy consumption act on the assumption that this fact is not going to change in the next few decades. Mineral oil as a primary energy source is divided according to its deposit into conventional and non conventional mineral oil. Non conventional mineral oil includes oil sand (tars, difficult to flow), oil shale (bitumen is mined and mineral oil is extracted by heating to 500 °C) and heavy oil. The regional allocation of the total potential of conventional mineral oil of 2004 can be seen in figure 1-2.

The worldwide total potential of conventional mineral oil has a value of 381 Gt. From the beginning of the industrial age mineral oil extraction until 2004 was about 139 Gt, more than half of it in the last 22 years. For this reason 46 % of the proved reserves of conventional mineral oil have been extracted. Considering predicted resources of 82 Gt, 36 % of the expected total potential of conventional mineral oil is exhausted. The "depletion mid-point", where half of the conventional mineral oil is extracted, will be reached in the next 10 – 20 years. A successive reduction of extraction is bound to occur soon.
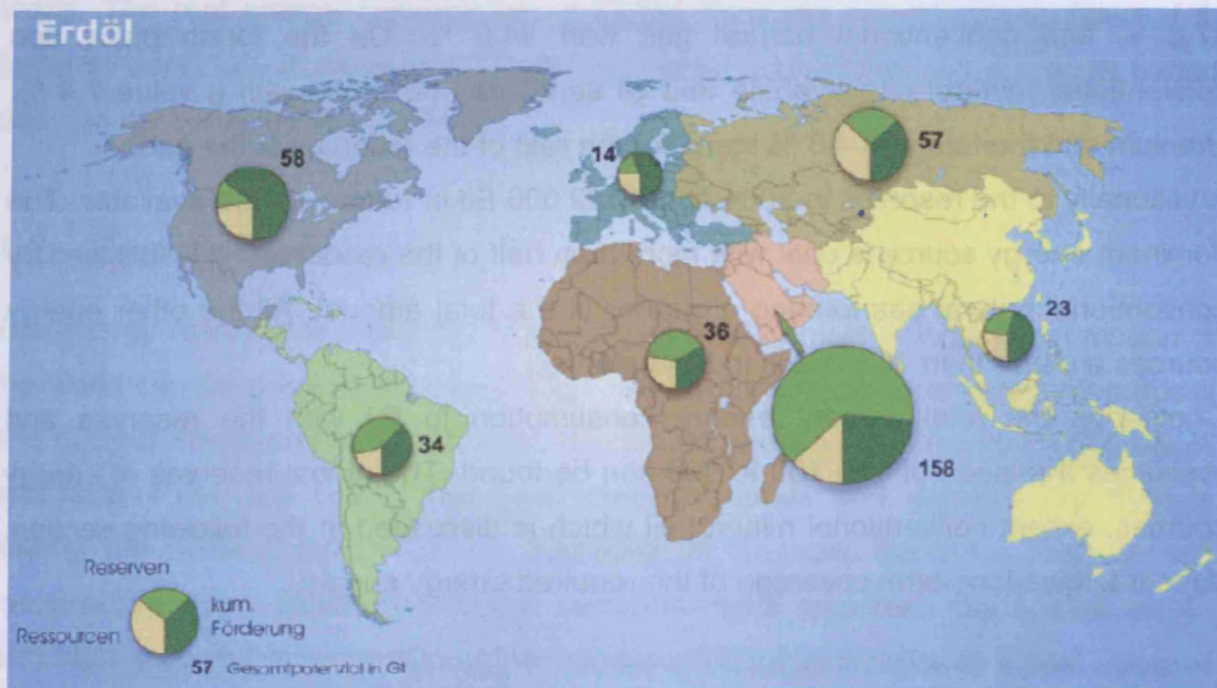
Figure 1-2: Regional allocation of the total potential of conventional mineral oil [1]

Besides conventional mineral oil an important potential of non-conventional mineral oil can be displayed. The reserves of non conventional mineral oil have a level of about 41 % of the reserves of conventional mineral oil, the resources rise above those of conventional mineral oil by a factor three. It has to be kept in mind that more than 80 % of the resources are bound as oil shale. The commercial use of these resources is problematic because of higher production costs and immense environmental pollution. For the extraction of oil sands and heavy oils many projects have been started in Canada and Venezuela in the few last years. The production costs are close to the ones of conventional mineral oil. The market share of non conventional mineral oil will rise in the next years if the oil price stays at a high level, but will not exceed a value of 5 – 10 % of the total extraction till the year 2020. The reason is that these projects have only a fractional capacity of conventional plants and will take decades to reach higher values. These projects bring further problems. In Canada oil sand are found underneath vast forests that have to be cleared. For the production process vast quantities of water mixed with various chemicals is needed to wash the oil from the sand. The polluted water is kept in huge lakes.

Despite the possibilities shown in the last section, in the conceivable future mineral oil will not be available in infinite amounts. Because of this fact and the long term need for a change in the energy sector alternatives are needed.

Another element of uncertainty in the use of fossil energy sources are the discussions about climate change and especially the role of CO_2 emissions.

1.3 Greenhouse effect

The exhaustion of the fossil energy sources, especially of mineral oil is not the only problem the energy supply of the future has to face. The surface of the earth is heated up by solar irradiation and emits heat at a mean temperature of about 15 °C. Due to trace gases like water vapour and CO_2 this thermal radiation is reflected in the atmosphere back to the surface of the earth like in a greenhouse. The greenhouse effect can be divided into a natural and an anthropogenic greenhouse effect. The existing natural greenhouse effect makes life possible on our planet. Without it the temperature on the surface would be 33 °C lower. Due to rising fossil energy consumption and other effects on the environment huge masses of trace gases are emitted into the atmosphere and cause the anthropogenic greenhouse effect. Data from the most important green house gases can be found in table 1.2.

Green-house gas	Concentration [ppm]	Dwell period in the atmosphere [a]	Rise in concentration [%/a]	Specific greenhouse potential	Percentage on the green house effect [%]
CO_2	362	50-200	0,4	1	61
CH_4	1,7	10	0,4	32	15
N_2O	0,31	120	0,26	150	4
O_3	0,03	0,1	0,5	2'000	<9
R11	0,0003	50	0,9	14'000	11
R12	0,0005	103	2,6	17'000	

Table 1.2: Data on the greenhouse gases in the atmosphere [1]

With a share of about 60 % of the total green house effect, CO_2, due to the combustion of fossil combustibles and the use of biomass, is by far the most important greenhouse gas. Whilst biomass, which is used at a rate where it can grow again in the same period, is extensively CO_2-neutral the slash and burn of tropical rainforests liberates huge masses of CO_2 that were bound in the last decades or even hundred years. The combustion of fossil energy sources is responsible for the greatest part of the anthropogenic CO_2 emissions. The concentration has increased in the last 150 years from 280 ppm in the year 1850 to 370 ppm in the year 2000.

Today's CO_2 concentration in the atmosphere is higher than at any time in the last 250'000 years. Anthropogenic methane is set free as mine gas with coal mining, with the extraction of mineral oil, at landfill sites, with the farming of rice and with cattle breeding. In large part the methane emissions can be traced back to the use of fossil energy sources. Even if the share of methane in the atmosphere is less than 1 % of the share of CO_2, methane has immense climate relevance, because the greenhouse potential of methane is 32 times larger than the one of CO_2. N_2O is generated with the slash and burn of tropic rainforests and especially with the use of mineral nitrogen fertiliser in farming. Atmospheric concentrations of N_2O in 1996 were 0,31 ppm, only 8 % over the preindustrialized value, but because of the long dwell period of N_2O in the atmosphere it has to be evaluated seriously. The creation of ground level ozone is increased by pollutants, arising from road traffic as well as stationary combustion of fossil energy sources. Halogenated hydrocarbons have been used as refrigerants or as expanding agents in aerosol cans in vast quantities. These substances have been phased out because of their damaging influence on the ozone layer. Since then the increase of the concentration of ozone in the atmosphere has slowed down considerably. The greenhouse potential of these substances are background to these discussions; most of the substitutes like R11 and R12 have a similar greenhouse potential.

The different anthropogenic green house gases can be assigned to the different origin groups shown in the following:

> Use of fossil energy sources: 50 %
> Chemistry (halogenated hydrocarbons):   20 %
> Slash and burn of tropic rainforests: 15 %
> Farming: 15 %

A detailed forecast of the consequences of the anthropogenic greenhouse effect is not possible. With the help of different climate models attempts are being made to simulate the effect of the increase of greenhouse gases. If the anthropogenic greenhouse effect and especially the consumption of fossil energy sources is not slowed down the CO_2 concentration in the atmosphere will double compared to pre-industrial values within this century. The predictions of the rise of the global mean temperature range between 1 and 5 °C. In a large part the emissions are caused by the industrial countries, developing countries lag far behind, although China now produces as much greenhouse gas emission as the USA. As a result the industrial

countries have to make relatively much larger reduction in their emissions. In February 2005 the Kyoto protocol became effective and requires industrial countries to reduce their greenhouse gas emissions in the period from 2008 to 2012 compared to the values of 1990 by at least of 5 %. The European Union has to realize a mean reduction of 8 %, Germany 21 % and the United Kingdom 12,5 %.

1.4 Renewable energy sources

Besides the fossil and nuclear energy sources renewable (inexhaustible) energy sources are available for energy supply. The term inexhaustible is not meant in a thermodynamic sense, but in human time measure. Renewable energy sources can be divided into three groups:

> ➢ Break up of isotopes in the earth's interior (geothermal energy)
> ➢ Motion of the planets in combination with gravitation (tide energy)
> ➢ Thermonuclear conversion in the sun (solar energy)

The highest energy flux results from solar irradiation, which contributed to the formation of coal, mineral oil and natural gas. The sun is a ball of hot gas with a diameter of $1,4 \cdot 10^6$ km and a distance of $1,49 \cdot 10^8$ km (= 1 AU = 1 astronomical unit) from our planet earth. The energy emitted by the sun is produced in the inner by nuclear fusion, where hydrogen is turned to helium. The surface temperature of the sun has a value of about 6'000 K, while the temperature in the centre is about 15 million K. The irradiation emitted by the sun reduces with the square of the distance. Beyond the atmosphere of the earth an energy of $5,59 \cdot 10^9$ PJ, which is 13'000 times more than the total primary energy consumption of the earth in 2004, is irradiated by the sun. Problems with the use of the solar energy are the low energy density and the resulting high space requirement as well as the issues of energy storage and transport, because solar energy is a time and location dependent energy source.

The energy balance of the earth is basically determined by the sun. About 30 % of the irradiated solar energy is reflected unchanged and 45 % is sent to outer space as thermal radiation. Approximately 22 % of the irradiated energy cause water evaporation and is stored momentary. This part of the solar energy keeps the water circuit in the oceans and around the earth's atmosphere in balance. All other contributions are very low: only 2,5 % contribute to wind, wave energy and ocean current, 0,1 % are used for the production of biomass. Planetary gravitation and geothermal energy

have an ineffectual share of 0,02 % on the energy balance of the earth. The possibilities of the usage of renewable energy sources are listed in the following:

- ➢ Direct usage of solar energy:
  - Solar cell   →   electrical energy
  - Thermal collector   →   thermal energy
  - Thermal power plant   →   electrical energy
- ➢ Indirect usage of solar energy:
  - Hydroelectric power plant   →   electrical energy
  - Wind energy converter   →   electrical energy
  - Power plant using wave energy   →   electrical energy
  - Ocean current power plant   →   electrical energy
  - Heat pump (surface heat)   →   thermal energy
  - Ocean heat power plant   →   electrical energy
  - Biomass power plant   →   electrical energy
  - Biomass conversion plant   →   chemical energy
  - Combustion of biomass   →   thermal energy
- ➢ Usage of planet gravitation:
  - Tide power plant   →   electrical energy
- ➢ Usage of geothermal energy:
  - Geothermal power plant   →   electrical energy
  - Geothermal heating station   →   thermal energy

Until now only hydropower is used in an appreciable amount for the commercial fulfilment of the energy demand. All other conversion methods have exclusively regional meaning or have lost their former relevance especially in industrial countries like wind energy or wood. The known technologies for the usage of renewable energy sources have the ability to provide all the required kinds of secondary energies: heat, electrical current and combustibles. The share of hydropower of the total energy consumption of the earth has a value of about 6 %, for the use of wood and other biomasses only assumptions can be made (5 – 17 %). Wood plays a major role as a non commercial energy source, especially in developing countries, where up to 80 % of the primary energy consumption is provided by wood. In Germany the contribution of renewable energy sources is limited primarily to hydropower and wind energy. The reasons for the marginal usage of renewable energy sources can be found in two principle physical disadvantages. The solar irradiation and the evolving

energies wind, heat and bio energy have a low energy density. Today's technologies for the usage of energy have performance and energy densities that are considerably higher than the ones of renewable energy sources. When appreciable amounts of energy are needed, vast collector areas have to be built, broad agricultural land has to be cropped with biomass or a huge number of wind turbines has to be aligned. The consequence is a large material requirement, high costs and environmental effects. Another disadvantage is the restricted availability of solar and wind energy caused by changes due to the daytime and the season as well as variations caused by the weather. The reliability of the energy supply around the clock can not be guaranteed, because wind and solar energy are not predictable. For the assurance of the energy supply a system based on renewable energy sources normally is coupled with a second energy supply system.

With the use of renewable energy sources the following advantages arise:

- ➢ Infinite amount available
- ➢ No release of the greenhouse gas CO_2 (eg. wind energy or direct irradiation) or CO_2 neutrality (eg. biomass combustion)
- ➢ Low environmental pollution
- ➢ All kinds of energy can be generated (electrical current, heat and chemical energy)
- ➢ Lots of central and decentral technologies can be used
- ➢ No costs for combustibles (except biomass)

In this thesis two systems for the usage of renewable energies are described in detail. One is a biomass Stirling CHP system converting energy out of the combustion of biomass (wooden pellets) to electrical current and heat. The second one is a Dish / Stirling system concentrating direct irradiation on the heater of a Stirling engine and producing electrical current.

1.5 Aims of the thesis

As it was said, this thesis is written to improve γ-type Stirling engines in a low power range up to about 2,5 kW. Its aim is to describe all important existing calculation methods found in the last century and to modify them to give good results for this engine type. The influence of parameter variations is another important fact to find ideal process parameters and geometry data together with the CFD analysis of the

heat exchangers. The values for the variation of the parameters are compared to the ones of measurements to show the accuracy of the methods. Also the results of the different calculation methods are compared to each other and to the measurements processed. The existing experimental Stirling engine systems are modified in a way to be able to measure the system parameters and make them run properly.

The Stirling engines can help to reduce the greenhouse effect and the environmental pollution, by producing electrical current with the use of biomass in CHP systems and with solar irradiation in Dish / Stirling systems. With the use of low power CHP systems in households a better utilization factor of the used combustible can be reached. In conventional power plants the efficiency is only about 40 %, in central combined heat and power plant the utilization factor reaches values of up to 80 % and in decentralized CHP systems this factor can rise up to 90 %. The Stirling engine is an encouraging technology. With properly designed and improved Stirling engines high efficient CHP systems and Dish / Stirling systems can be built up which can help to secure the power supply in the future. With this work attempts are made to understand the complex processes within the Stirling engine, show weaknesses of existing systems and bring the technology a bit closer to the mass production readiness.

1.6   Structure of the thesis

In this section the structure of the thesis is described to show the chronology and the structure of the work.

In chapter 2 the Stirling engine is defined at first and the history is described with examples from the last 200 years. Also characteristics and different types of Stirling engines are shown. As a first calculation method the ideal Stirling cycle calculation method is derived. A comparison of the real and ideal Stirling process is given to define where losses arise. The two experimental systems, a biomass CHP and a solar Dish / Stirling system, are described in first overview. For these engines the ideal process calculation method is used to calculate the efficiency and performance of the cycle. In this chapter also the 0th order calculation methods of West and Beale are described and values for the experimental engines are determined.

In chapter 3 the 1st order calculation method, the so called Schmidt analysis is discussed. The equation set that can be found in the literature is modified in a way to fit the γ-type geometry of the experimental engines. With the methods of Hirata and

Hargreaves the performance and efficiency of the experimental solar and biomass engine are calculated and compared to each other. With these methods the pressure as a function of the crank angle can be displayed. Combining these values with the volumes as a function of the crank angle p-V diagrams for the expansion space, the compression space and the total engine can be derived.

Chapter 4 is added to describe the 2nd order calculation methods in detail. The sinusoidal piston movement is replaced by the real one. The first part shows the ideal adiabatic five cell analysis method. The equation set of Urieli and Berchowitz is modified to fit γ-type Stirling engines and make the results more convenient. Out of these equations a program text is derived in Fortran. With the boundary conditions of the two experimental engines parameters like the p-V diagrams for the different spaces, the temperature as a function of the crank angle for the expansion and compression space, the masses and mass flows of the different spaces, the heat, work, performance and efficiency can be displayed. The second section of this chapter deals with the quasi steady flow model of Urieli. Here the equations are modified to fit the experimental engines and to make the results more exact by using less simplifying assumptions. Non ideal heat exchangers are introduced and values like the pressure drop and the convection losses are determined for the experimental engines additionally to the values calculated in the ideal adiabatic analysis. The pressure and temperature as a function of the crank angle for all the spaces can be calculated and the results are compared with the ideal adiabatic ones. In the third section a parameter variation based on the quasi steady flow analysis is added. Here the influence of the working gas, the preload pressure, the speed, the swept volumes, the phase shift angle and the parameters of the heater, cooler and regenerator on the experimental engines performances and efficiencies is determined and described in detail. In a last step an optimized engine with completely changed parameters is compared to the original one.

In chapter 5 the 4th order multidimensional analysis with CFD is described. With the methods of numerical flow analysis the existing geometry of the heat exchangers heater, cooler and regenerator are analysed. In the result section values for the gas temperatures, heat flux, stream lines (gas velocities) and pressure drops including the inlet and outlet losses are displayed. One of the most interesting sections of this chapter is the FSI analysis of the regenerator where the linear temperature profile of the matrix and the working gas assumed in former chapters is proved.

Chapter 6 is added to show the results of the experiments on the biomass CHP, the Dish / Stirling system and on the gamma type Stirling test bench. Parameters of the different engine concepts are analysed and compared to the different calculation methods to show how successfully the real process can be simulated with the calculation methods shown in the chapters before. With the test bench it is tried to reproduce the results of the parameter variation of chapter 4 according to the heater temperature, preload pressure and phase shift angle.

The conclusion is given in chapter 7 and the possibilities of further research projects are discussed. In chapter 8 the publications done during the writing of this thesis are shown and in chapter 9 the references used are displayed.

2 Stirling cycle engines

2.1 Definition of a Stirling cycle engine

Figure 2-1: Rev. Dr. Robert Stirling (1790-1878) [2]

Rev. Dr. Robert Stirling, Minister at the Church of Scotland and Inventor Extraordinaire wrote in 1876, two years before he died:

"...These imperfections have been in great measure removed by time and especially by the genius of the distinguished Bessemer. If Bessemer iron or steel had been known thirty five or forty years ago there is scarce a doubt that the air engine would have been a great success... It remains for some skilled and ambitious mechanist in a future age to repeat it under favourable circumstances and with complete success..." [3]

The following definition of the Stirling cycle machine is taken from Graham Walkers book "Stirling engines" (1980) [3], that some call the bible of Stirling engines:

"...A Stirling engine is a mechanical device which operates on a closed regenerative thermodynamic cycle, with cyclic compression and expansion of the working fluid at

different temperature levels. The flow is controlled by volume changes and there is a net conversation of heat to work or vice versa...." [3]

This generalized definition embraces a large family of machines with different functions, characteristics and configurations. It includes both rotating and reciprocating machines, utilizing mechanisms of varying complexity. It covers machines capable of operating as prime movers, heat pumps, refrigerating engines or pressure generators.

Other machines exist which operate on an open regenerative cycle, where the flow of working fluid is controlled by valves. For convenience, these may be called Ericsson engines. Unfortunately the distinction is not widely established in practice and the name "Stirling engine" is frequently indiscriminately applied to all types of regenerative machines.

2.2   History of Stirling cycle engines and its origin

The Stirling cycle has its origins in 1816, being first described in a patent granted in that year to a Scottish minister, Reverend Dr. Robert Stirling (see figure 2-1). A part of these original patent drawings, modified for clarity by Finkelstein [4], is shown in figure 2-2. The Stirling engine is the second oldest heat engine, while the oldest is the steam engine. In a time when boiler explosions of steam engines happened very often, Stirling wanted to make work in quarries and coal mines safer. Beside the advanced security for workers also the better efficiency in contrast to the steam engine played a significant role in its invention.

This was undoubtedly one of the most amazing inventions of its kind, being well in advance of all pertinent scientific knowledge of the time. In this context it is worth recalling that Sadi Carnot published his *"Reflections on the motive power of fire"* in 1824, whilst Joule established the mechanical equivalent of heat, and thus laid the foundations for the first law of thermodynamics in 1849 – more than 30 years after the invention of the Stirling engine. [3]

Several aspects of Stirlings invention are unique when compared with other reciprocating prime movers of that time and for some considerable time thereafter:

> ➤ It did not make use of any valves or piston-actuated port openings.
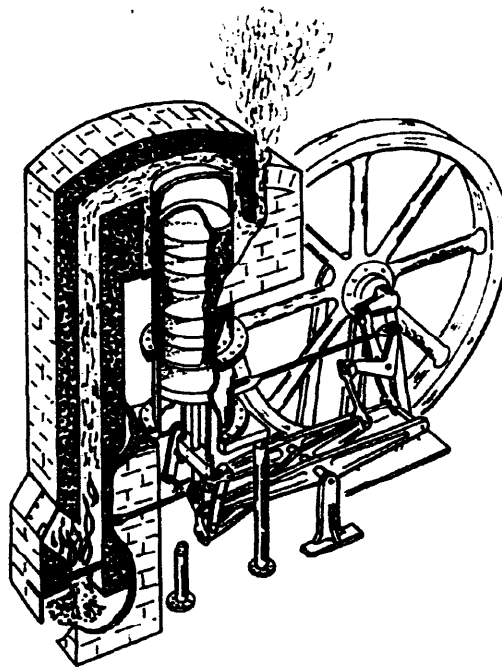
Figure 2-2: Stirling's 2hp engine of 1818 [4]

➤ It operated on a closed cycle so that the working gas is being used over and over again. This allows the minimum cycle pressure to be raised above that of the atmosphere, thereby proportionately increasing the specific work output. Stirling used this feature in his most successful engine built in 1843.

➤ The power piston was located entirely in the cold zone of the engine.

➤ Stirling introduced an "economiser" (now known as a regenerator) for storing heat during one part of the cycle for re-use during another part. This was the most important aspect of Stirling's invention. The following 100 years similar engines were still being "invented" without recognising the full significance of the regenerator, whose importance Stirling must have intuitively appreciated. The regenerator substantially improves the efficiency of the cycle.

Stirling originally envisaged his engine as a perpetual motion engine of the second kind, where all the heat supplied would be converted to work. This is born out by the fact that his patent of 1816 did not include a cooler – only a heater was indicated (see figure 2-2).

The Carnot theorem states that the efficiency of all reversible engines operating between the same two temperatures is the same, and that an irreversible engine working between the same two temperatures must necessarily have lower efficiency than this (Carnot 1824).

At the beginning of the 20th century there were about 250'000 Stirling machines used worldwide for table ventilators, water pumps and engines for small machines. They provided houses and small companies with electrical and mechanical energy. As the Otto-, Diesel- and electrical engines spread, Stirling engines were displaced. Only the military was interested in Stirling engines, because they appreciated the advantages of this concept. To give an example, in the USA a so called "Ground power unit" (figure 2-3) was invented. In Sweden the Koksums AB built an air independent engine for a submarine based upon the Stirling technology.
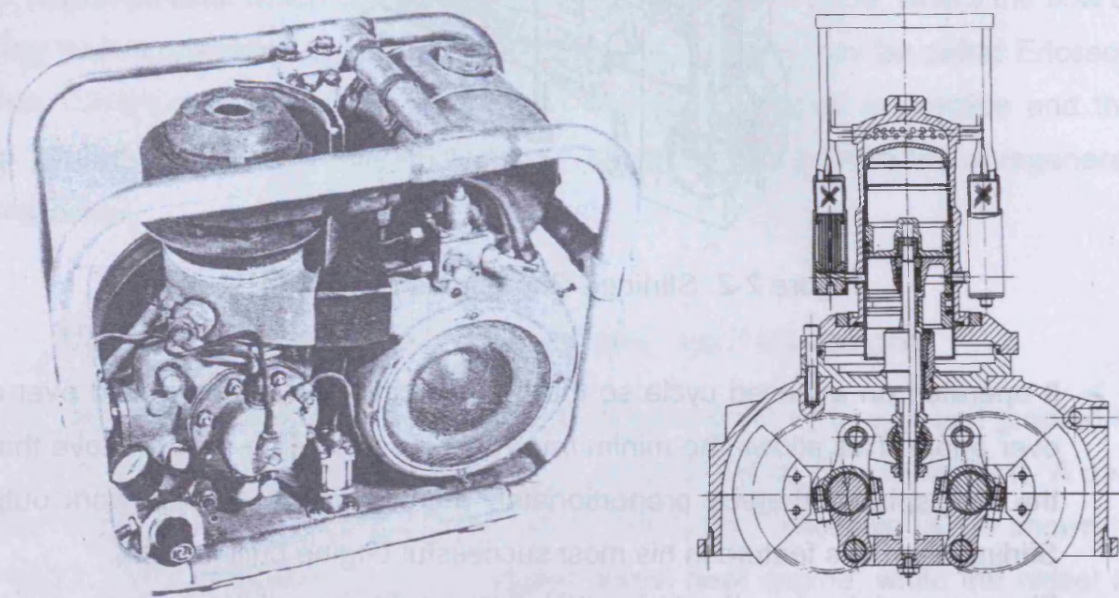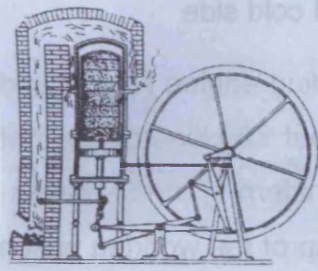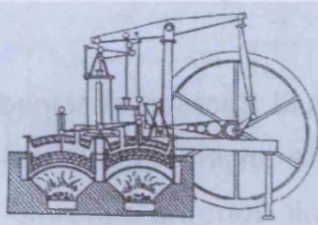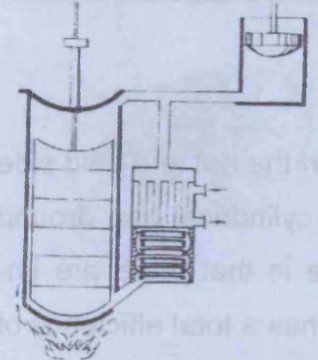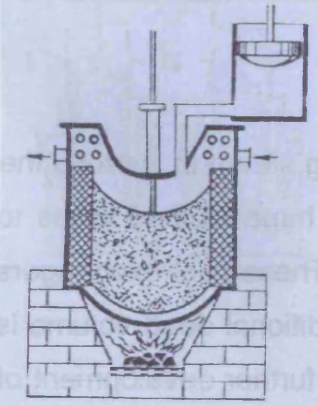
Figure 2-3: Ground power unit of 1958 [3]
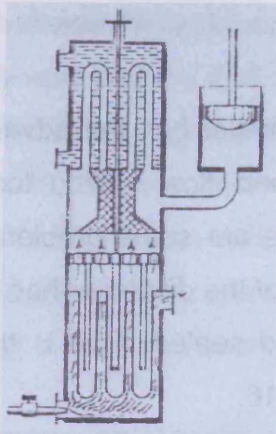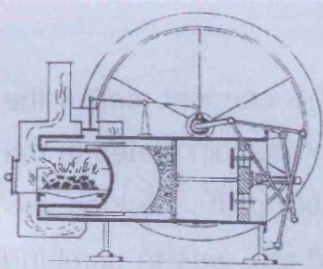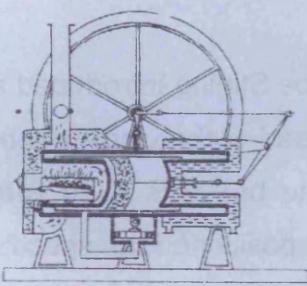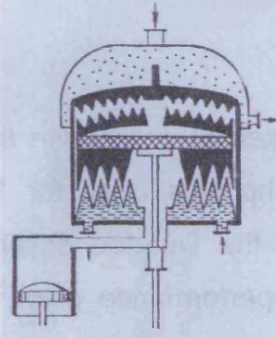
In the following the most important steps in the history of the Stirling engine from the first engine of James Stirling, Robert Stirling's brother, to modern engines, like the main drive of a submarine are shown and described. Some of the pictures and descriptions are taken from Ivo Kolins book "Historische Stirlingmotoren" [5].

	1 - Stirling – 1815 Two separated cylinders This is the first Stirling engine ever built. Today it is at the university of Edinburgh. It was invented in 1815, one year before the first patent. Using the qualification of Chapter 2.4 it is a gamma-type engine. In contrast to a typical gamma type, like the one of Heinrici (pos. 17), it is cooled by air and not by water.
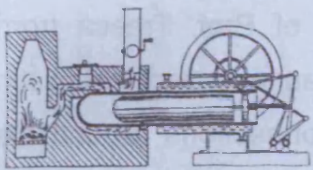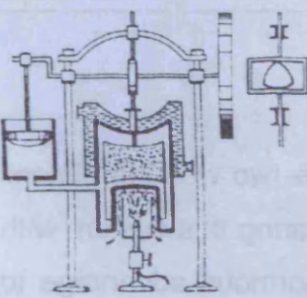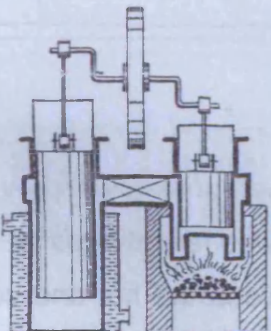
	2 – Stirling – 1816 Two pistons in one cylinder The use of two pistons in only one cylinder has the advantage of avoiding the dead volume and flow friction loss aroused by the connecting pipe. There are some problems with this concept – the connecting rod of the displacer has to be led through the working piston and sealed. This is the typical beta type engine patented in 1816.
	3 – Stirling - 1827 First engine with regenerator Two improvements were realized in this concept, called the Stirling-method. The first one was to place thin plates in the displacer piston to store heat and heat up the working gas when it enters the heater. The second one was to combine two or more of these displacers with one working piston to make the motion of the engine more regular.
	4 – Stirling - 1840 Separated regenerator To enlarge the heat transferring surface Stirling introduced a heat exchanger built up of pipes. Instead of the word regenerator it was named "plate box". The box was filled with sheets of metal (1/40 inches thick) positioned at specific spacing (1/50 inches).
	5 – Stirling - 1845 Cycle under pressure An external pump (not shown) was used to pressurise the engine. This engine with about 2,5 hp was used for 10 months to drive all the machines of the Dundee casting company in Britain. As the need for performance grew, it was displaced by a larger one of the same type. It ran for more than two years without interruption.
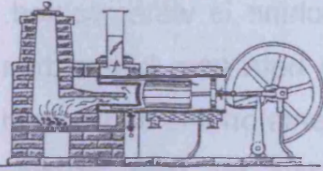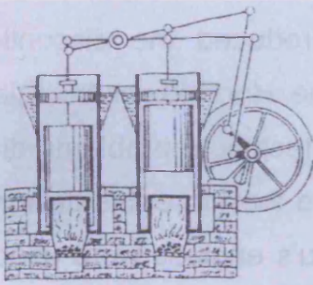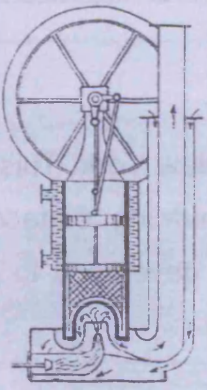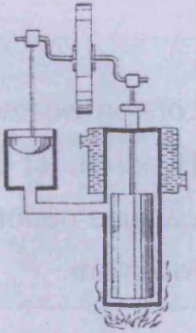
	6 – Napier-Rankine - 1854 Heat exchanging pipes on the hot and cold side Less than ten years after the last Stirling engine Napier and Rankine designed an engine with about 20 pipes on the hot and cold side to enlarge the heat transferring area. The engine had several rods to adjust the gap of the working piston and the displacer. It is not known if this kind of engine ever ran because of the immense dead volume.
	7 – Ericsson - 1860 Open Stirling cycle To avoid problems with the cooling fluid Ericsson designed the open cycle. At each rotation of the engine the hot, expanded gas was displaced by fresh air from the surroundings. Although the losses were huge and the engine only had a total efficiency of 2 % it found numerous applications for large pumps and presses.
	8 – Laubereau - 1861 Enlarged heat exchanging surfaces Laubereau enlarged these surfaces on the hot and cold side by designing an engine with a small cylindrical gap around one central piston. The disadvantage is that there are immense flow losses and so the engine has a total efficiency of only ~1,8 %.
	9 – Young and Kirk - 1865 Toothed heat transferring areas This engine was driven by condensing steam to improve the heat exchange. The designers used huge toothed areas to improve the Stirling engine (pos. 3). These heat exchangers are better than pipes because no additional dead volume is raised. There are no reports about a further development of this concept.
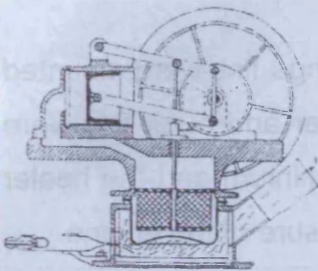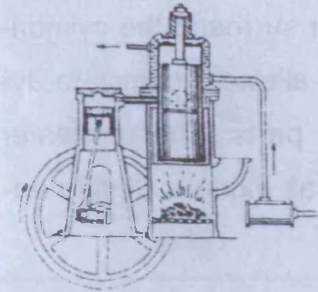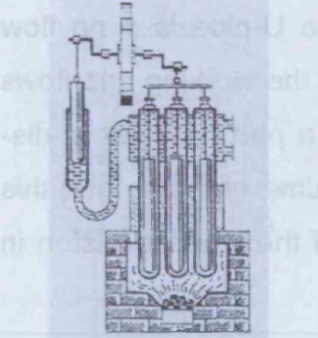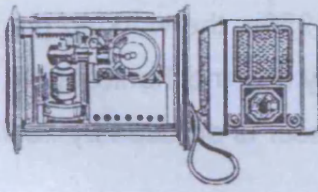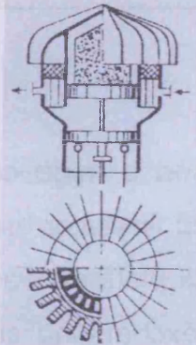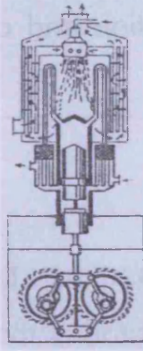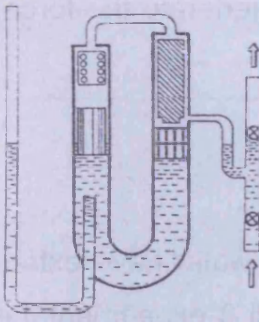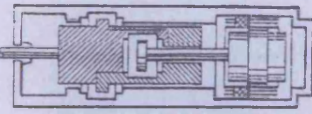
	10 – Lehmann - 1866 The characteristical beta type In contrast to other engines this machine is water cooled. The Lehmann engine represents the beta type better than Stirling's design (pos. 2) did. Experiments on this engine and comments of Delabar were the basis for Prof. Gustav Schmidt's theory (1871) concerning Stirling engines.
	11 – Laubereau - 1869 Discontinuous piston movement The French inventor Laubereau introduced the discontinuous piston movement. He used the Hornblower triangle for the motion of the displacer. The technical problems diminished the practical advantages and therefore this design was not developed further. Laubereau's engines were used for mixers and pumps in chemical laboratories of that time.
	12 – Ericsson - 1870 The first Dish/Stirling unit This first sun driven engine was built in New York. This engine producing 1 hp needed a concentrating surface of about 10 square feet. This concept was developed to produce energy where coal was not available.
	13 – Rider – 1875 The characteristical alpha type The Rider air engine, built by M.H.T. in London worked for up to 15 years without any interruption. Hundreds of these engines were sold all over the world. The engine performed so well that little thought was given to improvement.
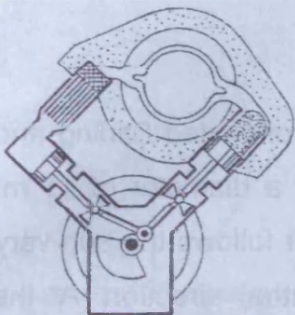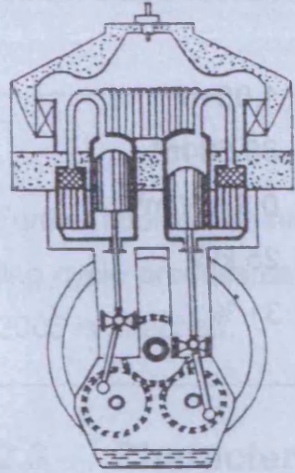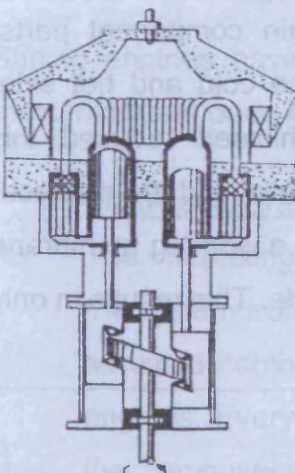
	14 – Stenberg – 1877 Combination of earlier engines Based on the experimental reports of Prof. Tresca from Paris, it became clear that Laubereau was very optimistic about the design of the complex connections around his central piston. Because of this Stenberg only took the hot part of Laubereau (pos. 9) and combined it with the cold part of Lehmann (pos. 10). In addition he improved the burner and the boiler in a way that this engine was quite successful.
	15 – Van Rennes – 1879 Simplified working mechanism Two connection rods are used to drive two working pistons and displacers in two cylinders. Comparing this system with a conventional crank drive it is an enormous advantage to design and maintain only these connection rods.
	16 – Robinson - 1880 Air preheater This invention tripled the performance of air engines without making it more complex. It made the Stirling engine more efficient than the best steam engine but it was too late as the Otto engine was already introduced and the Diesel engine was just being invented.
	17 – Heindrici - 1884 Characteristical gamma type The original Stirling concept (pos. 1) was primarily improved by the water cooler. The performance was raised because of the larger temperature difference between the hot and cold side. As a result Heindrici built a small engine with good performance that found a large market.
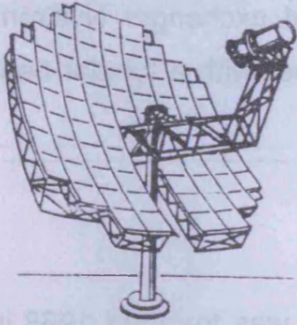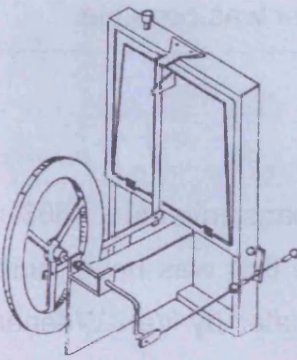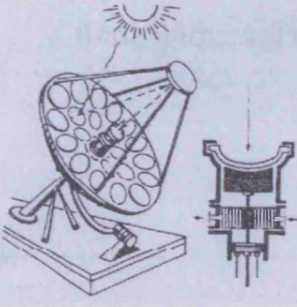
	18 – Robinson - 1889 Engine with cooling platform Instead of a water cooler Robinson used a huge cooling platform. It was built with a kind of cooling fins later used for the cylinders of the Otto engine. The thick platform was also modified by holes to enlarge the heat exchanging surface and to improve the heat transfer by radiation and convection.
	19 – Ringbom - 1905 Mixed form This engine is one of the first hybrid machines. The displacer is free oscillating and the working piston is moun-ted on a conventional crank shaft. In the patent description the weight of the displacer is supposed to generate the force to return the displacer to its lower position.
	20 – Malone - 1931 Hot water instead of air Experiments showed that thin layers of water have extreme high thermal conductivities. Malone built 3 experimental engines with a heater temperature of 400 °C and a pressure of 10'000 psi. No further engines were built using this concept until 2003.
	21 – Philips - 1938 Air engine for Radios Before world war 2 Philips searched for a power unit for its radios. It was to be sold in regions where it is difficult to obtain batteries and where there were good supplies of wood or coal. Philips made enormous steps in the development of Stirling engines and began in the 1960's to build refrigeration systems using the Stirling concept.

	22 – De Brey and Andere - 1947 Inner and outer fins at the heater In order to develop better heat exchange fins were mounted at the outside of the heater. The inner and outer fins were made of materials like bronze or aluminium and the heater itself out of steel to withstand the pressure of the engine.
	23 – Meijer - 1958 Rhombic drive The cooler, regenerator and preheater surround the cylindrical working space. The rhombic drive allows a complete dynamic balanced motion of all driven parts. The preheater system shown became part of almost all modern Stirling engines.
	24 – West - 1970 Engine with liquid pistons The oscillating motion of water in the U-pipe is a no flow process but a displacement. Thereby the working gas flows from the hot to the cold side. When a part of water is displaced from the U-pipe, the total volume changes and this has the same effect as the motion of the working piston in gamma type engines.
	25 – Beale - 1974 Free piston machine In this system, first described in the 1950s, the working piston and displacer are not connected by any mechanical part. The motion of the free swinging displacer is aroused by flow forces of the working fluid.

	26 – Nyström - 1977 Special tubular heat exchanger Almost 20 years after Meijer's invention of the parallel device of combustion chamber and heat exchanger Nyström designed a tubular combustion chamber with a tubular heat exchanger in a radial position.
	27 – United Stirling - 1978 Enlarged pipe preheater The Swedish company United Stirling was founded 1968 in Malmö as part of the Swedish department of defence. Soon after it became part of the Philips Company. One of the later inventions was a double acting Stirling engine with four cylinders. The parallel cylinders needed a complex working mechanism but because of the compact assembly the use of a heater in combination with a preheater was possible.
	28 – Meijer - 1982 Wobble plate engine The British scientist Sir William Siemens invented 1863 a Stirling engine with wobble plate drive that was never built. This concept was modified 80 years later by Van Weenan for the early Philips program. In 1978 Meijer built a wobble plate engine with adjustable angles. This system was used for a double acting Siemens Stirling engines to control the movement of the displacer and to drive the crank shaft.

	29 – McDonnell Douglas - 1985 An enormous solar engine Mc Donnell Douglas used the engine of United Stirling and mounted it on a parabolic mirror with a diameter of 11 m. Using an exocentric, kardanical drive it follows the sun very precisely in the horizontal and azimuthal direction. At the focus of the engine 1430 °C can be produced. Some technical data are as follows: Surface of 1 mirror: 1,08 m² Surface of 82 mirrors: 88,56 m² Irradiation: 0,9 kW/m² Electrical performance: 25 kW Total efficiency 31 %
	30 – Kolin - 1985 Only three main parts needed Stirling's concept is based on 5 main component parts: working piston, heat exchanger on the cold and hot side, displacer and regenerator. Stirling himself reduced this number to 4 by combining the regenerator and the displacer (pos. 4). Kolin's engine also combines a working membrane with the heat exchanger on the cold side. This results in only 3 main parts of the engine
	31 – Isshiki - 1988 Stirling engine with internal heating The Isshiki-engine receives concentrated solar radiation, which heats up the wire mesh in the engine through a glass cover. It can be said that Stirlings design of an external heated engine is changed to an internal one. This system resembles Otto or Diesel engines.
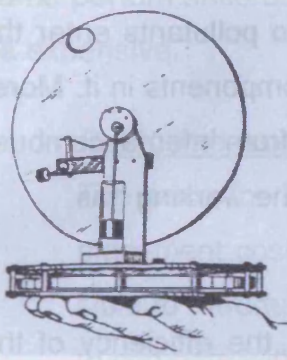
	<u>32 – Senft - 1990</u> Engine with very low ΔT This engine keeps running down to a temperature difference of only 0,5 °C. This was realised by reducing the friction and flow losses to a minimum. For this concept the compression ratio is about 1,004:1. The engine starts moving when it is held in the hand after 15 s and runs with about 60 rotations per minute.

Table 2.1: History of the Stirling engine (pictures taken from [5])

Further information about the history and the different inventions based upon the Stirling cycle process can be found in appendix A where a list of patents from 1816 till 2005 is attached.

2.3   Characteristics of Stirling cycle engines
2.3.1   Advantages of Stirling engines

Stirling engines have many advantages compared to other engine concepts; the most important ones are listed in the following.

➢ <u>Multifuel operation</u>

The interesting thing about this kind of engine is that the heat is brought into the system from the outside. Because of that fact it is not dependent on the intermitted combustion of a certain fuel like it is required in the Otto or Diesel engines. Every kind of heat source can be used, e.g. solar energy, heat from the combustion of biomass, waste gases from processes and all the other solid, fluid and gaseous fuels, even nuclear energy can be used. Because of the external combustion of the fuel, very good, continuous reaction of fuel with oxygen is possible, with low pollutant emissions of NO_x, SO_x, CO etc.

➢ <u>Quiet running</u>

Because of the small number of moving parts in the engine and the avoidance of intermitted combustion the level of noise and vibrations is set to a minimum for this concept.

> ➢ Robustness and long maintenance intervals

The engine parts in their closed case don't have any direct contact to their surroundings. There is also no exchange of fluids. Thus no pollutants enter the engine, which naturally improves the lifetime of all the components in it. Moreover the lubrication oil is not polluted and no acids arise from internal combustion. This leads to extended life for the components and the working gas.

> ➢ Good efficiency

When Stirling engines are designed and built properly, the efficiency of the process is potentially same or even higher as high loaded Diesel engines. For the future new materials like ceramics will be used to increase temperatures and to improve this value. Stirling engines are also able to achieve good efficiencies even at part load.

> ➢ Less pollution

Using solar driven engines there is no pollution; biomass powered engines are CO_2 neutral; even engines driven by fossil energy produce less pollution than Otto or Diesel engines, because of their high efficiencies and continuous mode of combustion

2.3.2 Disadvantages and hindrances to the introduction of Stirling engines

From all the advantages listed above there's the question why there are only so few Stirling engines available for today's civil market.

> ➢ Technical reasons

Common Stirling engines only have high efficiencies when used with enormous swept volumes. Thus these engines cannot be used in cars. Small engines can achieve a high performance, but then the working gas has to be helium or hydrogen and must be set at high pressures (up to 220 bar). Heat and pressure resistant materials for the cylinders, heaters, bearings and bushings are needed which makes this machine quite expensive. Also significant money is needed for the fast and often very complex performance control system. Stirling engines have little chance for introduction into markets

2 Stirling engines

where they have to compete with Otto and Diesel engines. A Stirling engine with the same performance as an Otto engine is either twice as large or twice to three times as expensive.

> Political reasons

The price for fossil and nuclear energies does not reflect their historical replacement cost. At present they are sold too cheaply. It is thus almost impossible to introduce new alternative technologies in existing markets. They have to compete with polluting, but cheap technologies.

> Low level of public recognition

Today only a small percentage of the public is able to describe how and why a Stirling engine works in contrast to the not less complex Otto process. Most persons haven't even heard of Stirling engines.

2.4 Types of Stirling engines

Stirling engines can be distinguished by the configuration of the working spaces and by the kind of mechanical piston control. Classifying them by working space configuration there are three main types of Stirling cycle engines:

> α-type machines

> β-type machines

> γ-type machines

Classifying them by means of piston control there are:

> Machines with kinematical transmission gear (crankshaft drive)

> Free piston machines

In this concept the two pistons oscillate against a gas volume that works as a spring. There is no mechanical connection of the pistons. The energy is brought out using linear generators or pneumatic or hydraulic circuits.

> Hybrid machines

This type is a combination of the two listed above. One piston works with the mechanical transmission gear, the other one is a free oscillating piston. The

Ringbom machine is such a unit and is named after Ossian Ringbom, who patented this machine in 1907.

In the following the first criterion will be defined more exactly.

2.4.1 α-type engines
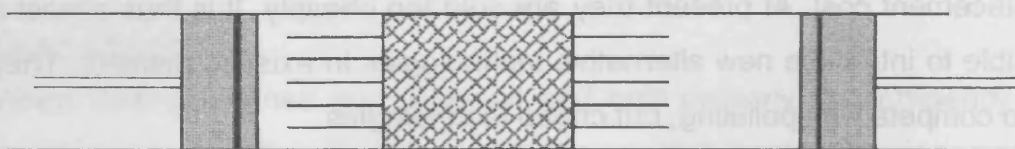
Figure 2-4: Scheme of a α-type machine [3]

The α-type Stirling (figure 2-4) engine has two working pistons, named compression and expansion piston. They are clearly arranged and use a conventional crankshaft drive. Here two pistons have to be sealed from their surroundings, while for β- and γ-type engines only one piston and one connecting rod of the displacer have to be sealed. The sealing of a rod is much simpler than the one of a piston, because the diameter is essentially smaller. The gap in the sealing rises proportional to its diameter. Another feature is that there are no shuttle heat losses (described later) in α-type machines, because both pistons work in spaces with a homogenous temperature.

2.4.2 β-type engines

β-machines (figure 2-5) work like the γ-machines with one working piston and one displacer. They have the advantage in contrast to γ-machines that when moving the
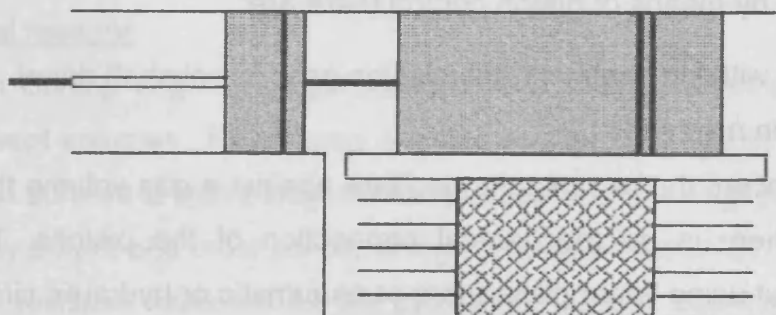
Figure 2-5: Scheme of a β-type machine [3]

two pistons are able to overlap, as they use only one cylinder. Thus higher compression ratios can be achieved and dead volumes are reduced. This can easily be seen,

28

because the position of the displacer does not have any influence on the value of the whole volume (as for α-type Stirling engines). Only the working piston changes the volume. If now the working piston uses a part of the displacers space the swept volume and with it the ratio of maximum to minimum volume rises. Thus β-machines also have the disadvantage that they need to have very exotic transmission gears like the rhombic drive (see figure 2-3 – Ground Power Unit).

2.4.3 γ-type engines

γ-machines (figure 2-6) also have a working piston and a displacer. Here the two pistons are placed in different cylinders. These cylinders can be positioned parallel as well as at an angle of 90° (Figure 2-7). It also works with conventional crankshaft drives. A disadvantage is that it has a large dead volume and therefore the compression ratio and the efficiency are lower compared to the other concepts.

Figure 2-6: Scheme of a γ-type machine [3]

Regenerator
Expansion space
Compression space
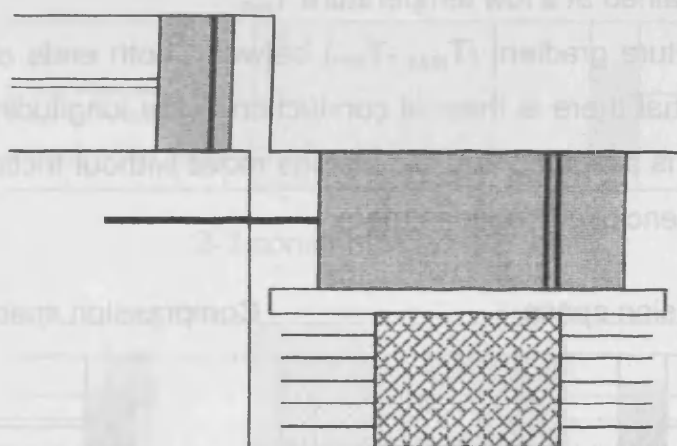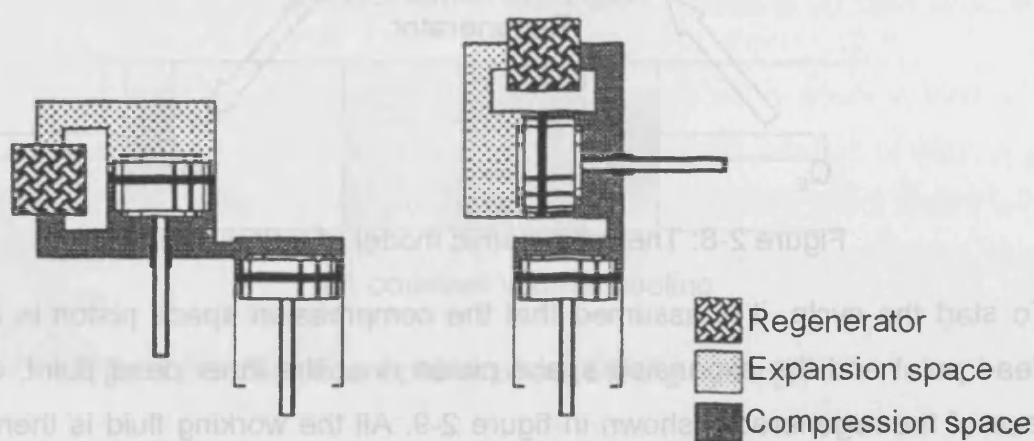
Figure 2-7: Different cylinder configurations of the γ-type machine [3]

2.5   Ideal Stirling process
2.5.1   Ideal Stirling cycle

The basic principle of the Stirling cycle, as for the Otto and Diesel process, is the compression of cold gas and the expansion of hot gas. For these processes the work needed for the compression is less than the resulting work for the expansion. Thus the machine changes heat to work.

Analysing specific steps for the motion, the process becomes clearer. Figure 2-8 shows the thermodynamic scheme of the Stirling engine. The Stirling cycle is similar, in some respects, to the Carnot cycle. The scheme is built up of a cylinder containing two opposed pistons, with a regenerator between the pistons. The regenerator can be supposed to be a thermodynamic sponge, alternately releasing and absorbing heat. It is a matrix of finely divided metal in the form of wires or strips. One of the two volumes between the regenerator and the pistons is called the expansion space and is maintained at a high temperature T_{max}. The other volume is called the compression space, and is maintained at a low temperature T_{min}.

There is a temperature gradient (T_{max} -T_{min}) between both ends of the regenerator, and it is assumed that there is thermal conduction in the longitudinal direction. As in the Carnot cycle, it is assumed that the pistons move without friction or leakage loss of the working fluid enclosed between them.
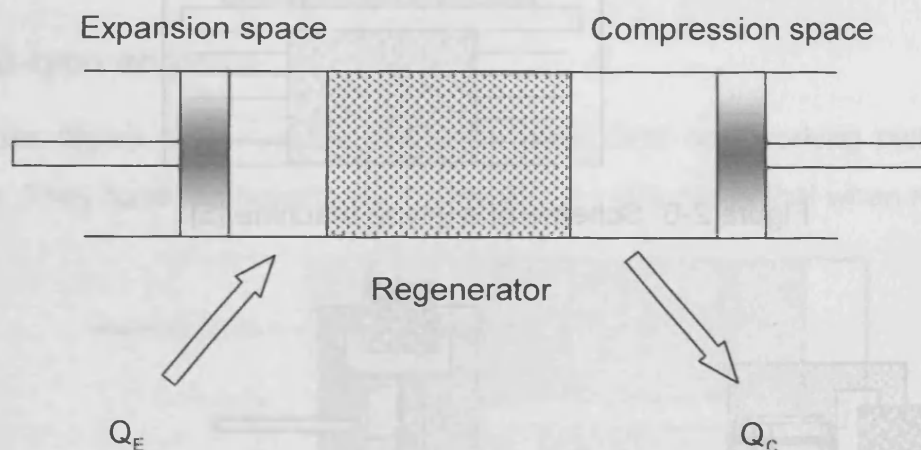
Figure 2-8: Thermodynamic model of a Stirling engine [6]

To start the cycle, it is assumed that the compression space piston is at the outer dead point and the expansion space piston is at the inner dead point, close to the face of the regenerator, shown in figure 2-9. All the working fluid is then in the cold compression space. The volume is at a maximum and thus the pressure and tem-

perature are at their minimum values, represented by point 1 in the p-v and T-s diagrams, shown in figure 2-10 and 2-11.

During compression (process step 1-2 in figure 2-9), the compression space piston moves towards the inner dead point and the expansion space piston remains stationary. The working fluid is compressed in the compression space and the pressure increases. The temperature is maintained constant because the heat Q_C is transported from the compression space cylinder to the surroundings.

1-2 isothermal compression

2-3 constant volume heating

3-4 isothermal expansion

4-1 constant volume cooling
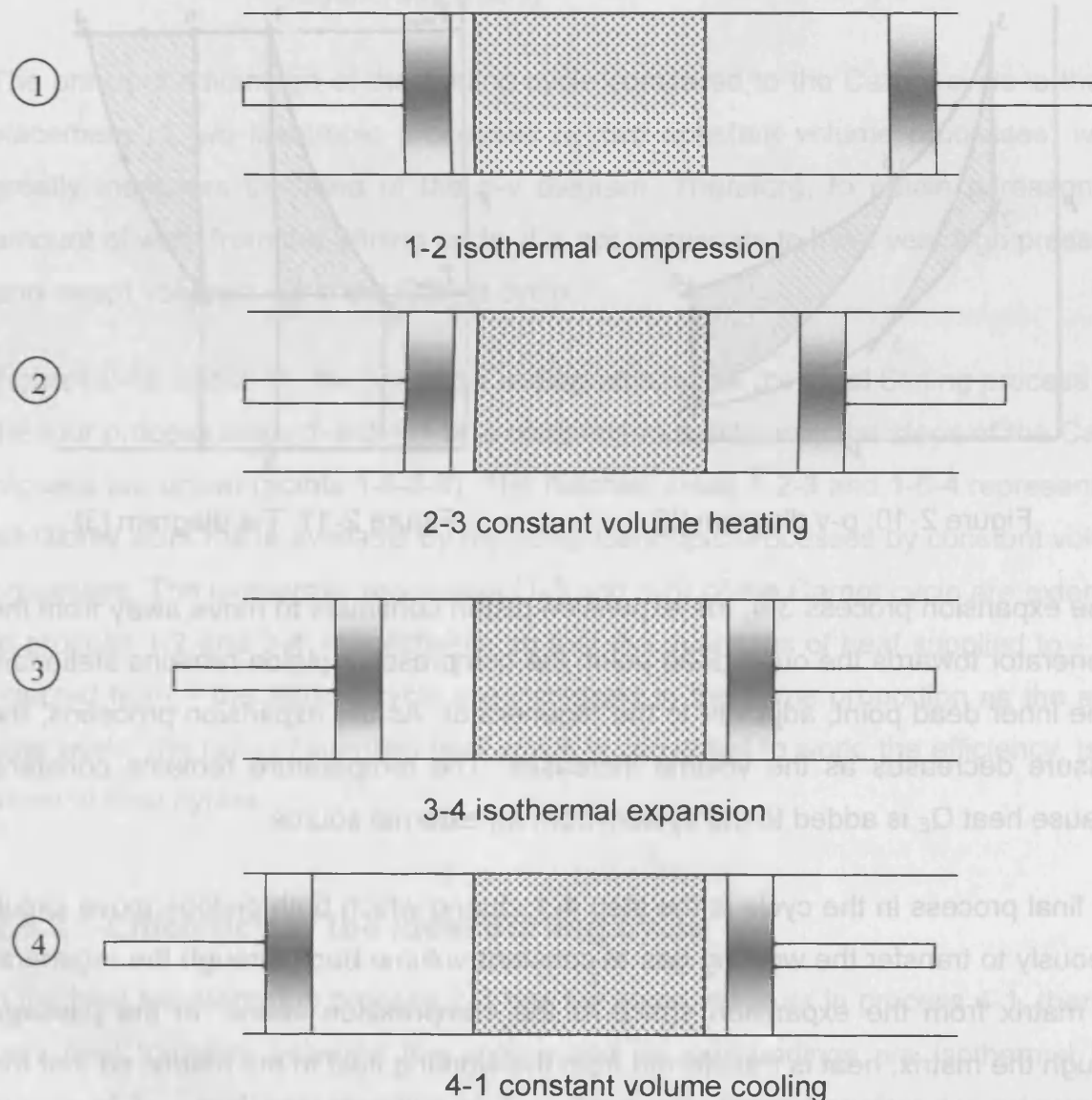
Figure 2-9: Significant points of the Stirling cycle [6]

In the process step 2-3 both pistons move simultaneously, the compression piston towards and the expansion piston away from the regenerator, so that the volume between them remains constant. Therefore, the working fluid is transferred through the porous metallic matrix of the regenerator from the compression space to the expansion space. In the passage through the regenerator, the working fluid is heated from T_{min}, by heat transfer from the matrix and emerges from the regenerator into the expansion space at temperature T_{max}. The gradual increase in temperature in the passage through the matrix, at constant volume, causes an increase in pressure.
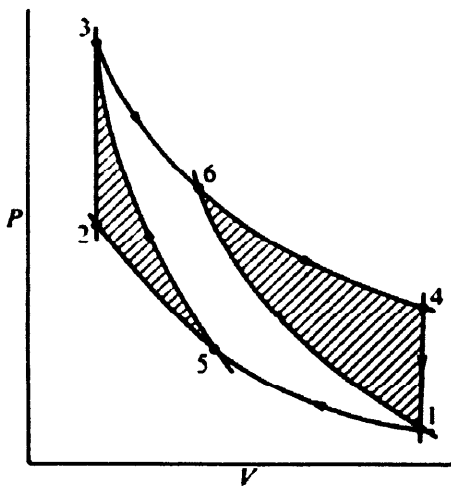
Figure 2-10: p-v diagram [3]   Figure 2-11: T-s diagram [3]
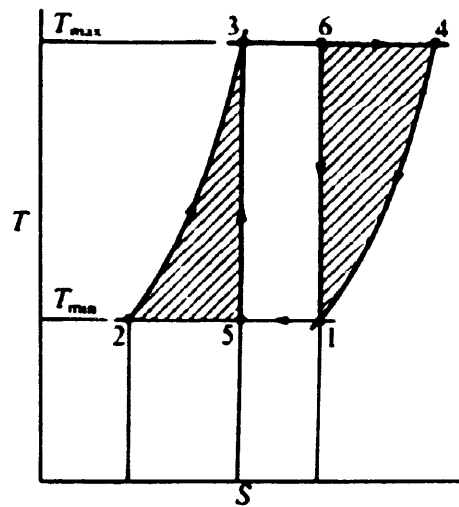
In the expansion process 3-4, the expansion piston continues to move away from the regenerator towards the outer dead point; the compression piston remains stationary at the inner dead point, adjacent to the regenerator. As the expansion proceeds, the pressure decreases as the volume increases. The temperature remains constant, because heat Q_E is added to the system from an external source.

The final process in the cycle is the step 4-1, during which both pistons move simultaneously to transfer the working gas at constant volume back through the regenerative matrix from the expansion space to the compression space. In the passage through the matrix, heat is transferred from the working fluid to the matrix, so that the working fluid decreases in temperature and emerges at T_{min} into the compression space. Heat transferred during the process is stored in the matrix, for transfer to the gas in process 2-3 of the subsequent cycle.

The cycle is therefore composed of four heat transfer processes:

> Process 1-2:   isothermal compression; heat transfer from the working fluid at T_{min} to the external heat sink

> Process 2-3:   constant volume; heat transfer to the working fluid from the regenerator matrix

> Process 3-4:   isothermal expansion; heat transfer to the working fluid at T_{max} from an external source

> Process 4-1:   constant volume; heat transfer from the working fluid to the regenerator matrix

The principal advantage of the Stirling cycle compared to the Carnot cycle is the replacement of two isentropic processes by two constant volume processes, which greatly increases the area of the p-v diagram. Therefore, to obtain a reasonable amount of work from the Stirling cycle, it is not necessary to have very high pressures and swept volumes, as in the Carnot cycle.

Figures 2-10 and 2-11, the p-v and T-s diagrams, show the ideal Stirling process with the four process steps 1-2-3-4. For a comparison additionally the steps of the Carnot process are drawn (points 1-5-3-6). The hatched areas 5-2-3 and 1-6-4 represent the additional work made available by replacing isentropic processes by constant volume processes. The isothermal processes (1-5 and 3-6) of the Carnot cycle are extended to process 1-2 and 3-4, respectively, so that the quantities of heat supplied to – and rejected from – the Stirling cycle are increased in the same proportion as the available work. The ratio of supplied heat which is converted to work, the efficiency, is the same in both cycles.

2.5.2   Efficiency of the ideal Stirling cycle

If the heat transferred in process 2-3 has the same value as in process 4-1, then the only heat transfers between the engine and its surroundings are isothermal heat supply at T_{max} and heat rejection at T_{min}. Thus only these transfers are relevant for the calculation of the efficiency. From the cycle definition the working fluid has to have the same state at the beginning as at the end of each cycle. Thus the internal energy U has to be the same at the beginning and the end. Using the second Law of Thermodynamics it can be shown that:

$$\int dQ + \int dW = \Delta U = 0 \tag{2.1}$$

$$Q_{12} + Q_{34} = -W \tag{2.2}$$

Thus the efficiency of the Stirling engine follows:

$$\eta_{th} = \frac{|W|}{Q_{34}} \tag{2.3}$$

$$\eta_{th} = \frac{Q_{12} + Q_{34}}{Q_{34}} = 1 + \frac{Q_{12}}{Q_{34}} \tag{2.4}$$

For the isothermal changes of state:

$$Q_{12} = m \cdot R \cdot T_1 \cdot \ln\left(\frac{V_2}{V_1}\right) \tag{2.5}$$

$$Q_{34} = m \cdot R \cdot T_3 \cdot \ln\left(\frac{V_4}{V_3}\right) = m \cdot R \cdot T_3 \cdot \ln\left(\frac{V_1}{V_2}\right) = -m \cdot R \cdot T_3 \cdot \ln\left(\frac{V_2}{V_1}\right) \tag{2.6}$$

Putting these equations into (2.4):

$$\eta_{th} = 1 - \frac{m \cdot R \cdot T_1 \cdot \ln\left(\frac{V_2}{V_1}\right)}{m \cdot R \cdot T_3 \cdot \ln\left(\frac{V_2}{V_1}\right)} = 1 - \frac{T_1}{T_3} \tag{2.7}$$

With

$$T_1 = T_2 = T_C \qquad \text{Compression space temperature} \tag{2.8}$$

$$T_3 = T_4 = T_E \qquad \text{Expansion space temperature} \tag{2.9}$$

The efficiency of the ideal process is thus

$$\eta_{th} = 1 - \frac{T_C}{T_E} = 1 - \frac{T_{min}}{T_{max}}. \tag{2.10}$$

This has the same value as the Carnot cycle efficiency and is only a function of the two extreme process temperatures.

2.5.3 Heat and work of the ideal Stirling cycle

From above the work of the Stirling cycle can by described. It is proportional to the performance of the engine:

$$Q_{12} = m \cdot R \cdot T_1 \cdot \ln\left(\frac{V_2}{V_1}\right) \tag{2.11}$$

$$Q_{34} = m \cdot R \cdot T_3 \cdot \ln\left(\frac{V_4}{V_3}\right) \tag{2.12}$$

$$W = -[Q_{12} + Q_{34}] = -m \cdot R \cdot (T_3 - T_1) \cdot \ln\left(\frac{V_1}{V_2}\right) \tag{2.13}$$

2.5.4 Motion in an ideal Stirling engine and the sinusoidal approximation

In the ideal process model the Stirling engine uses three different kinds of spaces (shown in figure 2-12) – the expansion and compression space and the regenerator with the dead volume.

| Expansion space | Regenerator | Compression space |
| V_E | V_R | V_C |
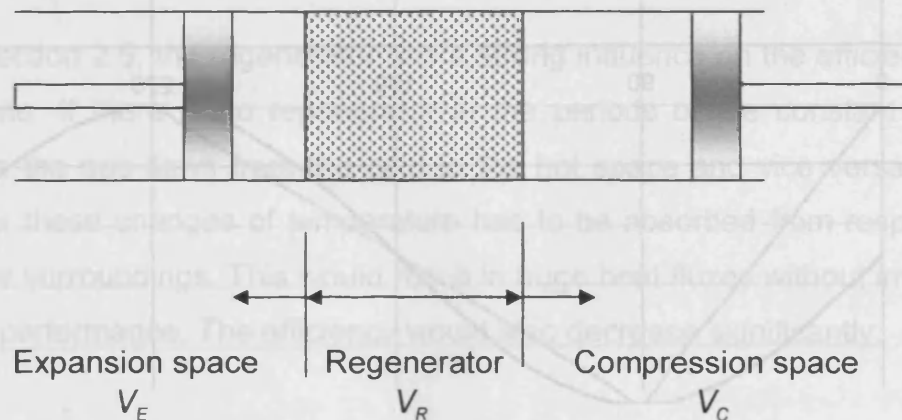
Figure 2-12: Volumes of a Stirling engine [6]

Figure 2-13 shows how the volumes of the expansion space, the compression space and the regenerator relate to the crank angle for a real, continuous and an ideal, discontinuous motion. Here the angle φ stands for the phase shift of the expansion and compression piston. The volume of the regenerator stays constant for the whole cycle. The motion of the ideal Stirling cycle is discontinuous. The pistons are stopped for certain periods in each cycle and remain at their position. Such a motion is almost

impossible to be realised in an engine. A very complex crank drive would be needed. This would lead to immense accelerations and thus to very high forces on the moving parts and generation of noise.

Hence conventional crankshaft drives, like the ones of Otto and Diesel engines, are used. Here the pistons follow a continuous almost sinusoidal movement. Near the dead points the speed of the pistons is very low, which approximates to the still standing period of the discontinuous process. Because of this reason the corners of the p-v diagram are round (figure 2-14). The area enclosed by the curve of the p-v diagram represents the net work that can be produced in a process. Thus the corners are rounded, the area becomes smaller and the performance decreases (see equation in figure 2-14).
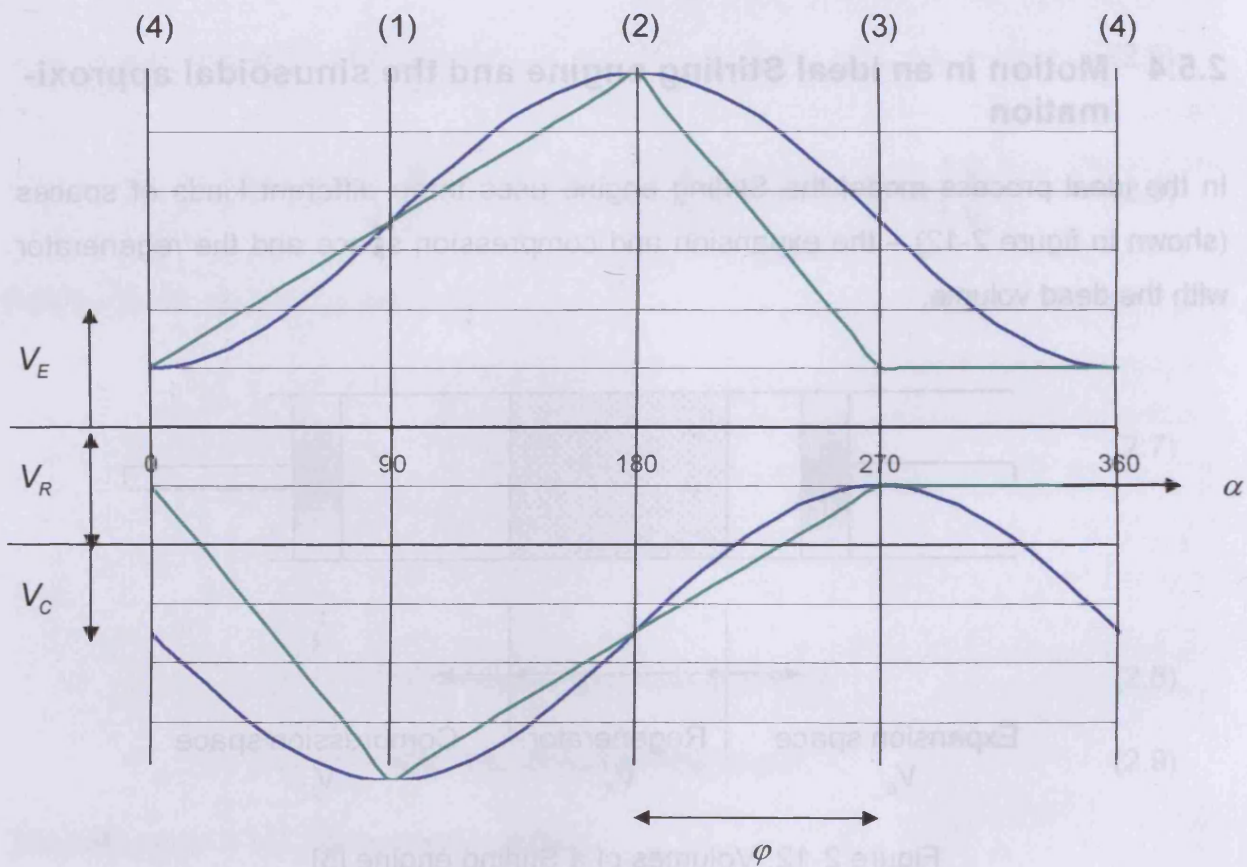
Figure 2-13: Continuous and discontinuous motion
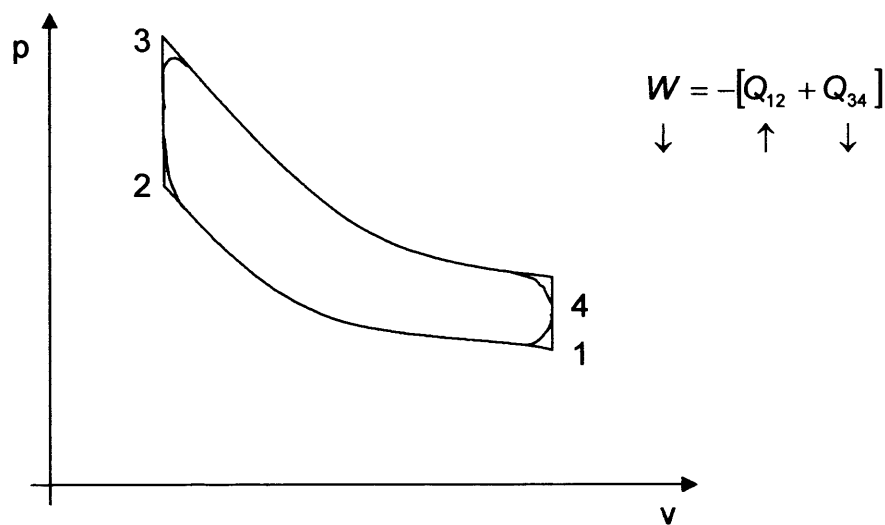
Figure 2-14: p-v diagram for the continuously moving Stirling engine

2.5.5 Direction of rotation

The two pistons in a Stirling engine move with a phase shift of 90°. Thus the direction of the rotation is reversed, the hot space changes to the cold and vice versa. This applies for heat engines as well as for heat pumps and refrigeration machines.

2.5.6 Regenerator

As stated in section 2.5, the regenerator has a strong influence on the efficiency of a Stirling machine. If there is no regenerator in the periods of the constant volume process, when the gas flows from the cold to the hot space and vice versa the required heat for these changes of temperature has to be absorbed from respectively released to the surroundings. This would result in huge heat fluxes without improving the machines performance. The efficiency would also decrease significantly.

2.5.6.1 Temperature profile

The heat capacity of the regenerator should be sufficiently high, that the temperature of the regenerator's material doesn't change when the gas flows through. Then the linear and constant temperature profile shown in figure 2-15 can be achieved. It is assumed that the heat capacity and heat transfer coefficient of the regenerator is infinitely high and the gas flow always adapts to the regenerator's local temperature.
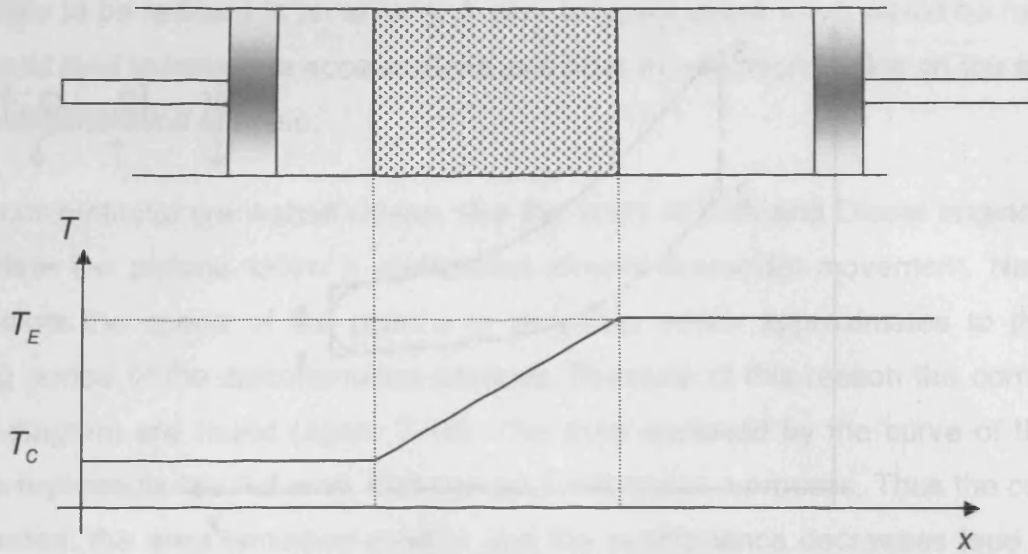
Figure 2-15: Temperature profile of an ideal regenerator

2.5.6.2 Stored heat of the regenerator

In this chapter it is shown how the relation between the stored energy of the regenerator and the work done in the process can be calculated. For heat exchange at constant specific volume:

$$Q_{23} = m \cdot c_v \cdot [T_3 - T_2] \qquad (2.14)$$

$$Q_{41} = m \cdot c_v \cdot [T_1 - T_4] \qquad (2.15)$$

with $T_4 = T_3$ and $T_1 = T_2$

$$Q_{23} = -Q_{41} = m \cdot c_v \cdot [T_3 - T_1] \qquad (2.16)$$

The work done by the process

$$W = -m \cdot R \cdot (T_3 - T_1) \cdot \ln\left(\frac{V_1}{V_2}\right) \qquad (2.17)$$

and the ratio of the volumes at process steps 1 and 2

$$\varepsilon = \frac{V_1}{V_2} \qquad (2.18)$$

Substituting into equation (2.16)

$$Q_{23} = -c_v \cdot \frac{W}{R \cdot \ln(\varepsilon)} \qquad (2.19)$$

Referring the heat of the regenerator to the work done by the cycle:

$$\frac{Q_{23}}{|W|} = \frac{c_v}{R \cdot \ln(\varepsilon)} \tag{2.20}$$

The term $\frac{c_v}{R}$ can be transformed to:

$$\frac{c_v}{R} = \frac{1}{\kappa - 1} \tag{2.21}$$

Thus finally:

$$\frac{Q_{23}}{|W|} = \frac{1}{(\kappa - 1) \cdot \ln(\varepsilon)} \tag{2.22}$$

For a given work the energy which has to be stored in the regenerator rises with a decreasing compression ratio. The volume of the regenerator has to be adapted to the heat storage requirements and here the dead volume must also be considered. Thus for high heat storage capacities there has to be a large regenerator with its associated dead volume which decreases the performance of the machine.

Different working fluids produce different effects in equation (2.22) as:

$$\kappa_a = 1{,}402 \qquad \text{for air} \tag{2.23}$$

$$\kappa_{He} = 1{,}630 \qquad \text{for helium} \tag{2.24}$$

$$\kappa_{H_2} = 1{,}410 \qquad \text{for hydrogen} \tag{2.25}$$

Equation (2.22) combined with the values of equations (2.23) – (2.25) results in figure 2-16.

For example: a machine with a compression ratio of 2 and air as working fluid has to store 3,6 times more energy in the regenerator than the work which can be used. Using helium as the working fluid, only 2,5 times more energy has to be stored.

$$\frac{Q_{23}}{W}$$
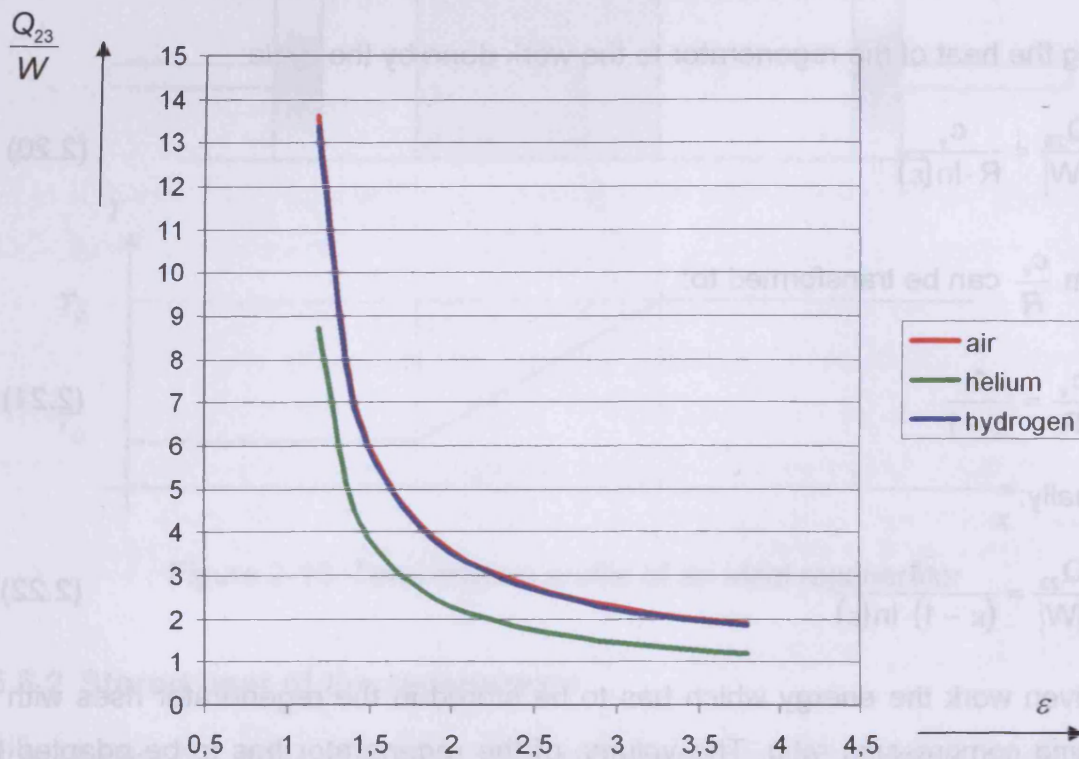
Figure 2-16: Heat stored in the regenerator relative to the work of the process as a function of the compression ratio

2.5.7 Compression ratio for gamma type engines

For Otto and Diesel engines the compression ratio is given by the extreme positions of the piston. The compression ratio of Stirling engines is a function of the crank angle. Because of the heat exchanger and regenerator large dead volumes, Stirling engines only reach compression ratios of about 2 - 3, while Otto and Diesel machines have values of about 9 - 22.

The derivation of the equation for the compression ratio is made with the assumption of a sinusoidal motion of the pistons without dead volumes. The volume of the expansion space is a sinusoidal function of the swept expansion space volume. The compression space volume is composed of two parts (see figure 2-17), because γ-type machines use both the compression space piston and the displacer for compressing the working gas.

$$V_E = \frac{V_{SE}}{2} \cdot [1 - \cos(\alpha)] \tag{2.26}$$

$$V_C = \frac{V_{SE}}{2} \cdot [1 + \cos(\alpha)] + \frac{V_{SC}}{2} \cdot [1 - \cos(\alpha - \varphi)] \tag{2.27}$$

Figure 2-17: Volumes of the Stirling engine [3]

The total volume is the sum of these volumes and the dead volume.

$$V(\alpha) = \frac{V_{SE}}{2} \cdot [1 - \cos(\alpha)] + \frac{V_{SE}}{2} \cdot [1 + \cos(\alpha)] + \frac{V_{SC}}{2} \cdot [1 - \cos(\alpha - \varphi)] + V_D \tag{2.28}$$

$$V(\alpha) = V_{SE} + \frac{V_{SC}}{2} \cdot [1 - \cos(\alpha - \varphi)] + V_D \tag{2.29}$$

The crank angles at the extreme volumes V_{min} and V_{max}, which are needed to calculate the compression ratio, result from the differentiation of the function $V(\alpha)$.

$$\frac{dV(\alpha)}{d\alpha} = \frac{V_{SC}}{2} \cdot \sin(\alpha - \varphi) \tag{2.30}$$

$$0 = \sin(\alpha - \varphi) \tag{2.31}$$

This function reaches the value zero obviously for:

$$\alpha = \varphi \qquad \text{Minimum} \tag{2.32}$$

$$\alpha = \pi + \varphi \qquad \text{Maximum} \tag{2.33}$$

The compression ratio follows:

$$\varepsilon = \frac{V_{max}}{V_{min}} = \frac{V_1}{V_2} \qquad (2.34)$$

$$\varepsilon = \frac{V_{SE} + V_{SC} + V_D}{V_{SE} + V_D} = 1 + \frac{V_{SC}}{V_{SE} + V_D} \qquad (2.35)$$

2.6   Real Stirling process

Like all other cycles, the ideal Stirling process is not exactly reproduceable in a real machine. Reasons for this difference between ideal and real process are listed in the following.

> **Regenerator losses and its efficiency**

The ideal regenerator heats up the working fluid to the heater temperature, when the gas flows from the compression to the expansion space. The working gas has no need to absorb further energy in the heater. In a non-ideal regenerator, shown in figure 2-17, the thermal conductivity is not infinite and thus the working gas leaves the regenerator with a temperature T_{Ro-I} that is below the heater temperature. Thus there is a temperature difference ΔT_{L-I} that has to be compensated by energy brought from the heater.

The heat losses arise from the energies that have to be transferred by the cooler and the heater and can be calculated as:

$$Q_{L-I} = Q_{heater} = m \cdot c_v \cdot \Delta T_{L-I} \qquad (2.36)$$

$$Q_{L-II} = Q_{cooler} = m \cdot c_v \cdot \Delta T_{L-II} \qquad (2.37)$$

The thermal efficiency is:

$$\eta_I = \frac{|Q_{23}| - |Q_{L-I}|}{|Q_{23}|} \qquad (2.38)$$

$$\eta_{II} = \frac{|Q_{41}| - |Q_{L-II}|}{|Q_{41}|} \qquad (2.39)$$
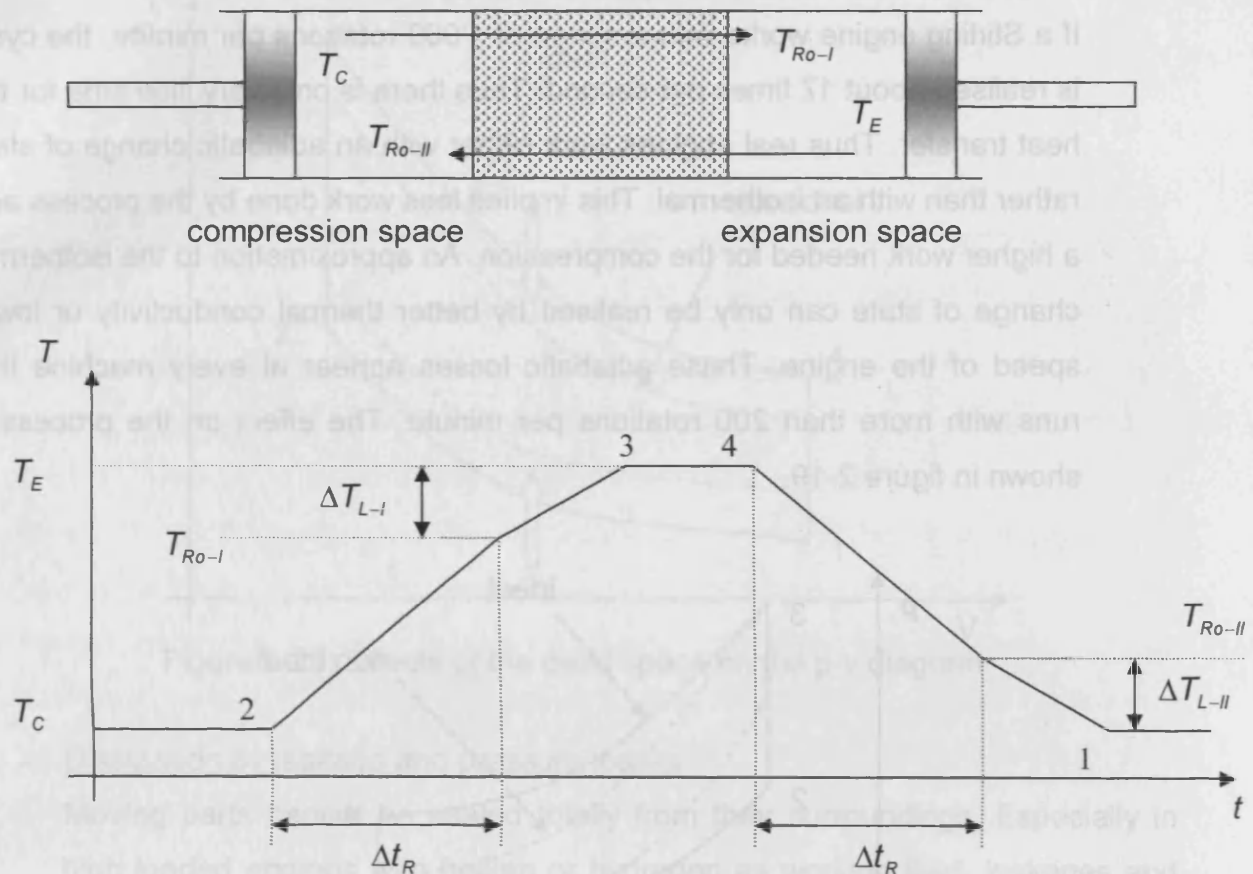
Figure 2-18: Losses of the regenerator

The pressure losses in the regenerator are flow losses due to the velocity of the gas and are not described here. Of course they reduce the mechanical work of the machine.

The working gas reaches the cold space warmer and the hot space colder. This leads to the fact that the cooler has to purge more energy and the heater has to add more energy as it is needed in the ideal process. For the regenerator generally it can be said: the higher the efficiency, the higher are the flow losses owing to the higher gas velocities. In real machines regenerator efficiencies of about 95 % can be reached.

➢ Technical feasibility of the discontinuous piston motion

As stated before, the discontinuous piston movement can only be realised with very complex crank shaft geometry. High accelerations and loads on the engine parts and a high noise level would be the result. Because of this, conventional crank shafts with their continuous, sinusoidal piston movement are used. Thus the corners of the p-v diagram are rounded (figure 2-14) and losses are taken into account.

> Feasibility of the isothermal changes of state

If a Stirling engine works with a speed of 1'000 rotations per minute, the cycle is realised about 17 times per second. Thus there is only very little time for the heat transfer. Thus real engines work rather with an adiabatic change of state rather than with an isothermal. This implies less work done by the process and a higher work needed for the compression. An approximation to the isothermal change of state can only be realised by better thermal conductivity or lower speed of the engine. These adiabatic losses appear at every machine that runs with more than 200 rotations per minute. The effect on the process is shown in figure 2-19.
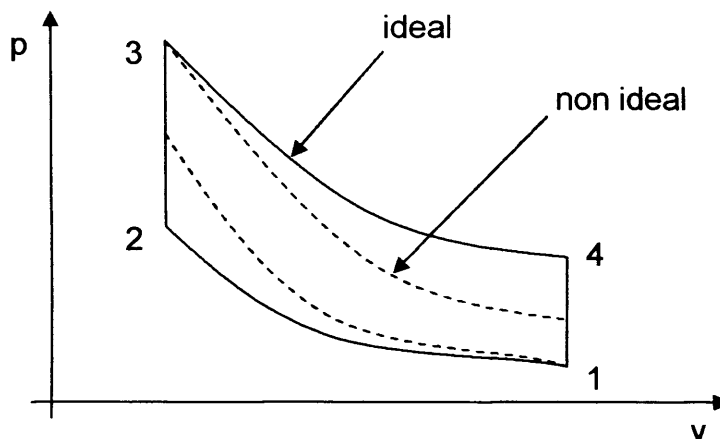
Figure 2-19: Effects of the adiabatic change of state on the p-v diagram

> Dead volume effects

In the ideal case all the working fluid is located in the expansion and the compression space. However in most of the real engines the dead volume amounts 40 – 50 % of the total volume. The main part of this dead volume arises through the volume of the heat exchangers (cooler, regenerator and heater). These dead volumes cause a reduced pressure level and also a decrease of the total efficiency, shown in the following figure.
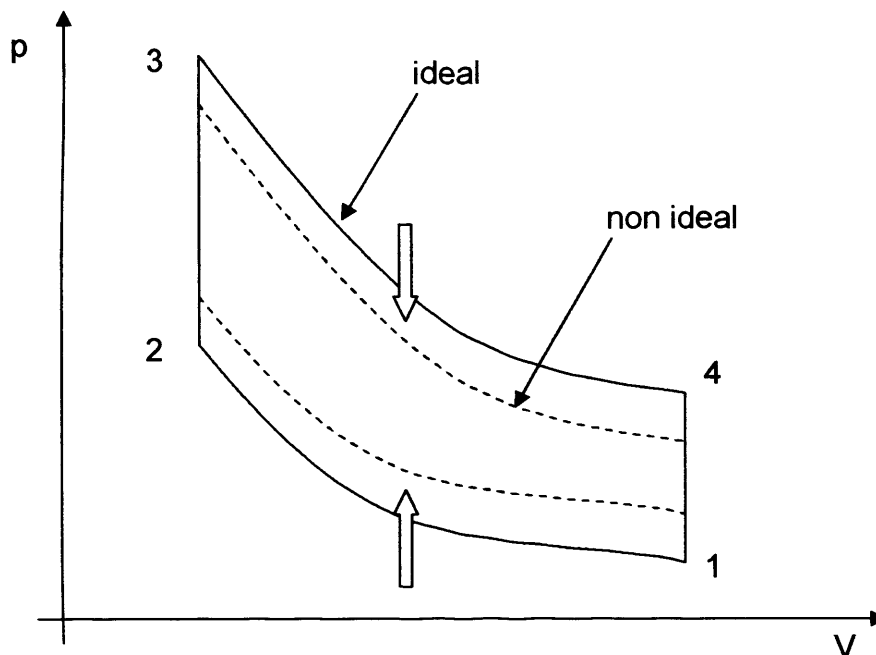
Figure 2-20: Effects of the dead space on the p-v diagram

➤ Dissipation by leakage and pressure losses

Moving parts cannot be sealed totally from their surroundings. Especially in high loaded engines with helium or hydrogen as working fluid, leakages and pressure losses cannot be avoided. This results in a decrease of efficiency. Particularly the working piston has to be sealed, because here the most performance can be lost. The sealing problem was one of the limiting parameters of Stirling engines in the past. In new generation engines the generator is positioned right in the crank case, so that no rotating parts have to be led out and only cables have to be sealed.

➤ Dissipation by non ideal working fluid

Here flux losses can be mentioned, like they appear by vorticity generation in the regenerator or through gas velocity effects. Their exergy is converted to pressure loss.

➤ Dissipation by mechanical friction

These losses appear at all areas of contact (bearings, piston in the cylinder, gear wheels), where mechanical energy is converted to useless heat.

> Heat losses through the material

The thermal conductivity losses arise by the heat flux in direction of the temperature gradient along the cylinder and outwards to the surrounding.

> Total losses

The effect of all the different kinds of losses together on the process is shown in a p-v diagram in figure 2-21.
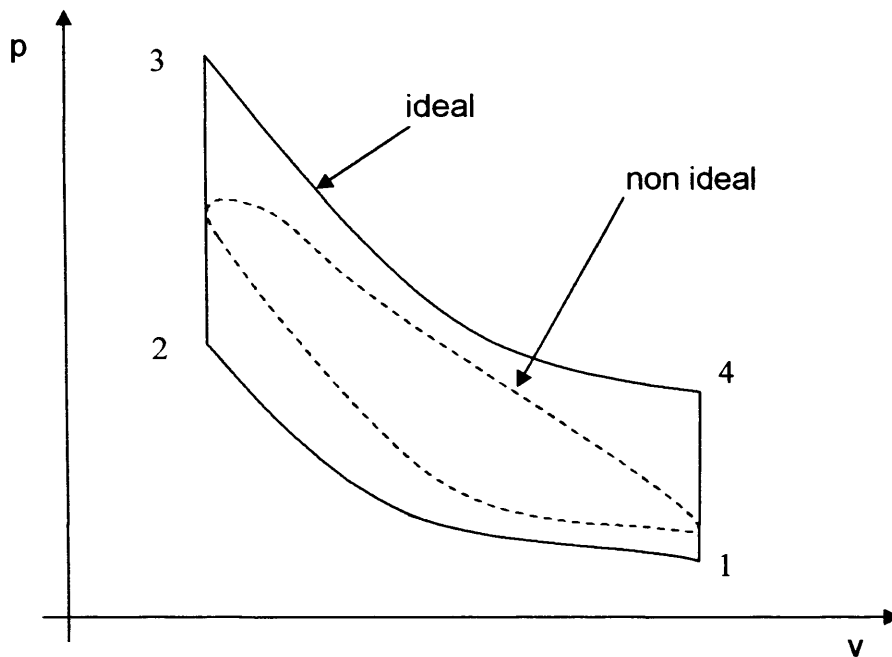
Figure 2-21: The real Stirling process in the p-v diagram

2.7 The experimental engines
2.7.1 Description of the systems
2.7.1.1 The Dish/Stirling system

The Dish/Stirling system EPAS S400 with a mean process performance of 200 W belongs to a group of very small solar power plants. This low power output was chosen by the producer, to support agrarian areas and secluded farms with electrical current. About 2,4 billion people living in sunny regions all over the world have no access to electrical power and therefore there is an immense requirement for economic small power plants. As these systems are used in agrarian regions the following properties were taken as a basis for the development.

> ➢ Automatic operation (starting motor, tracking, charging accumulators)
> ➢ Low maintenance
> ➢ Robustness to environmental conditions
> ➢ Simplicity and availability of spare parts
> ➢ Low fabrication and operating costs

Dish/Stirling systems belong to the class of parabolic power plants and are mainly used for the decentralized energy supply. The electrical power output of such systems is between the 200 W of the EPAS S400 and 50 kW of a plant built in Riad by the Arabian ministry of research and development. The maximum system efficiencies are about 30 % and so the Dish/Stirling technology is one of the most efficient solar technologies. There is also the possibility to combine single plants to a so called solar farm. Performances of up to some megawatts can be generated. These Dish/Stirling plants can remove the polluting decentralized diesel driven generator sets and also be an alternative to the very expensive generation of electrical current by photovoltaics.

Figure 2-22: The solar Stirling engine

Dish/Stirling systems concentrate direct radiation and generate electrical energy. As it can be seen in figure 2-22 it is built up of the following components:

> Concentrator (parabolic mirror)

> Solar heat exchanger / receiver (mounted on the hot side of the Stirling engine)

> Stirling engine with generator

> Tracking equipment

The parabolic concentrator (Dish) focuses the solar radiation. The receiver of the Stirling engine fixed in the focus absorbs the energy and heats up the working gas of the engine. There heat is changed to rotation of the crank shaft. The generator produces electrical current. The electrical performance is proportional to the intensity of the radiation and to the diameter of the parabolic mirror. Influences which reduce the performance include the optical, mechanical, thermal and electrical efficiencies of the single components. To focus the reflected irradiation on the receiver at every time of the day, the aperture of the concentrator has to be tracked continuously towards the sun. There are two kinds of tracking systems:

> Polar tracking

For the polar tracking the system revolves in the daily routine around a polar axis which is parallel to the earth's axis. Once a day the angle of this polar axis – depending on the season – is adapted to the angle of incidence of the sun. Control is carried out by a process computer.

> Azimuthal tracking

For the azimuthal tracking the concentrator is moved continuously and biaxially by two actuators according to the azimuthal and elevation angle of the sun. These actuators are either controlled by the process computer or by two sensor units.

Table 2.2 shows the technical data of the Dish/Stirling system EPAS S400. Further Information about this system can be found in section 6.3.

Dish/Stirling system operating with concentrated irradiation	
Motor type	γ-type Stirling
Motor mean power	200 W
Motor rated speed	500 rpm
Generator type	3 phase a.c. motor permanent magnetic
Generator output power	350 W$_{peak}$
Parabolic collector	Float glass divided into 8 sections
Mirror diameter	2,2m
Aperture area	3m^2
Automatic location of the sun	Biaxial tracking
Motor weight	43kg
Working gas	Nitrogen
Working gas preload pressure	5,5bar
Heater temperature	~700 °C
Coolant temperature	~50 °C
Manufacturer	EPAS GmbH Zweinaundorfer Str. 2077 04316 Leipzig Germany

Table 2.2: Technical data of the solar engine

2.7.1.2 The cogeneration system with the biomass engine

This system, the EPAS BM1000, with a mean process performance of 600 W is a combination of a biomass Stirling engine for the generation of electrical current and a heating and hot water boiler. The main components of the system are:

➢ Blow pipe

➢ Heater and hot water boiler

➢ Stirling engine

➢ Water supply with pumps for the Stirling engine and the hot water boiler

➢ Electrical installations

Pictures of the system are shown in figure 2-23 and important details are listed in table 2-3. A detailed description of the system is given in section 6.1.

49

Figure 2-23: The biomass Stirling engine

Motor type	γ-type Stirling
Motor mean power	600 W
Motor rated speed	700 rpm
Generator type	3 phase a.c. motor permanent magnetic
Generator output power	820 W_{peak}
Boiler	SBS Axiom
Boiler thermal performance	21,4 kW
Blow pipe	SBS Janfire flex-a
Fired by	Wooden pellets
Motor weight	43kg
Working gas	Nitrogen
Working gas preload pressure	7,5bar
Heater temperature	~1100 °C
Coolant temperature	~50 °C
Manufacturer	EPAS GmbH Zweinaundorfer Str. 2077 04316 Leipzig Germany

Table 2.3: Technical data of the biomass engine

2.7.2 Drawings

To illustrate further details about the engines a cross section of the biomass engine is shown in figure 2-24 and 2-25. It is the same as the solar Stirling engine except the heater (can be seen at the top of the figures with its 36 pipes).

gap hot
side 28cm³

36 pipes 478cm³

dead space above regenerator 38cm³

dead space around regenerator 85cm³

dead space above cooler 26cm³

regenerator
150cm³

displacer

stoke 75mm
working piston Ø 87,5mm
displacer Ø 98mm
displacer rod Ø 10mm

cooling water
connection

cooler
95cm³

swept volume 450cm³
displacer space volume:
hot side 565cm³
cold side 559 cm³

cooling water
connection

connection to the
cooler 24cm³

head connec-
tion 23cm³

transfer port
72cm³

gap cold
side 32cm³

cooling water
connection

cooling water
connection

cooling water
connection

working piston

head port
18cm³

gap working piston
4cm³

total dead volume
1'073cm³

Figure 2-24: Cross section of the biomass driven Stirling engine
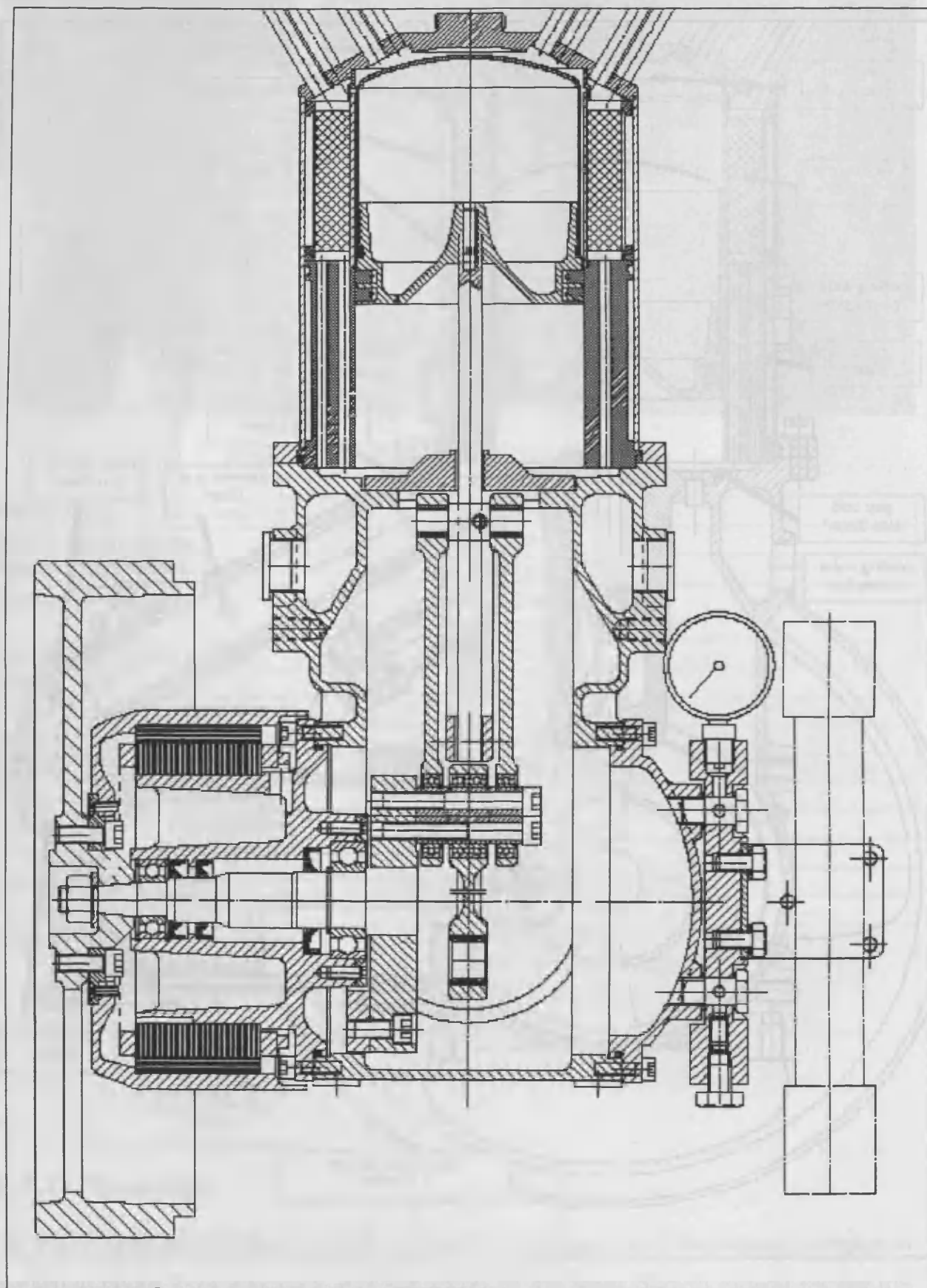
Figure 2-25: Cross section of the biomass driven Stirling engine

2.7.3 Performance of both engines using the ideal cycle model

Using the model of chapter 2 performance and critical parameters are calculated for the two experimental engines. Index s stands for the solar and b for the biomass engine. Values without an index are for both engines.

> ## Thermal efficiency

The thermal efficiency of the ideal process (equation (2.10)) can be calculated from the two process temperatures in the cooler and the heater. Measurements give the following values:

$$T_{C,s} = 331 K \tag{2.40}$$

$$T_{E,s} = 628 K \tag{2.41}$$

$$T_{C,b} = 328 K \tag{2.42}$$

$$T_{E,b} = 1173 K \tag{2.43}$$

$$\eta_{th,s} = 1 - \frac{331 K}{628 K} = 0{,}473 \tag{2.44}$$

$$\eta_{th,b} = 1 - \frac{328 K}{1173 K} = 0{,}720 \tag{2.45}$$

The biomass Stirling has a very high ideal efficiency, potentially higher than that of an Otto or Diesel engine.

> ## Volumes as a function of the crank angle

The stoke of the two engines is the same with a value of:

$$h = 75 \, mm \tag{2.46}$$

The piston diameters are:

$$d_d = 98 \, mm \qquad \text{displacer} \tag{2.47}$$

$$d_w = 87{,}5 \, mm \qquad \text{working piston} \tag{2.48}$$

Using equations (2.46) – (2.48) and figure 2-24 the different swept and dead volumes can be derived:

$$V_{SE} = \frac{\pi}{4} \cdot d_d^2 \cdot h = 5{,}65 \cdot 10^{-4} \ m^3 \tag{2.49}$$

$$V_{SC} = \frac{\pi}{4} \cdot d_w^2 \cdot h = 4{,}51 \cdot 10^{-4} \ m^3 \tag{2.50}$$

$$V_{DE,s} = 2{,}50 \cdot 10^{-4} \ m^3 \tag{2.51}$$

$$V_{DE,b} = 5{,}44 \cdot 10^{-4} \ m^3 \tag{2.52}$$

$$V_{DC} = 3{,}79 \cdot 10^{-4} \ m^3 \tag{2.53}$$

$$V_R = 1{,}50 \cdot 10^{-4} \ m^3 \tag{2.54}$$

$$V_{D,s} = 7{,}80 \cdot 10^{-4} \ m^3 \tag{2.55}$$

$$V_{D,b} = 10{,}73 \cdot 10^{-4} \ m^3 \tag{2.56}$$

The phase shift angle is:

$$\varphi = 90° \tag{2.57}$$

Setting the values (2.49) to (2.57) into equation (2.26) and (2.27) figures 2-26 and 2-27 can be derived.
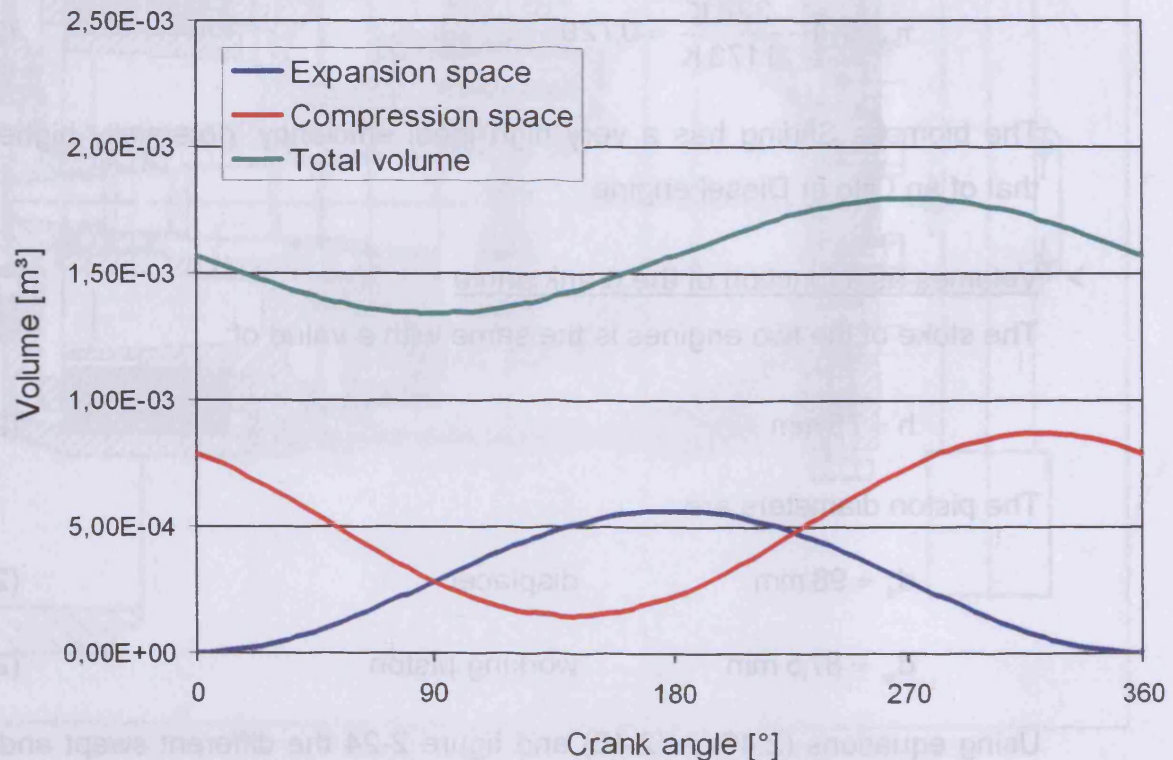
Figure 2-26: Volume as a function of the crank angle for the solar engine
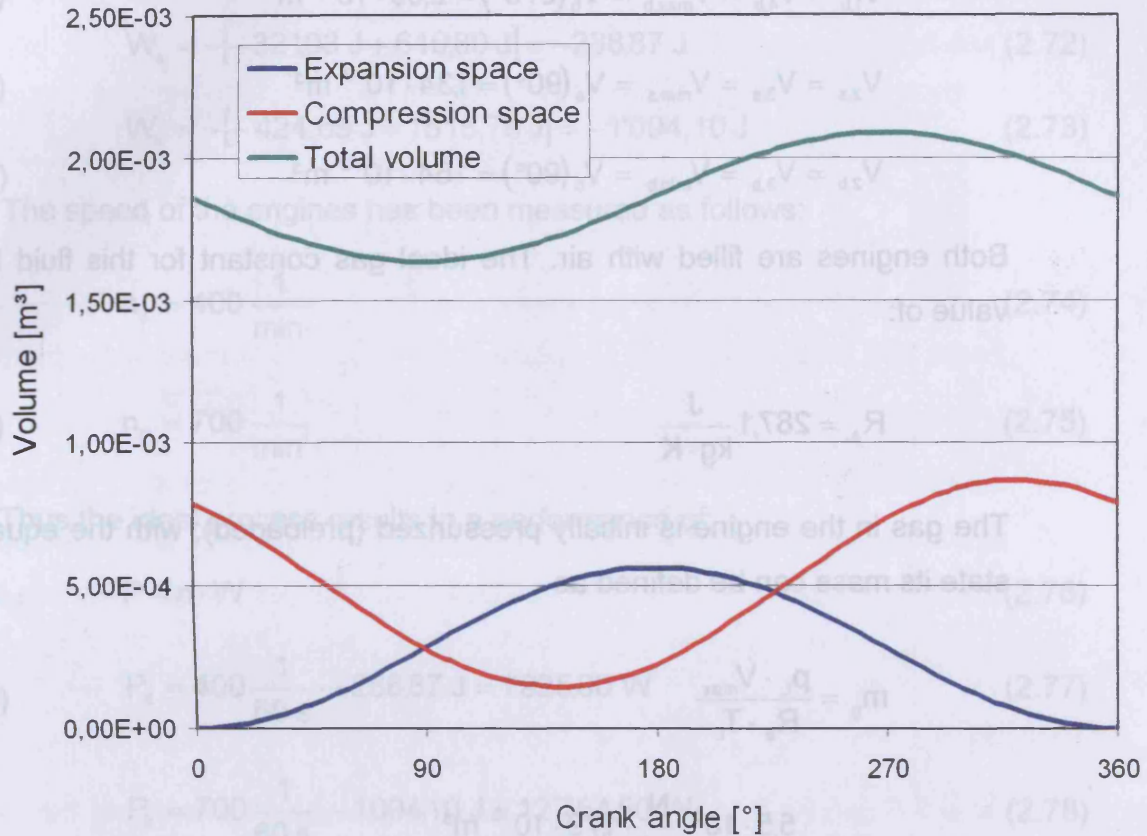
Figure 2-27: Volume as a function of the crank angle for the biomass engine

> Compression ratio

The compression ratio of the two engines is calculated with equation (2.35) and has the values:

$$\varepsilon_s = 1 + \frac{4{,}51 \cdot 10^{-4} \ m^3}{5{,}65 \cdot 10^{-4} \ m^3 + 7{,}80 \cdot 10^{-4} \ m^3} = 1{,}34 \qquad (2.58)$$

$$\varepsilon_b = 1 + \frac{4{,}51 \cdot 10^{-4} \ m^3}{5{,}65 \cdot 10^{-4} \ m^3 + 10{,}73 \cdot 10^{-4} \ m^3} = 1{,}28 \qquad (2.59)$$

> Heat, work and performance of the ideal Stirling cycle

To obtain the heat, which must be transferred in the steps of the cycle, the volumes at the corner points of the thermodynamic cycle have to be determined. The maximum and minimum total volumes can be seen in figures 2-26 and 2-27.

$$V_{1,s} = V_{4,s} = V_{max,s} = V_s(270°) = 1{,}79 \cdot 10^{-3} \ m^3 \qquad (2.60)$$

$$V_{1,b} = V_{4,b} = V_{max,b} = V_b(270°) = 2{,}09 \cdot 10^{-3} \ m^3 \qquad (2.61)$$

$$V_{2,s} = V_{3,s} = V_{min,s} = V_s(90°) = 1{,}34 \cdot 10^{-3} \ m^3 \qquad (2.62)$$

$$V_{2,b} = V_{3,b} = V_{min,b} = V_b(90°) = 1{,}64 \cdot 10^{-3} \ m^3 \qquad (2.63)$$

Both engines are filled with air. The ideal gas constant for this fluid has an value of:

$$R_a = 287{,}1 \frac{J}{kg \cdot K} \qquad (2.64)$$

The gas in the engine is initially pressurized (preloaded); with the equation of state its mass can be defined as

$$m_g = \frac{p_L \cdot V_{max}}{R_a \cdot T_L} \qquad (2.65)$$

$$m_{g,s} = \frac{5{,}5 \cdot 10^5 \ \frac{N}{m^2} \cdot 1{,}79 \cdot 10^{-3} \ m^3}{287{,}1 \frac{J}{kg \cdot K} \cdot 293 \ K} = 11{,}7 \cdot 10^{-3} \ kg \qquad (2.66)$$

$$m_{g,b} = \frac{7{,}5 \cdot 10^5 \ \frac{N}{m^2} \cdot 2{,}09 \cdot 10^{-3} \ m^3}{287{,}1 \frac{J}{kg \cdot K} \cdot 293 \ K} = 18{,}6 \cdot 10^{-3} \ kg \qquad (2.67)$$

Putting the values (2.40) – (2.43), (2.60) – (2.64), (2.66) and (2.67) into equations (2.11) – (2.13) the transferred heat and work can be calculated as:

$$Q_{12,s} = 11{,}7 \cdot 10^{-3} kg \cdot 287{,}1 \frac{J}{kg \cdot K} \cdot 331K \cdot \ln\left(\frac{1{,}34}{1{,}79}\right) = -321{,}93 \ J \qquad (2.68)$$

$$Q_{12,b} = 18{,}6 \cdot 10^{-3} kg \cdot 287{,}1 \frac{J}{kg \cdot K} \cdot 328 \ K \cdot \ln\left(\frac{1{,}64}{2{,}09}\right) = -424{,}69 \ J \qquad (2.69)$$

$$Q_{34,s} = 11{,}7 \cdot 10^{-3} kg \cdot 287{,}1 \frac{J}{kg \cdot K} \cdot 628 \ K \cdot \ln\left(\frac{1{,}79}{1{,}34}\right) = 610{,}80 \ J \qquad (2.70)$$

$$Q_{34,b} = 18{,}6 \cdot 10^{-3} \ kg \cdot 287{,}1 \frac{J}{kg \cdot K} \cdot 1173K \cdot \ln\left(\frac{2{,}09}{1{,}64}\right) = 1'518{,}79 \ J \qquad (2.71)$$

$$W_s = -[-321{,}93 \text{ J} + 610{,}80 \text{ J}] = -288{,}87 \text{ J} \qquad (2.72)$$

$$W_b = -[-424{,}69 \text{ J} + 1518{,}79 \text{ J}] = -1'094{,}10 \text{ J} \qquad (2.73)$$

The speed of the engines has been measured as follows:

$$n_s = 400 \frac{1}{\text{min}} \qquad (2.74)$$

$$n_b = 700 \frac{1}{\text{min}} \qquad (2.75)$$

Thus the ideal process results in a performance of:

$$P = n \cdot W \qquad (2.76)$$

$$P_s = 400 \frac{1}{60 \text{ s}} \cdot -288{,}87 \text{ J} = 1'925{,}80 \text{ W} \qquad (2.77)$$

$$P_b = 700 \frac{1}{60 \text{ s}} \cdot -1094{,}10 \text{ J} = 12'764{,}50 \text{ W} \qquad (2.78)$$

This large difference in the performance arises from the fact that in the ideal process no dead volumes are considered. The complete gas mass is always in the working spaces. The other point is, that the speed of the biomass engine is higher.

➤ Heat stored in the regenerator relative to the work of the process
With equation (2.22), (2.23), (2.58) and (2.59) this value can be determined. It shows how much more heat the regenerator has to store, compared to the work of the process. These high values arise from the low compression ratio, which is typical for γ-type engines.

$$\left(\frac{Q_{23}}{W}\right)_s = \frac{1}{(1{,}402 - 1) \cdot \ln(1{,}34)} = 8{,}50 \qquad (2.79)$$

$$\left(\frac{Q_{23}}{W}\right)_b = \frac{1}{(1{,}402 - 1) \cdot \ln(1{,}28)} = 10{,}08 \qquad (2.80)$$

➤ p-V diagram of the ideal process
At process step points 1 - 4 of the ideal process, volume and temperature is calculated in this chapter (equations (2.40) – (2.43) and (2.60) – (2.63)). Using

the equation of state, the pressure at each of the points can be determined (see table 2-4 and 2-5).

<table>
<thead>
<tr><th></th><th>V</th><th>T</th><th>p</th></tr>
<tr><th></th><th>m³</th><th>K</th><th>bar</th></tr>
</thead>
<tbody>
<tr><td>1</td><td>1,79E-03</td><td>331</td><td>6,21</td></tr>
<tr><td>2</td><td>1,34E-03</td><td>331</td><td>8,30</td></tr>
<tr><td>3</td><td>1,34E-03</td><td>628</td><td>15,7</td></tr>
<tr><td>4</td><td>1,79E-03</td><td>628</td><td>11,8</td></tr>
</tbody>
</table>

<table>
<thead>
<tr><th></th><th>V</th><th>T</th><th>p</th></tr>
<tr><th></th><th>m³</th><th>K</th><th>bar</th></tr>
</thead>
<tbody>
<tr><td>1</td><td>2,09E-03</td><td>328</td><td>8,38</td></tr>
<tr><td>2</td><td>1,64E-03</td><td>328</td><td>1,07</td></tr>
<tr><td>3</td><td>1,64E-03</td><td>1173</td><td>38,2</td></tr>
<tr><td>4</td><td>2,09E-03</td><td>1173</td><td>30,0</td></tr>
</tbody>
</table>

Table 2.4: Values of the solar engine   Table 2.5: Values of the biomass engine

Interpolating some of the values between points 2 - 3 and 4 - 1 (volume there is constant and the pressure can be linearly interpolated) and calculating values between point 1 - 2 and 3 - 4 (isothermal change of state) with equation

$$\frac{p_1}{p_2} = \frac{V_2}{V_1} \qquad (2.81)$$

table 2-6 can be built up. Figure 2-28 – the p-V diagram showing the total volume – is derived from of table 3-4.
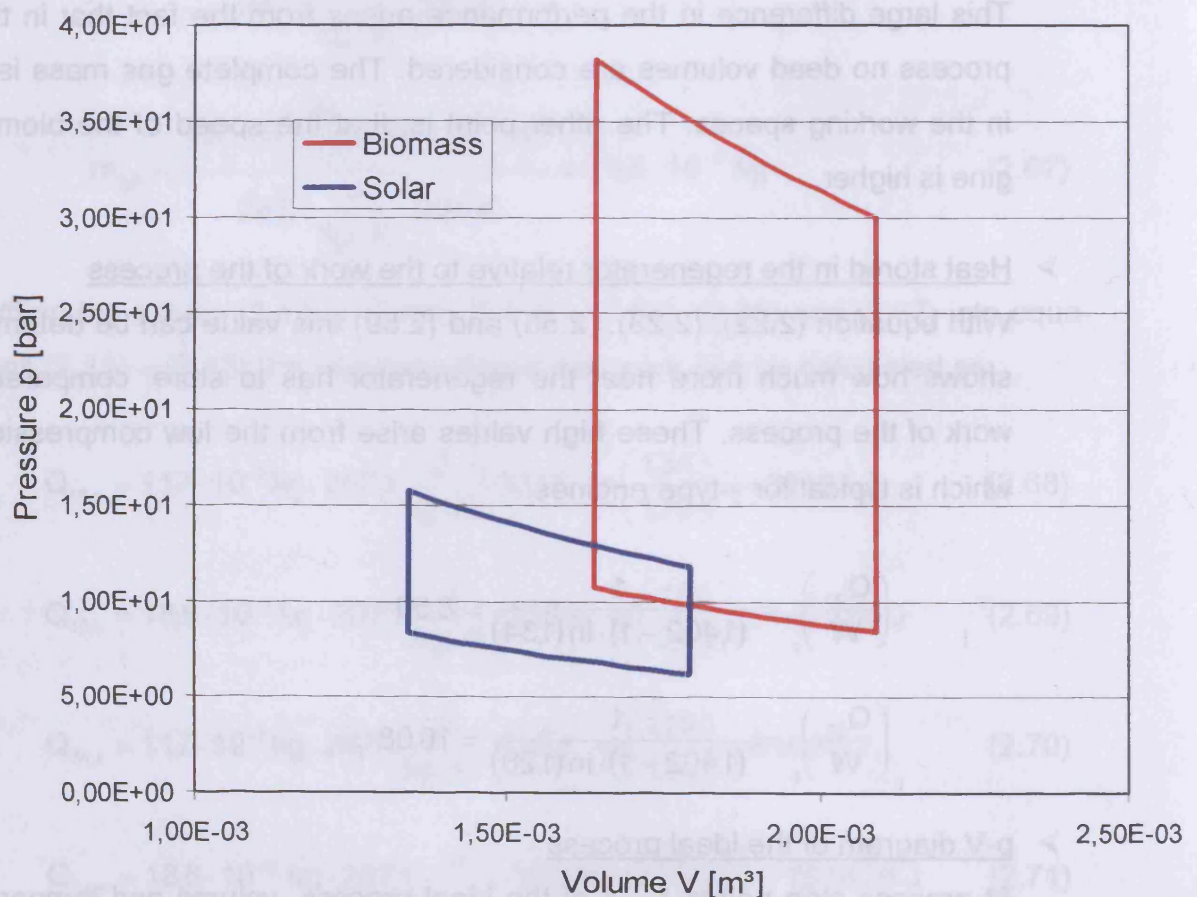
Figure 2-28: p-V diagram for the ideal process

58

	solar		biomass	
	V	p	V	p
	m³	bar	m³	bar
1	1,79E-03	6,21	2,09E-03	8,38
	1,75E-03	6,37	2,05E-03	8,56
	1,70E-03	6,54	2,00E-03	8,76
	1,66E-03	6,72	1,96E-03	8,96
	1,61E-03	6,91	1,91E-03	9,17
	1,57E-03	7,10	1,87E-03	9,39
	1,52E-03	7,31	1,82E-03	9,62
	1,48E-03	7,54	1,78E-03	9,87
	1,43E-03	7,78	1,73E-03	10,10
	1,39E-03	8,03	1,69E-03	10,40
2	1,34E-03	8,30	1,64E-03	10,70
	1,34E-03	9,04	1,64E-03	13,40
	1,34E-03	9,79	1,64E-03	16,20
	1,34E-03	10,50	1,64E-03	18,90
	1,34E-03	11,30	1,64E-03	21,70
	1,34E-03	12,00	1,64E-03	24,40
	1,34E-03	12,80	1,64E-03	27,20
	1,34E-03	13,50	1,64E-03	29,90
	1,34E-03	14,30	1,64E-03	32,70
	1,34E-03	15,00	1,64E-03	35,40
3	1,34E-03	15,70	1,64E-03	38,20
	1,39E-03	15,20	1,69E-03	37,20
	1,43E-03	14,80	1,73E-03	36,20
	1,48E-03	14,30	1,78E-03	35,30
	1,52E-03	13,90	1,82E-03	34,40
	1,57E-03	13,50	1,87E-03	33,60
	1,61E-03	13,10	1,91E-03	32,80
	1,66E-03	12,70	1,96E-03	32,00
	1,70E-03	12,40	2,00E-03	31,30
	1,75E-03	12,10	2,05E-03	30,60
4	1,79E-03	11,80	2,09E-03	30,00
	1,79E-03	11,20	2,09E-03	27,80
	1,79E-03	10,70	2,09E-03	25,70
	1,79E-03	10,10	2,09E-03	23,50
	1,79E-03	9,56	2,09E-03	21,30
	1,79E-03	9,00	2,09E-03	19,20
	1,79E-03	8,44	2,09E-03	17,00
	1,79E-03	7,88	2,09E-03	14,90
	1,79E-03	7,33	2,09E-03	12,70
	1,79E-03	6,77	2,09E-03	10,50
1	1,79E-03	6,21	2,09E-03	83,80

Table 2.6: Values for the p-V diagramm

This very high performance in equation (2.77) and (2.88) and high pressures (figure 2-28) can be explained by the assumption that the total mass of working gas is in the compression space at points 2 and 3 and in the expansion space at points 4 and 1. No dead volumes with lower temperatures are considered and the whole mass of gas

is heated up to expansion space temperature and cooled down to compression space temperature. In real machines only about 30 % of the gases are in the hot and cold space and so the ideal process does not give exact values.

2.8   0th order calculation
2.8.1   Definition

A 0th order calculation method is a very simple paper based method of analysis. It relates the power output and efficiency of a machine to the heater and cooler temperature, the engine displacement and the speed. There is no need to specify the engine in any more detail than this. Therefore, this method is good for preliminary system analysis. It is assumed that an experienced Stirling engine design and manufacture team executes the engine. 0th order methods are used to predict the efficiency as well as the power output much better than the ideal cycle method can. Because of its simplicity no extra main chapter is used to describe it. In the following different estimation methods for performance and efficiency are shown. The most important methods were invented by Carlquist, Beale and West in the 1950s and 1960s.

2.8.2   Efficiency Prediction by the method of Carlquist

This is not a very common way to predict the efficiency of a Stirling engine. It is documented in Martinis "Stirling engine design manual Vol. 2" [7] and states that the efficiency of a Stirling engine is related to the cycle efficiency of a Stirling engine which is the same as the Carnot efficiency, which of course is related to the heat source and heat sink temperatures specified.

Carlquist [6] gives the following formula for well optimized engines operating on hydrogen at their maximum efficiency points. The overall effective efficiency is:

$$\eta_{eff} = \left(1 - \frac{T_C}{T_E}\right) \cdot C \cdot \eta_H \cdot \eta_M \cdot f_A \qquad (2.82)$$

with

    C   Carnot efficiency ratio of indicated efficiency to Carnot efficiency, normally from 0,65 to 0,75.

η_H heater efficiency, ratio between the energy flow to the heater and the fuel energy flow, normally between 0,85 and 0,90.

η_M mechanical efficiency, ratio of indicated to brake power, normally between 0,85 and 0,90.

f_A auxiliary ratio; at maximum efficiency point 0,95

Taking an average value of these figures, equation (2.82) can be reduced to

$$\eta_{eff} = \left(1 - \frac{T_C}{T_E}\right) \cdot 0{,}512 \qquad (2.83)$$

2.8.3 Power estimation by the method of Beale

Some attempts have been made to relate the power actually realized in a Stirling engine to the power calculated from the dimensions and operating conditions of the engine using the applicable Schmidt equation (see chapter 3). Usually, the actual power realized has been quoted to be 30 – 40 % of the Schmidt power [6]. The recommended way of estimating the Stirling engine power output is to use the Beale number method as described by Walker [3]. To quote from Walker, "William Beale, of Sunpower, Inc. in Athens, Ohio, observed several years ago that the power output of many Stirling engines conformed approximately to the simple equation:" [3]

$$P = Be \cdot p_m \cdot f \cdot V_0 \qquad (2.84)$$

where

Be   Beale number

P   engine Power in W

p_m mean cycle pressure in bar

f   cycle frequency of engine speed in Hz

V_0 displacement of power piston in cm^3

This can be rearranged as

$$Be = \frac{P}{p_m \cdot f \cdot V_0} = const. \qquad (2.85)$$

61

The equation was found by Beale to apply approximately to all types and sizes of Stirling engines for which data were available including free piston machines and those with crank mechanisms. In most instances the engines operated with heater temperatures of 650° C and cooler temperatures of 65° C.

The result of equation (2.85) is a dimensionless group that may be called the Beale number. It is self evident that the Beale number is a function of both heater and cooler temperatures. Recent work suggests the relationship of Beale number to heater temperature may be of the form shown in figure 2-29 by the full line. Although for the sake of clarity the relationship is shown as a single line, it must of course be understood that the relationship is a gross approximation and particular examples of engines that depart widely may be cited. Nevertheless, a surprisingly large number of engines will be found to lie within the bounds of the confidence limits (broken lines) drawn on either side of the proposed relationship. Well designed, high efficiency units with low cooler temperatures will be concentrated near the upper bound. Less well designed units of moderate efficiency with high cooler temperatures will be located at the lower extremity [3].

It should be carefully noted that the abscissa of figure 2-29 is absolute temperature, degrees Kelvin; engines with the hot parts made of conventional stainless steels will be confined to operate at temperatures limited to the region indicated by the line A-A. High alloy steels for the hot parts will permit the elevation of heater temperature to the limit of B-B. Above this temperature ceramic components would likely be used in the heater assembly [7].

Figure 2-29 is the best information generated by Walker and his students based upon information available to them, both proprietary and non-proprietary.

2.8.4 Power estimation by the method of West

As shown in Schleder's work [8] another method exists to estimate the performance of a Stirling engine. In contrast to Beale's equation (2.84) the equation uses the process temperatures. The following equation was found by West in the 1980s by testing various types of engines

$$P = F \cdot n \cdot p_m \cdot V_0 \cdot \frac{T_E - T_C}{T_E + T_C} \qquad (2.86)$$
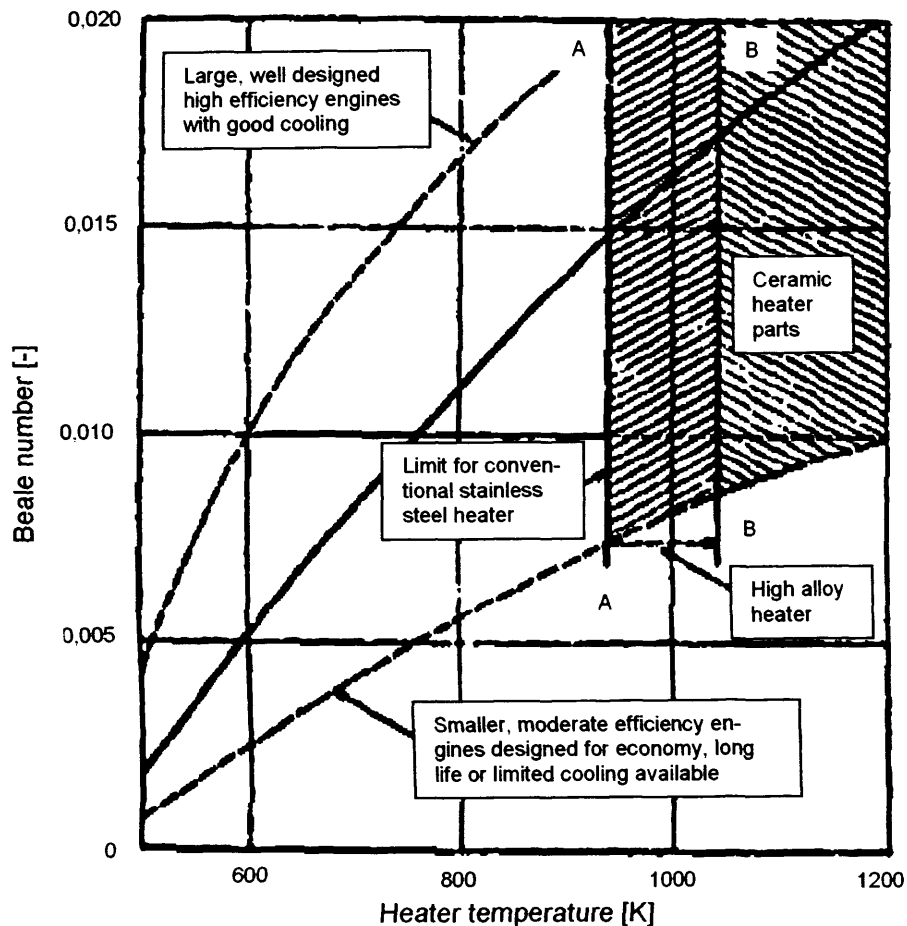
Figure 2-29: Beale number as a function of the heater temperature [7]

where

F = 0,35	West factor	(2.87)
n	speed of the engine in Hz	
p_m	mean cycle pressure in Pa	
V_0	displacement of power piston in m³	
T_E	expansion space temperature in K	
T_C	compression space temperature in K	

The equations of Beale and West cannot be used for designing a new machine and calculating the work and heat. They give an excellent overview of the performance and enable easy comparison of different technologies and machines to be made

2.8.5 Experimental engine analysis

➢ Efficiency by the method of Carlquist

The total efficiency of an experimental engines can by calculated with equation (2.83) and the approximate values from equations (2.40) – (2.43).

$$\eta_{eff,s} = \left(1 - \frac{331\,K}{628\,K}\right) \cdot 0{,}512 = 24{,}21\%$$ (2.88)

$$\eta_{eff,b} = \left(1 - \frac{328\,K}{1173\,K}\right) \cdot 0{,}512 = 36{,}88\%$$ (2.89)

➢ Performance by the method of Beale

Using figure 2-30 for the heater temperature of the experimental engines, the mean pressures from chapter 3 (equations (3.145) and (3.146)), the speed of the engine (equation (2.74) and (2.75)) and the swept volume of the compression space (equation (2.50)) the following values for the performance can be derived.

$$P_s = 0{,}0065 \cdot 8{,}962bar \cdot \frac{400}{60s} \cdot 4{,}51 \cdot 10^2 cm^3 = 175{,}15\,W$$ (2.90)

$$P_b = 0{,}019 \cdot 15{,}308bar \cdot \frac{700}{60s} \cdot 4{,}51 \cdot 10^2 cm^3 = 1'530{,}37\,W$$ (2.91)
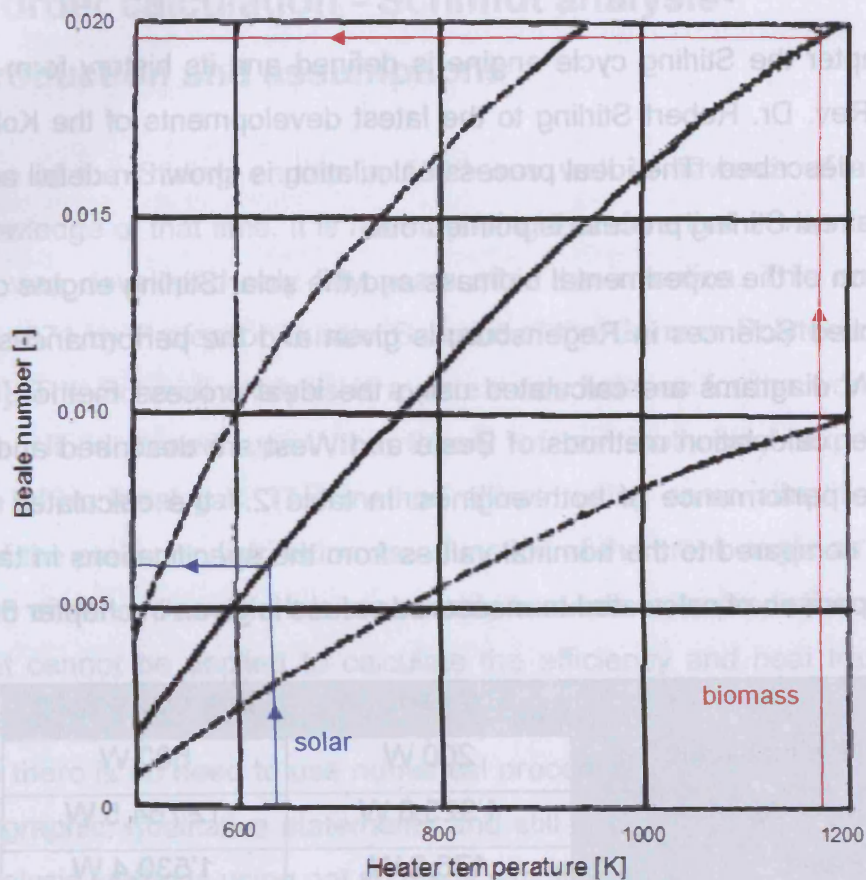
Figure 2-30: Beale diagram for the experimental engines

> Performance by the method of West

Using equation (2.86) in combination with the West factor (2.87), the speed of the engine ((2.74) and (2.75)) the mean pressure ((3.125) and (3.146)), the volume of the compression space (2.50) and the process temperatures ((2.40) – (2.43)) the performance can be estimated as

$$P_s = 0,35 \cdot \frac{400}{60s} \cdot 8,962 \cdot 10^5 \frac{N}{m^2} \cdot 4,51 \cdot 10^{-4} m^3 \cdot \frac{628 - 331}{628 + 331} K$$

(2.92)

$$= 292,08 \, W$$

$$P_b = 0,35 \cdot \frac{700}{60s} \cdot 15,308 \cdot 10^5 \frac{N}{m^2} \cdot 4,51 \cdot 10^{-4} m^3 \cdot \frac{1173 - 328}{1173 + 328} K$$

(2.93)

$$= 1'587,03 \, W$$

2.9   Summary

In this chapter the Stirling cycle engine is defined and its history form the first machines of Rev. Dr. Robert Stirling to the latest developments of the Koksums AB in Sweden is described. The ideal process calculation is shown in detail and the difference to the real Stirling process is pointed out.

A description of the experimental biomass and the solar Stirling engine of the University of Applied Sciences in Regensburg is given and the performances, efficiencies and the p-V diagrams are calculated using the ideal process method. Furthermore the 0th order calculation methods of Beale and West are described and used to determine the performance of both engines. In table 2.7 the calculated performance values are compared to the nominal values from the specifications in tables 2.2 and 2.3. A comparison of calculated to measured values is given in chapter 6.

	Solar engine	Biomass engine
Nominal value	200 W	600 W
Ideal process	1'925,8 W	12'764,5 W
Beale	175,2 W	1'530,4 W
West	292,1 W	1'587,0 W

Table 2.7: Comparison of calculated and nominal performance values

It can be stated that the calculated performances of the ideal process method are far away from the nominal values as the complete working gas in all the cells is assumed to have a common temperature. This results in an extremely high pressure level and process performance.

The results of the 0th order methods are closer to the nominal ones but there is the disadvantage that with these simple calculations no process parameters, like working gas temperatures and mass flows, can be defined and no parameter variation can be processed. Hence higher order calculation methods like the 1st order Schmidt analysis are needed to get more parameters with values that are closer to the real ones.

3 1st order calculation - Schmidt analysis

3.1 Introduction and assumptions

The invention of the Stirling engine in 1816 was well in advance of all pertinent scientific knowledge of that time. It is not surprising therefore that a scientific analysis of the cycle was developed only fifty years after the invention. This analysis was published in 1871 by Professor Gustav Schmidt of the German Polytechnic Institute in Prague [6]. The Schmidt analysis is a pure mass balance for the working gas of the machine. It is based upon the theory of an isothermal expansion and compression of an ideal gas. This method allows, using some simplifications, the calculation of the pressure distribution as a function of the crank angle as well as the determination of the cycle work. It is reasonably accurate in its prediction of the cycle power, but it cannot be applied to calculate the efficiency and heat transferred. A special advantage of this analysis is that the equation set can be solved in a closed form and so there is no need to use numerical procedures. Because of its clarity it is suitable for graphic, qualitative statements and still is widely spread, although there are other analysis methods using not so many simplifications.

The Schmidt analysis is based upon the following assumptions:

> ➢ The working gas is an ideal gas, so the equation of state can be used.
> ➢ The gas in each of the spaces is ideal homogeneous mixed throughout the cycle.
> ➢ There are three dead volumes taken into account:
>   One for the compression space a second one for the expansion space and a third one for the gas volume of the regenerator. This is an important advantage compared to the ideal process. The constant volume V_2 (volume after compression) doesn't have the same effect like a dead volume in the calculation, because in the ideal process, there is the assumption that the working gas in all the spaces at a given time interval has the same temperature. Thus for the Schmidt analysis the temperature of each gas space has a constant value for the complete cycle. The resulting reduction of the pressure level is, using the Schmidt analysis, taken into account.
> ➢ Compression and expansion processes are isothermal. This assumption of isothermal working spaces and heat exchangers implies that the heat exchangers (including the regenerator) are perfectly effective.

> ➢ The speed of the machine is constant and the motion is sinusoidal.
> ➢ The temperature profile of the regenerator is linear and constant. There are no losses and therefore the working gas leaves the regenerator with the temperature of the space it enters.
> ➢ There are no fluid losses and dissipation effects in the cycle which leads to one constant pressure over the whole machine.

At first the Schmidt analysis derived by C. M. Hargreaves is shown. The differences to the one of K. Hirata are on one hand in the way of defining the regenerator temperature and on the other that Hirata takes the fife spaces (expansion, compression, heater, cooler and regenerator space) all along the calculation, while Hargreaves sums up the dead volumes. [6]

3.2   Calculation model of a γ-type Stirling engine

Figure 3-1 shows the different volumes and simplified components of an γ-type Stirling engine used for the Schmidt analysis.
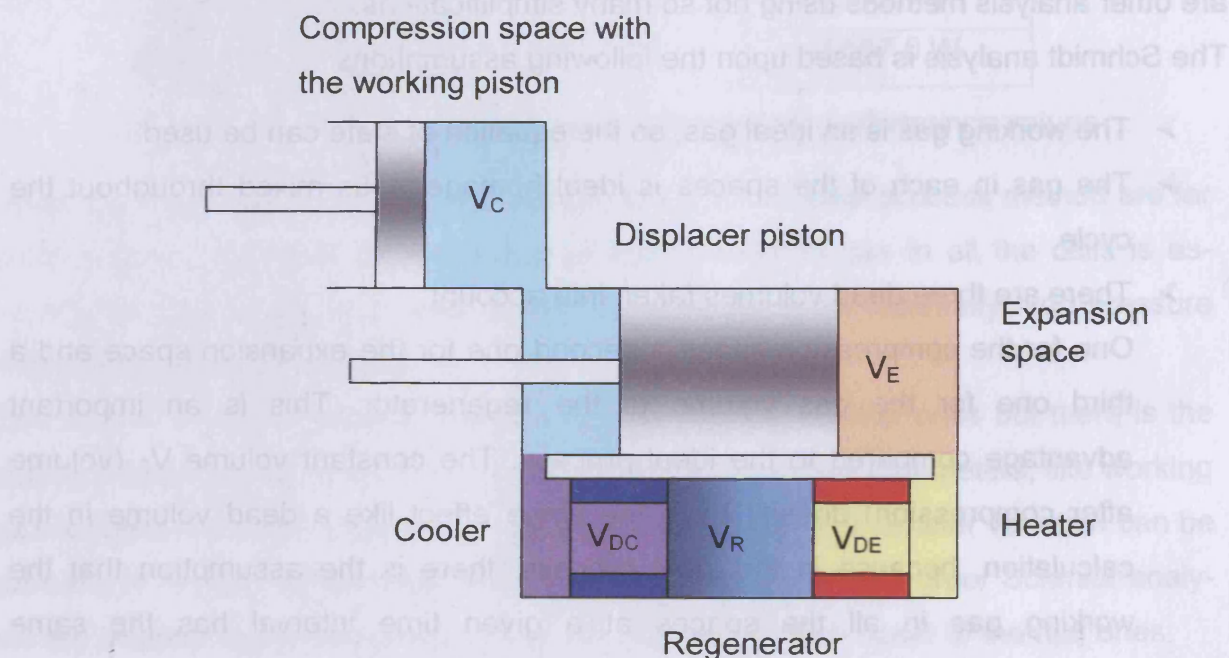
Figure 3-1: Model of a γ-type Stirling

3.3 Calculation by HARGREAVES

3.3.1 Equations for the volumes

For this type of machine the compression space is defined by the position of the working piston as well as by the position of the displacer. As shown in chapter 2, the expansion and compression volume can be calculated with the following equations:

$$V_E = \frac{V_{SE}}{2} \cdot [1 - \cos(\alpha)] \tag{3.1}$$

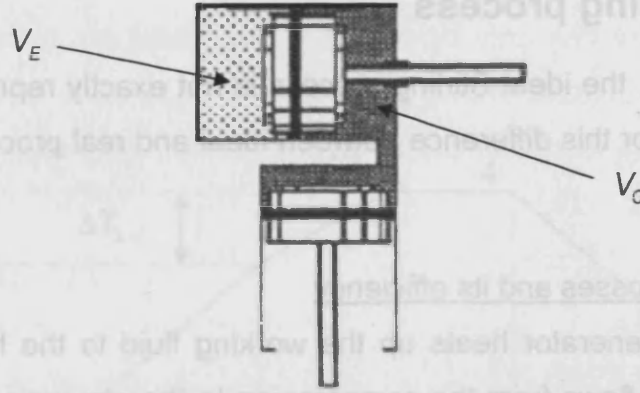$$V_C = \frac{V_{SE}}{2} \cdot [1 + \cos(\alpha)] + \frac{V_{SC}}{2} \cdot [1 - \cos(\alpha - \varphi)] \tag{3.2}$$

The crank angle α reaches the value of zero when the displacer is at the upper dead point. A positive value for the angle φ means that the working piston reaches his upper dead point after the displacer has reached it.

3.3.2 Effective dead volume temperature

To simplify further calculations Hargreaves sums up all the different dead volumes (expansion space dead volume, compression space dead volume und the regenerator dead volume – see figure 3-1). The effective temperature of this gas space can be described by balancing these spaces and using the equation of state:

$$m = \frac{p}{R} \cdot \left[\frac{V_{DE}}{T_E} + \frac{V_R}{T_R} + \frac{V_{DC}}{T_C} \right] = \frac{p}{R} \cdot \frac{V_D}{T_D} \tag{3.3}$$

$$\frac{V_{DE}}{T_E} + \frac{V_R}{T_R} + \frac{V_{DC}}{T_C} = \frac{V_D}{T_D} \tag{3.4}$$

$$V_D = V_{DE} + V_R + V_{DC} \tag{3.5}$$

$$T_D = \frac{V_{DE} + V_R + V_{DC}}{\dfrac{V_{DE}}{T_E} + \dfrac{V_R}{T_R} + \dfrac{V_{DC}}{T_C}} \tag{3.6}$$

3.3.3 Effective regenerator gas temperature

It is assumed that the regenerator theoretically has a linear temperature profile. Urieli analysed this and came to the solution that this temperature profile in real machines is linear. [9] Thus this assumption is a near to reality. A temperature must be found, which represents the regenerator as a large space of constant pressure. A mass balance for the regenerator gives this temperature. For the gas mass in the regenerator:

$$m_R = \int_0^{l_R} \rho \cdot dV_R = \int_0^{l_R} \frac{p}{R \cdot T} \cdot dV_R \tag{3.7}$$

As fluid losses are neglected the pressure of the regenerator is constant and the specific mass is only a function of temperature:

$$m_R = \frac{p}{R} \cdot \int_0^{l_R} \frac{1}{T} \cdot dV_R \tag{3.8}$$

The assumption of a linear temperature profile can be mathematically defined by the equation of a straight line shown in figure (3-2).

$$T(x) = \frac{(T_E - T_C)}{l_R} \cdot x + T_C \tag{3.9}$$

A combination of equation (3.8) and (3.9) gives:

$$m_R = \frac{p}{R} \cdot \int_0^{l_R} \frac{1}{\frac{(T_E - T_C)}{l_R} \cdot x + T_C} \cdot dV_R \tag{3.10}$$

The volume element dV_R can be displaced by $A_R \cdot dx$ (A_R is there the constant cross section of the regenerator):

$$m_R = \frac{p}{R} \cdot \int_0^{l_R} \frac{1}{\frac{(T_E - T_C)}{l_R} \cdot x + T_C} \cdot A_R \cdot dx \tag{3.11}$$

The area A_R can be written as:

$$A_R = \frac{V_R}{l_R} \tag{3.12}$$
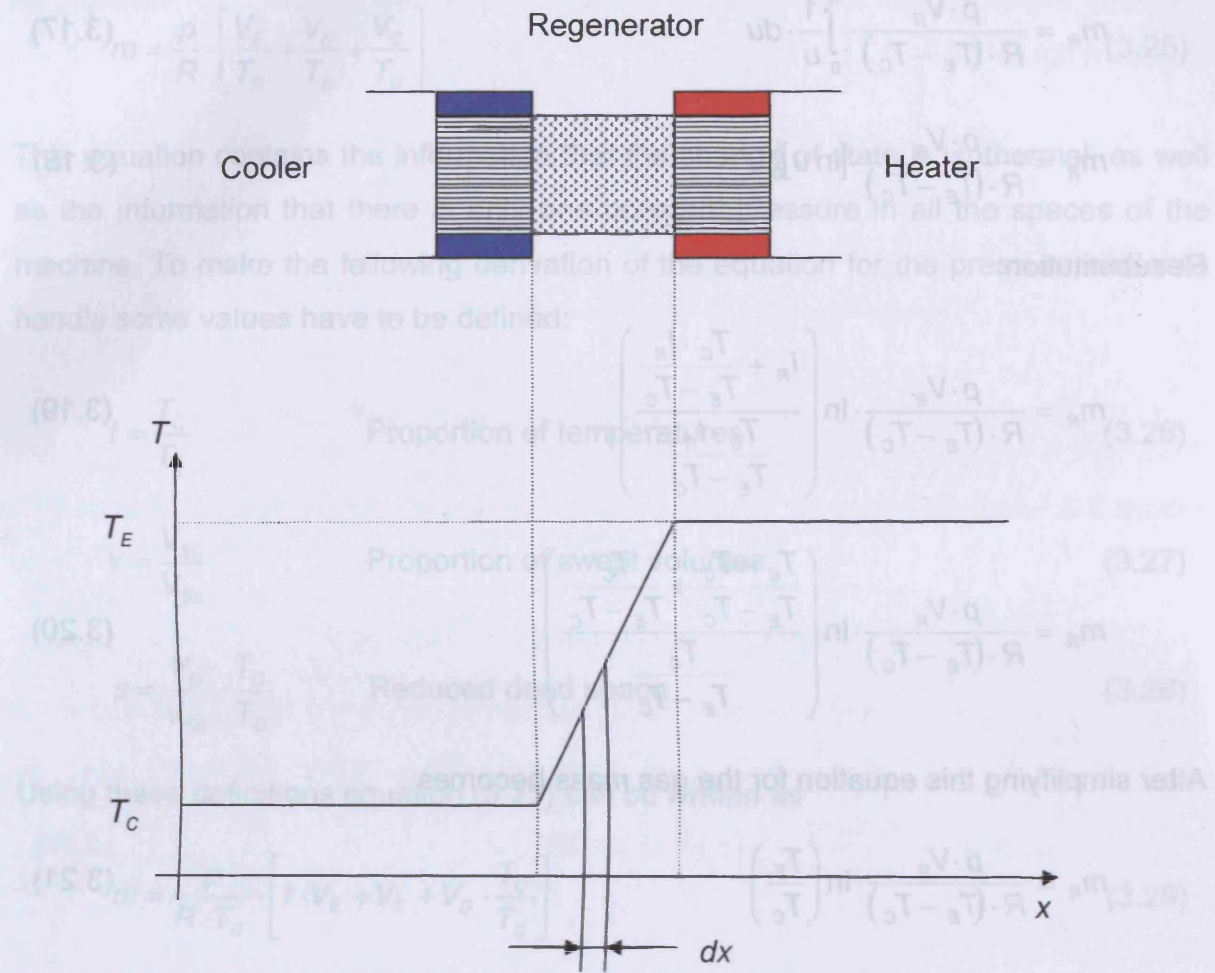
Figure 3-2: The regenerator temperature profile [6]

$$m_R = \frac{p \cdot V_R}{R} \cdot \int_0^{l_R} \frac{1}{(T_E - T_C) \cdot x + T_C \cdot l_R} \cdot dx \tag{3.13}$$

$$m_R = \frac{p \cdot V_R}{R \cdot (T_E - T_C)} \cdot \int_0^{l_R} \frac{1}{x + \frac{T_C \cdot l_R}{T_E - T_C}} \cdot dx \tag{3.14}$$

Substitution:

$$u = x + \frac{T_C \cdot l_R}{T_E - T_C} \tag{3.15}$$

$$\frac{du}{dx} = 1 \tag{3.16}$$

$$m_R = \frac{p \cdot V_R}{R \cdot (T_E - T_C)} \cdot \int_0^{I_R} \frac{1}{u} \cdot du \qquad (3.17)$$

$$m_R = \frac{p \cdot V_R}{R \cdot (T_E - T_C)} \cdot [\ln u]_0^{I_R} \qquad (3.18)$$

Resubstitution:

$$m_R = \frac{p \cdot V_R}{R \cdot (T_E - T_C)} \cdot \ln \left(\frac{I_R + \dfrac{T_C \cdot I_R}{T_E - T_C}}{\dfrac{T_C \cdot I_R}{T_E - T_C}} \right) \qquad (3.19)$$

$$m_R = \frac{p \cdot V_R}{R \cdot (T_E - T_C)} \cdot \ln \left(\frac{\dfrac{T_E - T_C}{T_E - T_C} + \dfrac{T_C}{T_E - T_C}}{\dfrac{T_C}{T_E - T_C}} \right) \qquad (3.20)$$

After simplifying this equation for the gas mass becomes:

$$m_R = \frac{p \cdot V_R}{R \cdot (T_E - T_C)} \cdot \ln \left(\frac{T_E}{T_C} \right) \qquad (3.21)$$

The substituted space with the same gas volume has the homogeneous effective Temperature T_R and so:

$$m_R = \frac{p \cdot V_R}{R \cdot T_R} = \frac{p \cdot V_R}{R \cdot (T_E - T_C)} \cdot \ln \left(\frac{T_E}{T_C} \right) \qquad (3.22)$$

$$T_R = \frac{T_E - T_C}{\ln \left(\dfrac{T_E}{T_C} \right)} \qquad (3.23)$$

With this temperature the Schmidt analysis can be developed.

3.3.4 Pressure as function of the crank angle

Using the equation of state the mass of the whole working gas in the machine is:

$$m = \sum m_i = m_E + m_D + m_C \qquad (3.24)$$

$$m = \frac{p}{R} \cdot \left[\frac{V_E}{T_E} + \frac{V_D}{T_D} + \frac{V_C}{T_C} \right] \qquad (3.25)$$

This equation contains the information that the change of state is isothermal, as well as the information that there is only one constant pressure in all the spaces of the machine. To make the following derivation of the equation for the pressure easier to handle some values have to be defined:

$$t = \frac{T_C}{T_E} \qquad \text{Proportion of temperatures} \qquad (3.26)$$

$$v = \frac{V_{SC}}{V_{SE}} \qquad \text{Proportion of swept volumes} \qquad (3.27)$$

$$s = \frac{V_D}{V_{SE}} \cdot \frac{T_C}{T_D} \qquad \text{Reduced dead space} \qquad (3.28)$$

Using these definitions equation (3.25) can be written as

$$m = \frac{p}{R \cdot T_C} \cdot \left[t \cdot V_E + V_C + V_D \cdot \frac{T_C}{T_D} \right] \qquad (3.29)$$

Here in the analysis the functions for the volumes (3.1) and (3.2) are introduced:

$$m = \frac{p \cdot V_{SE}}{R \cdot T_C} \cdot \left[\frac{t}{2} \cdot [1 - \cos(\alpha)] + \frac{1}{2} \cdot [1 + \cos(\alpha)] + \frac{v}{2} \cdot [1 - \cos(\alpha - \varphi)] + \frac{V_D}{V_{SE}} \cdot \frac{T_C}{T_D} \right] (3.30)$$

$$m = \frac{p \cdot V_{SE}}{2 \cdot R \cdot T_C} \cdot [t + 1 + v + 2 \cdot s + (1 - t) \cdot \cos(\alpha) - v \cdot \cos(\alpha - \varphi)] \qquad (3.31)$$

Substitution:

$$B = t + 1 + v + 2 \cdot s \qquad (3.32)$$

Thus:

$$m = \frac{p \cdot V_{SE}}{2 \cdot R \cdot T_C} [B - (t - 1) \cdot \cos(\alpha) - v \cdot \cos(\alpha - \varphi)] \qquad (3.33)$$

$$m = \frac{p \cdot V_{SE}}{2 \cdot R \cdot T_C} [B - \{(t - 1) \cdot \cos(\alpha) + v \cdot \cos(\alpha - \varphi)\}] \qquad (3.34)$$

The two trigonometric functions can be summed up by geometrical addition, as shown in figure 3-3:
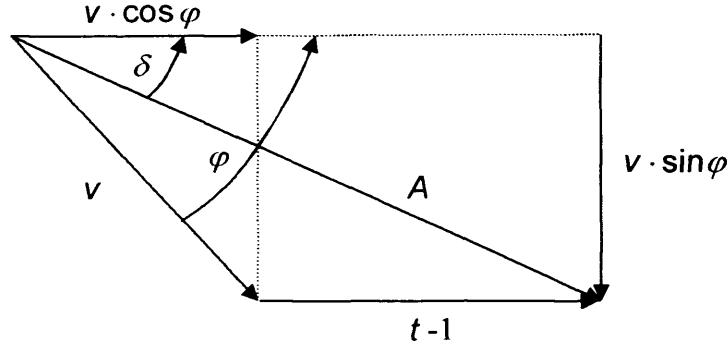
Figure 3-3: Vector diagram for the geometrical addition of trigonometric functions [11]

$$m = \frac{p \cdot V_{SE}}{2 \cdot R \cdot T_c} \cdot [B - A \cdot \cos(\alpha - \delta)] \qquad (3.35)$$

with

$$\delta = \arctan\left(\frac{v \cdot \sin\varphi}{t - 1 + v \cdot \cos\varphi}\right) \pm (0;\ \pi;\ 2\pi;\ 3\pi;\ ...) \qquad (3.36)$$

and

$$A = \sqrt{(t - 1 + v \cdot \cos\varphi)^2 + (v \cdot \sin\varphi)^2} \qquad (3.37)$$

$$A = \sqrt{t^2 - 2 \cdot t + 1 + 2 \cdot (t - 1) \cdot v \cdot \cos\varphi + v^2} \qquad (3.38)$$

At this point the π periodicity (180° periodicity) of the tangent function plays a role (see figure 3-4). The inverse function, the inverse tangent, does not give an unequivocal result. For values between $-\frac{\pi}{2} < \delta < \frac{\pi}{2}$ ($-90° < \delta < 90°$) a calculator gives correct results for the inverse tangent function. For the relevant values between $0 < \delta < \pi$ ($0° < \delta < 180°$) eventually the result has to be summed up with π (180°) to get the right sign.
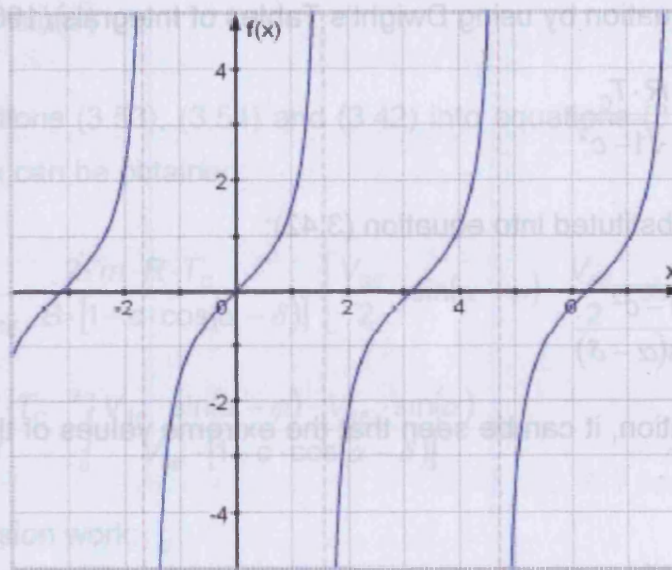
Figure 3-4: Periodicity of the tangent [75]

As a criterion, if this correction is needed or not, the sign of the term $t + v \cdot \cos\varphi$ can be used. When it is negative, the sign has to be turned to plus.

$$m = \frac{p \cdot V_{SE}}{2 \cdot R \cdot T_C} \cdot [B - A \cdot \cos(\alpha - \delta)] \qquad (3.39)$$

$$p = \frac{2 \cdot m \cdot R \cdot T_C}{V_{SE} \cdot [B - A \cdot \cos(\alpha - \delta)]} \qquad (3.40)$$

If c is considered as:

$$c = \frac{A}{B} \qquad (3.41)$$

the pressure can be calculated with this equation

$$p = \frac{2 \cdot m \cdot R \cdot T_C}{V_{SE} \cdot B \cdot [1 - c \cdot \cos(\alpha - \delta)]} \qquad (3.42)$$

Integrating the pressure as a function of the crank angle, the average pressure can be calculated with the equation:

$$p_m = \frac{1}{2 \cdot \pi} \int_0^{2\pi} p \cdot d\alpha \qquad (3.43)$$

$$p_m = \frac{1}{2 \cdot \pi} \int_0^{2\pi} \frac{2 \cdot m \cdot R \cdot T_C}{V_{SE} \cdot B \cdot [1 - c \cdot \cos(\alpha - \delta)]} \cdot d\alpha \qquad (3.44)$$

Urieli solved this equation by using Dwight's Tables of Integrals (1964) [9]:

$$p_m = \frac{2 \cdot m \cdot R \cdot T_C}{V_{SE} \cdot B \cdot \sqrt{1-c^2}}$$ (3.45)

This result is the substituted into equation (3.42):

$$p = \frac{p_m \cdot \sqrt{1-c^2}}{1-c \cdot \cos(\alpha - \delta)}$$ (3.46)

Analysing this equation, it can be seen that the extreme values of the pressure result for:

$$\cos(\alpha - \delta) = \pm 1$$ (3.47)

and have the values:

$$p_{max} = p_m \cdot \frac{\sqrt{1-c^2}}{1-c} = p_m \cdot \frac{\sqrt{(1+c) \cdot (1-c)}}{1-c} = p_m \cdot \frac{\sqrt{1+c}}{\sqrt{1-c}}$$ (3.48)

$$p_{min} = p_m \cdot \frac{\sqrt{1-c^2}}{1+c} = p_m \cdot \frac{\sqrt{(1+c) \cdot (1-c)}}{1+c} = p_m \cdot \frac{\sqrt{1-c}}{\sqrt{1+c}}$$ (3.49)

3.3.5 Work and performance

Work is done by the engine by virtue of the varying volumes of the working spaces V_C and V_E. The total work done by the engine is therefore the algebraic sum of the work of the compression and expansion spaces. Over the complete cycle the work is:

$$W_C = \int p \cdot dV_C = \int_0^{2 \cdot \pi} p \cdot \frac{dV_C}{d\alpha} \cdot d\alpha$$ (3.50)

$$W_E = \int p \cdot dV_E = \int_0^{2 \cdot \pi} p \cdot \frac{dV_E}{d\alpha} \cdot d\alpha$$ (3.51)

$$W = W_C + W_E$$ (3.52)

Differentiating equations (3.1) and (3.2), the volume derivatives are:

$$\frac{dV_C}{d\alpha} = -\frac{V_{SE}}{2} \cdot \sin(\alpha) + \frac{V_{SC}}{2} \cdot \sin(\alpha - \varphi)$$ (3.53)

$$\frac{dV_E}{d\alpha} = \frac{V_{SE}}{2} \cdot \sin(\alpha) \tag{3.54}$$

Substituting equations (3.53), (3.54) and (3.42) into equations (3.50) and (3.51), the compression work can be obtained:

$$W_C = \int_0^{2 \cdot \pi} \left[\frac{2 \cdot m \cdot R \cdot T_C}{V_{SE} \cdot B \cdot [1 - c \cdot \cos(\alpha - \delta)]} \cdot \left[\frac{V_{SC}}{2} \cdot \sin(\alpha - \varphi) - \frac{V_{SE}}{2} \cdot \sin(\alpha) \right] \right] d\alpha \tag{3.55}$$

$$W_C = \frac{m \cdot R \cdot T_C}{B} \cdot \int_0^{2 \cdot \pi} \frac{V_{SC} \cdot \sin(\alpha - \varphi) - V_{SE} \cdot \sin(\alpha)}{V_{SE} \cdot [1 - c \cdot \cos(\alpha - \delta)]} d\alpha \tag{3.56}$$

and for the expansion work:

$$W_E = \int_0^{2 \cdot \pi} \left[\frac{2 \cdot m \cdot R \cdot T_C}{V_{SE} \cdot B \cdot [1 - c \cdot \cos(\alpha - \delta)]} \cdot \frac{V_{SE}}{2} \cdot \sin(\alpha) \right] d\alpha \tag{3.57}$$

$$W_E = \frac{m \cdot R \cdot T_C}{B} \cdot \int_0^{2 \cdot \pi} \frac{\sin(\alpha)}{1 - c \cdot \cos(\alpha - \delta)} d\alpha \tag{3.58}$$

Equations (3.55) and (3.57) cannot be solved in a closed form, because of the complexity of the piston movement in γ-type machines. They can only be solved with numerical methods. The performance can be determined combining equation (2.76) with the speed of the engine and the work done in the process (equation (3.52)).

3.3.6 Mass flow through the machine

The layout of heater and cooler requires the knowledge of the volume or mass flow through the machine, which is carried out using the Schmidt analysis. In the literature this calculation is rarely shown only for the α-type engine and not published for the γ-type. Using the equation of state and the function of the pressure (equation (3.46)) the mass of a particular space can be derived. The gas mass in the expansion space is:

$$m_E = \frac{p \cdot V_E}{R \cdot T_E} \tag{3.59}$$

The volume for the expansion space is calculated with equation (3.1). Combining equations (3.1), (3.46) and (3.59):

$$m_E = \frac{p_m \cdot \sqrt{1-c^2}}{R \cdot T_E \cdot [1-c \cdot \cos(\alpha - \delta)]} \cdot \frac{V_{SE}}{2} \cdot [1-\cos(\alpha)] \qquad (3.60)$$

$$m_E = \frac{p_m \cdot V_{SE} \cdot \sqrt{1-c^2}}{2 \cdot R \cdot T_E} \cdot \frac{1-\cos(\alpha)}{1-c \cdot \cos(\alpha - \delta)} \qquad (3.61)$$

Differentiating this equation results in the mass flow into the expansion space

$$\frac{dm_E}{d\alpha} = \frac{d}{d\alpha} \left(\frac{p_m \cdot V_{SE} \cdot \sqrt{1-c^2}}{2 \cdot R \cdot T_E} \cdot \frac{1-\cos(\alpha)}{1-c \cdot \cos(\alpha - \delta)} \right) \qquad (3.62)$$

A positive sign means that gas flows into the expansion space. Solving this equation:

$$\frac{dm_E}{d\alpha} = \frac{p_m \cdot V_{SE} \cdot \sqrt{1-c^2}}{2 \cdot R \cdot T_E} \cdot \ldots$$
$$\ldots \cdot \frac{\sin(\alpha) \cdot [1-c \cdot \cos(\alpha - \delta)] - [1-\cos(\alpha)] \cdot c \cdot \sin(\alpha - \delta)}{[1-c \cdot \cos(\alpha - \delta)]^2} \qquad (3.63)$$

$$\frac{dm_E}{d\alpha} = \frac{p_m \cdot V_{SE} \cdot \sqrt{1-c^2}}{2 \cdot R \cdot T_E} \cdot \ldots$$
$$\ldots \cdot \frac{\sin(\alpha) - c \cdot [\sin(\alpha) \cdot \cos(\alpha - \delta) + \sin(\alpha - \delta) - \cos(\alpha) \cdot \sin(\alpha - \delta)]}{[1-c \cdot \cos(\alpha - \delta)]^2} \qquad (3.64)$$

Using the trigonometric theorem

$$\sin(u-v) = \sin(u) \cdot \cos(v) - \cos(u) \cdot \sin(v) \qquad (3.65)$$

equation (3.64) can be simplified to:

$$\frac{dm_E}{d\alpha} = \frac{p_m \cdot V_{SE} \cdot \sqrt{1-c^2}}{2 \cdot R \cdot T_E} \cdot \frac{\sin(\alpha) - c \cdot [\sin(\delta) + \sin(\alpha - \delta)]}{[1-c \cdot \cos(\alpha - \delta)]^2} \qquad (3.66)$$

These transformations can be made in the same way for the compression space and for the dead volume. The corresponding equations for the compression space are as follows:

$$m_C = \frac{p_m \cdot \sqrt{1-c^2}}{R \cdot T_C \cdot [1-c \cdot \cos(\alpha - \delta)]} \cdot \left[\frac{V_{SE}}{2} \cdot [1+\cos(\alpha)] + \frac{V_{SC}}{2} \cdot [1-\cos(\alpha - \varphi)] \right] \qquad (3.67)$$

$$m_C = \frac{p_m \cdot V_{SE} \cdot \sqrt{1-c^2}}{2 \cdot R \cdot T_C} \cdot \left[\frac{1+\cos(\alpha)+v-v\cdot\cos(\alpha-\varphi)}{1-c\cdot\cos(\alpha-\delta)}\right] \tag{3.68}$$

Differentiating this equation results in the mass flow into the compression space:

$$\frac{dm_C}{d\alpha} = \frac{d}{d\alpha}\left\{\frac{p_m \cdot V_{SE} \cdot \sqrt{1-c^2}}{2 \cdot R \cdot T_C} \cdot \left[\frac{1+\cos(\alpha)+v-v\cdot\cos(\alpha-\varphi)}{1-c\cdot\cos(\alpha-\delta)}\right]\right\} \tag{3.69}$$

Solving this equation:

$$\frac{dm_C}{d\alpha} = \frac{p_m \cdot V_{SE} \cdot \sqrt{1-c^2}}{2 \cdot R \cdot T_C} \cdot \cdots$$

$$\cdots \cdot \left[\frac{[-\sin(\alpha)+v\cdot\sin(\alpha-\varphi)]\cdot[1-c\cdot\cos(\alpha-\delta)]}{[1-c\cdot\cos(\alpha-\delta)]^2} - \cdots \right. $$
$$\left. \cdots - \frac{[1+\cos(\alpha)+v-v\cdot\cos(\alpha-\varphi)]\cdot c\cdot\sin(\alpha-\delta)}{[1-c\cdot\cos(\alpha-\delta)]^2}\right] \tag{3.70}$$

$$\frac{dm_C}{d\alpha} = \frac{p_m \cdot V_{SE} \cdot \sqrt{1-c^2}}{2 \cdot R \cdot T_C} \cdot \cdots \tag{3.71}$$

$$\cdots \cdot \left[\frac{-\sin(\alpha)+c\cdot\sin(\alpha)\cdot\cos\cdot(\alpha-\delta)+v\cdot\sin(\alpha-\varphi)-c\cdot v\cdot\sin(\alpha-\varphi)\cdot\cos(\alpha-\delta)}{[1-c\cdot\cos(\alpha-\delta)]^2} - \cdots \right.$$
$$\left. \cdots - \frac{c\cdot\sin(\alpha-\delta)+c\cdot\cos(\alpha)\cdot\sin(\alpha-\delta)+c\cdot v\cdot\sin(\alpha-\delta)-c\cdot v\cdot\cos(\alpha-\varphi)\cdot\sin(\alpha-\delta)}{[1-c\cdot\cos(\alpha-\delta)]}\right]$$

Using the trigonometric theorem (3.65) equation (3.71) can be simplified to:

$$\frac{dm_C}{d\alpha} = \frac{p_m \cdot V_{SE} \cdot \sqrt{1-c^2}}{2 \cdot R \cdot T_C} \cdot \cdots \tag{3.72}$$

$$\cdots \cdot \left[\frac{-\sin(\alpha)+c\cdot\sin(\delta)+v\cdot\sin(\alpha-\varphi)-c\cdot v\cdot\sin(\delta-\varphi)-c\cdot\sin(\alpha-\delta)-c\cdot v\cdot\sin(\alpha-\delta)}{[1-c\cdot\cos(\alpha-\delta)]^2}\right]$$

The dead volume can be considered as:

$$m_D = \frac{p_m \cdot V_{SE} \cdot X_D \cdot \sqrt{1-c^2}}{R \cdot T_D} \cdot \frac{1}{1-c\cdot\cos(\alpha-\delta)} \tag{3.73}$$

with

$$X_D = \frac{V_D}{V_{SE}} \tag{3.74}$$

$$\frac{dm_D}{d\alpha} = \frac{d}{d\alpha}\left[\frac{p_m \cdot V_{SE} \cdot X_D \cdot \sqrt{1-c^2}}{R \cdot T_D} \cdot \frac{1}{1-c \cdot \cos(\alpha-\delta)}\right] \tag{3.75}$$

Solving this equation:

$$\frac{dm_D}{d\alpha} = \frac{p_m \cdot V_{SE} \cdot X_D \cdot \sqrt{1-c^2}}{R \cdot T_D} \cdot \frac{c \cdot \sin(\alpha-\delta)}{[1-c \cdot \cos(\alpha-\delta)]^2} \tag{3.76}$$

With these equations the change of the masses in the different spaces is defined. These values do not show inevitably the mass flow through any cross-section of the machine.
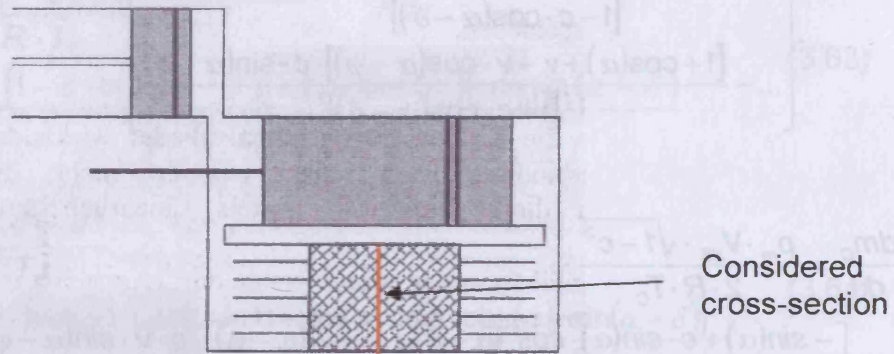
Figure 3-5: Mass flow in the γ-type machine [8]

The mass flow is thus defined for the considered cross-section right in the middle of the regenerator. For example 1 kg gas flows out of the compression space, the mass in the dead volume rises by 0,3 kg, so that 0,7 kg reaches the expansion space. The mass in the dead volume distributes steadily, so that 0,85 kg flow through the considered cross-section. Relocation of this cross-section to the border between the regenerator and the expansion space results in only 0,7 kg mass passing through. On the border of the regenerator and compression space it would be 1kg.

It is thus noticeable that the determination of the mass flow depends on the location of the cross section. Considering the middle of the regenerator as the cross-section, the mass flow is defined by:

$$\dot{m}_{MR} = -\dot{m}_C - \frac{\dot{m}_D}{2} \tag{3.77}$$

$$\dot{m}_{MR} = \dot{m}_E + \frac{\dot{m}_D}{2} \tag{3.78}$$

The flow through this cross-section is defined to be positive for the direction from the compression space to the expansion space.

3.4 Calculation by HIRATA

As it is mentioned in chapter 3 there are two main differences between the calculation methods of Hirata and Hargreaves. One is that Hirata uses for the regenerator temperature the average of the expansion gas temperature T_E and the compression gas temperature T_C. The other one is that Hirata uses five explicit volumes for his whole calculation, while Hargreaves sums up the dead volumes.

3.4.1 Compression and expansion space volume

In Hirata's method the equations of the compression and expansion space volumes (3.1) and (3.2) have the additional terms of the dead volumes.

$$V_E = \frac{V_{SE}}{2} \cdot [1 - \cos(\alpha)] + V_{DE} \tag{3.79}$$

$$V_C = \frac{V_{SE}}{2} \cdot [1 + \cos(\alpha)] + \frac{V_{SC}}{2} \cdot [1 - \cos(\alpha - \varphi)] + V_{DC} \tag{3.80}$$

The crank angle α reaches the value of zero when the displacer is at the upper dead point. A positive value for the angle φ means that the working piston reaches his upper dead point after the displacer has reached it.

3.4.2 Pressure as function of the crank angle

Using the equation of state (3.59) the mass of the whole working gas of the machine is:

$$m = \sum m_i = m_E + m_R + m_C \tag{3.81}$$

$$m = \frac{p}{R} \cdot \left[\frac{V_E}{T_E} + \frac{V_R}{T_R} + \frac{V_C}{T_C} \right] \tag{3.82}$$

To perform the following derivation of the equation for the pressure some parameters have to be defined:

$$t = \frac{T_C}{T_E}$$ Temperature ratio   (3.83)

$$v = \frac{V_{SC}}{V_{SE}}$$ Swept volume ratio   (3.84)

$$X_{DE} = \frac{V_{DE}}{V_{SE}}$$ Expansion space dead volume ratio   (3.85)

$$X_{DC} = \frac{V_{DC}}{V_{SE}}$$ Compression space dead volume ratio   (3.86)

$$X_R = \frac{V_R}{V_{SE}}$$ Regenerator volume ratio   (3.87)

The regenerator temperature is calculated by using the average value of the expansion gas temperature and the compression gas temperature:

$$T_R = \frac{T_E + T_C}{2}$$ Regenerator temperature   (3.88)

Replacing the volume functions (3.79) and (3.80) in (3.82):

$$m = \frac{p}{R} \cdot \begin{bmatrix} \left(\frac{V_{SE}}{T_E \cdot 2} - \frac{V_{SE}}{T_E \cdot 2} \cdot \cos(\alpha) + \frac{V_{DE}}{T_E} \right) + \frac{2 \cdot V_R}{T_E + T_C} + \dots \\ \dots + \left(\frac{V_{SE}}{T_C \cdot 2} + \frac{V_{SE}}{T_C \cdot 2} \cdot \cos(\alpha) + \frac{V_{SC}}{T_C \cdot 2} - \frac{V_{SC}}{T_C \cdot 2} \cdot \cos(\alpha - \varphi) + \frac{V_{DC}}{T_C} \right) \end{bmatrix} \quad (3.89)$$

$$m = \frac{p \cdot V_{SE}}{2 \cdot R \cdot T_C} \cdot \begin{bmatrix} t + 2 \cdot X_{DE} \cdot t + \frac{4 \cdot t \cdot X_R}{1+t} + 1 + v + 2 \cdot X_{DC} + \dots \\ \dots + (1-t) \cdot \cos(\alpha) - v \cdot \cos(\alpha - \varphi) \end{bmatrix} \quad (3.90)$$

Using the substitution:

$$B = t + 2 \cdot X_{DE} \cdot t + \frac{4 \cdot t \cdot X_R}{1+t} + 1 + v + 2 \cdot X_{DC} \quad (3.91)$$

in equation (3.90):

$$m = \frac{p \cdot V_{SE}}{2 \cdot R \cdot T_C} \cdot [B - (t-1) \cdot \cos \alpha - v \cdot \cos(\alpha - \varphi)] \quad (3.92)$$

$$m = \frac{p \cdot V_{SE}}{2 \cdot R \cdot T_c} \cdot [B - \{(t-1) \cdot \cos\alpha + v \cdot \cos(\alpha - \varphi)\}] \tag{3.93}$$

Now Hirata's equation has reached the same form as the one from Hargreaves and so no further calculations are shown. Only the results and the definition of the constant values are repeated to make this chapter complete (for the derivation see chapter 3.2.4).

$$\delta = \arctan\left(\frac{v \cdot \sin\varphi}{t - 1 + v \cdot \cos\varphi}\right) \pm (0; \pi; 2\pi; 3\pi; ...) \tag{3.94}$$

$$A = \sqrt{t^2 - 2 \cdot t + 1 + 2 \cdot (t-1) \cdot v \cdot \cos\varphi + v^2} \tag{3.95}$$

$$p = \frac{2 \cdot m \cdot R \cdot T_c}{V_{SE} \cdot [B - A \cdot \cos(\alpha - \delta)]} \tag{3.96}$$

$$c = \frac{A}{B} \tag{3.97}$$

$$p = \frac{2 \cdot m \cdot R \cdot T_c}{V_{SE} \cdot B \cdot [1 - c \cdot \cos(\alpha - \delta)]} \tag{3.98}$$

$$p_m = \frac{2 \cdot m \cdot R \cdot T_c}{V_{SE} \cdot B \cdot \sqrt{1 - c^2}} \tag{3.99}$$

$$p = \frac{p_m \cdot \sqrt{1 - c^2}}{1 - c \cdot \cos(\alpha - \delta)} \tag{3.100}$$

$$p_{max} = p_m \cdot \frac{\sqrt{1 - c^2}}{1 - c} = p_m \cdot \frac{\sqrt{(1+c) \cdot (1-c)}}{1 - c} = p_m \cdot \frac{\sqrt{1+c}}{\sqrt{1-c}} \tag{3.101}$$

$$p_{min} = p_m \cdot \frac{\sqrt{1 - c^2}}{1 + c} = p_m \cdot \frac{\sqrt{(1+c) \cdot (1-c)}}{1 + c} = p_m \cdot \frac{\sqrt{1-c}}{\sqrt{1+c}} \tag{3.102}$$

The equations for the pressures are the same as in Hargreaves. However some of the constants used are different. Thus the values of the pressure may differ. A comparison of these two methods with values for a real engine is shown in the following section 3.4.

3.5   Values for the experimental engines

3.5.1   The Hargreaves method

> Effective regenerator gas temperature

With equation (3.23) and the values (2.40) to (2.43) the effective regenerator gas temperature can be calculated for the biomass and the solar engine:

$$T_{R,s} = \frac{628K - 331K}{\ln\left(\dfrac{628K}{331K}\right)} = 463,76K \tag{3.103}$$

$$T_{R,b} = \frac{1173K - 328K}{\ln\left(\dfrac{1173K}{328K}\right)} = 663,11K \tag{3.104}$$

> Effective dead volume temperature

Using equation (3.6) and the values (2.51) to (2.54), (2.40) to (2.43) and (3.103) and (3.104) this value can be determined.

$$T_{D,s} = \frac{2,50 \cdot 10^{-4} m^3 + 1,50 \cdot 10^{-4} m^3 + 3,79 \cdot 10^{-4} m^3}{\dfrac{2,50 \cdot 10^{-4} m^3}{628K} + \dfrac{1,50 \cdot 10^{-4} m^3}{463,76K} + \dfrac{3,79 \cdot 10^{-4} m^3}{331K}} = 417,35K \tag{3.105}$$

$$T_{D,b} = \frac{5,44 \cdot 10^{-4} m^3 + 1,50 \cdot 10^{-4} m^3 + 3,79 \cdot 10^{-4} m^3}{\dfrac{5,44 \cdot 10^{-4} m^3}{1173K} + \dfrac{1,50 \cdot 10^{-4} m^3}{663,11K} + \dfrac{3,79 \cdot 10^{-4} m^3}{328K}} = 581,43K \tag{3.106}$$

> Pressure as a function of the crank angle

For the calculation of the pressure, the substitution variables have to be analysed. For the temperature ratio the values (2.40) to (2.43) are put into equation (3.26):

$$t_s = \frac{331K}{628K} = 0,527 \tag{3.107}$$

$$t_b = \frac{328K}{1173K} = 0,280 \tag{3.108}$$

For the swept volume ratios (equation 3.27) values (2.49) and (2.50) are used.

$$V = \frac{4,51 \cdot 10^{-4} m^3}{5,65 \cdot 10^{-4} m^3} = 0,798 \qquad (3.109)$$

The reduced dead space (equation 3.28) can be defined with the values (2.40), (2.42), (2.49), (2.55), (2.56), (3.105) and (3.106).

$$S_s = \frac{7,80 \cdot 10^{-4} m^3 \cdot 331K}{5,65 \cdot 10^{-4} m^3 \cdot 417,35K} = 1,095 \qquad (3.110)$$

$$S_b = \frac{10,73 \cdot 10^{-4} m^3 \cdot 328K}{5,65 \cdot 10^{-4} m^3 \cdot 581,43K} = 1,071 \qquad (3.111)$$

The substitution variable B (equation 3.32) is used together of the values (3.107) to (3.111).

$$B_s = 0,527 + 1 + 0,798 + 2 \cdot 1,095 = 4,515 \qquad (3.112)$$

$$B_b = 0,280 + 1 + 0,798 + 2 \cdot 1,071 = 4,220 \qquad (3.113)$$

Combining the values (3.107) to (3.111) and (2.57) with equation (3.38) the substitution variable A can be determined.

$$A_s = \sqrt{0,527^2 - 2 \cdot 0,527 + 1 + 2 \cdot (0,527 - 1) \cdot 0,798 \cdot \cos\left(\frac{\pi}{2}\right) + 0,798^2} =$$
$$= 0,928 \qquad (3.114)$$

$$A_b = \sqrt{0,280^2 - 2 \cdot 0,280 + 1 + 2 \cdot (0,280 - 1) \cdot 0,798 \cdot \cos\left(\frac{\pi}{2}\right) + 0,798^2} =$$
$$= 1,075 \qquad (3.115)$$

Equation (3.41) can be solved:

$$c_s = \frac{0,928}{4,515} = 0,205 \qquad (3.116)$$

$$c_b = \frac{1,075}{4,220} = 0,255 \qquad (3.117)$$

The substituted angle δ is defined with equation (3.36). Using values (2.57) and (3.107) to (3.109):

$$\delta_s = \arctan\left(\frac{0{,}798 \cdot \sin\left(\frac{\pi}{2}\right)}{0{,}527 - 1 + 0{,}798 \cdot \cos\left(\frac{\pi}{2}\right)}\right) = -1{,}036 \tag{3.118}$$

$$\delta_b = \arctan\left(\frac{0{,}798 \cdot \sin\left(\frac{\pi}{2}\right)}{0{,}280 - 1 + 0{,}798 \cdot \cos\left(\frac{\pi}{2}\right)}\right) = -0{,}837 \tag{3.119}$$

The value of δ is not in the relevant area (0°< δ<180°) and has to be summed up with π.

$$\delta_s = 2{,}106 \tag{3.120}$$

$$\delta_b = 2{,}305 \tag{3.121}$$

The average value of the pressure p_m can be calculated with equation (3.35) using the values (2.66), (2.67), (2.64), (2.40), (2.42), (2.49), (3.112), (3.113), (3.116) and (3.117).

$$p_{m,s} = \frac{2 \cdot 11{,}7 \cdot 10^{-3}\,m^3 \cdot 287{,}1\frac{J}{kg \cdot K} \cdot 331K}{5{,}65 \cdot 10^{-4}\,m^3 \cdot 4{,}515 \cdot \sqrt{1 - (0{,}205)^2}} = 8{,}929bar \tag{3.122}$$

$$p_{m,b} = \frac{2 \cdot 18{,}6 \cdot 10^{-3}\,m^3 \cdot 287{,}1\frac{J}{kg \cdot K} \cdot 328K}{5{,}65 \cdot 10^{-4}\,m^3 \cdot 4{,}220 \cdot \sqrt{1 - (0{,}255)^2}} = 15{,}195bar \tag{3.123}$$

To obtain the maximum and minimum values of the pressure, values (3.122), (3.123), (3.116) and (3.117) have to be combined with equation (3.101) and (3.102).

$$p_{max,s} = 8{,}929bar \cdot \frac{\sqrt{1 + 0{,}205}}{\sqrt{1 - 0{,}205}} = 11{,}008bar \tag{3.124}$$

$$p_{max,b} = 15{,}195bar \cdot \frac{\sqrt{1 + 0{,}255}}{\sqrt{1 - 0{,}255}} = 19{,}72bar \tag{3.125}$$

$$p_{min,s} = 8{,}929bar \cdot \frac{\sqrt{1-0{,}205}}{\sqrt{1+0{,}205}} = 7{,}253bar \qquad (3.126)$$

$$p_{min,b} = 15{,}195bar \cdot \frac{\sqrt{1-0{,}255}}{\sqrt{1+0{,}255}} = 11{,}707bar \qquad (3.127)$$

Using equation (3.46) the pressure p can be shown as a function of the crank angle α in figure 3-6.
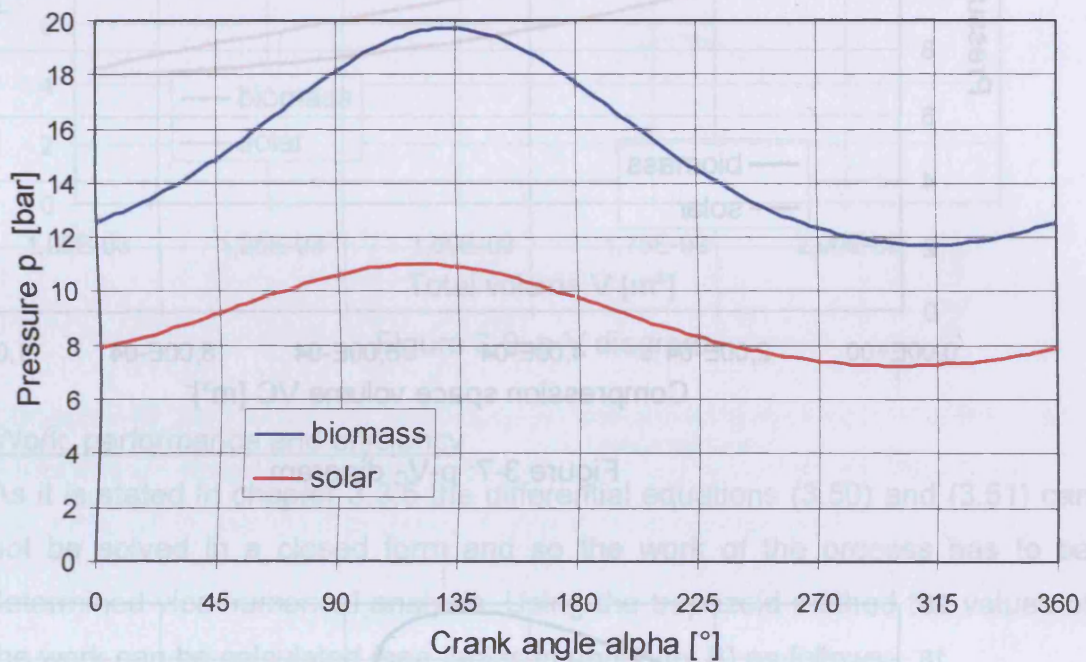
Figure 3-6: Pressure as a function of the crank angle

Combining the values of the figures 2-26 and 2-27 (volume as a function of the crank angle) with the ones of figure 3-6 (pressure as a function of the crank angle) p-V-diagrams for the expansion space, compression space and total volume can be derived. They are shown in figures 3-7, 3-8 and 3-9 both for the solar engine and for the biomass engine. The corresponding values can be seen in appendix B.
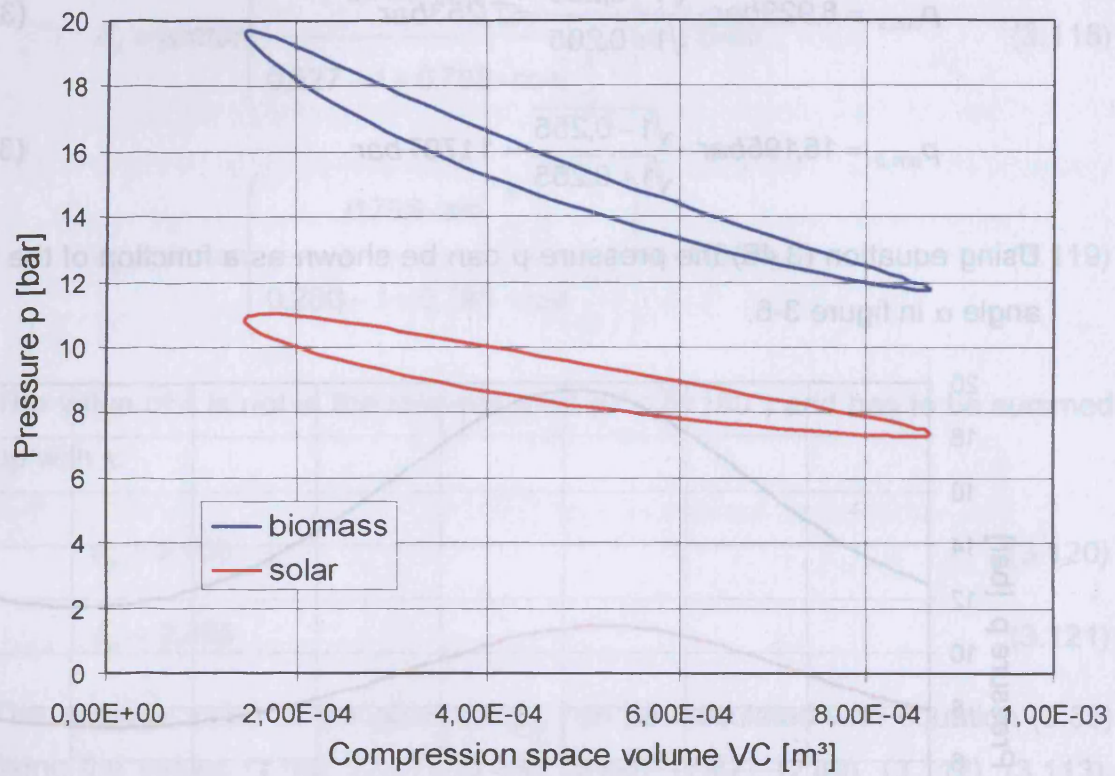
Figure 3-7: p-V_C diagram
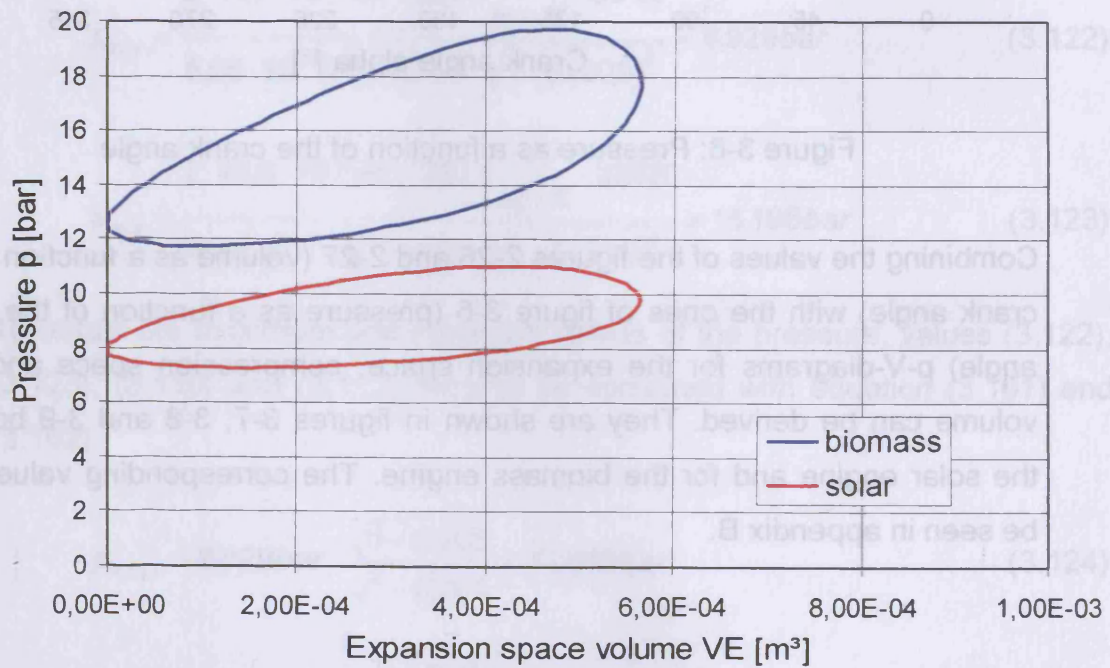
Figure 3-8: p-V_E diagram
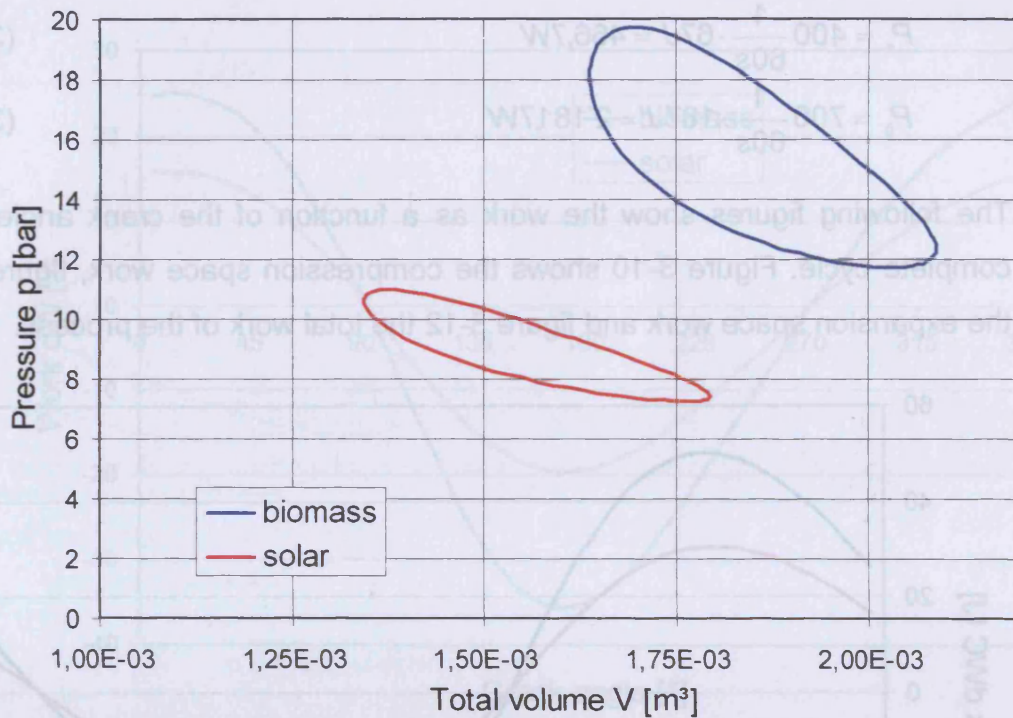
Figure 3-9: p-V diagram

> **Work, performance and efficiency**

As it is stated in chapter 3.3.5 the differential equations (3.50) and (3.51) can not be solved in a closed form and so the work of the process has to be determined vice numerical analysis. Using the trapezoid method the values of the work can be calculated (see tables in appendix B) as follows:

$$W_{C,s} = -142J \qquad (3.128)$$

$$W_{E,s} = 75J \qquad (3.129)$$

$$W_s = 67J \qquad (3.130)$$

$$W_{C,b} = -259J \qquad (3.131)$$

$$W_{E,b} = 72J \qquad (3.132)$$

$$W_b = 187J \qquad (3.133)$$

Combining equation (2.74), (2.75) and (2.76) with the work done by the engines (equations 3.130 and 3.133) the overall performance obtains values of:

$$P_s = 400 \frac{1}{60s} \cdot 67J = 466,7W \tag{3.134}$$

$$P_b = 700 \frac{1}{60s} \cdot 187J = 2'181,7W \tag{3.135}$$

The following figures show the work as a function of the crank angle for a complete cycle. Figure 3-10 shows the compression space work, figure 3-11 the expansion space work and figure 3-12 the total work of the process.
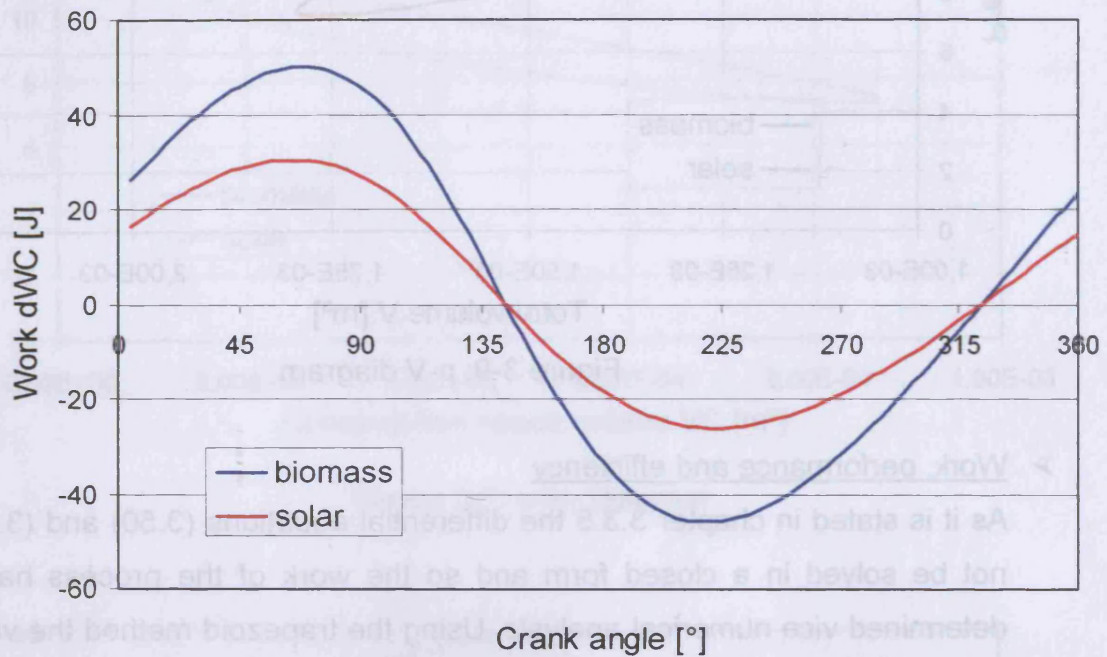
Figure 3-10: Compression space work as a function of the crank angle
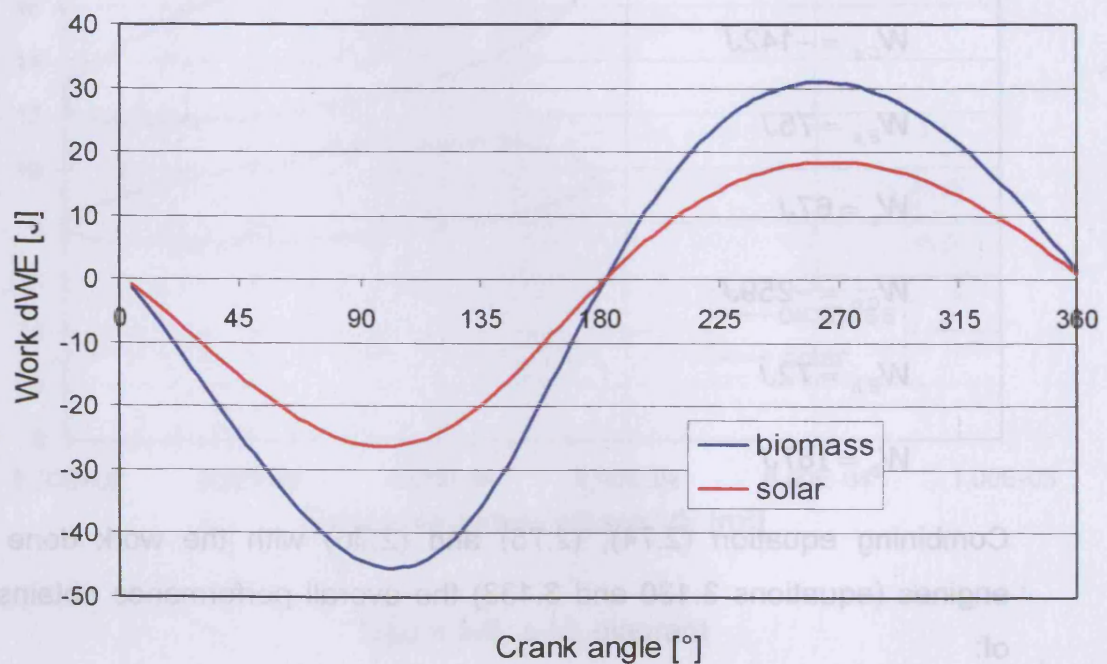
Figure 3-11: Expansion space work as a function of the crank angle

90
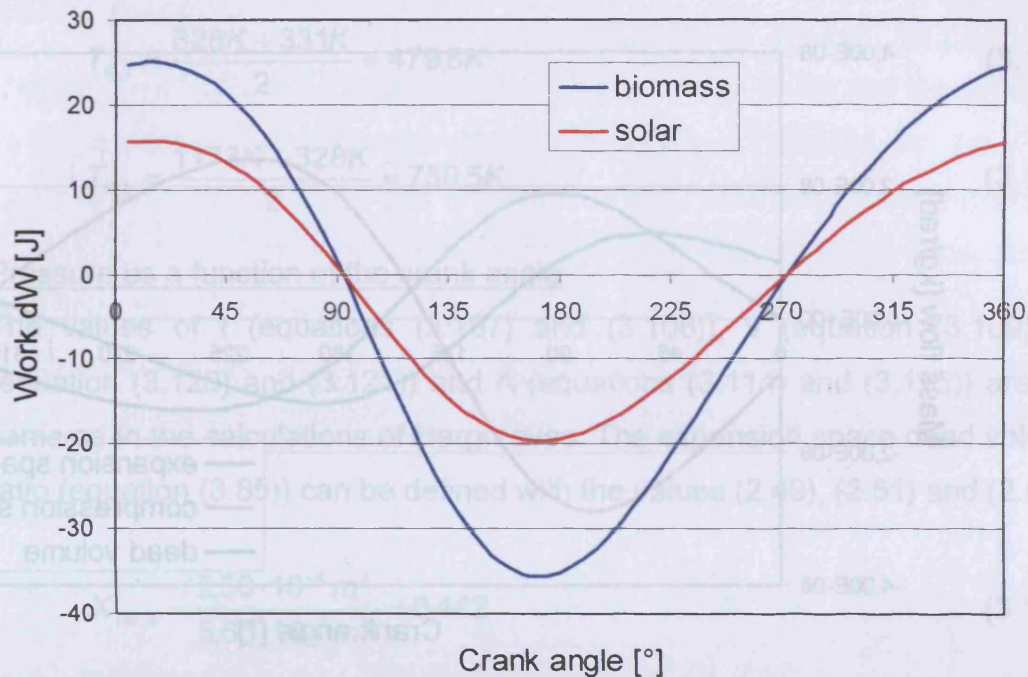
Figure 3-12: Total work as a function of the crank angle

Because of the isothermal conditions in the working spaces (expansion and compression space) the efficiency for the two experimental engines is exactly the same as in the ideal process. There is thus no change in the heat source and heat sink temperature compared to the conditions of the ideal process.

➢ Mass flow through the machine

The mass flow through the machines, defined in chapter 3.26 by equation (3.66) for the change of mass of working gas in the expansion space and by equation (3.76) for the change in the compression space, is calculated in the tables in appendix B. Also the change of mass in the dead space is shown. Figures 3-13 and 3-14 show how these values change as a function of the crank angle.
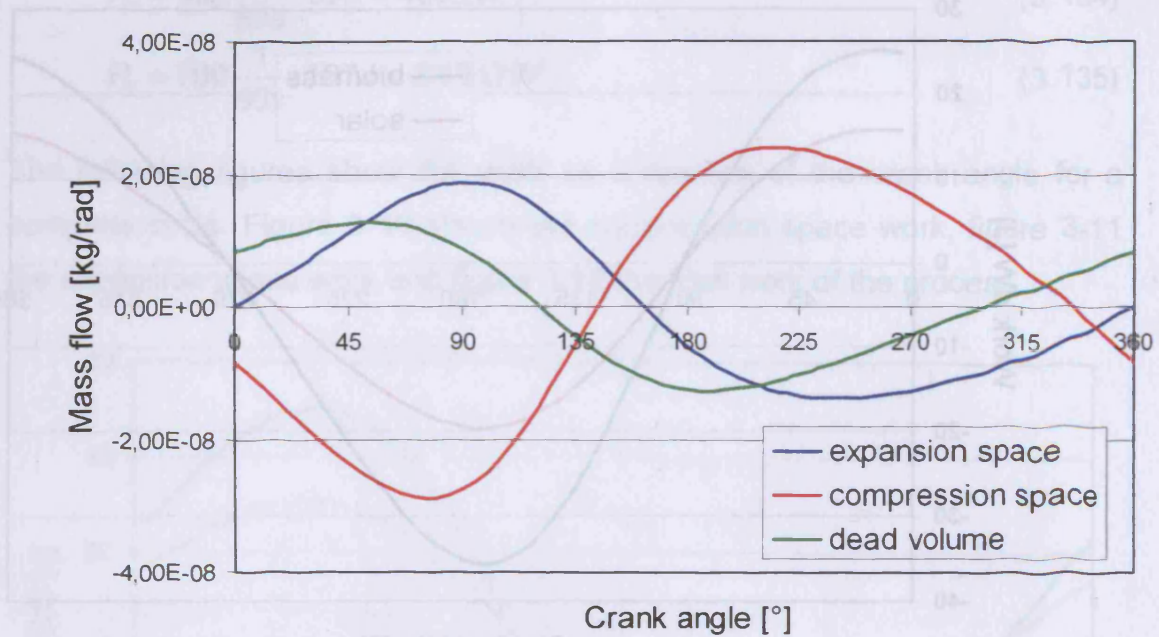
Figure 3-13: Mass flow as a function of the crank angle for the solar engine
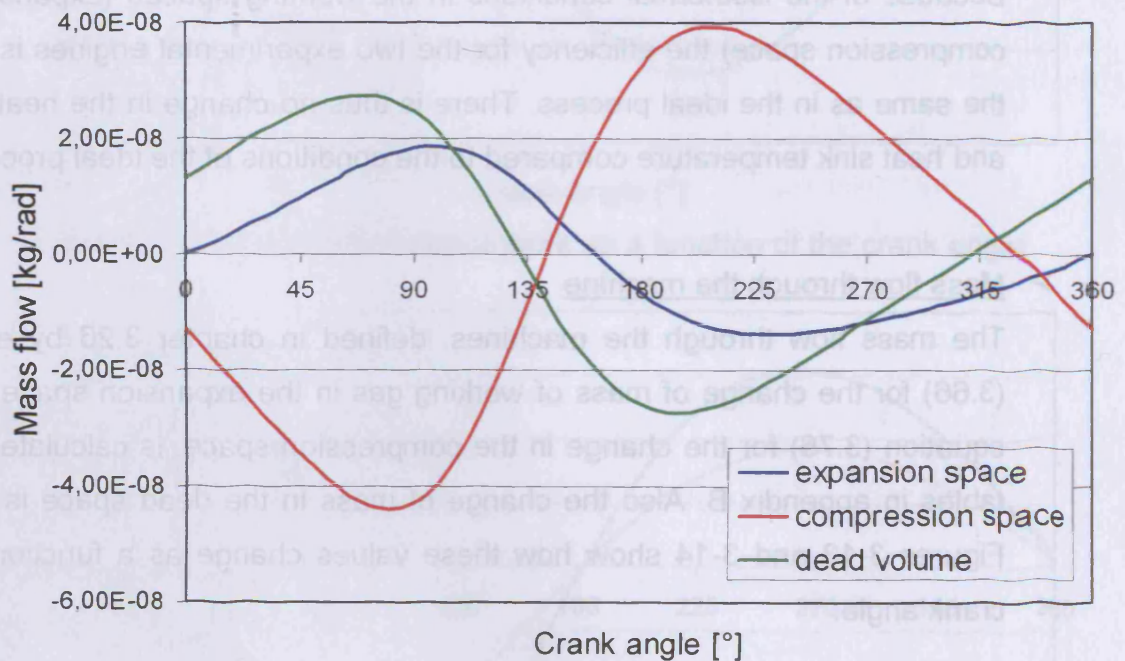
Figure 3-14: Mass flow as a function of the crank angle for the biomass engine

3.5.2   The Hirata method

➢ Effective regenerator gas temperature

The values of equation (2.40) to (2.43) set into equation (3.88) results in the effective regenerator temperature:

$$T_{R,s} = \frac{628K + 331K}{2} = 479,5K \tag{3.136}$$

$$T_{R,b} = \frac{1173K + 328K}{2} = 750,5K \tag{3.137}$$

> **Pressure as a function of the crank angle**

The values of t (equations (3.107) and (3.108)), v (equation (3.109)), δ (equation (3.120) and (3.121)) and A (equations (3.114) and (3.115)) are the same as in the calculations of Hargreaves. The expansion space dead volume ratio (equation (3.85)) can be defined with the values (2.49), (2.51) and (2.52):

$$X_{DE,s} = \frac{2,50 \cdot 10^{-4} m^3}{5,65 \cdot 10^{-4} m^3} = 0,442 \tag{3.138}$$

$$X_{DE,s} = \frac{5,44 \cdot 10^{-4} m^3}{5,65 \cdot 10^{-4} m^3} = 0,963 \tag{3.139}$$

With the equations (2.49) and (2.53) the compression space dead volume ratio (equation (3.86)) has a value of:

$$X_{DC} = \frac{3,79 \cdot 10^{-4} m^3}{5,65 \cdot 10^{-4} m^3} = 0,671 \tag{3.140}$$

Combining equations (2.49) and (2.54) the regenerator volume ratio (equation (3.87)) is:

$$X_R = \frac{1,50 \cdot 10^{-4} m^3}{5,65 \cdot 10^{-4} m^3} = 0,265 \tag{3.141}$$

The substitution variable B (equation (3.91)) can be determined with equation (3.107), (3.108), (3.109), (3.138), (3.139), (3.140) and (3.141).

$$\begin{aligned} B_s &= 0,527 + 2 \cdot 0,442 \cdot 0,527 + \frac{4 \cdot 0,527 \cdot 0,265}{1 + 0,527} + 1 + 0,798 + 2 \cdot 0,671 = \\ &= 4,500 \end{aligned} \tag{3.142}$$

$$\begin{aligned} B_b &= 0,280 + 2 \cdot 0,963 \cdot 0,280 + \frac{4 \cdot 0,280 \cdot 0,265}{1 + 0,280} + 1 + 0,798 + 2 \cdot 0,671 = \\ &= 4,191 \end{aligned} \tag{3.143}$$

Equation (3.97) and the substitution variable c can be solved with the values (3.114), (3.115), (3.142) and (3.143).

$$c_s = \frac{0,928}{4,500} = 0,206 \qquad (3.144)$$

$$c_b = \frac{1,075}{4,191} = 0,257 \qquad (3.145)$$

Combining the values (2.40), (2.42), (2.49), (2.64), (2.66), (2.67) and (3.142) to (3.145) with equation (3.99) the average value of the pressure can be determined.

$$p_{m,s} = \frac{2 \cdot 11,7 \cdot 10^{-3} kg \cdot 287,1 \frac{J}{kg \cdot K} \cdot 331K}{5,65 \cdot 10^{-4} m^3 \cdot 4,500 \cdot \sqrt{1 - 0,206^2}} = 8,962 bar \qquad (3.146)$$

$$p_{m,b} = \frac{2 \cdot 18,6 \cdot 10^{-3} kg \cdot 287,1 \frac{J}{kg \cdot K} \cdot 328K}{5,65 \cdot 10^{-4} m^3 \cdot 4,191 \cdot \sqrt{1 - 0,257^2}} = 15,308 bar \qquad (3.147)$$

To get the maximum and minimum values of the pressure, equations (3.101) and (3.102) have to be calculated with the values (3.144) to (3.147).

$$p_{max,s} = 8,962 bar \cdot \frac{\sqrt{1 + 0,206}}{\sqrt{1 - 0,206}} = 11,047 bar \qquad (3.148)$$

$$p_{max,b} = 15,308 bar \cdot \frac{\sqrt{1 + 0,257}}{\sqrt{1 - 0,257}} = 19,911 bar \qquad (3.149)$$

$$p_{min,s} = 8,962 bar \cdot \frac{\sqrt{1 - 0,206}}{\sqrt{1 + 0,206}} = 7,272 bar \qquad (3.150)$$

$$p_{min,b} = 15,308 bar \cdot \frac{\sqrt{1 - 0,257}}{\sqrt{1 + 0,257}} = 11,769 bar \qquad (3.151)$$

3.6   Summary

In this chapter the so called Schmidt analysis is discussed in detail and the complete equation set is derived with the methods of Hirata and Hargreaves for the γ-type engine. This is felt to be new and was presented at the "International Stirling Engine Conference" in Durham, GB in 2005 (see chapter 8.2). All the parameters that can be calculated with the Hargreaves method are shown for the solar and biomass experimental engines. At this point it can be seen that there is almost no difference between the calculation methods of Hirata and Hargreaves. Values for these differences are:

$$\Delta p_s = 0,033 bar \tag{3.152}$$

$$\Delta p_b = 0,113 bar \tag{3.153}$$

The percentage difference can be determined by

$$\Delta p_s = 0,37\% \tag{3.154}$$

$$\Delta p_b = 0,74\% \tag{3.155}$$

Thus there is little point in further developing the analysis via the Hirata method. In table 3.1 the main values of the Hirata and Hargreaves method are shown for comparison. Hence for the following chapters of this work only the method of Hargreaves is used.

	Hargreaves	Hirata
$T_{R,s}$	463,76 K	479,50 K
$T_{R,b}$	663,11 K	750,50 K
$p_{m,s}$	8,929 bar	8,962 bar
$p_{m,b}$	15,195 bar	15,308 bar
$p_{max,s}$	11,008 bar	11,047 bar
$p_{max,b}$	19,720 bar	19,911 bar
$p_{min,s}$	7,253 bar	7,272 bar
$p_{min,b}$	11,707 bar	11,769 bar

Table 3.1: Values of the calculation methods of Hargreaves and Hirata

It is of special interest how the calculated values correspond with the specified ones of chapter 2. A comparison of the nominal values from the specifications in tables 2.2 and 2.3 with the calculated ones using the Hargeaves method can be found in table 3.2.

	Solar engine	Biomass engine
Nominal value	200 W	600 W
Hargreaves	466,7 W	2'181,7 W

Table 3.2: Comparison of calculated and nominal performance values

It can be seen that the calculated performance values for both engines differ by factors from the specified ones. Another disadvantage of the Schmidt method is the isothermal assumption of the working spaces which avoids that the transferred heat of heater and cooler can be calculated. In order to get more process parameters that are closer to real ones the 2nd order calculation methods are discussed in the following chapter.

4 2nd order calculation – adiabatic analysis

4.1 Ideal adiabatic analysis by Urieli and Berchowitz

4.1.1 Non-isothermal working spaces

The theory described in this chapter originates from one of the most interesting books about Stirling engine analysis. This is "Stirling cycle engine analysis" [9] and was written by the famous Stirling engine scientists Urieli and Berchowitz. The equations and calculation methods are modified to make the program more structured, easier to solve and fit gamma type engines.

In chapter 3 a Stirling cycle engine model is considered in which the compression and expansion spaces are assumed to be isothermal. This leads to the paradoxical situation that neither the heater nor the cooler contribute any net heat transfer over the cycle and hence are redundant. All the required heat transfer occurs across boundaries of the isothermal working spaces. The practical requirements for effective heat exchange generally conflict with those attainable in the working spaces designed for expanding and compressing the working gas. In real machines the working spaces will tend to be adiabatic rather than isothermal. This implies that the net heat transferred over the cycle must be provided by the heat exchangers.

Unfortunately, if the attempt is made to depart from the isothermal assumption, the equations are no longer explicitly integrable and can only be solved with a differential equation set. The resulting set of differential equations is non-linear and numerical methods have to be used.

There are advantages to this approach. The detailed behaviour of all the variables is available throughout the cycle, in particular the considerable amount of heat stored in the regenerator, from which the importance of the regenerator can be derived. The method can be extended to include heat transfer and flow friction analysis of the heat exchanger components (see section 4.2). With the recent proliferation of digital computers, the so called ideal adiabatic model is considered by the author to be far more representative of what can be understood as the ideal cycle to compare with the performance of real machines.

Stirling cycle machines having non-isothermal working spaces were first analysed by Finkelstein (in 1960) and this analysis represented the most significant theoretical development in nearly a century [10]. His model assumed finite heat transfer in the working spaces by means of a heat transfer coefficient. The resulting temperature

variation of the gas in the working spaces leads to a temperature discontinuity at the working space interfaces. Finkelstein introduced the concept of "conditional temperatures" in which the gas, flowing in or out of the working spaces, always takes the immediate upstream value of temperature.

It is of interest to note that, given the same mass of working gas, the non-isothermal analysis does not result in a significantly different performance from that due to the isothermal Schmidt analysis. The indicated power output will usually be higher since the polytrophic processes involved tend to produce larger pressure swings than the isothermal ones [9]. The thermal efficiency will inevitably be reduced from the Carnot efficiency, owing to the irreversibility introduced by the temperature discontinuities. A comparison of the results of the different calculation methods is given in chapter 6.

The theory presented by Finkelstein was explored by Walker and Kahn (1965) with particular emphasis [10] on the limiting case of adiabatic compression and expansion processes. A study of the effect of the four principal design parameters, temperature ratio, phase angle advance, swept volume ratio and dead volume ratio was made using a specific typical example. Because of the non-linearity introduced by conditional temperatures, it is extremely difficult to generalise the results and every engine concept should be calculated on its own.

The adiabatic analysis has also been reconsidered by Lee (1976) and Berchowitz (1978) [9], both of whom include the complete mathematical developments and computer program listings. Urieli also analysed several engines with the ideal adiabatic model. As experimental engines he used alpha-type machines and free piston machines – but no gamma-type machines. Thus the following calculations are a new step in the calculation of the processes occurring in a gamma-type engine.

The ideal adiabatic model is defined in the following section whilst the equation set is developed. The method of solution is outlined and the analysis is used both to determine the effects of the adiabatic working spaces on the engine performance and to examine the detailed behaviour of various variables over the cycle.

4.1.2 Ideal adiabatic model and assumptions

In the following the ideal adiabatic model is defined and its relevant nomenclature and various assumptions are made with reference to figure 4-1.
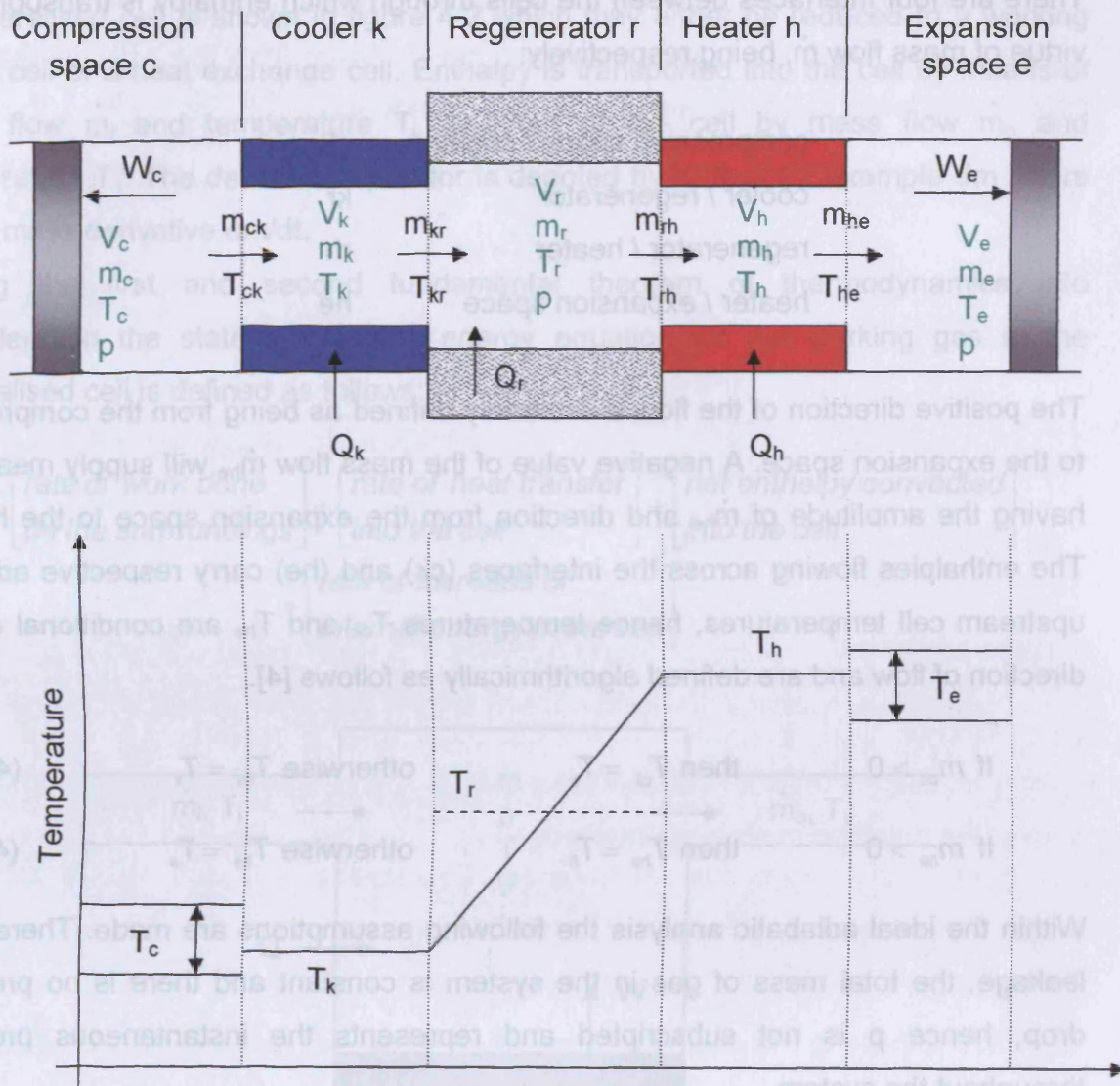
Figure 4-1: The ideal adiabatic model (basis from [9])

The engine is configured as a five-component serially connected model having perfectly effective heat exchangers (heater, cooler and regenerator) and thus is similar to the ideal isothermal model. The gas in the cooler and heater spaces is maintained under isothermal conditions at temperatures T_k and T_h respectively. Both the regenerator matrix and the gas in the regenerator void volume have the identical linear temperature profile, the gas flowing through the regenerator / cooler interface being at the cooler temperature T_k and through the regenerator / heater interface at the heater temperature T_h. The resulting equivalent mixed mean temperature of the gas in the regenerator is the logarithmic mean temperature difference between T_k and T_h as was derived in the first order calculation. The working spaces are assumed to be adiabatic and thus temperatures T_c and T_e vary over the cycle in accordance with the adiabatic nature of these spaces.

There are four interfaces between the cells through which enthalpy is transported by virtue of mass flow ṁ, being respectively:

compression space / cooler	ck
cooler / regenerator	kr
regenerator / heater	rh
heater / expansion space	he

The positive direction of the flow is arbitrarily defined as being from the compression to the expansion space. A negative value of the mass flow ṁ$_{he}$ will supply mean flow having the amplitude of ṁ$_{he}$ and direction from the expansion space to the heater. The enthalpies flowing across the interfaces (ck) and (he) carry respective adjacent upstream cell temperatures, hence temperatures T$_{ck}$ and T$_{he}$ are conditional on the direction of flow and are defined algorithmically as follows [4].

$$\text{If } \dot{m}_{ck} > 0 \qquad \text{then } T_{ck} = T_c \qquad \text{otherwise } T_{ck} = T_k \qquad (4.1)$$

$$\text{If } \dot{m}_{he} > 0 \qquad \text{then } T_{he} = T_h \qquad \text{otherwise } T_{he} = T_e \qquad (4.2)$$

Within the ideal adiabatic analysis the following assumptions are made. There is no leakage, the total mass of gas in the system is constant and there is no pressure drop, hence p is not subscripted and represents the instantaneous pressure throughout the system.

Work W is done on the surroundings by virtue of the varying volumes of the working spaces V$_c$ and V$_e$ and heat Q$_k$ and Q$_h$ is transferred from the external environment to the working gas in the cooler and heater cells. The regenerator is externally adiabatic, heat Q$_r$ is transferred internally from the regenerator matrix to the gas flowing through the regenerator dead volume V$_r$.

4.1.3 Development of the equation set

The general approach for deriving the differential and algebraic equation set is to apply the equations of energy and state to each of the cells, which are considered as control volumes. The resulting equations are linked by applying the continuity equation across the entire system.

A generalised cell is shown in figure 4-2 which may either be reduced to a working space cell or a heat exchange cell. Enthalpy is transported into the cell by means of mass flow $\dot{m}_i$ and temperature T_i, and out of the cell by mass flow $\dot{m}_o$ and temperature T_o. The derivative operator is denoted by d: thus for example dm refers to the mass derivative dm/dt.

Taking the first and second fundamental theorem of thermodynamics into consideration the statement of the energy equation for the working gas in the generalised cell is defined as follows:

$$\begin{bmatrix} rate\ of\ work\ done \\ on\ the\ surroundings \end{bmatrix} + \begin{bmatrix} rate\ of\ heat\ transfer \\ into\ the\ cell \end{bmatrix} + \begin{bmatrix} net\ enthalpy\ convected \\ into\ the\ cell \end{bmatrix}$$
$$= \begin{bmatrix} rate\ of\ increase\ of \\ internal\ energy\ in\ the\ cell \end{bmatrix}$$
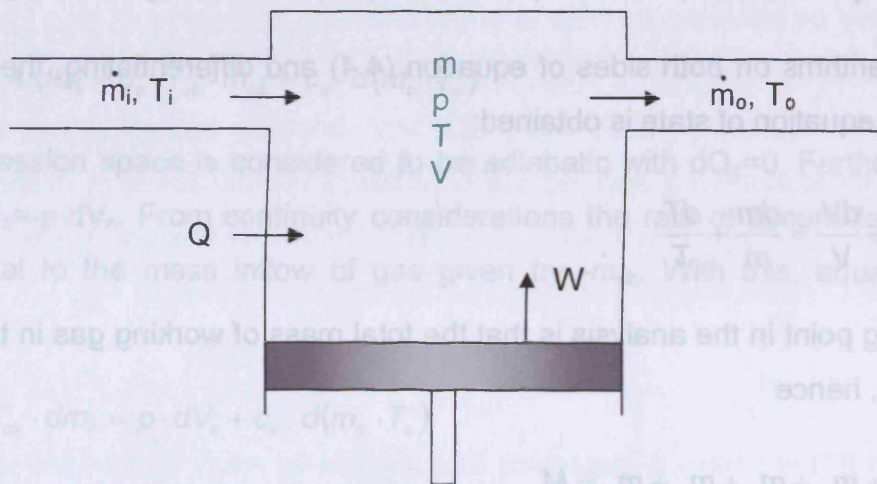
Figure 4-2: Generalised cell [11]

Mathematically, the word statement becomes

$$dW + dQ + \left(c_p \cdot T_i \cdot \dot{m}_i - c_p \cdot T_o \cdot \dot{m}_o\right) = c_v \cdot d(m \cdot T) \tag{4.3}$$

This equation is well known as the energy equation for non-steady flow in which kinetic and potential energy terms have been neglected. The equation of state is given by

$$p \cdot V = m \cdot R \cdot T \tag{4.4}$$

Equation (4.4) assumes that the working gas is ideal, which is valid for Stirling engines since the working gas processes are far away from the critical point. This assumption leads to the following additional equations.

$$c_p - c_v = R \tag{4.5}$$

Hence

$$c_p = R \cdot \frac{\kappa}{\kappa - 1} \tag{4.6}$$

$$c_v = R \cdot \frac{1}{\kappa - 1} \tag{4.7}$$

with

$$\kappa = \frac{c_p}{c_v}. \tag{4.8}$$

Taking logarithms on both sides of equation (4.4) and differentiating, the differential form of the equation of state is obtained:

$$\frac{dp}{p} + \frac{dV}{V} = \frac{dm}{m} + \frac{dT}{T} \tag{4.9}$$

The starting point in the analysis is that the total mass of working gas in the machine is constant, hence

$$m_c + m_k + m_r + m_h + m_e = M \tag{4.10}$$

Differentiating this equation leads to

$$dm_c + dm_k + dm_r + dm_h + dm_e = 0 \tag{4.11}$$

For all the heat exchanger cells (k, r and h), since the respective volumes and temperatures are constant,

$$V = const. \qquad dV = 0 \tag{4.12}$$

$$T = const. \qquad dT = 0 \tag{4.13}$$

the differential form of the equation of state (4.9) reduces to

$$\frac{dm}{m} = \frac{dp}{p} \qquad (4.14)$$

Applying equation (4.14) to each of the three heat exchangers and substituting them in equation (4.11)

$$dm_c + dm_e + dp \cdot \left(\frac{m_k}{p} + \frac{m_r}{p} + \frac{m_h}{p} \right) = 0 \qquad (4.15)$$

and substituting the equation of state (4.4)

$$dm_c + dm_e + \left(\frac{dp}{R} \right) \cdot \left(\frac{V_k}{T_k} + \frac{V_r}{T_r} + \frac{V_h}{T_h} \right) = 0 \qquad (4.16)$$

dm$_c$ and dm$_e$ have to be eliminated in equation (4.16) to get to an explicit equation in dp. Applying the energy equation (4.3) to the compression space, it is obtained:

$$dW_c + dQ_c - c_p \cdot T_{ck} \cdot \dot{m}_{ck} = c_v \cdot d(m_c \cdot T_c) \qquad (4.17)$$

The compression space is considered to be adiabatic with dQ$_c$=0. Furthermore, the work is dW$_c$=-p·dV$_c$. From continuity considerations the rate of accumulation of gas dm$_c$ is equal to the mass inflow of gas given by -$\dot{m}_{ck}$. With this, equation (4.17) reduces to:

$$c_p \cdot T_{ck} \cdot dm_c = p \cdot dV_c + c_v \cdot d(m_c \cdot T_c) \qquad (4.18)$$

Substituting the equation of state (4.4) and associated ideal gas relations (4.6) and (4.7) into equation (4.18)

$$c_p \cdot T_{ck} \cdot dm_c = p \cdot dV_c + \frac{c_v}{R} \cdot d(p \cdot V_c) \qquad (4.19)$$

$$\frac{R \cdot \kappa}{\kappa - 1} \cdot T_{ck} \cdot dm_c = p \cdot dV_c + \frac{1}{\kappa - 1} \cdot (p \cdot dV_c + V_c \cdot dp) \qquad (4.20)$$

$$dm_c = \frac{p \cdot (\kappa - 1) \cdot dV_c + p \cdot dV_c + V_c \cdot dp}{R \cdot \kappa \cdot T_{ck}} \qquad (4.21)$$

$$dm_c = \frac{p \cdot \kappa \cdot dV_c + V_c \cdot dp}{R \cdot \kappa \cdot T_{ck}} \qquad (4.22)$$

Similarly for the expansion space:

$$dm_e = \frac{p \cdot \kappa \cdot dV_e + V_e \cdot dp}{R \cdot \kappa \cdot T_{he}}$$

(4.23)

Substituting equations (4.22) and (4.23) into equation (4.16) and simplifying:

$$\frac{p \cdot \kappa \cdot dV_c + V_c \cdot dp}{R \cdot \kappa \cdot T_{ck}} + \frac{p \cdot \kappa \cdot dV_e + V_e \cdot dp}{R \cdot \kappa \cdot T_{he}} + \left(\frac{dp}{R}\right) \cdot \left(\frac{V_k}{T_k} + \frac{V_r}{T_r} + \frac{V_h}{T_h}\right) = 0$$

(4.24)

$$dp = \frac{-p \cdot \kappa \cdot \left[\dfrac{dV_c}{T_{ck}} + \dfrac{dV_e}{T_{he}}\right]}{\left(\dfrac{V_c}{T_{ck}}\right) + \kappa \cdot \left[\dfrac{V_k}{T_k} + \dfrac{V_r}{T_r} + \dfrac{V_h}{T_h}\right] + \left(\dfrac{V_e}{T_{he}}\right)}$$

(4.25)

It can be observed that equations (4.25) and (4.22) are two simultaneous differential equations in the variables p and m_c. Once p and m_c are evaluated, the rest of the variables may be obtained by means of the equation of state (4.4) and mass balance (4.10). Volume variations dV_c, dV_e, V_c and V_e are available analytically and all other parameters in equations (4.25) and (4.22) are constant, excluding T_{ck} and T_{he}. The interface temperatures T_{ck} and T_{he} are conditional on the direction of the mass flow defined in equations (4.1) and (4.2). In order to evaluate the mass flow $\dot{m}$, and thus the direction of mass flow, the continuity equation is given by:

$$dm = \dot{m}_i - \dot{m}_o$$

(4.26)

Equation (4.26) is simply a statement that the rate of mass accumulation in a cell is equal to the net mass flow into that cell and is obvious by inspection. Successively applying equation (4.26) to each of the cells in figure 4-1 gives:

$$\dot{m}_{ck} = -dm_c$$

(4.27)

$$\dot{m}_{kr} = \dot{m}_{ck} - dm_k$$

(4.28)

$$\dot{m}_{rh} = \dot{m}_{kr} - dm_r$$

(4.29)

$$\dot{m}_{he} = \dot{m}_{rh} - dm_h$$

(4.30)

In order to complete the equation set the various required energy variables, these being the work W and the heat transferred respectively to the gas in the cooler Q_k, regenerator Q_r and heater Q_h are required. Since the energy variables are dependent

on the flow direction they can only be obtained by integrating the corresponding differential equations over the cycle. The total work done by the engine is given by the algebraic sum of the work done by compression and expansion spaces.

$$dW = -p \cdot dV_c - p \cdot dV_e$$

(4.31)

Substituting equations (4.4) and (4.5) into equation (4.3) and simplifying:

$$dW + dQ + c_p \cdot T_i \cdot \dot{m}_i - c_p \cdot T_o \cdot \dot{m}_o = \frac{c_v \cdot V \cdot dp}{R} + \frac{c_v \cdot p \cdot dV}{R}$$

(4.32)

In the heat exchanger spaces no work is done (4.33), since the respective volumes are constant (4.12).

$$dW = 0$$

(4.33)

Applying equation (4.32) to the individual heat exchanger spaces:

$$dQ_k = \frac{V_k \cdot dp \cdot c_v}{R} - c_p \cdot \left(T_{ck} \cdot \dot{m}_{ck} - T_{kr} \cdot \dot{m}_{kr} \right)$$

(4.34)

$$dQ_r = \frac{V_r \cdot dp \cdot c_v}{R} - c_p \cdot \left(T_{kr} \cdot \dot{m}_{kr} - T_{rh} \cdot \dot{m}_{rh} \right)$$

(4.35)

$$dQ_h = \frac{V_h \cdot dp \cdot c_v}{R} - c_p \cdot \left(T_{rh} \cdot \dot{m}_{rh} - T_{he} \cdot \dot{m}_{he} \right)$$

(4.36)

Since the heat exchangers are isothermal and the regenerator is ideal, the definition

$$T_{kr} = T_k$$

(4.37)

$$T_{rh} = T_h$$

(4.38)

can be given. The final set of pertinent differential and algebraic equations required for a solution is gathered in table 4.1

105

dp	$$= \frac{-p \cdot \kappa \cdot \left[\dfrac{dV_c}{T_{ck}} + \dfrac{dV_e}{T_{he}}\right]}{\left(\dfrac{V_c}{T_{ck}}\right) + \kappa \cdot \left[\dfrac{V_k}{T_k} + \dfrac{V_r}{T_r} + \dfrac{V_h}{T_h}\right] + \left(\dfrac{V_e}{T_{he}}\right)}$$	pressure
p	$= p_{old} + dp$	
m_c	$= m_{c,old} + dm_c$	masses
m_k	$= m_{k,old} + dm_k$	
m_r	$= m_{r,old} + dm_r$	
m_h	$= m_{h,old} + dm_h$	
m_e	$= m_{e,old} + dm_e$	
dm_c	$$= \frac{p \cdot \kappa \cdot dV_c + V_c \cdot dp}{R \cdot \kappa \cdot T_{ck}}$$	mass accumulations and flows
dm_k	$= m_k \cdot \dfrac{dp}{p}$	
dm_r	$= m_r \cdot \dfrac{dp}{p}$	
dm_h	$= m_h \cdot \dfrac{dp}{p}$	
dm_e	$= -dm_c - dm_k - dm_r - dm_h$	
$\dot{m}_{ck}$	$= -dm_c$	
$\dot{m}_{kr}$	$= \dot{m}_{ck} - dm_k$	
$\dot{m}_{rh}$	$= \dot{m}_{kr} - dm_r$	
$\dot{m}_{he}$	$= \dot{m}_{rh} - dm_h$	
T_c	$= \dfrac{p \cdot V_c}{m_c \cdot R}$	temperatures
T_e	$= \dfrac{p \cdot V_e}{m_e \cdot R}$	

If $\dot{m}_{ck} > 0$	then $T_{ck} = T_c$	otherwise $T_{ck} = T_k$	conditional
If $\dot{m}_{he} > 0$	then $T_{he} = T_h$	otherwise $T_{he} = T_e$	temperatures

dQ_k	$= \dfrac{V_k \cdot dp \cdot c_v}{R} - c_p \cdot \left(T_{ck} \cdot \dot{m}_{ck} - T_k \cdot \dot{m}_{kr}\right)$	energies
dQ_r	$= \dfrac{V_r \cdot dp \cdot c_v}{R} - c_p \cdot \left(T_k \cdot \dot{m}_{kr} - T_h \cdot \dot{m}_{rh}\right)$	
dQ_h	$= \dfrac{V_h \cdot dp \cdot c_v}{R} - c_p \cdot \left(T_h \cdot \dot{m}_{rh} - T_{he} \cdot \dot{m}_{he}\right)$	

dW_c	$= -p \cdot dV_c$	energies
dW_e	$= -p \cdot dV_e$	
W	$= W_{old} + dW_c + dW_e$	
Q_k	$= Q_{k,old} + dQ_k$	
Q_r	$= Q_{r,old} + dQ_r$	
Q_h	$= Q_{h,old} + dQ_h$	

Table 4.1: Ideal adiabatic model equation set

4.1.4 The real crank drive motion

In chapter 2.5.4 a pure sinusoidal motion of the crank drive was taken into consideration. This was made for simplifying reasons and to be able to solve the equation set with the Schmidt analysis in a closed form. Also in the literature for second order calculation methods this sinusoidal motion is used. But the second order calculation has to be solved with numerical methods by using digital computers. Because of this fact more exact equations [12] for describing the motion of the crank drive can be introduced.

4.1.4.1 Derivation of the equations for the real piston movement

The pistons of engines with conventional crank drives carry out an asymmetric, accelerated and decelerated motion. The crank shaft rotates with an almost simultaneous angular velocity. The movement of the connecting rods arises from the actions of the pistons and the crank shaft. The current distance of the piston to its upper dead point is called the piston motion s. For the derivation of the real piston motion figure 4-3 is needed. Thus:

$$s(\alpha) + x(\alpha) = r + l \tag{4.39}$$

$$s(\alpha) = r + l - x(\alpha) \tag{4.40}$$

The distance of the piston to the bearing point of the crank shaft x can be derived as:

$$x(\alpha) = r \cdot \cos(\alpha) + l \cdot \cos(\beta) \tag{4.41}$$
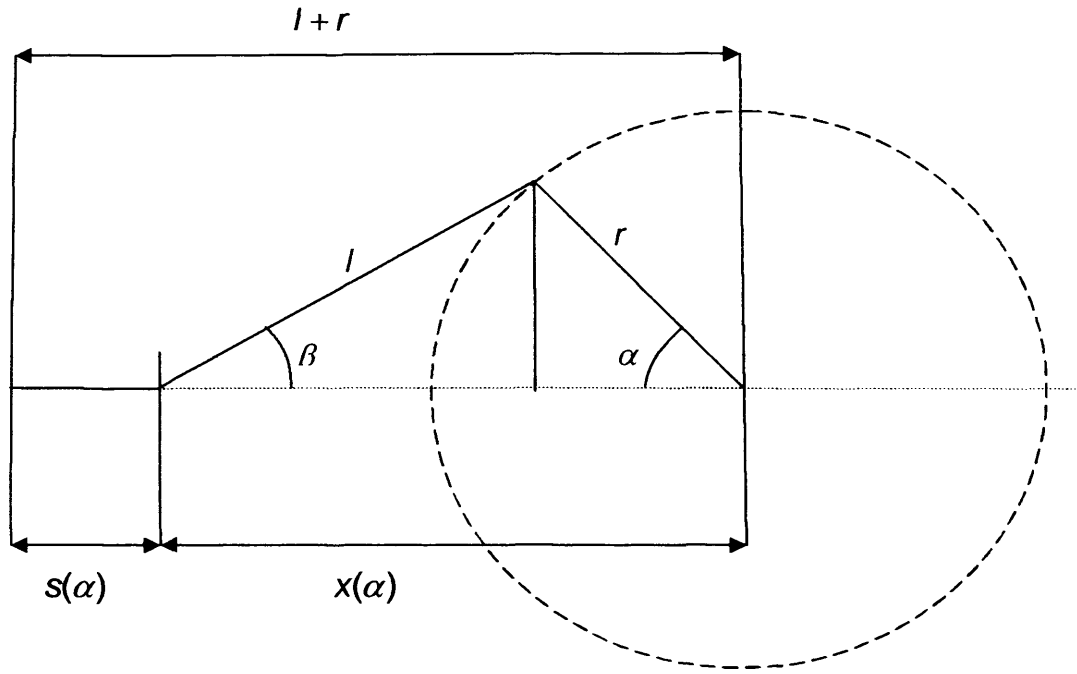
Figure 4-3: Geometry of a conventional crank drive [12]

With

$$l^2 = (l \cdot \cos(\beta))^2 + (r \cdot \sin(\alpha))^2 \qquad (4.42)$$

$$l \cdot \cos(\beta) = \sqrt{l^2 - (r \cdot \sin(\alpha))^2} \qquad (4.43)$$

equation (4.41) can be written as:

$$x(\alpha) = r \cdot \cos(\alpha) + \sqrt{l^2 - (r \cdot \sin(\alpha))^2} \qquad (4.44)$$

Defining the connecting rod ratio λ as

$$\lambda = \frac{r}{l} \qquad (4.45)$$

equation (4.44) can be simplified in the following way:

$$x(\alpha) = r \cdot \cos(\alpha) + l\sqrt{1 - (\lambda \cdot \sin(\alpha))^2} \qquad (4.46)$$

Setting this equation for x into equation (4.40)

$$s(\alpha) = r + l - r \cdot \cos(\alpha) - l\sqrt{1 - (\lambda \cdot \sin(\alpha))^2} \qquad (4.47)$$

$$s(\alpha) = r \cdot (1 - \cos(\alpha)) + l \cdot \left(1 - \sqrt{1 - \lambda^2 \cdot \sin^2(\alpha)}\right) \qquad (4.48)$$

108

This leads to the exact definition of the piston motion s without any approximations:

$$s(\alpha) = r \cdot \left[1 - \cos(\alpha) + \frac{1}{\lambda} \cdot \left(1 - \sqrt{1 - \lambda^2 \cdot \sin^2(\alpha)} \right) \right]$$
(4.49)

4.1.4.2 Real volumes for a gamma type engine

Modifying the approximate, sinusoidal equations for the volumes (2.26) and (2.27) with equation (4.49) it can be obtained:

$$V_e = \frac{V_{se}}{2} \cdot \left[1 - \cos(\alpha) + \frac{1}{\lambda_e} \cdot \left(1 - \sqrt{1 - \lambda_e^2 \cdot \sin^2(\alpha)} \right) \right]$$
(4.50)

$$V_c = \frac{V_{se}}{2} \cdot \left[1 + \cos(\alpha) - \frac{1}{\lambda_e} \cdot \left(1 - \sqrt{1 - \lambda_e^2 \cdot \sin^2(\alpha)} \right) \right] + ...$$

$$... \frac{V_{sc}}{2} \cdot \left[1 - \cos(\alpha - \varphi) + \frac{1}{\lambda_c} \cdot \left(1 - \sqrt{1 - \lambda_c^2 \cdot \sin^2(\alpha - \varphi)} \right) \right]$$
(4.51)

4.1.4.3 Comparison of the values for the real and sinusoidal piston motion

➢ Values for the comparison

To set boundary conditions for the following calculations table 4.2 shows all values used. It is divided into biomass and solar engine and in expansion space (e) and compression space (c).

		Biomass engine		Solar engine	
		e	c	e	c
V_s	[m³]	5,65E-4	4,51E-4	5,65E-4	4,51E-4
V_d	[m³]	1,073E-3		7,80E-4	
ρ	[°]	90			
l	[m]	0,130	0,146	0,130	0,146
r	[m]	0,0375			
λ	[-]	0,288	0,257	0,288	0,257
n	[1/min]	700		400	

Table 4.2: Values for the calculation of the piston motion

➢ **Piston motion s**

The piston motion s is the same for the biomass and solar engine, because the crank drive geometry is exactly the same. s reaches 0 when the volume has its minimum. In Figure 4-4 it can be clearly seen that there is a difference between the sinusoidal and the real piston motion for the working piston (c) as well as for the displacer (e).
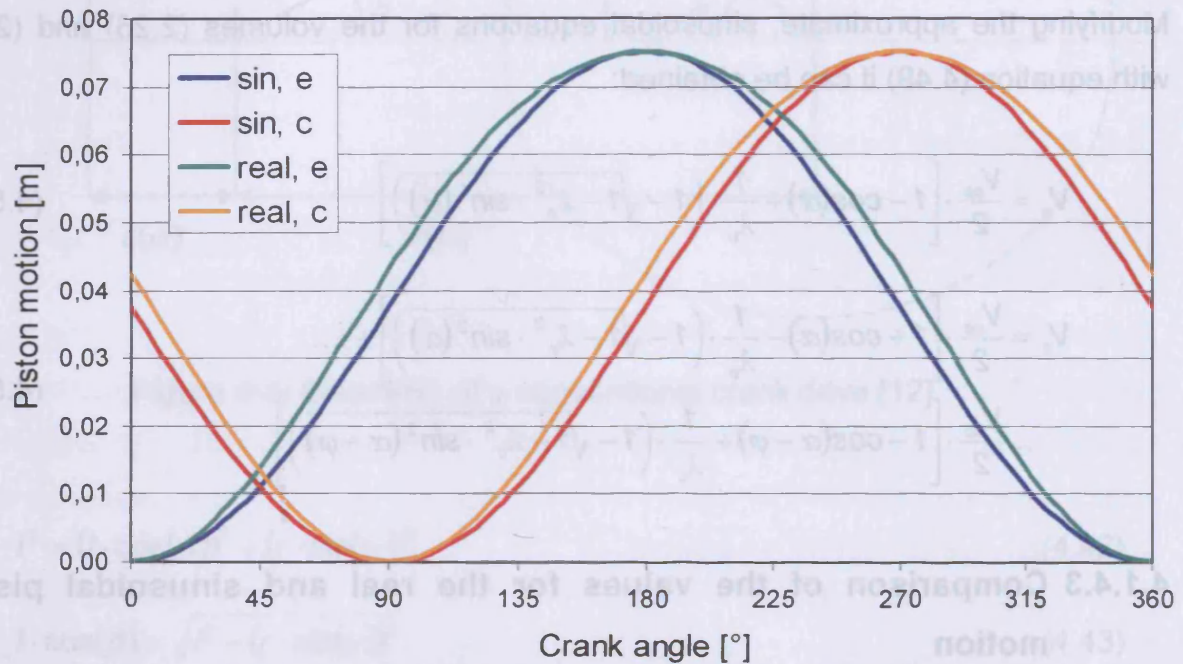
Figure 4-4: Sinusoidal and real piston motion for biomass and solar engine

➢ **Piston speed v**
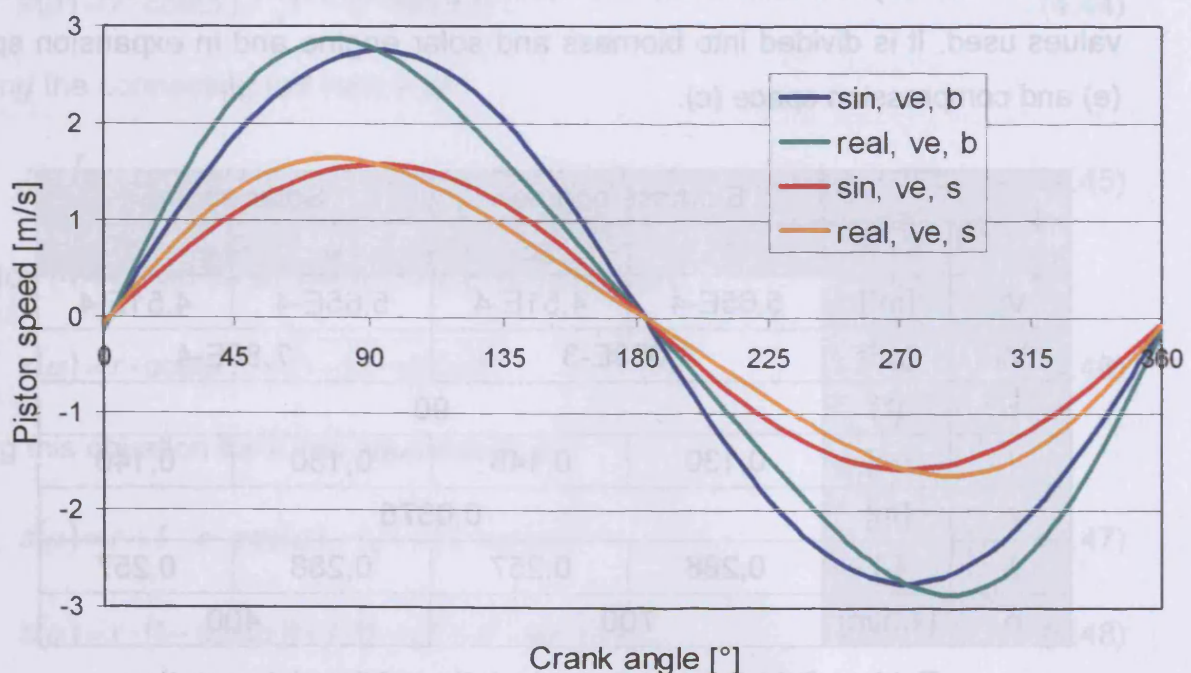
Figure 4-5: Speed of the displacer for biomass and solar engine

Figure 4-5 shows the speed of the displacer piston for the biomass and solar engine. The basis for this is the engine speed of the two engines given in table 4-2. Figure 4-6 shows this curve for the working piston
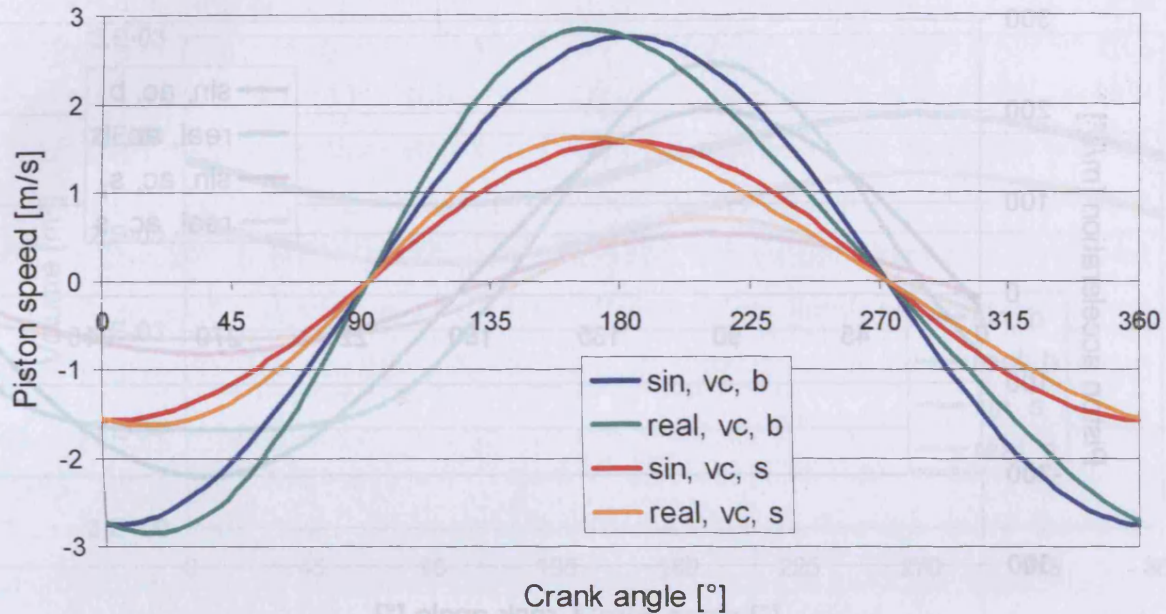
Figure 4-6: Speed of the working piston for biomass and solar engine

➢ Piston acceleration a

Another very interesting value is the piston acceleration a. Figure 4-7 and 4-8 show the acceleration of the displacer and working piston for both engines.
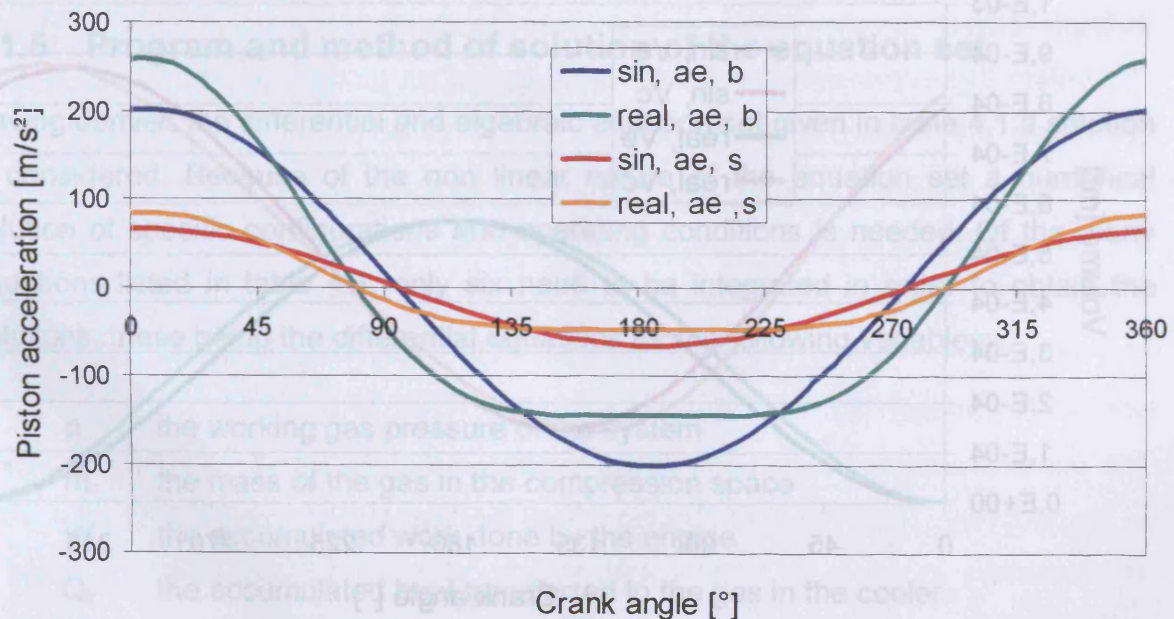
Figure 4-7: Acceleration of the displacer for biomass and solar engine

The real behaviour shows a plateau between 140° and 240° crank angle, where the acceleration is almost constant. This can also be seen in the speed curves (figure 4-5 and 4-6). For this crank angle range the speed changes linearly.
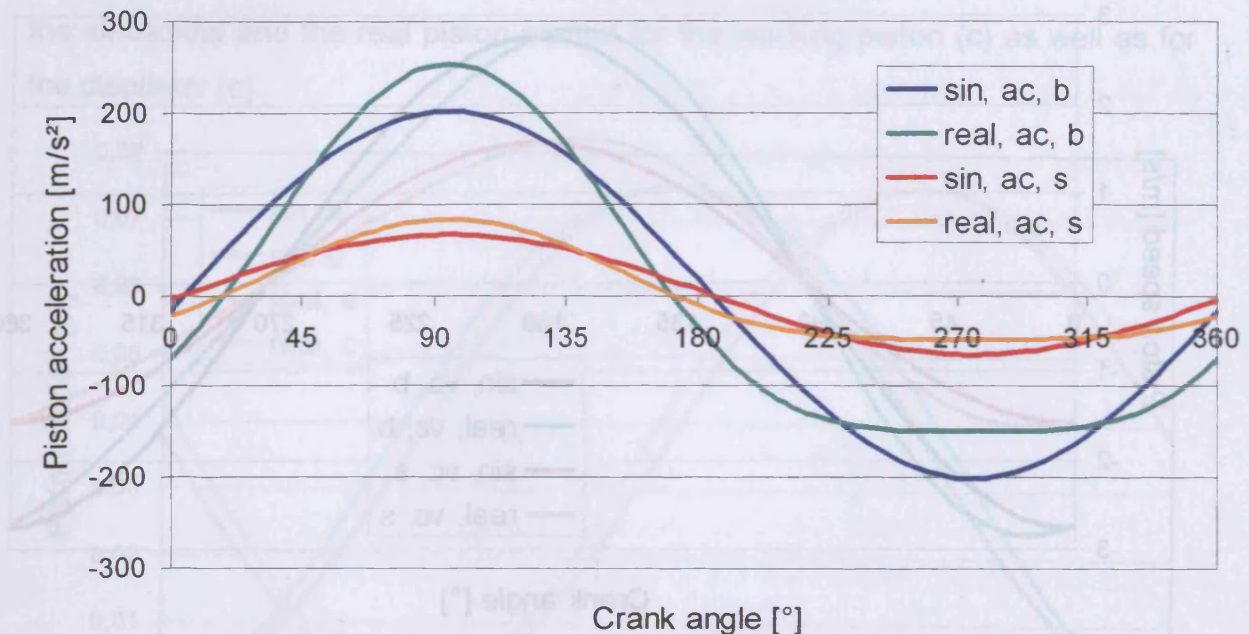
Figure 4-8: Acceleration of the working piston for biomass and solar engine

➤ Volumes

In figure 4-9 the expansion and compression space volume are compared for sinusoidal and real piston motion.
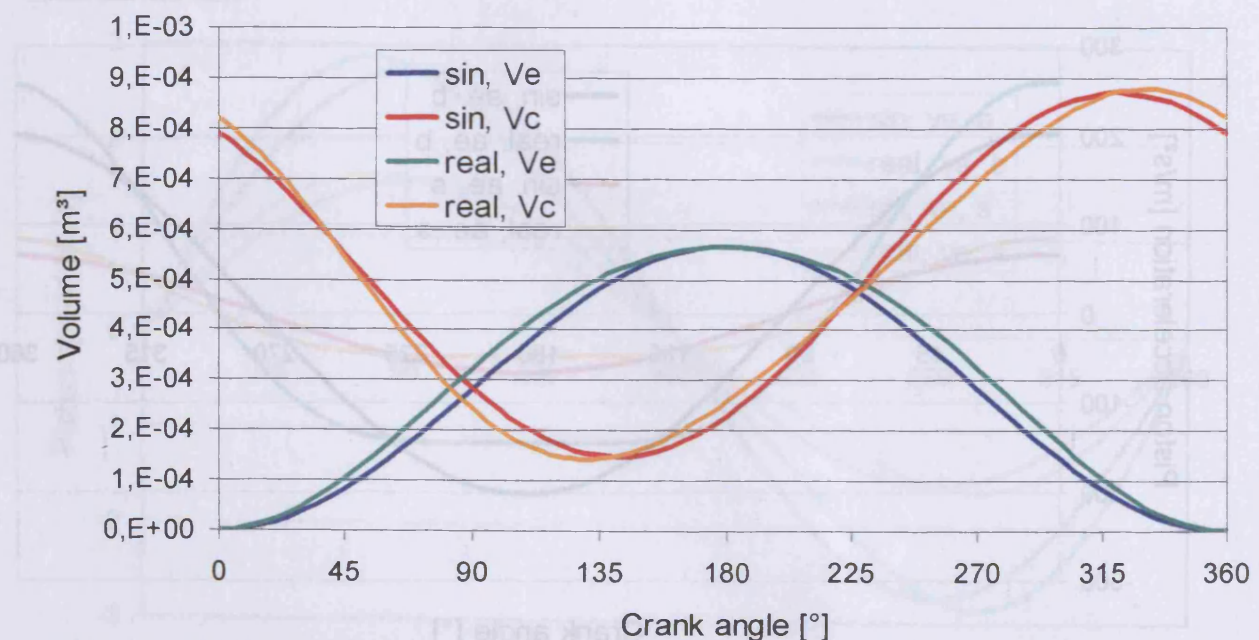
Figure 4-9: Expansion and Compression space volume for the biomass and solar engine

As in figure 4-4 these values are the same for the biomass and the solar engine because of the same geometry of the crank drive. Only the total volume (figure 4-10) differs because of the different dead volumes of the engines.
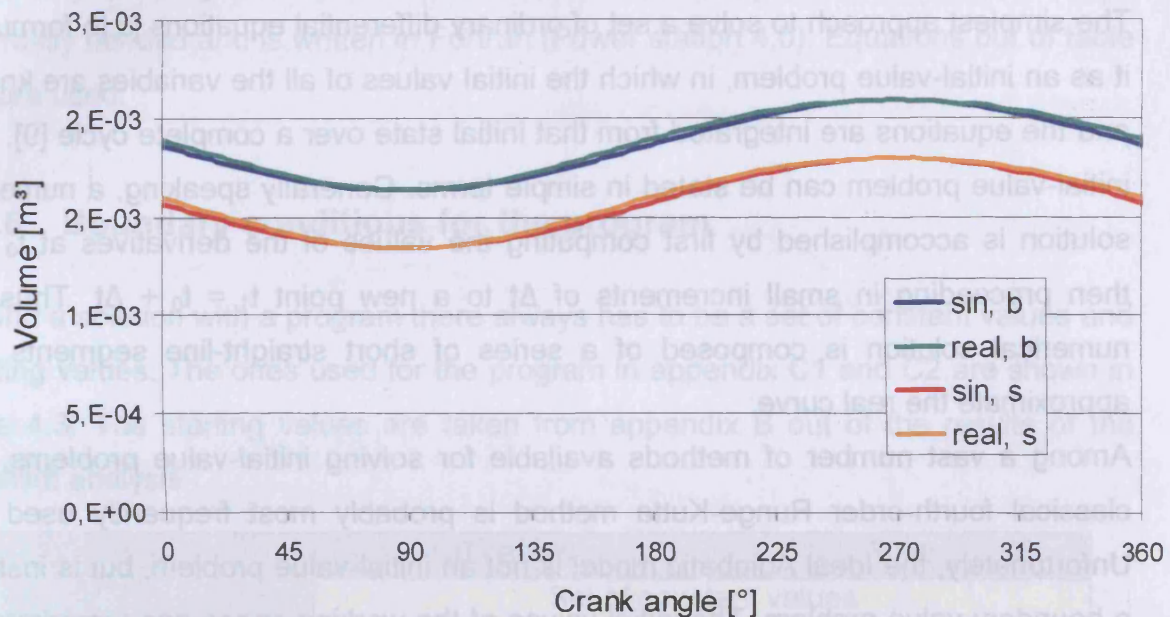
Figure 4-10: Total volume for the biomass and solar engine

In Figure 4-10 it can be seen that the maximum and minimum values of the total volume are the same. Thus the compression ratio calculated in section 2.7.3 remains without changes.

4.1.5   Program and method of solution of the equation set

Having derived the differential and algebraic equation set given in table 4.1 a solution is considered. Because of the non linear nature of the equation set a numerical solution of specific configurations and operating conditions is needed. Of the many equations listed in table 4.1, only six need to be integrated in order to obtain the solutions, these being the differential equations for the following variables:

p	the working gas pressure of the system
m_c	the mass of the gas in the compression space
W	the accumulated work done by the engine
Q_k	the accumulated heat transferred to the gas in the cooler
Q_r	the accumulated heat transferred to the gas in the regenerator
Q_h	the accumulated heat transferred to the gas in the heater

113

Of these, only the two differential equations in the variables p and m_c are independent and need to be solved simultaneously with the algebraic equations. The four energy derivatives can be solved by direct numerical integration after the rest of the equations have been solved.

The simplest approach to solve a set of ordinary differential equations is to formulate it as an initial-value problem, in which the initial values of all the variables are known and the equations are integrated from that initial state over a complete cycle [9]. The initial-value problem can be stated in simple terms. Generally speaking, a numerical solution is accomplished by first computing the values of the derivatives at t_0 and then proceeding in small increments of Δt to a new point $t_1 = t_0 + \Delta t$. Thus the numerical solution is composed of a series of short straight-line segments that approximate the real curve.

Among a vast number of methods available for solving initial-value problems, the classical fourth-order Runge-Kutta method is probably most frequently used [9]. Unfortunately, the Ideal Adiabatic model is not an initial-value problem, but is instead a boundary-value problem. The initial values of the working space gas temperatures T_c and T_e, are not known, because they result from adiabatic compression and enthalpy flow processes. The only guidance to their correct choice is that their values at the end of the steady state cycle should be equal to their values at the beginning of the cycle. Because of its cyclic nature, the system can be formulated as an initial-value problem by assigning arbitrary initial conditions and integrating the equations through several complete cycles until a cyclic steady state has been achieved. This is equivalent to the transient "warm-up" operation of an actual machine in which it will start from the stationary state, with T_c and T_e at ambient or any arbitrary initial temperature values and go through successive transient cycles until the values of all the state variables at the end of each cycle are equal to their values at the beginning of the cycle. Experience has shown that the most sensitive measure of convergence to cyclic steady state is the residual regenerator heat Q_r at the end of the cycle, which must be zero [9].

The compression and expansion space temperatures are initially specified at T_k and T_h respectively. The system of equations can then be solved through as many cycles as necessary in order to attain cyclic steady state. In the program presented in appendix C 1 and C2 about 100 cycles are needed to get good steady state values.

Many programs for second order calculation already exist, especially these developed by I. Urieli [9], who wrote programs in Fortran 90 and Matlab. These programs are very complex and contain numerous subroutines that are not essential. For clarity the program that is shown in appendix C1 only consists of the parts that are really needed and is written in Fortran (Power station 4.0). Equations out of table 4.1 are used.

4.1.6 Boundary conditions for the program

To find a solution with a program there always has to be a set of constant values and starting values. The ones used for the program in appendix C1 and C2 are shown in table 4.3. The starting values are taken from appendix B out of the results of the Schmidt analysis

		Biomass	Solar
		Set of constant values	
R	[J/kg/K]	287,1	
κ	[-]	1,4	
ρ	[°]	90	
V_{se}	[m³]	5,65E-4	
V_{sc}	[m³]	4,51E-4	
V_{de}	[m³]	0,28E-4	
V_{dc}	[m³]	0,04E-4	
V_r	[m³]	1,50E-4	
V_h	[m³]	5,44E-4	2,50E-4
V_k	[m³]	3,79E-4	
m_{gas}	[kg]	18,6E-3	11,7E-3
T_r	[K]	663,11	463,76
T_h	[K]	1'173,00	628,00
T_k	[K]	328,00	331,00
		Starting values	
T_c	[K]	300	300
T_e	[K]	800	500
T_{ck}		=Tc	
T_{he}		=Te	
p	[N/m²]	125'5940,8	791'519,3
m_c	[kg]	6,4E-3	4,3E-3

Table 4.3: Constant and starting values for the program

4.1.7   Results for the experimental engines

4.1.7.1 Convergence behaviour

Figure 4-11 and 4-12 show the convergence behaviour of the program for the ideal adiabatic analysis. It can be clearly seen, that after only about eight iterations all the values reach their stable state. Figures are only shown for the solar engine, because there is no difference to the biomass engine.
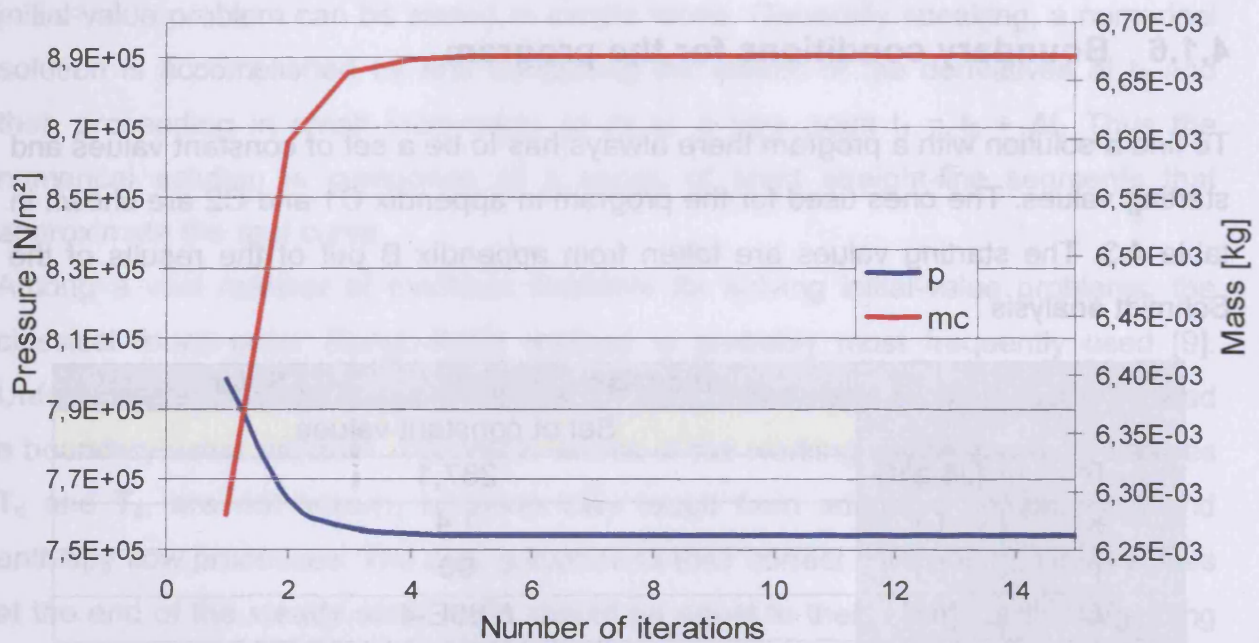
Figure 4-11: Convergence behaviour for the pressure and compression space mass of the solar engine
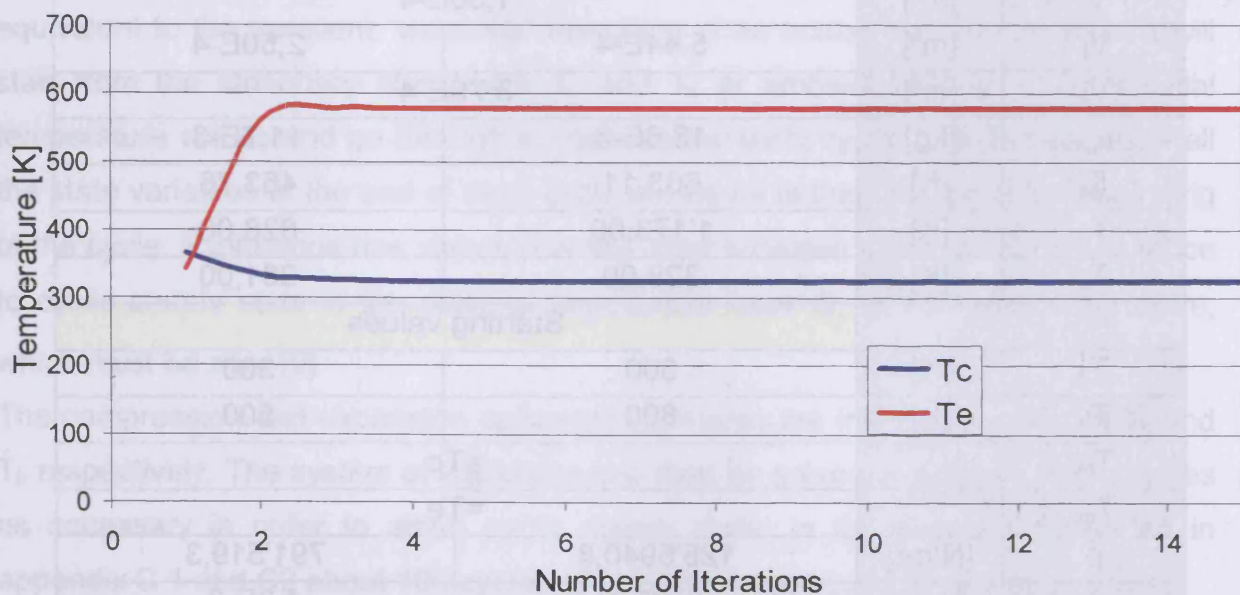
Figure 4-12: Convergence behaviour for T$_c$ and T$_e$ of the solar engine

116

In the following sections the results of the programs are shown and interpreted for the solar and biomass engine. These values are further required as initial values for the adiabatic analysis with losses, as boundary conditions of the CFD analysis in chapter 5 and as comparative values for the measurements.

4.1.7.2 Pressure as a function of the crank angle
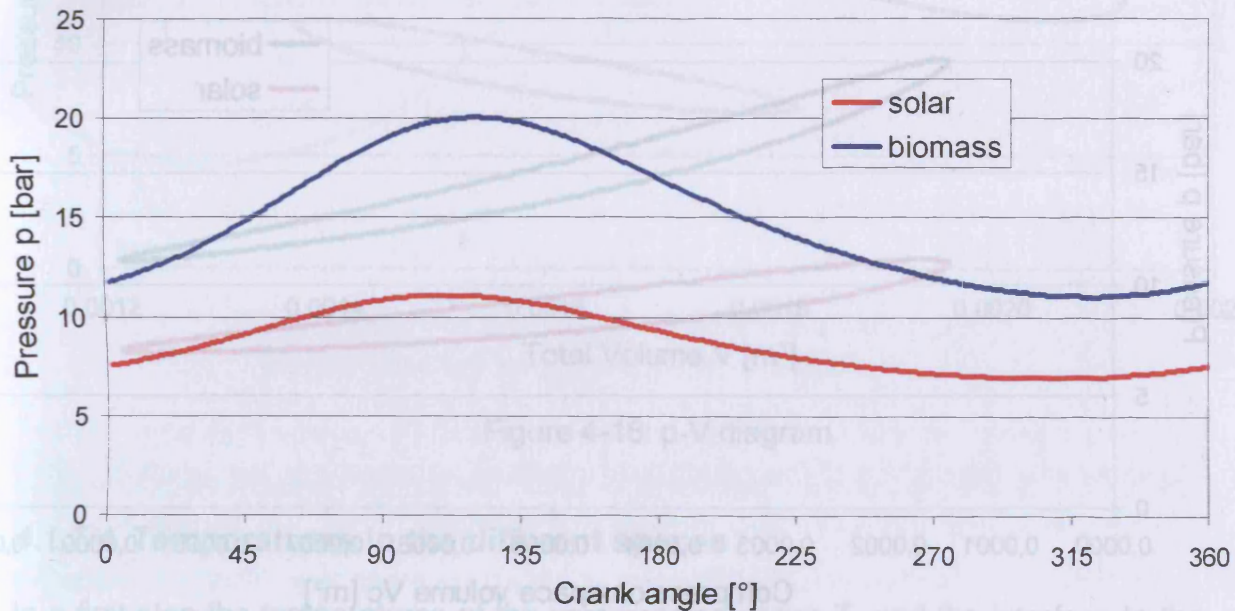
Figure 4-13: Pressure as a function of the crank angle

Figure 4-13 shows the pressure as a function of the crank angle. As characteristic values of the process the minimum, average and maximum values of the pressure are as follows.

$$p_{m,s} = 8{,}717 bar \tag{4.52}$$

$$p_{m,b} = 14{,}923 bar \tag{4.53}$$

$$p_{max,s} = 11{,}115 bar \tag{4.54}$$

$$p_{max,b} = 20{,}060 bar \tag{4.55}$$

$$p_{min,s} = 6{,}930 bar \tag{4.56}$$

$$p_{min,b} = 11{,}032 bar \tag{4.57}$$

4.1.7.3 p-V diagrams

Calculating the volumes with the equations from section 4.1.4 and taking the pressure as a function of the crank angle into consideration, p-V diagrams for the compression space, expansion space and total volume (figure 4-14 to 4-16) can be generated for both engines.
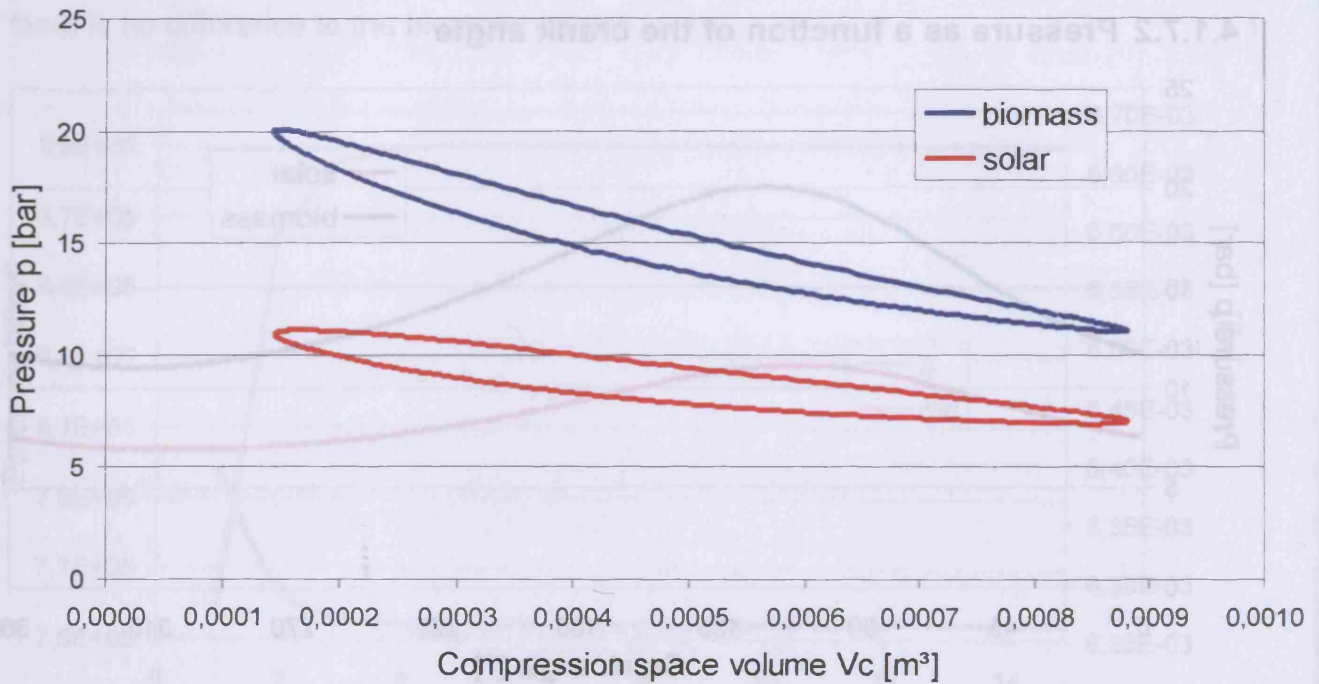
Figure 4-14: p-V$_c$ diagram
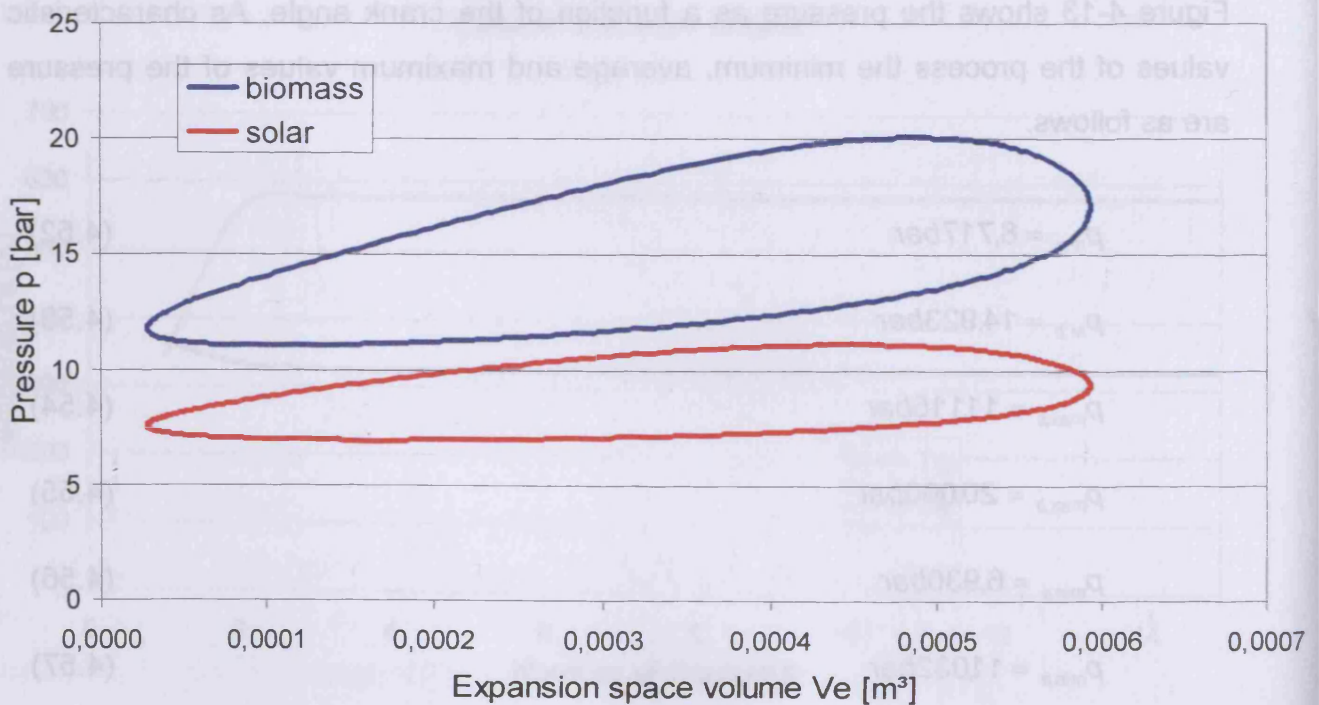
Figure 4-15: p-V$_e$ diagram

118
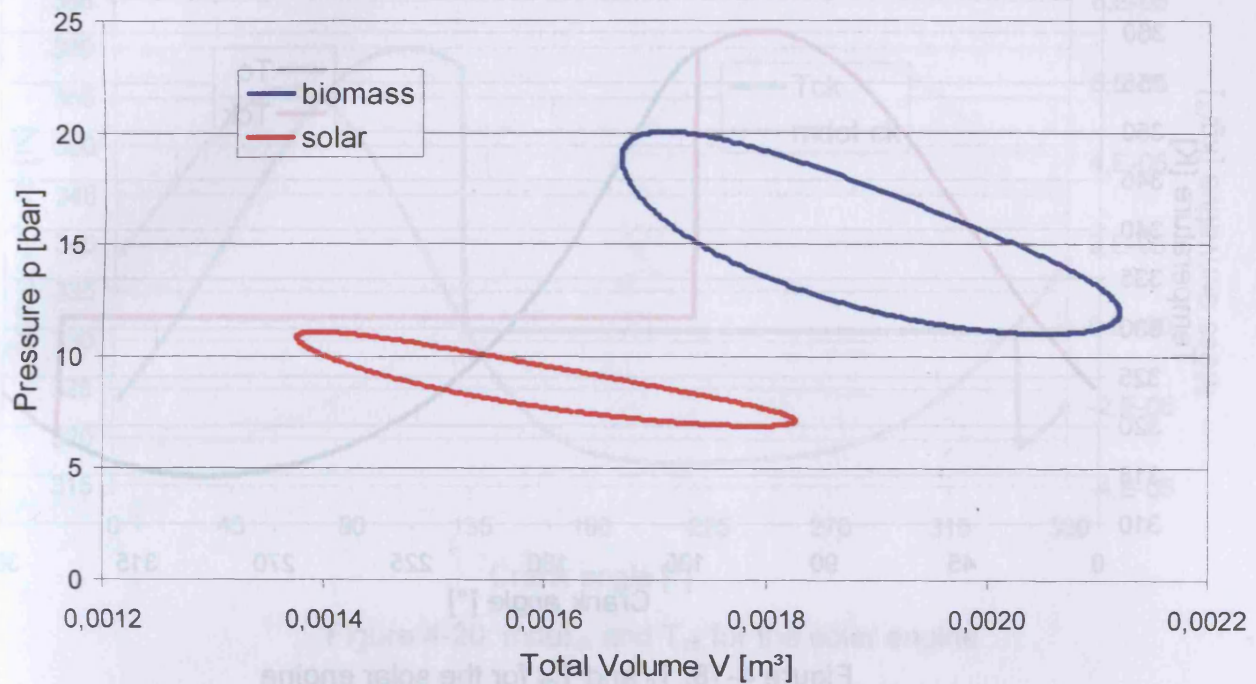
Figure 4-16: p-V diagram

4.1.7.4 Temperatures in the different spaces

In a first step the temperatures of the compression space T_c and the interface to the cooler T_{ck} are shown in figure 4-17 for the biomass engine and in figure 4-18 for the solar engine.
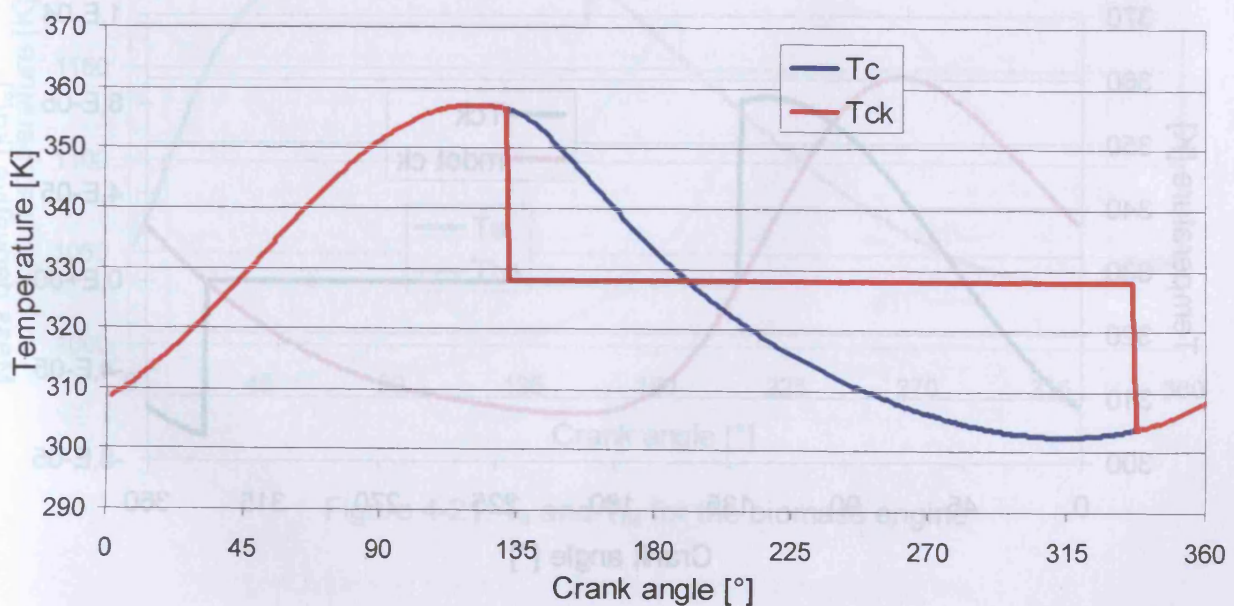
Figure 4-17: T_c and T_{ck} for the biomass engine
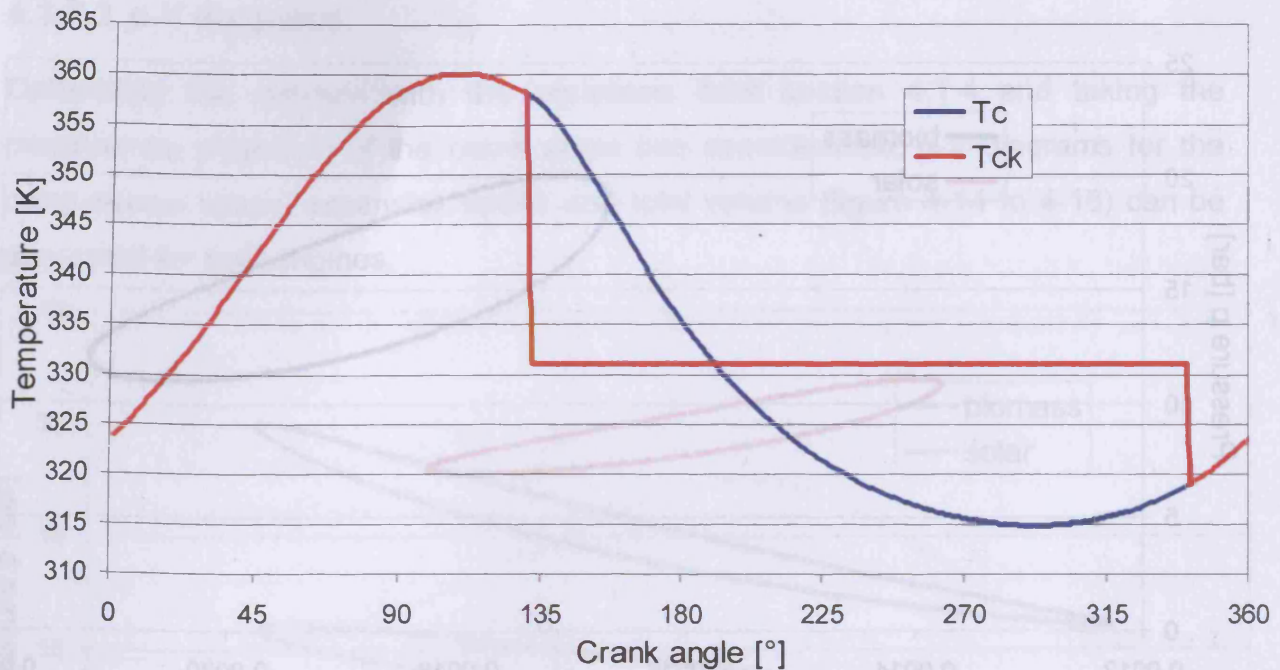
Figure 4-18: T_c and T_{ck} for the solar engine

To show why the curves of the conditional interface temperatures are unsteady they are combined with the mass flow through this interface (mdot$_{ck}$) in figures 4-19 and 4-20. It can be clearly seen that in case of changing mass flow direction (negative values turn positive and vice versa) the interface does not take the working spaces temperature any more, but the constant temperature of the heat exchangers.
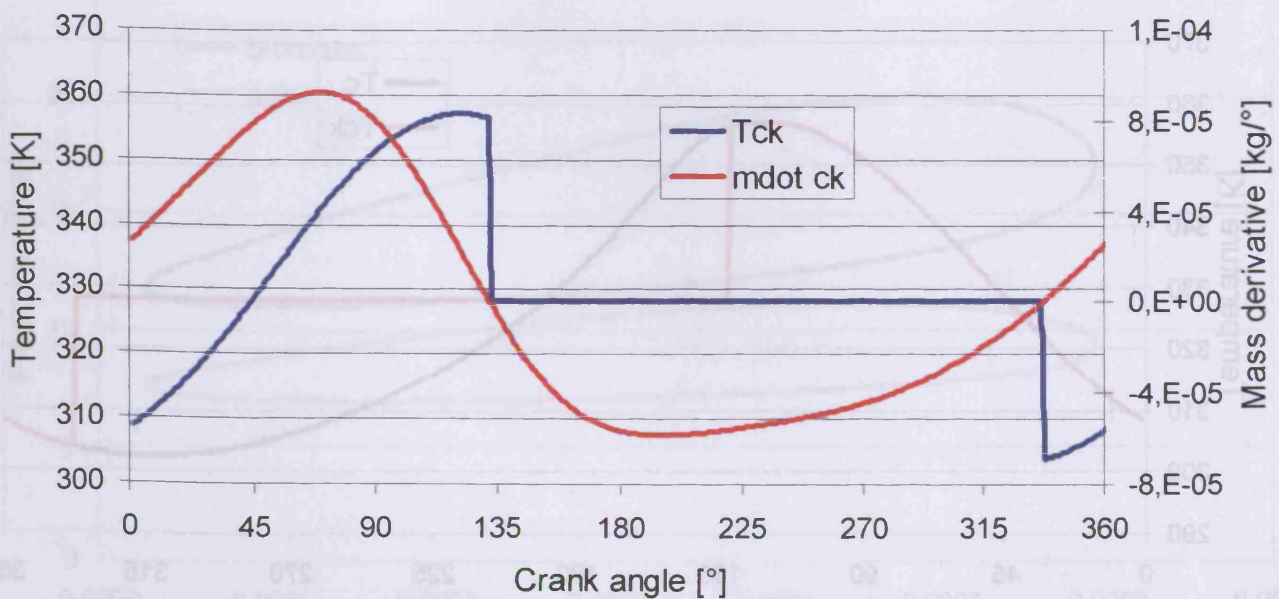
Figure 4-19: mdot$_{ck}$ and T_{ck} for the biomass engine

120
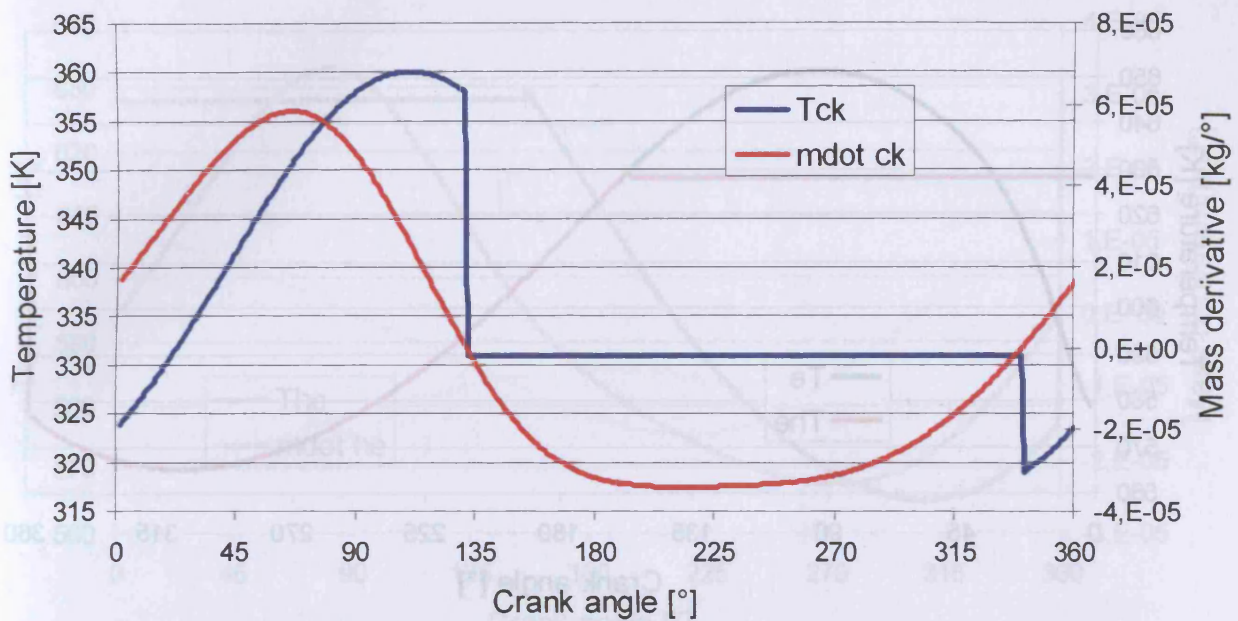
Figure 4-20: mdot$_{ck}$ and T$_{ck}$ for the solar engine

For the expansion space and its interface to the heater basically the same figures are shown in the following (figures 4-21 and 4-23 for the biomass engine and 4-22 and 4-24 for the solar engine).
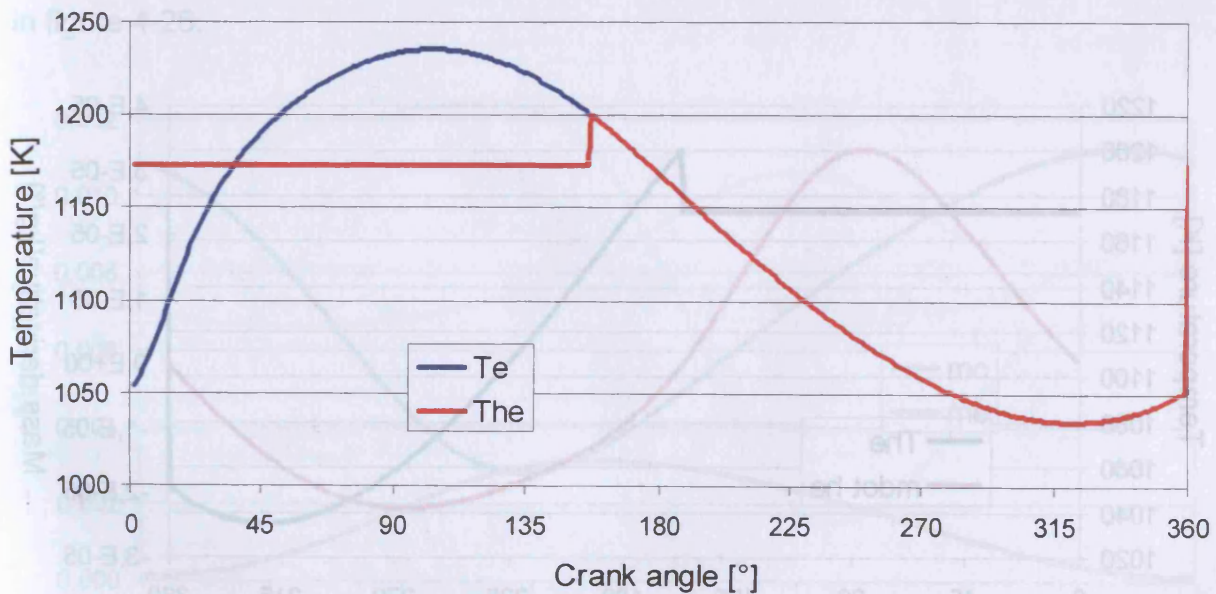
Figure 4-21: T$_e$ and T$_{he}$ for the biomass engine
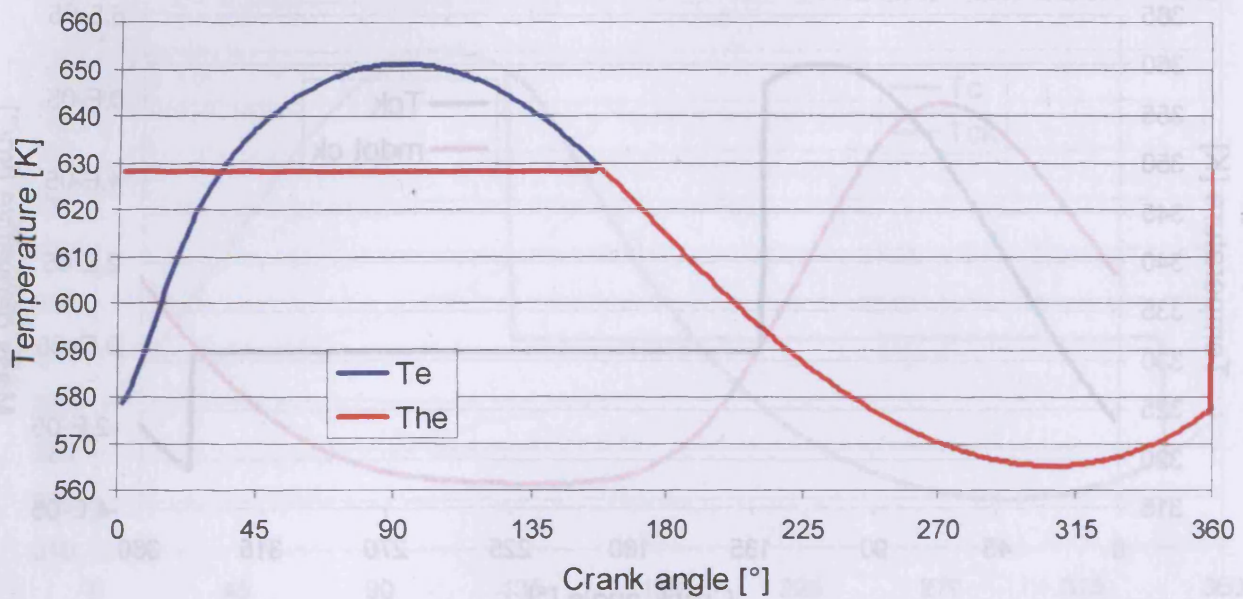
Figure 4-22: T_e and T_{he} for the solar engine

When the crank angle reaches the value 0°, the volume and mass in the expansion space also become 0 and the temperature of the gas is not defined. To avoid unsteady areas in the figures 4-21 to 4-24 for the expansion space the dead volume of the swept volumes is taken into consideration. For this it is also useful to avoid the crank angle 0°, by calculating the values for -0,5° and 0,5° instead.
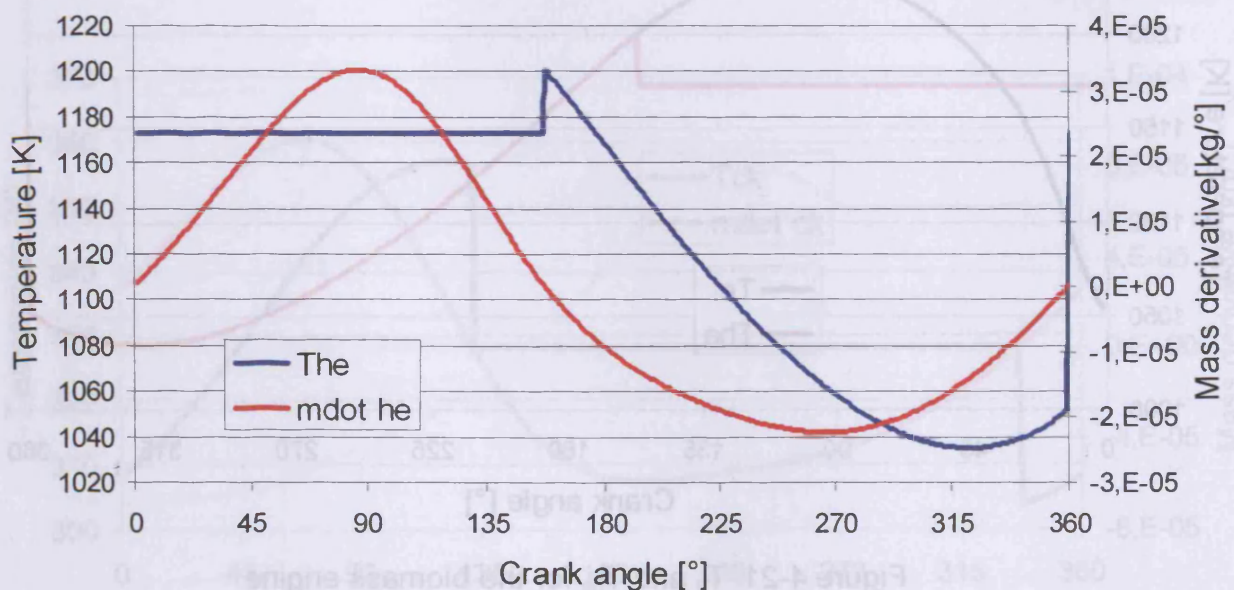
Figure 4-23: $mdot_{he}$ and T_{he} for the biomass engine

122
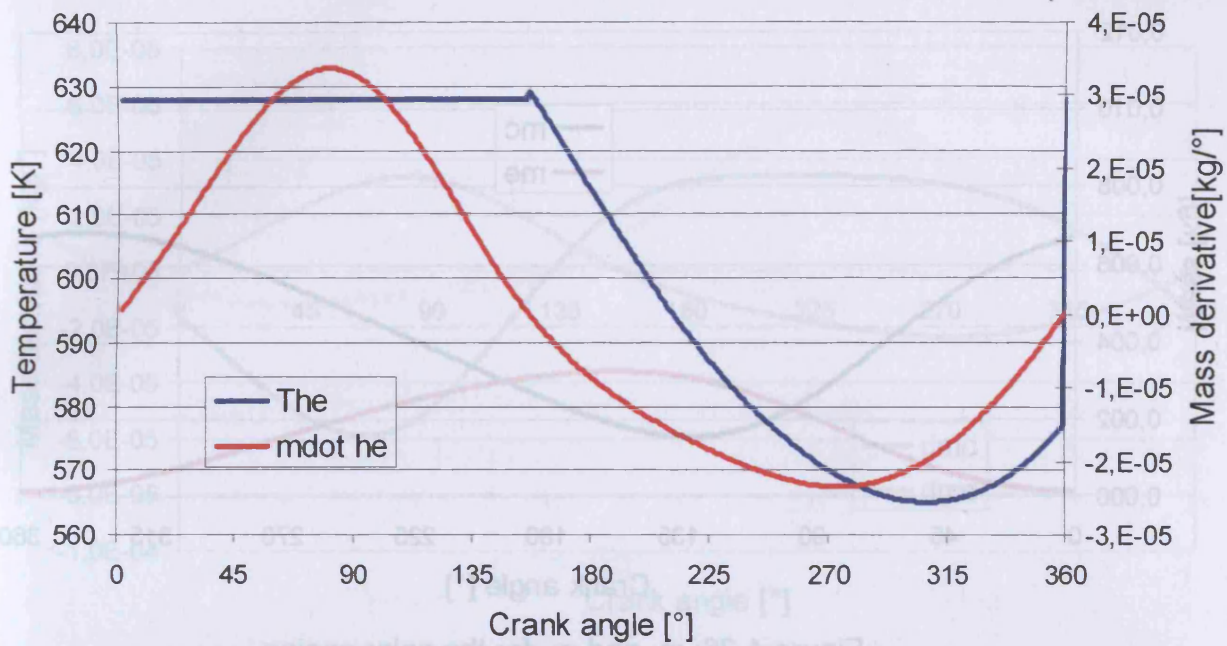
Figure 4-24: mdot$_{he}$ and T$_{he}$ for the solar engine

4.1.7.5 Masses and mass flows in the different spaces

In figure 4-25 the mass of working gas in the expansion and compression space is shown in comparison for the biomass engine. The same is done for the solar engine in figure 4-26.
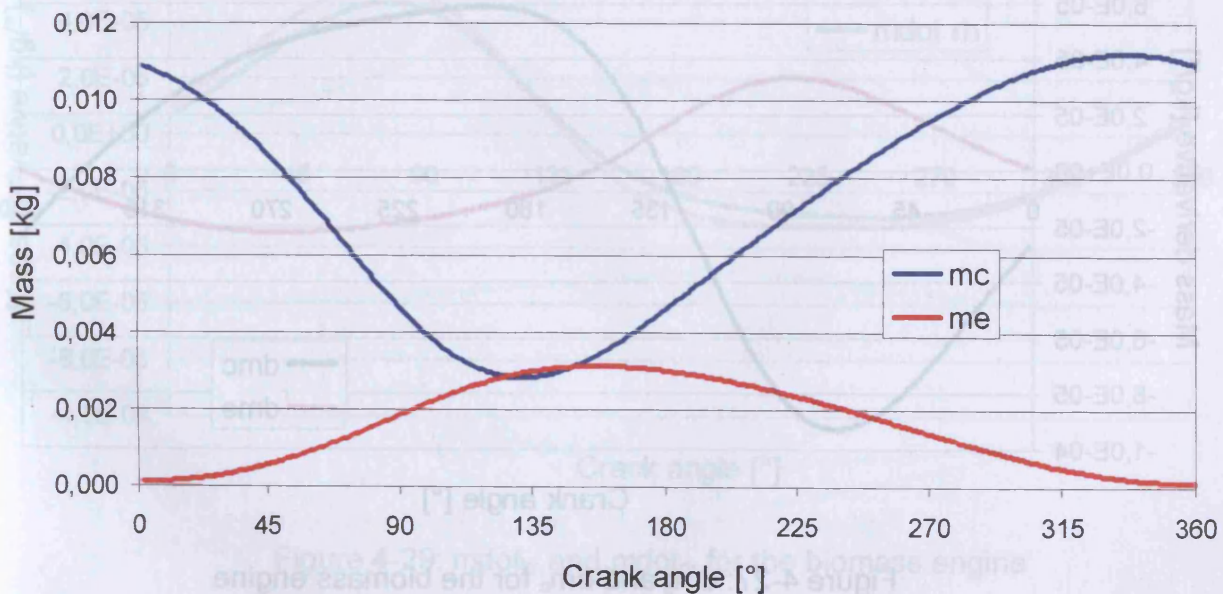
Figure 4-25: m$_e$ and m$_c$ for the biomass engine
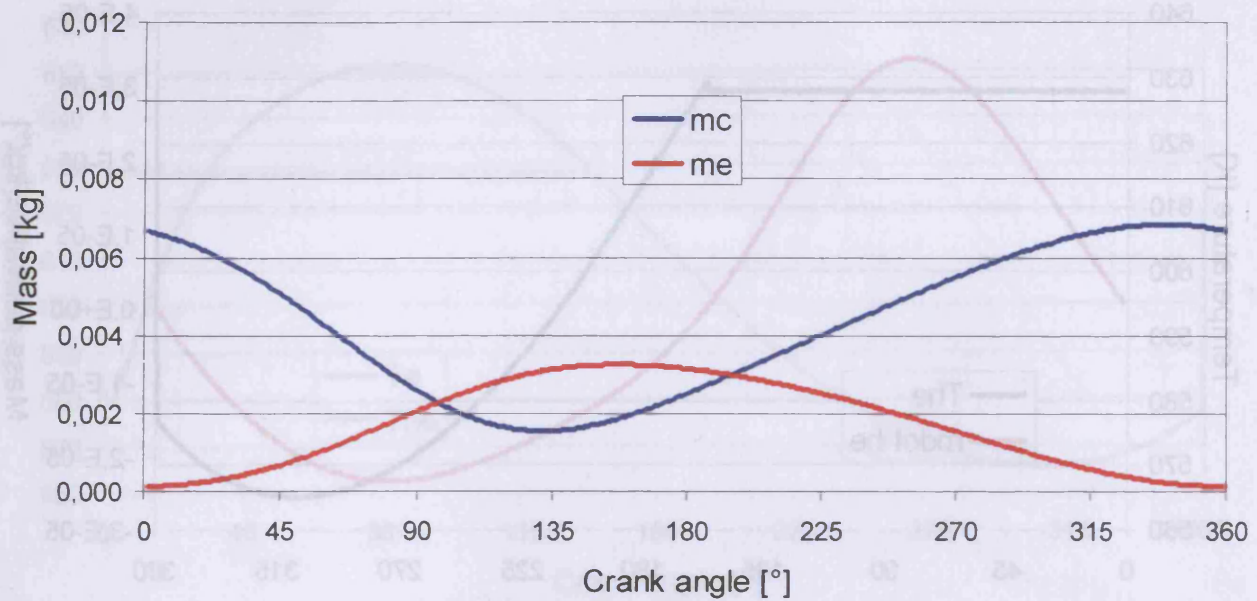
Figure 4-26: m_e and m_c for the solar engine

The mass derivatives dm_e and dm_c, shown in the following two figures (4-27 and 4-28), represent the mass flows through the surfaces between expansion space and heater ($mdot_{he}$) as well as for the mass flow from compression space to cooler ($mdot_{ck}$).
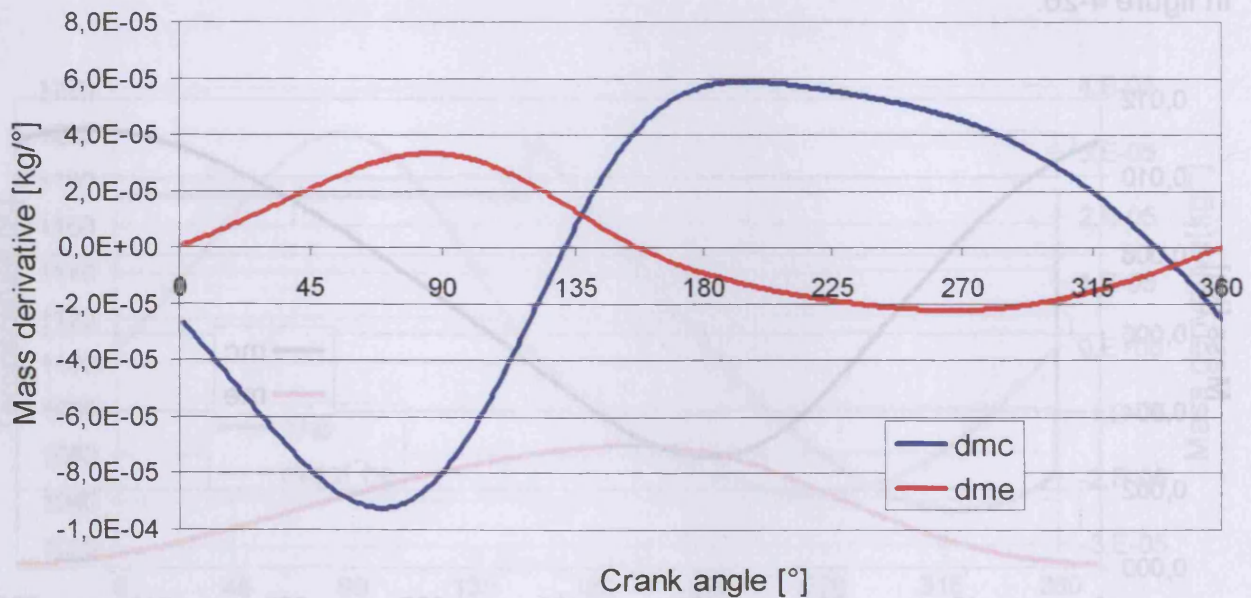
Figure 4-27: dm_e and dm_c for the biomass engine
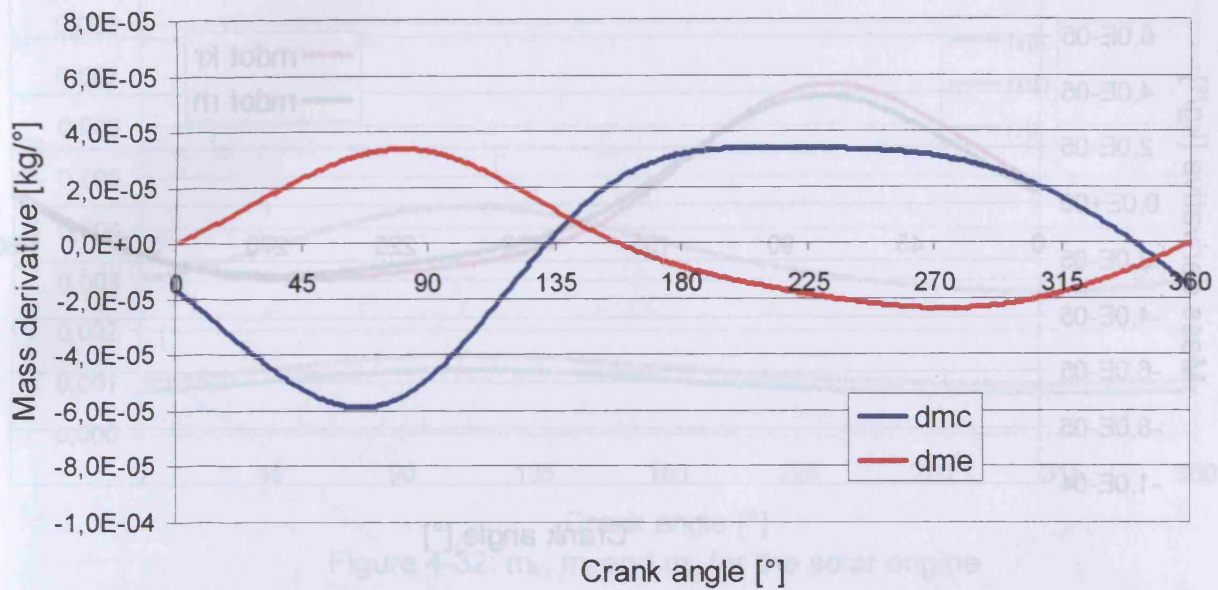
Figure 4-28: dm_e and dm_c for the solar engine

The mass flows through the surfaces between the cooler and regenerator and the regenerator and the heater (kr and rh) are shown in the figure 4-29 for the biomass engine and in figure 4-30 for the solar engine.
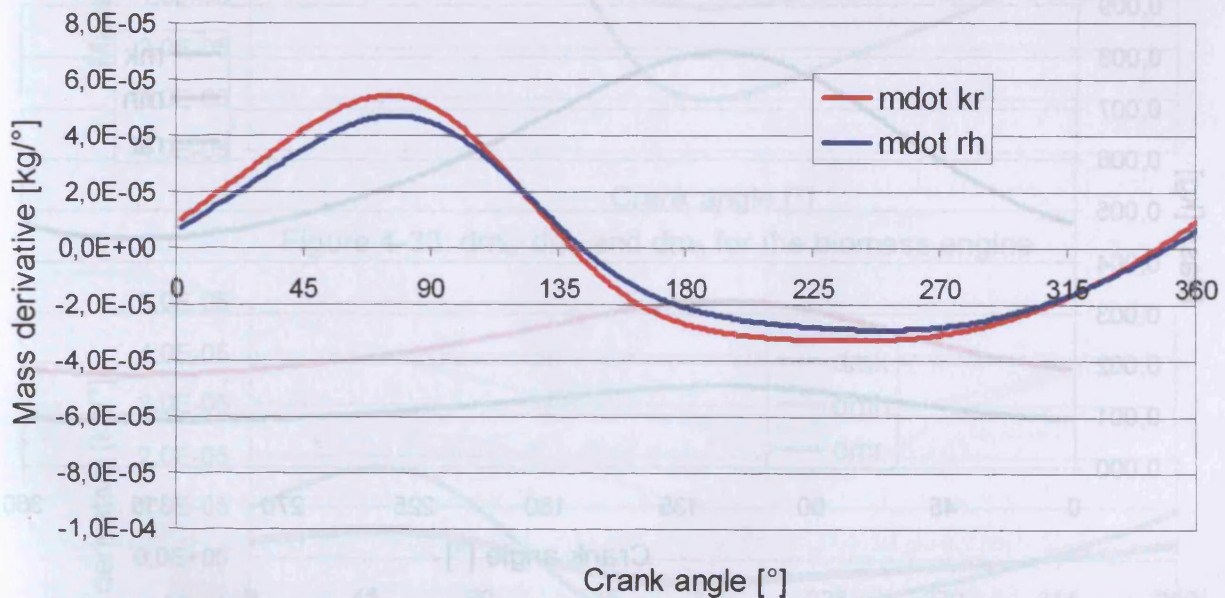
Figure 4-29: $mdot_{kr}$ and $mdot_{rh}$ for the biomass engine
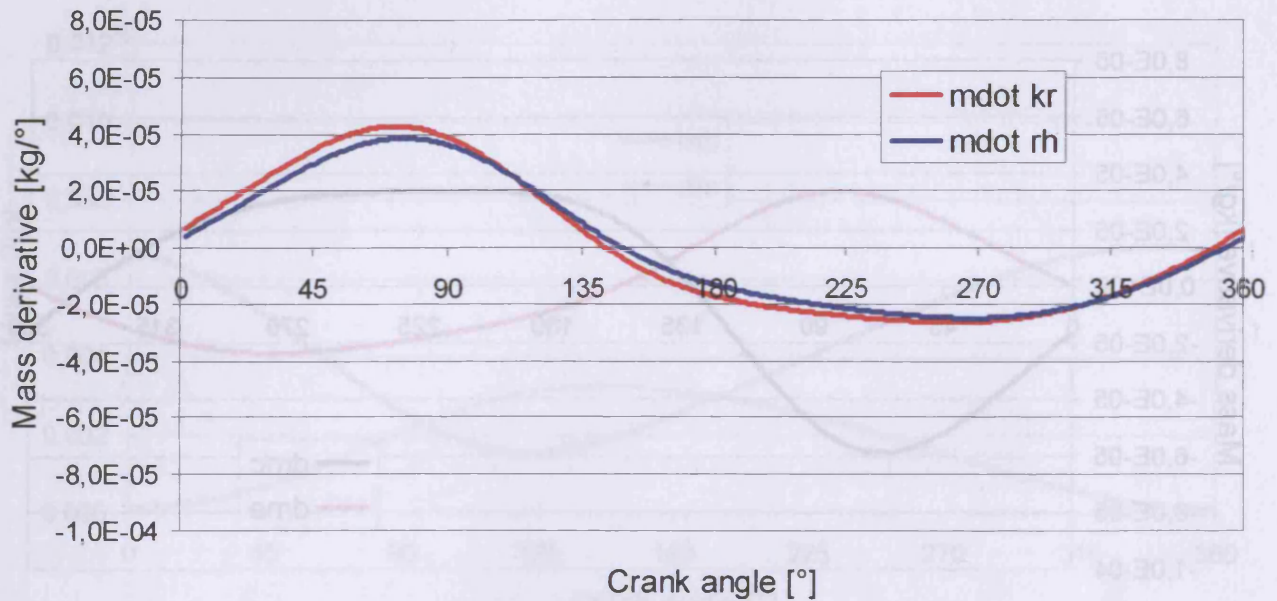
Figure 4-30: mdot$_{kr}$ and mdot$_{rh}$ for the solar engine

The absolute masses and their derivatives can not only be calculated for the working spaces, but also for the dead spaces like heater, regenerator and cooler, as shown in the following figures (4-31 to 4-34).
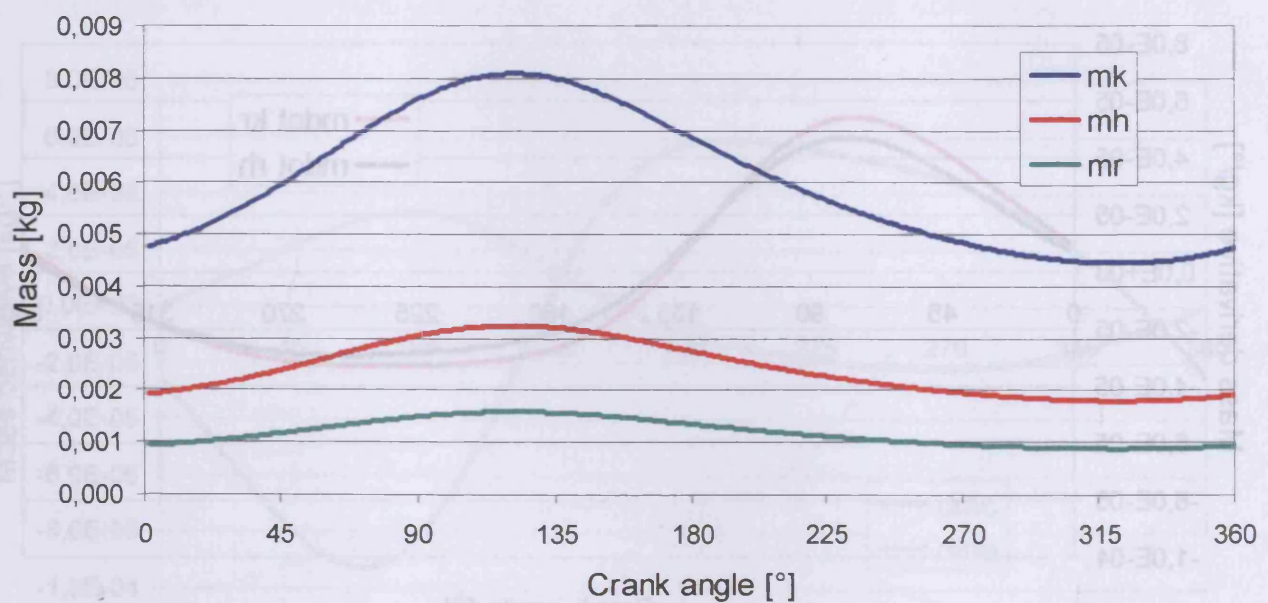
Figure 4-31: m$_k$, m$_r$ and m$_h$ for the biomass engine
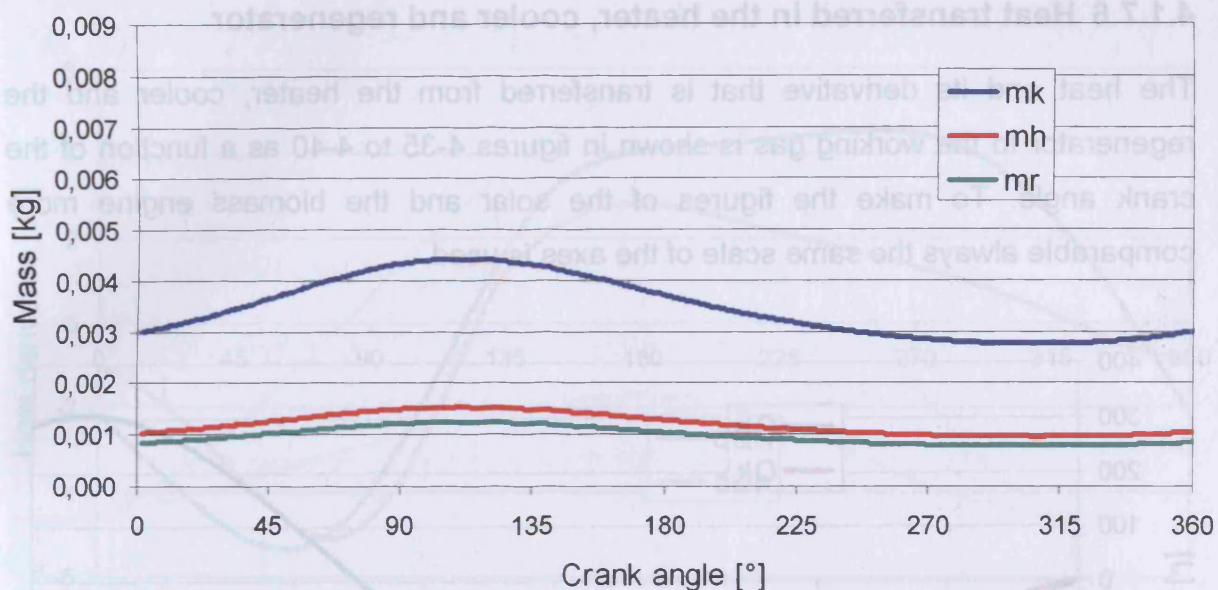
Figure 4-32: m_k, m_r and m_h for the solar engine
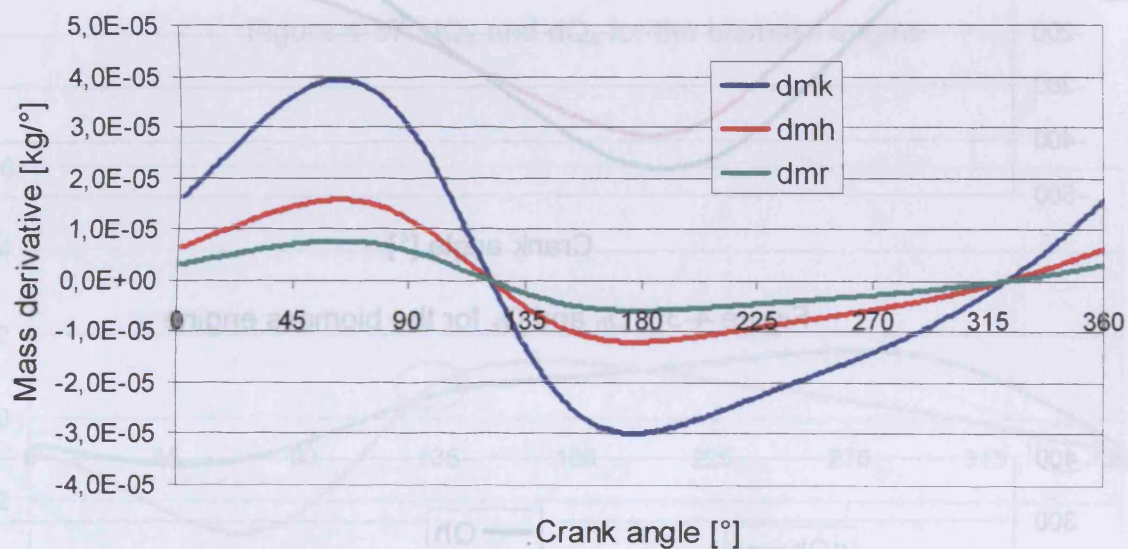
Figure 4-33: dm_k, dm_r and dm_h for the biomass engine
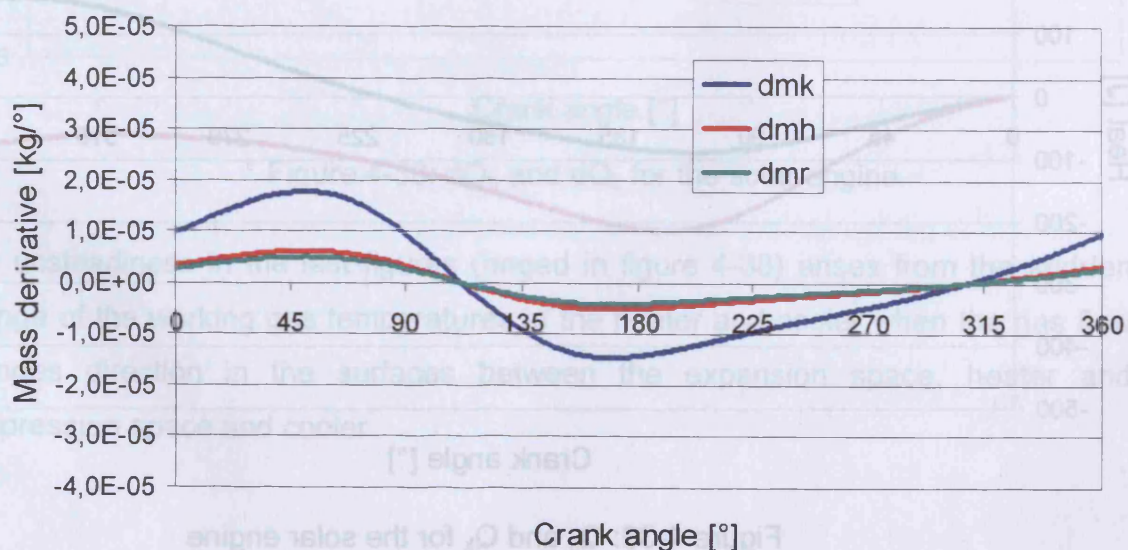
Figure 4-34: dm_k, dm_r and dm_h for the solar engine

127

4.1.7.6 Heat transferred in the heater, cooler and regenerator

The heat and its derivative that is transferred from the heater, cooler and the regenerator to the working gas is shown in figures 4-35 to 4-40 as a function of the crank angle. To make the figures of the solar and the biomass engine more comparable always the same scale of the axes is used.
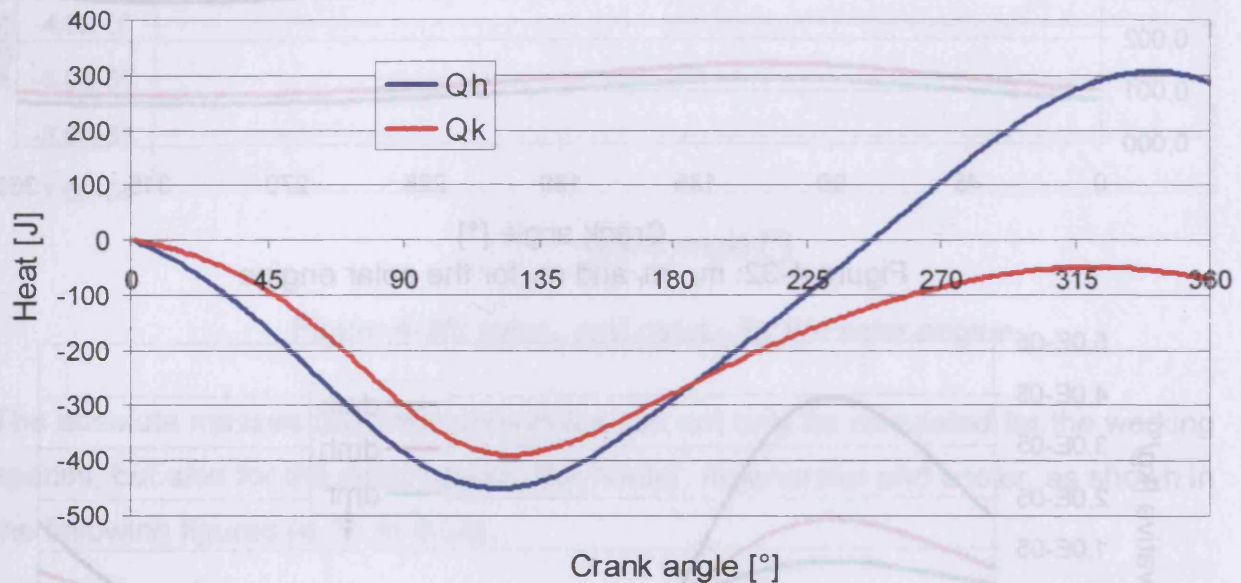
Figure 4-35: Q_h and Q_k for the biomass engine
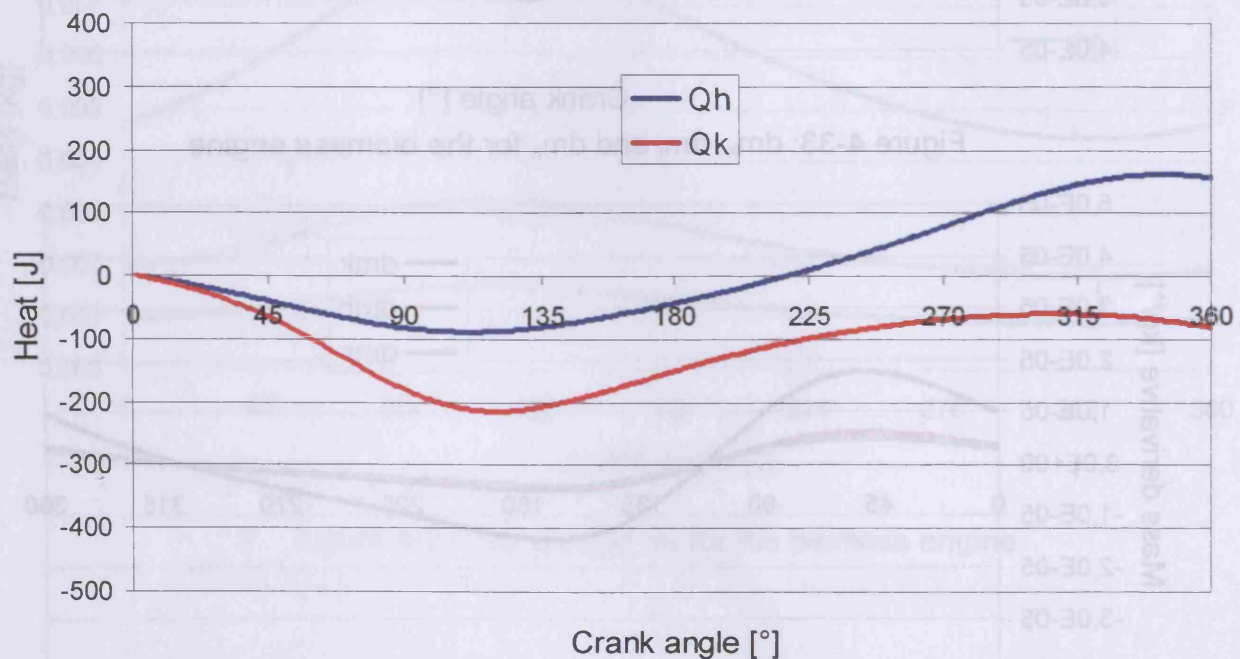
Figure 4-36: Q_h and Q_k for the solar engine
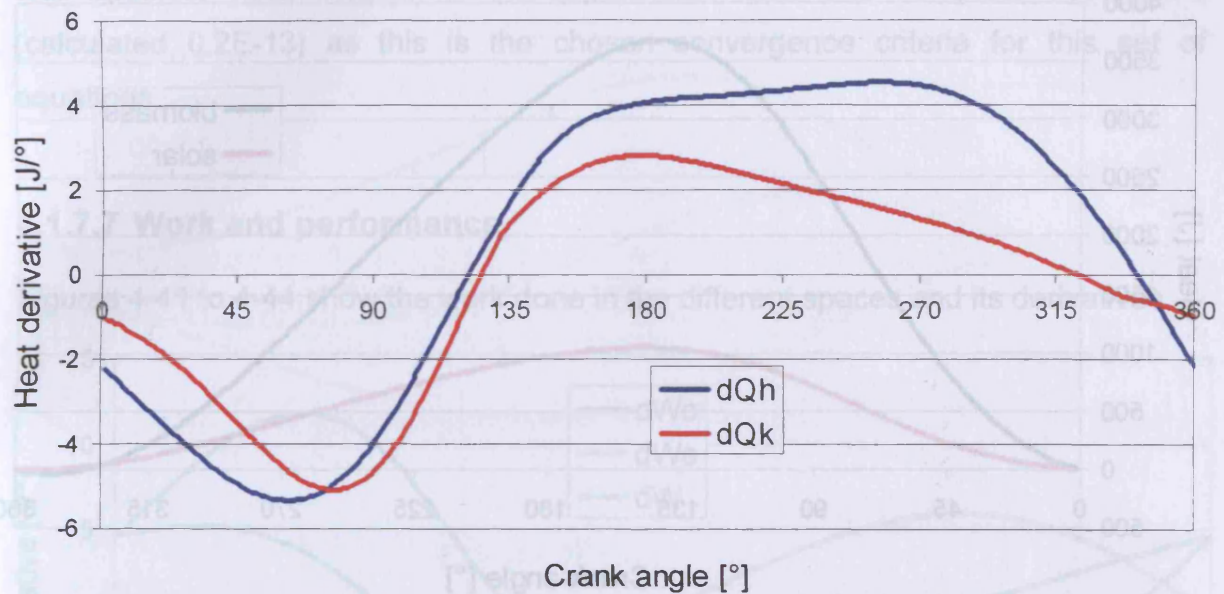
Figure 4-37: dQ$_h$ and dQ$_k$ for the biomass engine
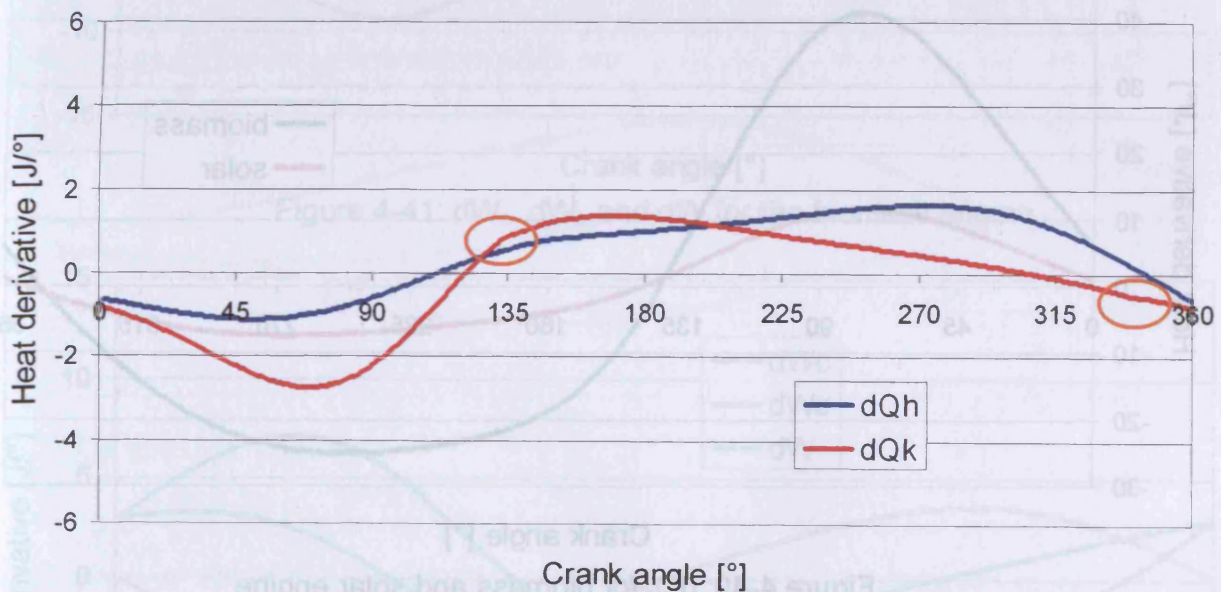
Figure 4-38: dQ$_h$ and dQ$_k$ for the solar engine

The unsteadiness in the last figures (ringed in figure 4-38) arises from the sudden change of the working gas temperatures in the heater and cooler when the gas flow changes direction in the surfaces between the expansion space, heater and compression space and cooler.
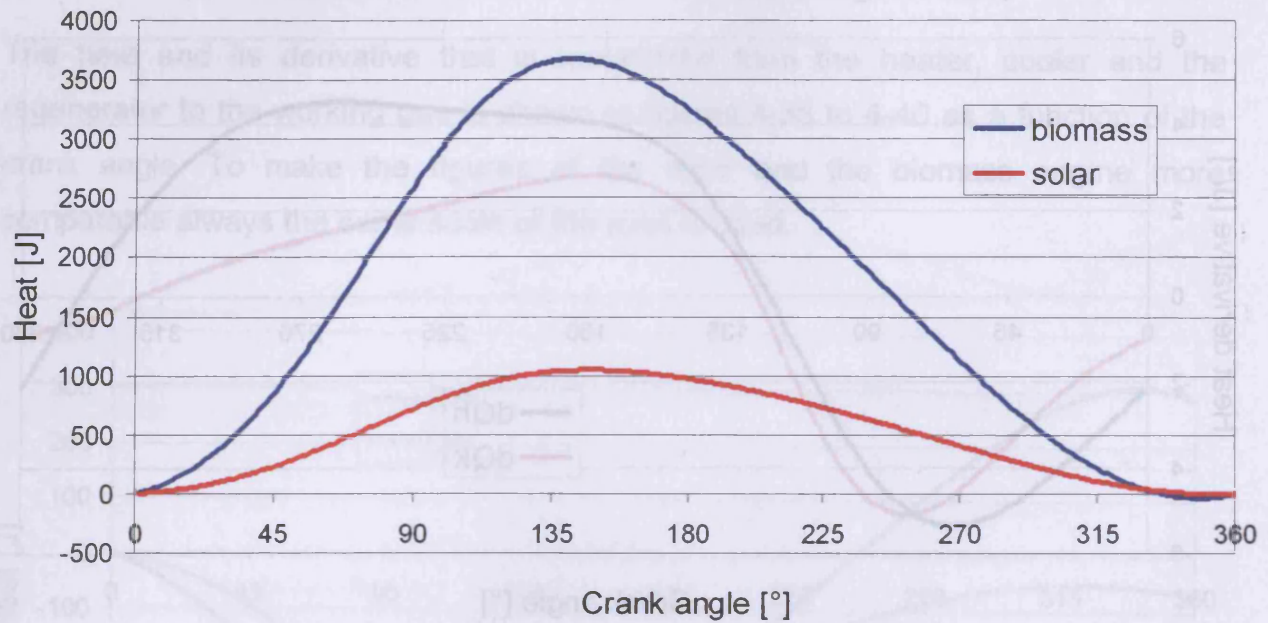
Figure 4-39: Q$_r$ for biomass and solar engine
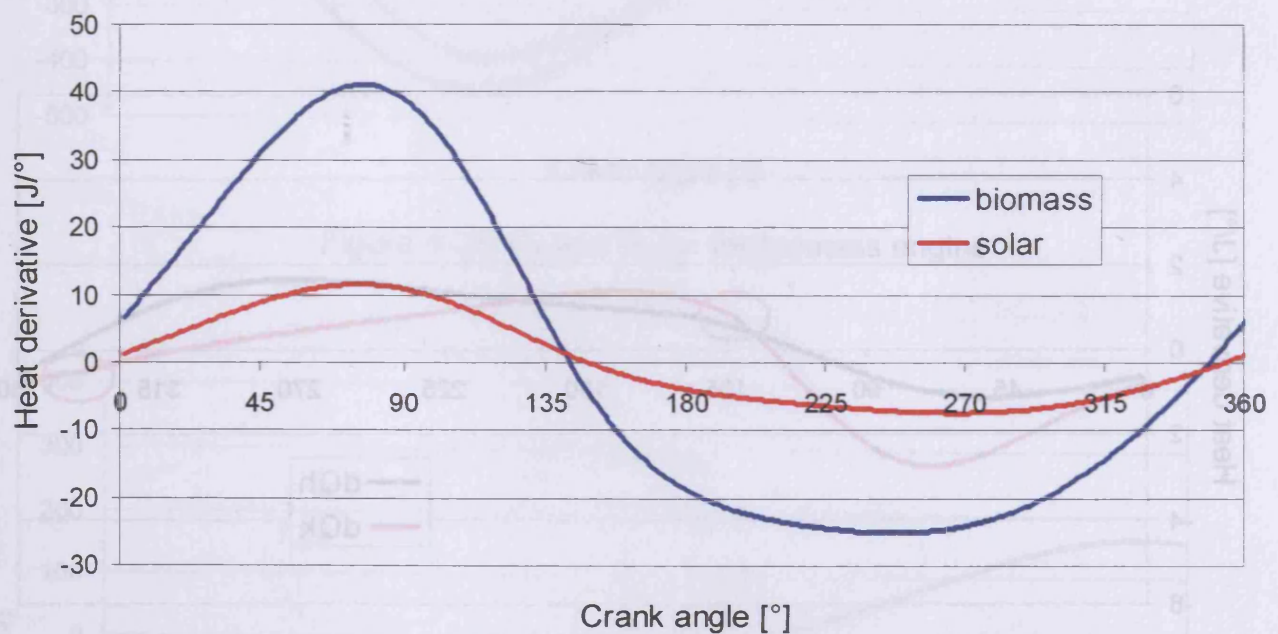
Figure 4-40: dQ$_r$ for biomass and solar engine

In addition to the figures the absolute values for the transferred heats are:

$$Q_{h,s} = 155{,}58\,J \tag{4.58}$$

$$Q_{h,b} = 283{,}75\,J \tag{4.59}$$

$$Q_{k,s} = -82{,}44\,J \tag{4.60}$$

$$Q_{k,b} = -71{,}66\,J \tag{4.61}$$

The absolute heat transfer of the regenerator over one complete cycle is 0 (calculated 0,2E-13) as this is the chosen convergence criteria for this set of equations.

4.1.7.7 Work and performance

Figures 4-41 to 4-44 show the work done in the different spaces and its derivatives.
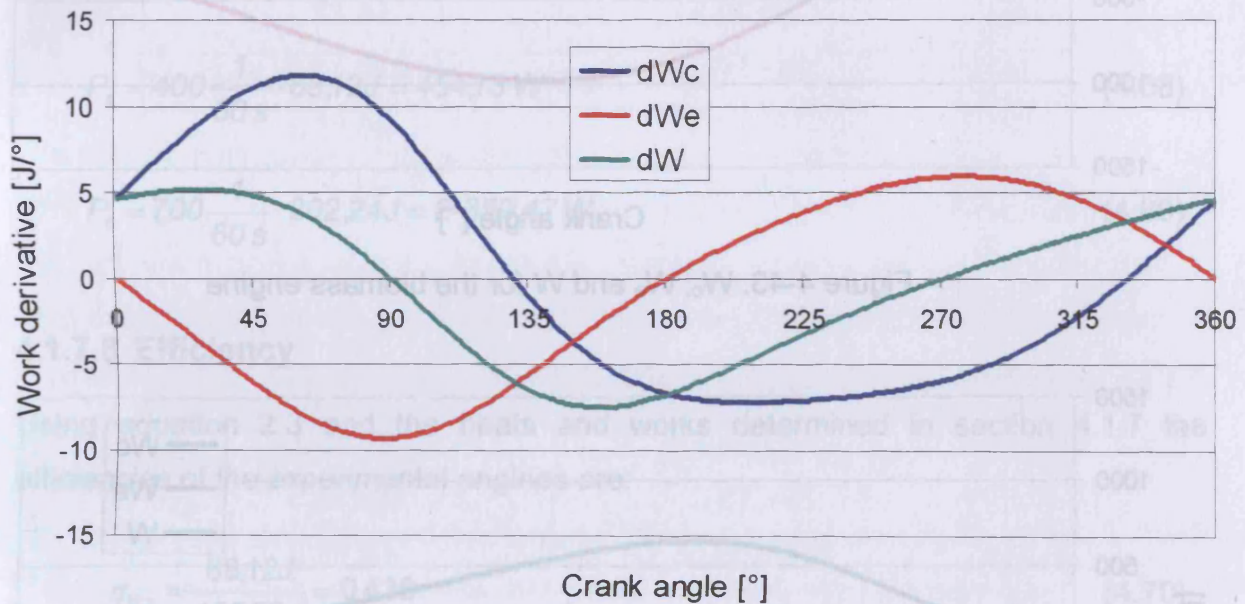
Figure 4-41: dW_c, dW_e and dW for the biomass engine
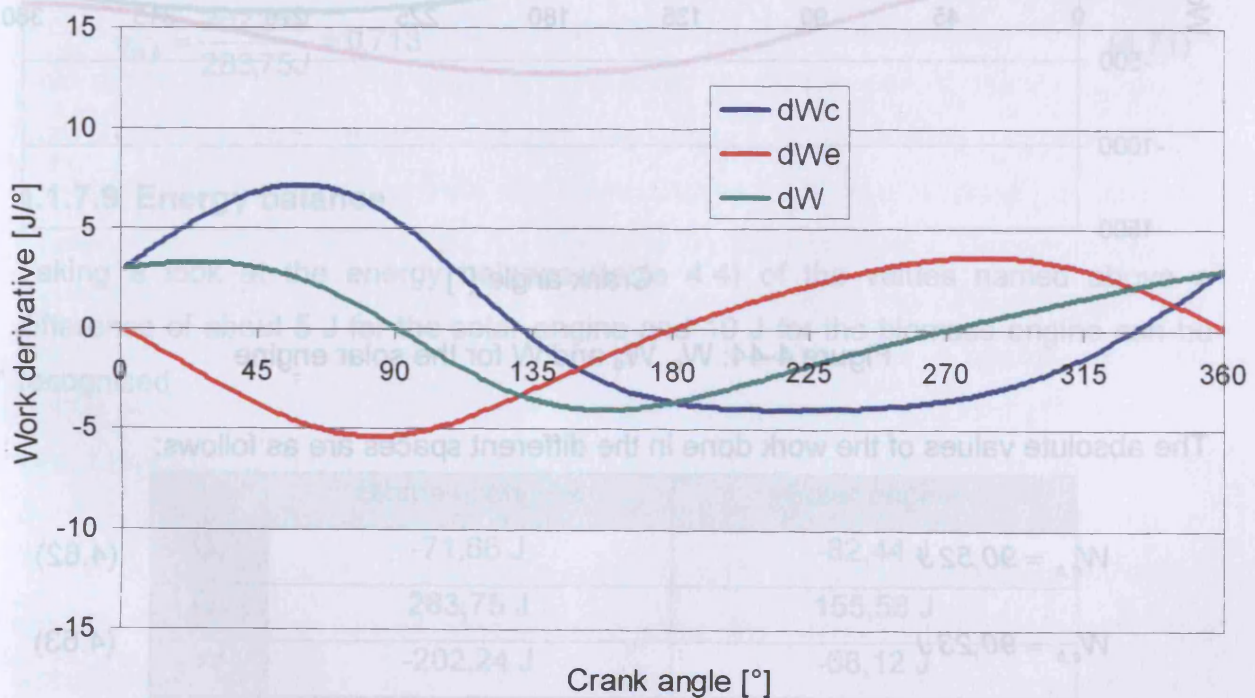
Figure 4-42: dW_c, dW_e and dW for the solar engine

131
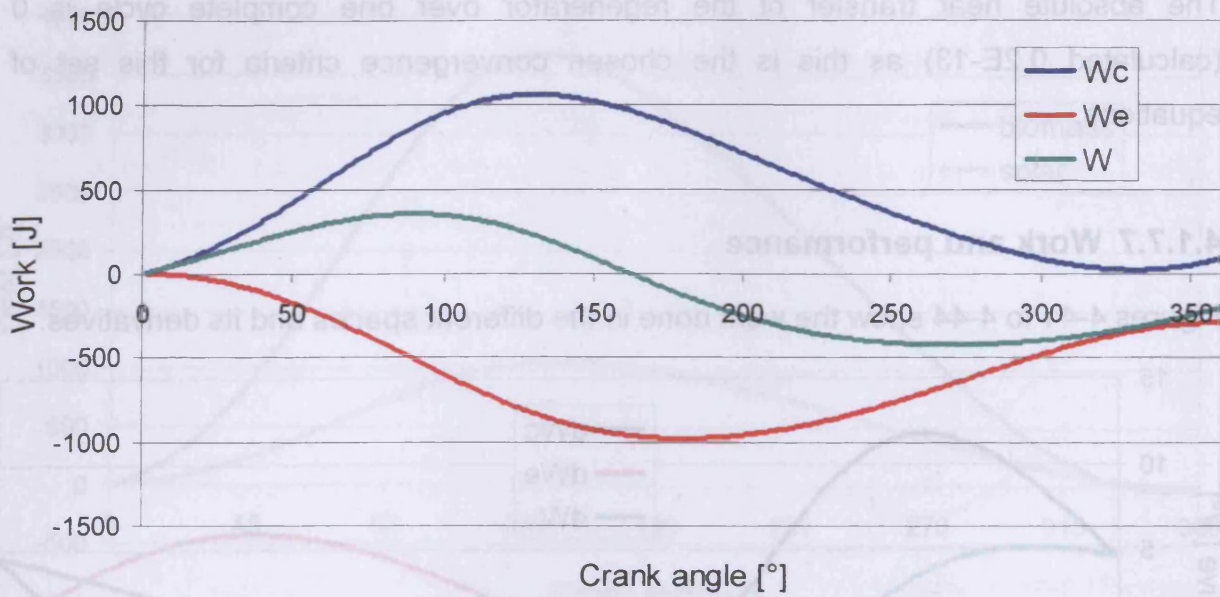
Figure 4-43: W_c, W_e and W for the biomass engine
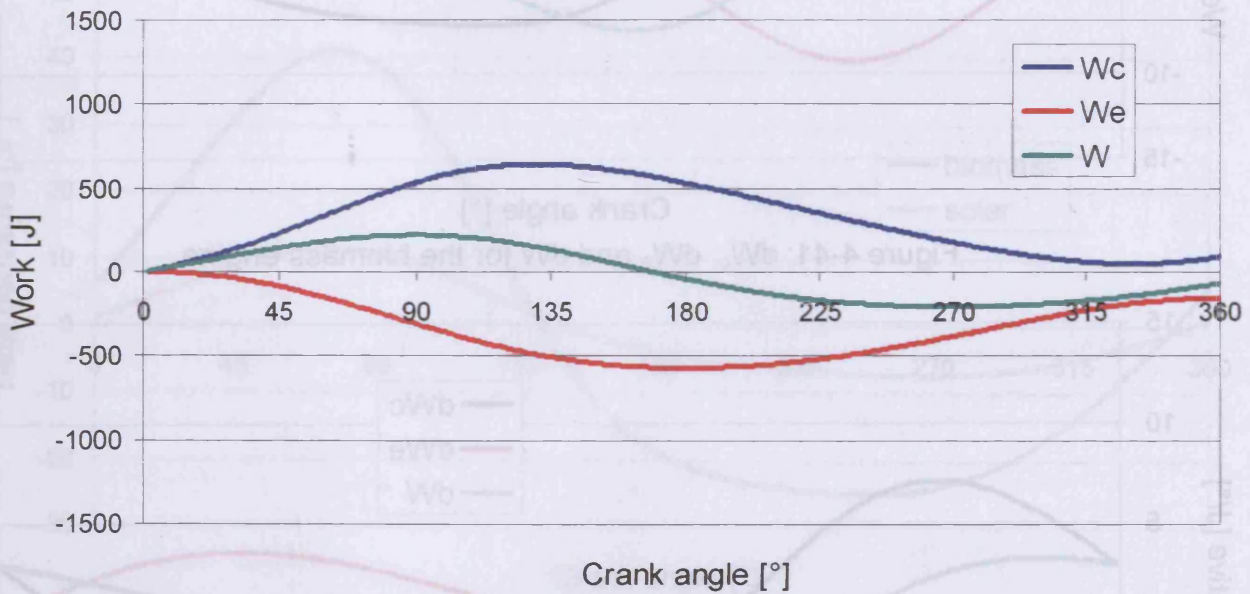
Figure 4-44: W_c, W_e and W for the solar engine

The absolute values of the work done in the different spaces are as follows:

$$W_{c,s} = 90,52\,J \tag{4.62}$$

$$W_{c,b} = 90,23\,J \tag{4.63}$$

$$W_{e,s} = -158,66\,J \tag{4.64}$$

$$W_{e,b} = -292,39 J \tag{4.65}$$

$$W_s = -68,12 J \tag{4.66}$$

$$W_b = -202,24 J \tag{4.67}$$

Combining equation (2.74), (2.75) and (2.76) with the work done by the engines (equations (4.66) and (4.67)) the performance has the values of:

$$P_s = 400 \frac{1}{60 s} \cdot 68,12 J = 454,13 W \tag{4.68}$$

$$P_b = 700 \frac{1}{60 s} \cdot 202,24 J = 2\;359,47 W \tag{4.69}$$

4.1.7.8 Efficiency

Using equation 2.3 and the heats and works determined in section 4.1.7 the efficiencies of the experimental engines are:

$$\eta_{th,s} = \frac{68,12 J}{155,58 J} = 0,438 \tag{4.70}$$

$$\eta_{th,b} = \frac{202,24 J}{283,75 J} = 0,713 \tag{4.71}$$

4.1.7.9 Energy balance

Taking a look at the energy balance (table 4.4) of the values named above a difference of about 5 J for the solar engine and 10 J for the biomass engine can be recognised.

1°	Biomass engine	Solar engine
Q_k	-71,66 J	-82,44 J
Q_h	283,75 J	155,58 J
W	-202,24 J	-68,12 J
Δ	9,85 J	5,02 J

Table 4.4: Energy balance for 360 steps per circle

These values were calculated with 360 steps per circle. Thus for every degree of the crank angle new values were defined. Raising the number of steps per circle the difference in the energy balance reduces and the values become more authentic. Table 4.5 and 4.6 show the values for 3'600 (0,1°) and 36'000 (0,01°) steps per circle.

0,1°	Biomass engine	Solar engine
Q_k	-93,20 J	-91,87 J
Q_h	293,78 J	159,02 J
W	-199,61 J	-66,65 J
Δ	0,97 J	0,50 J

Table 4.5: Energy balance for 3'600 steps per circle

0,01°	Biomass engine	Solar engine
Q_k	-95,33 J	-92,80 J
Q_h	294,78 J	159,36 J
W	-199,35 J	-66,51 J
Δ	0,12 J	0,05 J

Table 4.6: Energy balance for 36'000 steps per circle

4.2 Quasi steady flow model

The inspiration to this chapter was given by Urielis book "Stirling cycle engine analysis" [9]. A calculation method is described there that considers different kinds of losses like heat transfer losses and pressure drops. The equation set described there is modified in the following to fit gamma type engines and make the results more reasonable.

4.2.1 Non-ideal heat exchangers

The components having the most significant effect on performance and costs of the Stirling engine are undoubtedly the heat exchangers. The dead volume introduced by the heat exchangers must be kept to a minimum, which involves the use of small heat exchangers but still demands a high heat flow. The heater is required to absorb heat from the external heat source and to supply it to the working gas at the highest possible temperature and is usually required to operate continuously at high pressures close to its metallurgical limit.

The regenerator was invented by Robert Stirling as part of his original patent in 1816 (The engineer 1917) [4], and was without a doubt the most important aspect of his invention. In the following 100 years similar engines were being invented without recognising the significance of the regenerator. It is conceptually used for storing heat during one part of the cycle for re-use during another part. It usually is built up from a finely divided metallic matrix with alternating flows of working gas between the heater and the cooler in opposite directions. During the flow of working gas from the heater to the cooler section, the hot gas entering the regenerator dispenses heat to the matrix, which acts as a heat sink. During the subsequent flow of working gas from the cooler to the heater, the cold gas entering the regenerator is heated up by the matrix, which acts like a heat source. A regenerator having a reduced efficiency will result in an extra heating load burdened on the heater, as well similar cooling load burdened on the cooler, both of which lead to a reduction of the engine performance. It was noticed in chapter 2 that the quantity of heat transferred between the matrix and the working gas can be considerable about five times that of the heater. The accumulated heat flow in or out of the regenerator at the end of the cycle is zero.

In section 4.1 all heat exchanger components are considered to be ideal; the heater and cooler being isothermal and the regenerator having an ideal linear temperature

profile from the cooler temperature T_k to the heater temperature T_h. In practice there will be a difference in temperature between the cooler and heater wall temperatures T_{wk} and T_{wh} and the respective gas temperatures, which will vary over the cycle. Similarly, there will be a difference between the temperature profile of the gas flow through the regenerator and that of the regenerator matrix. In order to operate the engine at maximum efficiency it is necessary to reduce those wall to gas temperature differences to a minimum [9].

Considering the fundamental equation for heat transfer [9], given by:

$$dQ = U \cdot (T_w - T) \qquad (4.72)$$

where Q is the rate of heat transfer, U is the overall thermal conductivity (a product of the heat transfer coefficient and the wetted area) and T_w and T are the respective wall and gas temperatures. [9]

In the ideal adiabatic model it was found that for the limiting ideal case where $T_w = T$, the amount of heat transferred had a finite value depending on overall energy and mass conservation considerations. This implies that the heat exchangers of the ideal engine have infinite thermal conductance and that the real engine with heat exchangers having limited finite thermal conductance will always operate with a reduced thermal efficiency.

It is a need to design the heat exchangers to have as high thermal conductance as possible. The thermal conductance is directly proportional to the area of contact between the heat exchangers surface and the working gas (the so-called "wetted" area A_w) and therefore heat exchanger configurations are generally chosen to have as large wetted areas as it is practically possible. The regenerator matrix, in which the heat transfer is internal, is chosen to have a high surface area to dead volume ratio (up to 450 cm^2/cm^3). The heater and cooler, for which the heat transfer is both internal and external, usually comprise bundles of pipes in order to have large wetted areas, both internal and external. [9]

The nature of Stirling cycle engines involves transferring heat to the working gas by forced convection. Increasing the wetted area A_w in an attempt to increase the thermal efficiency will also cause an increase in the frictional drag force, with the resulting pressure drop tending to reduce the power output and efficiency [9]. Therefore a compromise has to be found.

The design of compact heat exchangers is well established in industry. The classic reference work on the subject is that that due to Kays and London (1964) [9]. All of the established design techniques assume steady flow and that the various flow regimes which govern both the thermal conductance and the friction drag force are well defined. Unfortunately, in Stirling engines the flow is unsteady, varying considerably over the cycle. Furthermore, because of the relative motion of the two pistons, at some periods in the cycle the gas of one cell can flow simultaneously in both directions. The field of unsteady or periodic flow in heat exchanger analysis is wide open. Initial work done by Kim (1970) [10] on periodic flow through spherical-bed regenerator matrices indicated that both the heat transfer and flow friction coefficients are significantly higher than in the equivalent steady flow case. In the absence of available periodic flow and heat transfer data the assumption is made that at each increment in the cycle steady flow conditions prevail. The so called quasi steady flow model is introduced to analyse the effects of non ideal heat exchangers on the engine performance.

4.2.2   Assumptions for the quasi steady flow model

The equation set for the quasi steady flow model is based upon several simplifying assumptions defined in the following.

> ➤ The method is not based on periodic flow regime but on quasi steady equations for certain increments of the cycle.

> ➤ Ideal gases with the gas equation are considered.

> ➤ Values like the heat capacity, dynamic viscosity and thermal conductivity are defined as a constant for each cell at average pressure and temperature.

> ➤ No leakage losses of the sealings and friction losses of the bearings are considered.

> ➤ The working and displacer piston space are defined as to not conduct any heat to the working gas.

> ➤ The wall temperatures of the cooler and heater are considered to be constant.

> ➤ The regenerator matrix is defined as having a linear temperature profile. To do this, the regenerator is divided into two cells and therefore the whole Stirling engine is built up as a six component system.

> ➤ The pressure drops are defined in a way considering only the flow friction along the walls of the heat exchangers (heater, cooler and regenerator). The inlet and outlet losses of these parts as well as all the drops caused by the connecting rods mounted in the working gas flow are neglected. The reason for this is that in case of the solar Stirling heater the determination of the exact inlet and outlet losses is difficult because of the geometry welded out of asymmetric parts of sheet metal (see figure 5-65). To keep the results of both engines comparable all the inlet and outlet losses are not considered in this chapter. Furthermore the inlet and outlet losses cause instability in the program and should not be included in this first step. The CFX analysis of the heat exchangers in chapter 5 shows what share of the total pressure drops these losses have.

The most simplifying assumptions for this calculation method are the neglect of the leakage losses and the inlet and outlet losses of the heat exchangers. A main part of the calculation is to show how far the tendencies of the performance and the efficiency subject to the geometry data and the boundary conditions match the measured values. To do this the assumptions made are justified.

4.2.3 Quasi steady flow model

The quasi steady flow model is defined with reference to figure 4-45. The major difference between the quasi steady flow model and the ideal adiabatic model defined in figure 4-1 is the heat exchanger section. The heater and cooler walls are maintained isothermally at constant source and sink temperatures T_{wh} and T_{wk} (see figure 4-46). The heat exchanger gas temperatures are no longer equal to their associated wall temperatures, nor are they constant over the cycle. The heater and cooler gas temperatures are represented by their respective mixed mean values T_h and T_k.
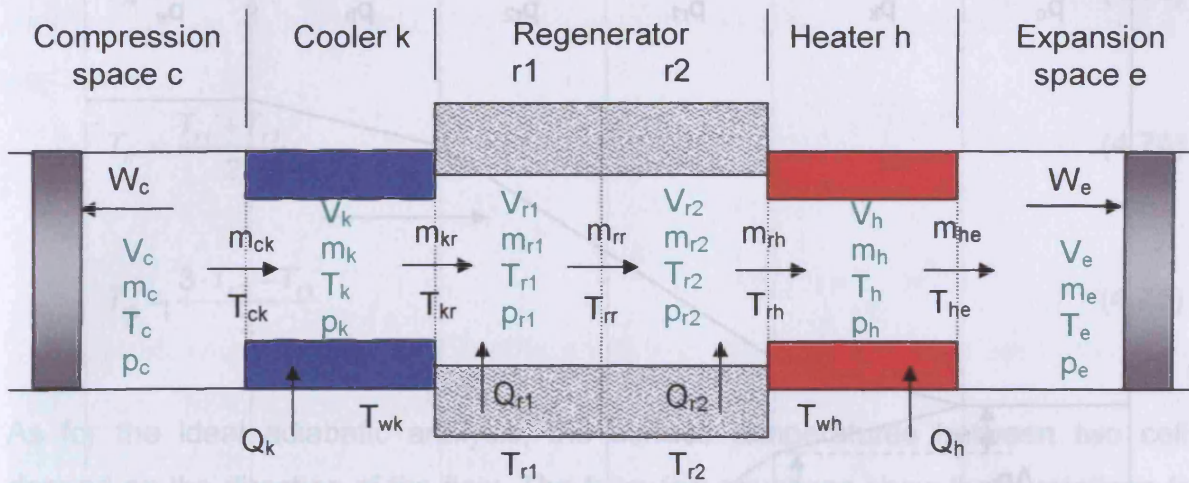
Figure 4-45: Quasi steady flow model of a Stirling engine (basis from [9])
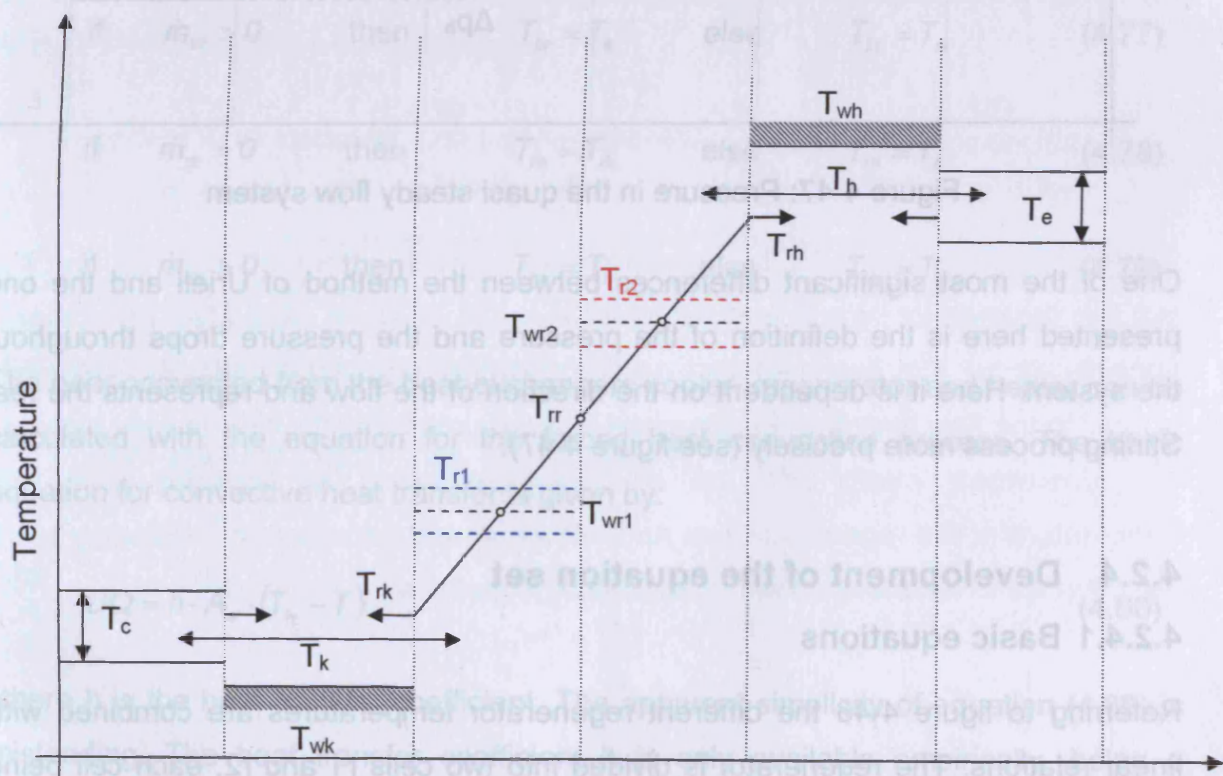
Figure 4-46: Temperature in the quasi steady flow system (basis from [9])
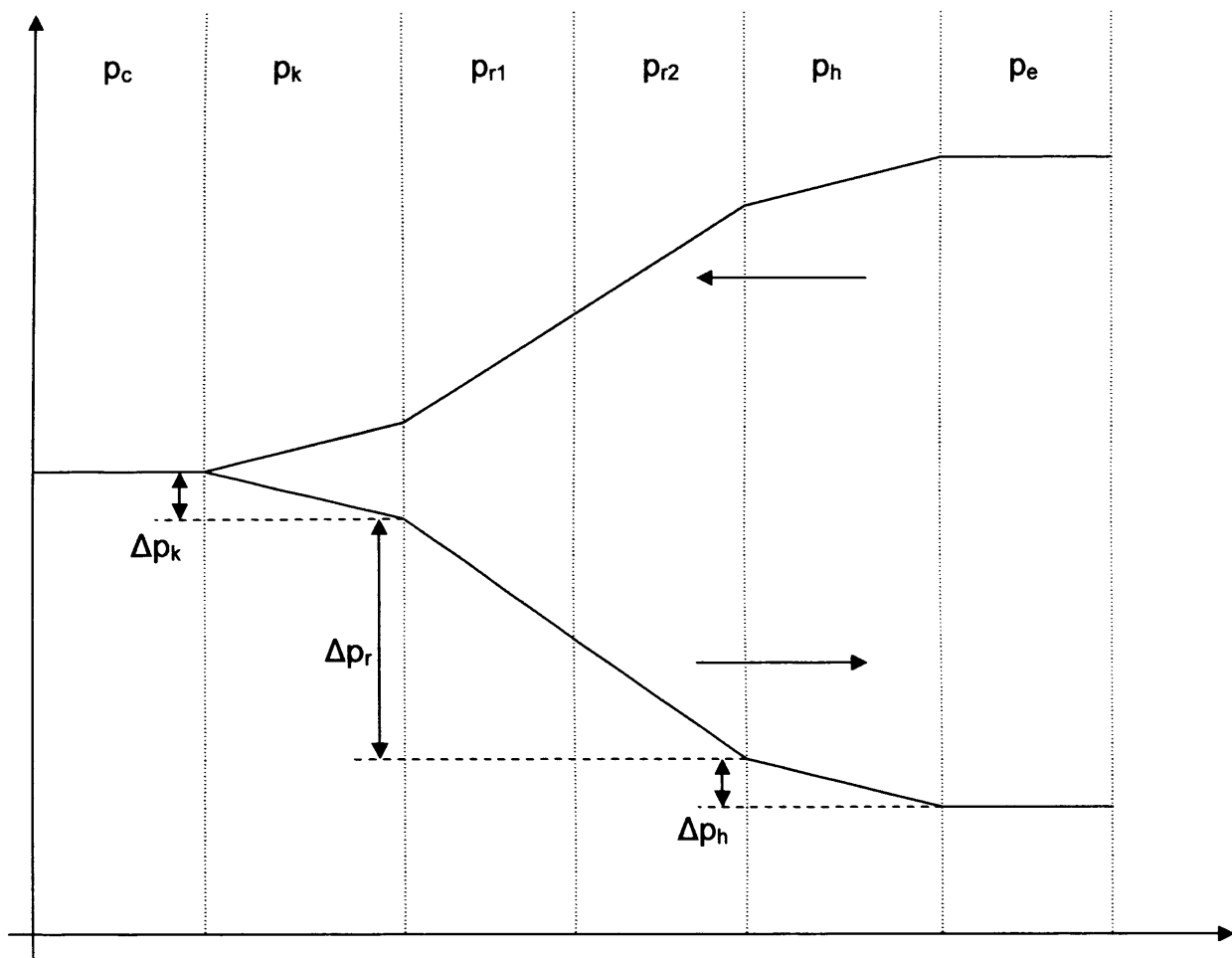
Figure 4-47: Pressure in the quasi steady flow system

One of the most significant differences between the method of Urieli and the one presented here is the definition of the pressure and the pressure drops throughout the system. Here it is dependent on the direction of the flow and represents the real Stirling process more precisely (see figure 4-47).

4.2.4 Development of the equation set

4.2.4.1 Basic equations

Referring to figure 4-46 the different regenerator temperatures are combined with linear relations. The regenerator is divided into two cells r1 and r2, each cell being associated with its respective mixed mean gas temperature T_{r1} and T_{r2} and corresponding effective matrix temperature T_{wr1} and T_{wr2}. T_{rk}, T_{rr} and T_{rh} can be calculated as follows:

$$T_{rk} = \frac{3 \cdot T_{r1} - T_{r2}}{2}$$ (4.73)

$$T_{rr} = \frac{T_{r1} + T_{r2}}{2}$$ (4.74)

$$T_{rh} = \frac{3 \cdot T_{r2} - T_{r1}}{2}$$ (4.75)

As for the ideal adiabatic analysis, the surface temperatures between two cells depend on the direction of the flow. The following equations show these relations for the model mentioned in figure 4-45.

if $\dot{m}_{ck} > 0$ then $T_{ck} = T_c$ else $T_{ck} = T_k$ (4.76)

if $\dot{m}_{kr} > 0$ then $T_{kr} = T_k$ else $T_{kr} = T_{rk}$ (4.77)

if $\dot{m}_{rh} > 0$ then $T_{rh} = T_{rh}$ else $T_{rh} = T_h$ (4.78)

if $\dot{m}_{he} > 0$ then $T_{he} = T_h$ else $T_{he} = T_e$ (4.79)

The heat convected from the heat exchangers cooler, regenerator and heater can be calculated with the equation for the forced heat convection process. The basic equation for convective heat transfer is given by:

$$DQ = h \cdot A_w \cdot (T_w - T)$$ (4.80)

where h is the heat transfer coefficient. The apparent simplicity of equation (4.80) is misleading. The heat transfer coefficient h is only available empirically, being a complicated function of the fluid transport properties (which are temperature dependent), the flow regime and the heat exchanger geometry.

The values for the heat transfer coefficients h_k, h_{r1}, h_{r2} and h_h are defined in section 4.2.4.2. Care needs to be taken to choose the correct units for the variables in these equations. Because of this the factor dz is used to compensate the unit of the

heat derivative ($J/°$ instead of W). Applying equation (4.80) on the four heat exchanger cells:

$$dQ_k = \frac{h_k \cdot A_{wk} \cdot (T_{wk} - T_k)}{dz}$$
(4.81)

$$dQ_{r1} = \frac{h_{r1} \cdot A_{wr1} \cdot (T_{wr1} - T_{r1})}{dz}$$
(4.82)

$$dQ_{r2} = \frac{h_{r2} \cdot A_{wr2} \cdot (T_{wr2} - T_{r2})}{dz}$$
(4.83)

$$dQ_h = \frac{h_h \cdot A_{wh} \cdot (T_{wh} - T_h)}{dz}$$
(4.84)

For clarity the important units of the variables from above are as follows:

$$dQ = \left[\frac{J}{°}\right] \qquad h = \left[\frac{W}{m^2 \cdot K}\right] \qquad dz = \left[\frac{°}{s}\right]$$

The heater and cooler walls are maintained isothermally at temperatures T_{wh} and T_{wk}, but the regenerator matrix temperatures T_{wr1} and T_{wr2} are evaluated from energy considerations. It is assumed that each matrix has an infinite thermal conductivity normal to the flow direction. Furthermore, it is assumed that the flow of heat between the regenerator matrix and the containing enclosure is negligible. The wall temperature of the regenerator has no fixed value and depends on the energy being stored in it and is described with the following equations.

$$dT_{wr1} = \frac{dQ_{r1}}{c_{mr}}$$
(4.85)

$$dT_{wr2} = \frac{dQ_{r2}}{c_{mr}}$$
(4.86)

c_{mr} is the heat capacity of the regenerator matrix and shows how much energy is needed to heat up the matrix. It is defined in the boundary conditions. The units are as follows:

$$dQ = \left[\frac{J}{\circ}\right] \qquad c_{mr} = \left[\frac{J}{K}\right] \qquad dT = \left[\frac{K}{\circ}\right]$$

The approach used to derive the differential and algebraic equation set is similar to that used for the ideal adiabatic model. The derivation of the equation for the pressure and its derivative is based on the energy balance for several cells. The main difference is that the energy equation has to be expanded to include flow dissipation and that the heat flow is determined from heat transfer considerations. The energy equation is used to determine the enthalpy flow and the associated mass flow. In section 4.1.3 it is considered that the energy equation is applied to a generalised cell, shown in figure 4-2. The energy equation to include flow dissipation effects can be written in a word statement as:

$$\begin{bmatrix} rate\ of\ work\ done \\ on\ the\ surroundings \end{bmatrix} + \begin{bmatrix} rate\ of\ heat\ transfer \\ into\ the\ cell \end{bmatrix} + \begin{bmatrix} rate\ of\ heat\ generation \\ due\ to\ flow\ dissipation \end{bmatrix}$$
$$+ \begin{bmatrix} net\ enthalpy\ convected \\ into\ the\ cell \end{bmatrix} = \begin{bmatrix} rate\ of\ increase\ of \\ internal\ energy\ in\ the\ cell \end{bmatrix}$$

Mathematically the word statement becomes

$$dW + dQ + Diss + (c_p \cdot T_i \cdot \dot{m}_i - c_p \cdot T_o \cdot \dot{m}_o) = c_v \cdot d(m \cdot T) \qquad (4.87)$$

With

$$d(m \cdot T) = \frac{p \cdot dV}{R} + \frac{V \cdot dp}{R} \qquad (4.88)$$

$$dW = -p \cdot dV \qquad (4.89)$$

$$c_p = R \cdot \frac{\kappa}{\kappa - 1} \qquad (4.90)$$

$$c_v = R \cdot \frac{1}{\kappa - 1} \qquad (4.91)$$

equation (4.87) can be modified in the following way:

$$dQ + Diss + \left(c_p \cdot T_i \cdot \dot{m}_i - c_p \cdot T_o \cdot \dot{m}_o\right) = \frac{c_v \cdot p \cdot dV}{R} + \frac{c_v \cdot V \cdot dp}{R} + p \cdot dV$$

$$dQ + Diss + \left(c_p \cdot T_i \cdot \dot{m}_i - c_p \cdot T_o \cdot \dot{m}_o\right) = \left(\frac{c_v}{R} + 1\right) \cdot p \cdot dV + \frac{c_v \cdot V \cdot dp}{R}$$

$$dQ + Diss + \left(c_p \cdot T_i \cdot \dot{m}_i - c_p \cdot T_o \cdot \dot{m}_o\right) = \left(\frac{1}{\kappa - 1} + \frac{\kappa - 1}{\kappa - 1}\right) \cdot p \cdot dV + \frac{c_v \cdot V \cdot dp}{R}$$

$$dQ + Diss + \left(c_p \cdot T_i \cdot \dot{m}_i - c_p \cdot T_o \cdot \dot{m}_o\right) = \left(\frac{\kappa}{\kappa - 1}\right) \cdot p \cdot dV + \frac{c_v \cdot V \cdot dp}{R}$$

$$dQ + Diss + \left(c_p \cdot T_i \cdot \dot{m}_i - c_p \cdot T_o \cdot \dot{m}_o\right) = \frac{c_p}{R} \cdot p \cdot dV + \frac{c_v}{R} \cdot V \cdot dp \qquad (4.92)$$

The assumption is made that the pressure derivative is the same in all the cells. In this step the pressure drops with their very small values in contrast to the pressure derivative are negligible. Because of this fact the pressure derivative dp is subscripted as dp_c in the following calculation. Simplifying equation (4.92) for the different working and heat transferring cells results in:

c: $\qquad -c_p \cdot T_{ck} \cdot \dot{m}_{ck} = \frac{c_p}{R} \cdot p_c \cdot dV_c + \frac{c_v}{R} \cdot V_c \cdot dp_c$ $\qquad (4.93)$

k: $\qquad dQ_k + Diss_k + \left(c_p \cdot T_{ck} \cdot \dot{m}_{ck} - c_p \cdot T_{kr} \cdot \dot{m}_{kr}\right) = \frac{c_v}{R} \cdot V_k \cdot dp_c$ $\qquad (4.94)$

r1: $\qquad dQ_{r1} + Diss_{r1} + \left(c_p \cdot T_{kr} \cdot \dot{m}_{kr} - c_p \cdot T_{rr} \cdot \dot{m}_{rr}\right) = \frac{c_v}{R} \cdot V_{r1} \cdot dp_c$ $\qquad (4.95)$

r2: $dQ_{r2} + Diss_{r2} + \left(c_p \cdot T_{rr} \cdot \dot{m}_{rr} - c_p \cdot T_{rh} \cdot \dot{m}_{rh}\right) = \dfrac{c_v}{R} \cdot V_{r2} \cdot dp_c$ (4.96)

h: $dQ_h + Diss_h + \left(c_p \cdot T_{rh} \cdot \dot{m}_{rh} - c_p \cdot T_{he} \cdot \dot{m}_{he}\right) = \dfrac{c_v}{R} \cdot V_h \cdot dp_c$ (4.97)

e: $c_p \cdot T_{he} \cdot \dot{m}_{he} = \dfrac{c_p}{R} \cdot p_e \cdot dV_e + \dfrac{c_v}{R} \cdot V_e \cdot dp_c$ (4.98)

Summing up all these equations from c to e - (4.93) to (4.98) -, where all the mass flow values are eliminated, a general energy balance for the whole system is built up.

Σ: $dQ + Diss = -\dfrac{c_p}{R} \cdot dW + \dfrac{c_v}{R} \cdot V \cdot dp_c$ (4.99)

dQ, Diss, dW and V in equation (4.99) are calculated as follows.

$dQ = dQ_k + dQ_{r1} + dQ_{r2} + dQ_h$ (4.100)

$Diss = Diss_k + Diss_{r1} + Diss_{r2} + Diss_h$ (4.101)

$dW = -p_c \cdot dV_c - p_e \cdot dV_e$ (4.102)

$V = V_c + V_k + V_{r1} + V_{r2} + V_h + V_e$ (4.103)

Rearranging equation (4.99):

$dp_c = \dfrac{R \cdot (dQ + Diss) + c_p \cdot dW}{c_v \cdot V}$ (4.104)

dp$_c$ is known and all the different pressures in the system can be calculated. The pressured drop values Δp are calculated in section 4.2.4.2. Taking a look at two related cells it always depends on the direction of flow in which one the pressure has the higher value (see figure 4-47). Pressure drops always match the flow direction

and therefore change with it. Because of that fact the pressure in the different cells is conditional and can be described as follows.

$$\text{if} \quad \dot{m}_{ck} > 0 \quad \text{then} \quad p_k = p_c - \frac{\Delta p_k}{2} \quad \text{else} \quad p_k = p_c + \frac{\Delta p_k}{2} \qquad (4.105)$$

$$\text{if} \quad \dot{m}_{kr} > 0 \quad \text{then} \quad p_{r1} = p_k - \frac{\Delta p_k + \Delta p_{r1}}{2} \quad \text{else} \quad p_{r1} = p_k + \frac{\Delta p_k + \Delta p_{r1}}{2} \qquad (4.106)$$

$$\text{if} \quad \dot{m}_{rr} > 0 \quad \text{then} \quad p_{r2} = p_{r1} - \frac{\Delta p_{r1} + \Delta p_{r2}}{2} \quad \text{else} \quad p_{r2} = p_{r1} + \frac{\Delta p_{r1} + \Delta p_{r2}}{2} \qquad (4.107)$$

$$\text{if} \quad \dot{m}_{rh} > 0 \quad \text{then} \quad p_h = p_{r2} - \frac{\Delta p_{r2} + \Delta p_h}{2} \quad \text{else} \quad p_h = p_{r2} + \frac{\Delta p_{r2} + \Delta p_h}{2} \qquad (4.108)$$

$$\text{if} \quad \dot{m}_{he} > 0 \quad \text{then} \quad p_e = p_h - \frac{\Delta p_h}{2} \quad \text{else} \quad p_e = p_h + \frac{\Delta p_h}{2} \qquad (4.109)$$

For the calculation of the absolute mass in each cell, the mass derivative and the mass flow across each cross section are calculated. Equation (4.110) shows that the mass flow across the cross section of compression space and cooler is directly proportional to the change of the mass in the compression space.

$$dm_c = -\dot{m}_{ck} \qquad (4.110)$$

Since there is no flow dissipation in the compression space, the compression space mass derivative equation (4.111) remains unchanged compared to the ideal adiabatic analysis.

$$dm_c = \frac{p_c \cdot dV_c + \frac{1}{\kappa} \cdot V_c \cdot dp_c}{R \cdot T_{ck}} \qquad (4.111)$$

Once dm$_c$ and with it the mass flow is known the energy balances for the different spaces (equation (4.94) to (4.97)) can be used to calculate the other mass flows in the cross sections of the cells.

$$\dot{m}_{kr} = \frac{c_p \cdot T_{ck} \cdot \dot{m}_{ck} + dQ_k + Diss_k - \frac{c_v}{R} \cdot V_k \cdot dp_c}{c_p \cdot T_{kr}}$$
(4.112)

$$\dot{m}_{rr} = \frac{c_p \cdot T_{kr} \cdot \dot{m}_{kr} + dQ_{r1} + Diss_{r1} - \frac{c_v}{R} \cdot V_{r1} \cdot dp_c}{c_p \cdot T_{rr}}$$
(4.113)

$$\dot{m}_{rh} = \frac{c_p \cdot T_{rr} \cdot \dot{m}_{rr} + dQ_{r2} + Diss_{r2} - \frac{c_v}{R} \cdot V_{r2} \cdot dp_c}{c_p \cdot T_{rh}}$$
(4.114)

$$\dot{m}_{he} = \frac{c_p \cdot T_{rh} \cdot \dot{m}_{rh} + dQ_h + Diss_h - \frac{c_v}{R} \cdot V_h \cdot dp_c}{c_p \cdot T_{he}}$$
(4.115)

With these equations the mass derivatives of the cells can be written as:

$$dm_k = \dot{m}_{ck} - \dot{m}_{kr}$$
(4.116)

$$dm_{r1} = \dot{m}_{kr} - \dot{m}_{rr}$$
(4.117)

$$dm_{r2} = \dot{m}_{rr} - \dot{m}_{rh}$$
(4.118)

$$dm_h = \dot{m}_{rh} - \dot{m}_{he}$$
(4.119)

As there is no leakage, the total mass of gas in the system m is constant and its derivative is zero. Therefore dm$_e$ can be determined as:

$$dm_e = -dm_c - dm_k - dm_{r1} - dm_{r2} - dm_h$$
(4.120)

As a last step in the derivation of the basic equation set for the quasi steady flow model, the cell temperatures have to be determined. This is carried out with the equation of state while all values needed were calculated previously.

$$T_c = \frac{p_c \cdot V_c}{R \cdot m_c}$$ (4.121)

$$T_k = \frac{p_k \cdot V_k}{R \cdot m_k}$$ (4.122)

$$T_{r1} = \frac{p_{r1} \cdot V_{r1}}{R \cdot m_{r1}}$$ (4.123)

$$T_{r2} = \frac{p_{r2} \cdot V_{r2}}{R \cdot m_{r2}}$$ (4.124)

$$T_h = \frac{p_h \cdot V_h}{R \cdot m_h}$$ (4.125)

$$T_e = \frac{p_e \cdot V_e}{R \cdot m_e}$$ (4.126)

4.2.4.2 Calculation of the loss values

The loss values have to be determined for the cells k, r1, r2 and h. Hence they are equal for all these cells in the following only the ones for the cooler k are described. The values for the others are calculated in an analogous manner and are shown in section 4.2.4.3.

➢ Density

$$\rho_k = \frac{m_k}{V_k}$$ (4.127)

> **Volume flux**

For the further calculation of the losses the volume flux has to be determined in the unit m³/s. Hence the mass derivative dm is in kg/° and has to be matched with the speed of the machine

$$V_k = \left| \frac{dm_k \cdot R \cdot T_k}{p_k} \cdot dz \right| \qquad (4.128)$$

$$\dot{V}_k = \left[\frac{m^3}{s} \right] \qquad dm_k = \left[\frac{kg}{°} \right] \qquad dz = \left[\frac{°}{s} \right]$$

> **Gas velocity**

The gas velocity in m/s can be determined with of the volume flux (equation (4.129)) and the free flow area of the heat exchanger A.

$$v_k = \frac{\dot{V}_k}{A_k} \qquad (4.129)$$

> **Reynolds number**

Reynolds is calculated with the gas velocity v, the characteristic dimension, which is the diameter of one pipe in the heat exchanger, the dynamic viscosity μ in [Pa·s] and the density.

$$Re_k = \frac{v_k \cdot D_k \cdot \rho_k}{\mu_k} \qquad (4.130)$$

> **Friction factor**

The friction factor λ_p is conditional to the value of Reynolds Re. In the literature three different regions are considered – laminar, transition and turbulent. [13]

if $Re_k < 2'320$ then $\lambda_{pk} = \dfrac{64}{Re_k}$ laminar   (4.131)

if $2'320 < Re_k < 10^5$ then $\lambda_{pk} = \dfrac{0,3164}{\sqrt[4]{Re_k}}$ transition   (4.132)

if $10^5 < Re_k$ then $\lambda_{pk} = 0,0032 + \dfrac{0,221}{Re_k^{0,237}}$ turbulent   (4.133)

The friction factor is only dependent on the Reynolds Number and the curve can be seen in figure 4-48.
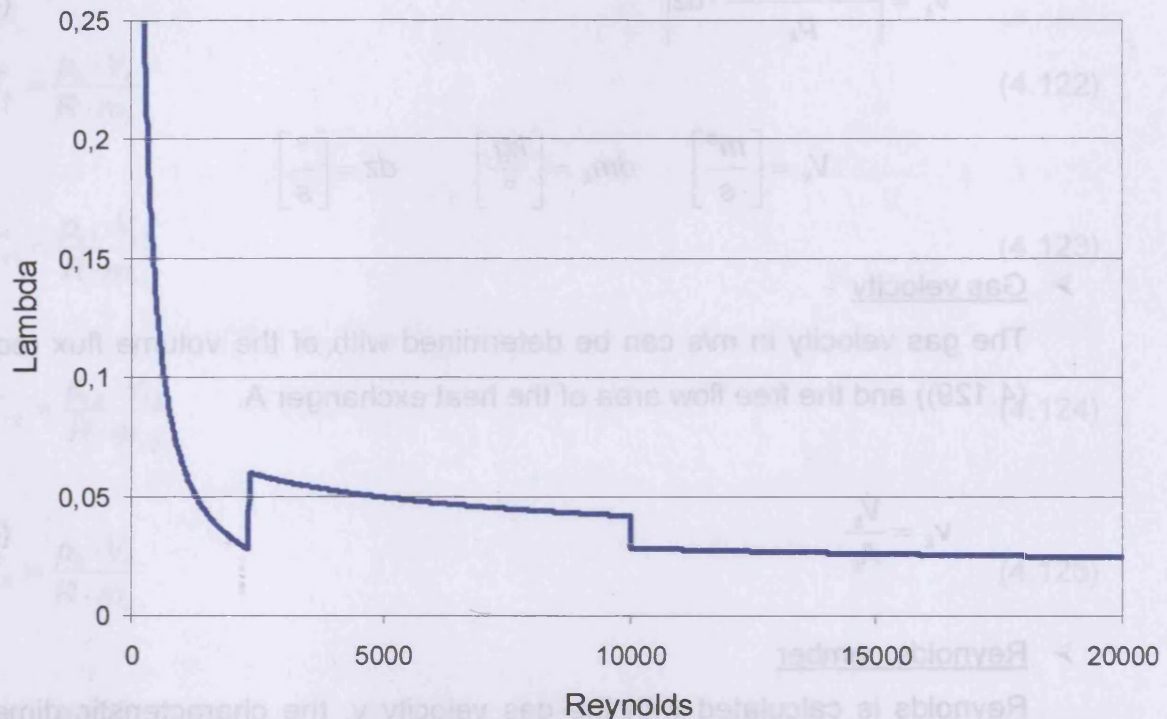
Figure 4-48: Friction factor as a function of Reynolds

> Pressure drop

The pressure drop is calculated only for the flow friction in the pipe. As it is stated in the assumptions additional pressure drops arising from pipe bends, inlets and outlets are neglected. L is the length and D the diameter of the heat exchanger pipe.

$$\Delta p_k = \left(\frac{\lambda_{pk} \cdot L_k}{D_k} \right) \cdot \frac{\rho_k \cdot v_k^2}{2}$$

(4.134)

> Dissipation

The dissipation generated by the pressure drop has to be determined to solve the energy balance (equation (4.87)). This is done as follows:

150

$$Diss_k = \left| \frac{\Delta p_k \cdot dm_k}{\rho_k} \right| \tag{4.135}$$

➤ Heat transfer coefficient

In the case of the Stirling engines described in this thesis the heater, cooler and regenerator sections are designed to be constructed from homogeneous bundles of smooth circular pipes. The Fanning friction factors versus Reynolds number curves for circular pipes have been in widespread use for some decades (Moody 1948 and Schlichting 1955 [9]) (see figure 4-49). The more up to date Dittus-Boelter correlation using the Nusselt number could not be taken into account as it caused oscillations in the solution process. The friction factor equations are defined as follows:

if $\qquad Re_k < 2'000 \qquad\qquad f_{rk} = 16 \tag{4.136}$

if $\qquad 2'000 < Re_k < 4'000 \qquad f_{rk} = 7{,}343 \cdot 10^{-4} \cdot Re_k^{1,3142} \tag{4.137}$

if $\qquad Re_k > 4'000 \qquad\qquad f_{rk} = 0{,}0791 \cdot Re_k^{0,75} \tag{4.138}$
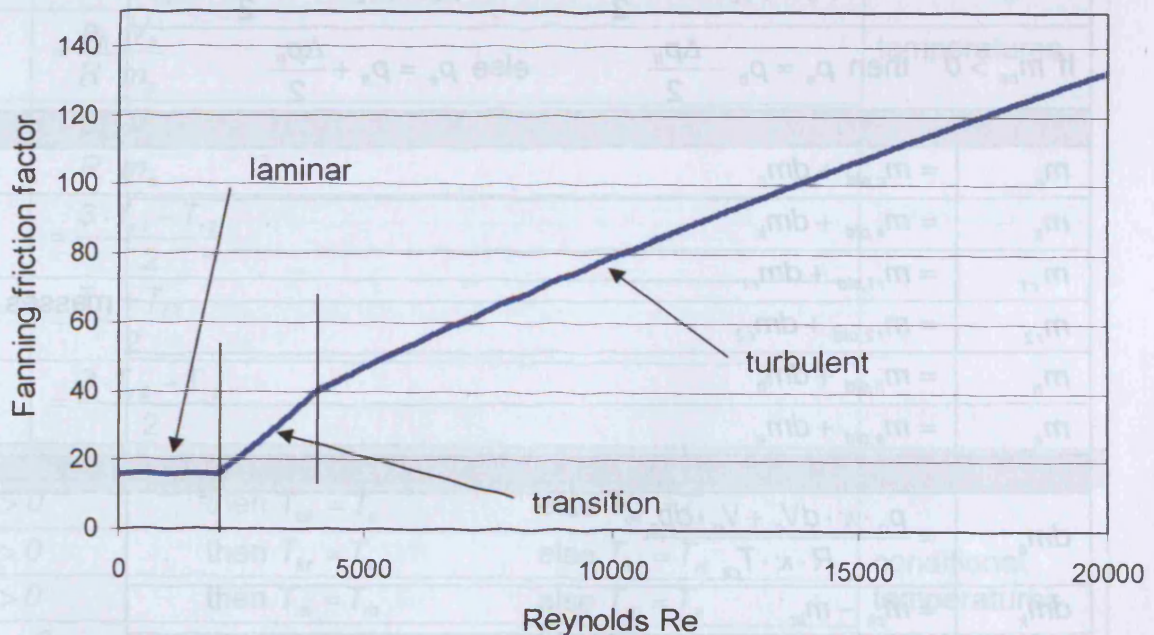
Figure 4-49: Fanning friction factor as a function of Reynolds

With the Fanning friction factor f_r the heat transfer coefficient can be calculated. The equation is taken from Urieli [9].

$$h_k = \frac{f_{rk} \cdot \mu_k \cdot c_{pk}}{2 \cdot D_k \cdot Pr_k} \tag{4.139}$$

The Prandtl number and specific heat capacity are considered to be constant. They are determined for each cell at average pressure and temperature.

4.2.4.3 Compete set of equations

To give a complete overview of the equations used and for clarity reasons, the complete equation set is given in the following table. It is there to show exactly how the program works and which values are calculated first.

dp_c	$= \dfrac{R \cdot (dQ + Diss) + c_p \cdot dW}{c_v \cdot V}$	
p_c	$= p_{c,old} + dp_c$	
If $\dot{m}_{ck} > 0$ then $p_k = p_c - \dfrac{\Delta p_k}{2}$ else $p_k = p_c + \dfrac{\Delta p_k}{2}$		
If $\dot{m}_{kr} > 0$ then $p_{r1} = p_k - \dfrac{\Delta p_k + \Delta p_{r1}}{2}$ else $p_{r1} = p_k + \dfrac{\Delta p_k + \Delta p_{r1}}{2}$		pressure
If $\dot{m}_{rr} > 0$ then $p_{r2} = p_{r1} - \dfrac{\Delta p_{r1} + \Delta p_{r2}}{2}$ else $p_{r2} = p_{r1} + \dfrac{\Delta p_{r1} + \Delta p_{r2}}{2}$		
If $\dot{m}_{rh} > 0$ then $p_h = p_{r2} - \dfrac{\Delta p_{r2} + \Delta p_h}{2}$ else $p_h = p_{r2} + \dfrac{\Delta p_{r2} + \Delta p_h}{2}$		
If $\dot{m}_{he} > 0$ then $p_e = p_h - \dfrac{\Delta p_h}{2}$ else $p_e = p_h + \dfrac{\Delta p_h}{2}$		

m_c	$= m_{c,old} + dm_c$	
m_k	$= m_{k,old} + dm_k$	
m_{r1}	$= m_{r1,old} + dm_{r1}$	
m_{r2}	$= m_{r2,old} + dm_{r2}$	masses
m_h	$= m_{h,old} + dm_h$	
m_e	$= m_{e,old} + dm_e$	

dm_c	$= \dfrac{p_c \cdot \kappa \cdot dV_c + V_c \cdot dp_c}{R \cdot \kappa \cdot T_{ck}}$	
dm_k	$= \dot{m}_{ck} - \dot{m}_{kr}$	
dm_{r1}	$= \dot{m}_{kr} - \dot{m}_{rr}$	mass accumulations and flows
dm_{r2}	$= \dot{m}_{rr} - \dot{m}_{rh}$	
dm_h	$= \dot{m}_{rh} - \dot{m}_{he}$	
dm_e	$= -dm_c - dm_k - dm_{r1} - dm_{r2} - dm_h$	
$\dot{m}_{ck}$	$= -dm_c$	

$\dot{m}_{kr}$	$= \dfrac{c_p \cdot T_{ck} \cdot \dot{m}_{ck} + dQ_k + Diss_k - \dfrac{c_v}{R} \cdot V_k \cdot dp_c}{c_p \cdot T_{kr}}$	mass accumulations and flows
$\dot{m}_{rr}$	$= \dfrac{c_p \cdot T_{kr} \cdot \dot{m}_{kr} + dQ_{r1} + Diss_{r1} - \dfrac{c_v}{R} \cdot V_{r1} \cdot dp_c}{c_p \cdot T_{rr}}$	
$\dot{m}_{rh}$	$= \dfrac{c_p \cdot T_{rr} \cdot \dot{m}_{rr} + dQ_{r2} + Diss_{r2} - \dfrac{c_v}{R} \cdot V_{r2} \cdot dp_c}{c_p \cdot T_{rh}}$	
$\dot{m}_{he}$	$= \dfrac{c_p \cdot T_{rh} \cdot \dot{m}_{rh} + dQ_h + Diss_h - \dfrac{c_v}{R} \cdot V_h \cdot dp_c}{c_p \cdot T_{he}}$	

T_c	$= \dfrac{p \cdot V_c}{m_c \cdot R}$	temperatures
T_k	$= \dfrac{p_k \cdot V_k}{R \cdot m_k}$	
T_{r1}	$= \dfrac{p_{r1} \cdot V_{r1}}{R \cdot m_{r1}}$	
T_{r2}	$= \dfrac{p_{r2} \cdot V_{r2}}{R \cdot m_{r2}}$	
T_h	$= \dfrac{p_h \cdot V_h}{R \cdot m_h}$	
T_e	$= \dfrac{p_e \cdot V_e}{R \cdot m_e}$	
T_{rk}	$= \dfrac{3 \cdot T_{r1} - T_{r2}}{2}$	
T_{rr}	$= \dfrac{T_{r1} + T_{r2}}{2}$	
T_{rh}	$= \dfrac{3 \cdot T_{r2} - T_{r1}}{2}$	

If $\dot{m}_{ck} > 0$	then $T_{ck} = T_c$	else $T_{ck} = T_k$	conditional temperatures
If $\dot{m}_{kr} > 0$	then $T_{kr} = T_k$	else $T_{kr} = T_{rk}$	
If $\dot{m}_{rh} > 0$	then $T_{rh} = T_{rh}$	else $T_{rh} = T_h$	
If $\dot{m}_{he} > 0$	then $T_{he} = T_h$	else $T_{he} = T_e$	

ρ_k	$= \dfrac{m_k}{V_k}$	densities
ρ_{r1}	$= \dfrac{m_{r1}}{V_{r1}}$	

ρ_{r2}	$= \dfrac{m_{r2}}{V_{r2}}$	densities
ρ_h	$= \dfrac{m_h}{V_h}$	
dV_k	$= \left\| \dfrac{dm_k \cdot R \cdot T_k}{p_k} \cdot dz \right\|$	volume fluxes
dV_{r1}	$= \left\| \dfrac{dm_{r1} \cdot R \cdot T_{r1}}{p_{r1}} \cdot dz \right\|$	
dV_{r2}	$= \left\| \dfrac{dm_{r2} \cdot R \cdot T_{r2}}{p_{r2}} \cdot dz \right\|$	
dV_h	$= \left\| \dfrac{dm_h \cdot R \cdot T_h}{p_h} \cdot dz \right\|$	
v_k	$= \dfrac{dV_k}{A_k}$	gas velocities
v_{r1}	$= \dfrac{dV_{r1}}{A_{r1}}$	
v_{r2}	$= \dfrac{dV_{r2}}{A_{r2}}$	
v_h	$= \dfrac{dV_h}{A_h}$	
Re_k	$= \dfrac{v_k \cdot D_k}{\upsilon_k}$	Reynolds
Re_{r1}	$= \dfrac{v_{r1} \cdot D_{r1}}{\upsilon_{r1}}$	
Re_{r2}	$= \dfrac{v_{r2} \cdot D_{r2}}{\upsilon_{r2}}$	
Re_h	$= \dfrac{v_h \cdot D_h}{\upsilon_h}$	
If $Re_k < 2320$ then $\lambda_{pk} = \dfrac{64}{Re_k}$		friction factors
If $2320 < Re_k < 10^5$ then $\lambda_{pk} = \dfrac{0{,}3164}{\sqrt[4]{Re_k}}$		
If $10^5 < Re_k$ then $\lambda_{pk} = 0{,}0032 + \dfrac{0{,}221}{Re_k^{0{,}237}}$		

If $Re_{r1} < 2320$	then	$\lambda_{pr1} = \dfrac{64}{Re_{r1}}$	
If $2320 < Re_{r1} < 10^5$	then	$\lambda_{pr1} = \dfrac{0{,}3164}{\sqrt[4]{Re_{r1}}}$	
If $10^5 < Re_{r1}$	then	$\lambda_{pr1} = 0{,}0032 + \dfrac{0{,}221}{Re_{r1}^{0,237}}$	
If $Re_{r2} < 2320$	then	$\lambda_{pr2} = \dfrac{64}{Re_{r2}}$	friction factors
If $2320 < Re_{r2} < 10^5$	then	$\lambda_{pr2} = \dfrac{0{,}3164}{\sqrt[4]{Re_{r2}}}$	
If $10^5 < Re_{r2}$	then	$\lambda_{pr2} = 0{,}0032 + \dfrac{0{,}221}{Re_{r2}^{0,237}}$	
If $Re_h < 2320$	then	$\lambda_{ph} = \dfrac{64}{Re_h}$	
If $2320 < Re_h < 10^5$	then	$\lambda_{ph} = \dfrac{0{,}3164}{\sqrt[4]{Re_h}}$	
If $10^5 < Re_h$	then	$\lambda_{ph} = 0{,}0032 + \dfrac{0{,}221}{Re_h^{0,237}}$	

Δp_k	$= \left(\dfrac{\lambda_{pk} \cdot L_k}{D_k} \right) \cdot \dfrac{\rho_k \cdot v_k^2}{2}$	
Δp_{r1}	$= \left(\dfrac{\lambda_{pr1} \cdot L_{r1}}{D_{r1}} \right) \cdot \dfrac{\rho_{r1} \cdot v_{r1}^2}{2}$	pressure drops
Δp_{r2}	$= \left(\dfrac{\lambda_{pr2} \cdot L_{r2}}{D_{r2}} \right) \cdot \dfrac{\rho_{r2} \cdot v_{r2}^2}{2}$	
Δp_h	$= \left(\dfrac{\lambda_{ph} \cdot L_h}{D_h} \right) \cdot \dfrac{\rho_h \cdot v_h^2}{2}$	

$Diss_k$	$= \left\| \dfrac{\Delta p_k \cdot dm_k}{\rho_k} \right\|$	
$Diss_{r1}$	$= \left\| \dfrac{\Delta p_{r1} \cdot dm_{r1}}{\rho_{r1}} \right\|$	dissipations
$Diss_{r2}$	$= \left\| \dfrac{\Delta p_{r2} \cdot dm_{r2}}{\rho_{r2}} \right\|$	
$Diss_h$	$= \left\| \dfrac{\Delta p_h \cdot dm_h}{\rho_h} \right\|$	

If $Re_k < 2000$	then $f_{rk} = 16$	Fanning friction factors
If $2000 < Re_k < 4000$	then $f_{rk} = 7{,}343 \cdot 10^{-4} \cdot Re_k^{1{,}3142}$	
If $Re_k > 4000$	then $f_{rk} = 0{,}0791 \cdot Re_k^{0{,}75}$	
If $Re_{r1} < 2000$	then $f_{rr1} = 16$	
If $2000 < Re_{r1} < 4000$	then $f_{rr1} = 7{,}343 \cdot 10^{-4} \cdot Re_{r1}^{1{,}3142}$	
If $Re_{r1} > 4000$	then $f_{rr1} = 0{,}0791 \cdot Re_{r1}^{0{,}75}$	
If $Re_{r2} < 2000$	then $f_{rr2} = 16$	
If $2000 < Re_{r2} < 4000$	then $f_{rr2} = 7{,}343 \cdot 10^{-4} \cdot Re_{r2}^{1{,}3142}$	
If $Re_{r2} > 4000$	then $f_{rr2} = 0{,}0791 \cdot Re_{r2}^{0{,}75}$	
If $Re_h < 2000$	then $f_{rh} = 16$	
If $2000 < Re_h < 4000$	then $f_{rh} = 7{,}343 \cdot 10^{-4} \cdot Re_h^{1{,}3142}$	
If $Re_h > 4000$	then $f_{rh} = 0{,}0791 \cdot Re_h^{0{,}75}$	

h_k	$= \dfrac{f_{rk} \cdot \mu_k \cdot c_{pk}}{2 \cdot D_k \cdot Pr_k}$	heat transfer coefficients
h_{r1}	$= \dfrac{f_{rr1} \cdot \mu_{r1} \cdot c_{pr1}}{2 \cdot D_{r1} \cdot Pr_{r1}}$	
h_{r2}	$= \dfrac{f_{rr2} \cdot \mu_{r2} \cdot c_{pr2}}{2 \cdot D_{r2} \cdot Pr_{r2}}$	
h_h	$= \dfrac{f_{rh} \cdot \mu_h \cdot c_{ph}}{2 \cdot D_h \cdot Pr_h}$	

dW_c	$= -p \cdot dV_c$	works
dW_e	$= -p \cdot dV_e$	
W	$= W_{old} + dW_c + dW_e$	
dQ_k	$= \dfrac{h_k \cdot A_{wk} \cdot (T_{wk} - T_k)}{dz}$	energies
dQ_{r1}	$= \dfrac{h_{r1} \cdot A_{wr1} \cdot (T_{wr1} - T_{r1})}{dz}$	
dQ_{r2}	$= \dfrac{h_{r2} \cdot A_{wr2} \cdot (T_{wr2} - T_{r2})}{dz}$	
dQ_h	$= \dfrac{h_h \cdot A_{wh} \cdot (T_{wh} - T_h)}{dz}$	
Q_k	$= Q_{k,old} + dQ_k$	
Q_{r1}	$= Q_{r1,old} + dQ_{r1}$	
Q_{r2}	$= Q_{r2,old} + dQ_{r2}$	
Q_h	$= Q_{h,old} + dQ_h$	

dQ	$= dQ_k + dQ_{r1} + dQ_{r2} + dQ_h$	energies
$Diss$	$= Diss_k + Diss_{r1} + Diss_{r2} + Diss_h$	

dT_{wr1}	$= \dfrac{dQ_{r1}}{c_{mr}}$	regenerator wall temperatures
dT_{wr2}	$= \dfrac{dQ_{r2}}{c_{mr}}$	
T_{wr1}	$= T_{wr1,old} + dT_{wr1}$	
T_{wr2}	$= T_{wr2,old} + dT_{wr2}$	

Table 4.7: Quasi steady flow complete equation set

4.2.5 Program and method of solution

The approach to the solution is identical to that of the ideal adiabatic model presented in section 4.1. Table 4-7 contains 90 equations of which 13 are differential equations in the following variables:

p_c compression space pressure

m_c mass of gas in the compression space

m_k, m_h mass of gas in the cooler and heater respectively

m_{r1}, m_{r2} mass of gas in the regenerator cells

T_{mr1}, T_{mr2} regenerator cell matrix temperatures

W accumulated work done by the engine

Q_k accumulated heat transferred to the gas in the cooler

Q_{r1}, Q_{r2} accumulated heat transferred to the gas in the regenerator cells

Q_h accumulated heat transferred to the gas in the heater

A consistent set of initial conditions has to be chosen for the system variables and the set of equations is subsequently integrated through several complete cycles until cyclic steady state has been attained. At each integration increment the values of heat transfer coefficient h and pressure drop Δp are evaluated in accordance with the methods presented before. The time needed for convergence is mainly dependent on the thermal capacitance of the system – in particular that of the regenerator matrix. For high performance engines the regenerator matrix thermal capacitance c_{mr} is chosen to be as high as possible. To minimise the variation of the matrix

temperatures T_{mr1} and T_{mr2}, some hundred crankshaft revolutions may be required before cyclic steady state has been attained. [9]

The numerical solution of such a complex system is prone to various effects of numerical instability which are often difficult to locate or identify, and various techniques are usually developed through trial and error in order to suppress the development of these instabilities. They are very often functions of the specific system being solved and the techniques are not universally applicable. One classical problem is the choice of the correct increment step size. Many numerical techniques automatically vary the step size to obtain the required accuracy. In the programme shown later it is preferred to leave the choice of step size an input parameter chosen by the user. The effect of changing the time step is shown in section 4.2.7.16.

The stepwise discretisation method is often a source of stability problems (Urieli 1977) [9]. It is difficult to find the right equation set which runs with the data of the experimental engines. One method is to introduce the Sutherland equations for the gas data and other equations rather than the simplifying equations of Fanning for the heat transfer coefficient. This attempt caused large instabilities and the program would not run. The programs developed for gamma type engines are presented in appendix C3 and C4.

4.2.6 Boundary conditions for the program

For the ideal adiabatic program shown in section 4.1 there are only a few boundary conditions needed. For the quasi steady flow model the geometry data of the heat exchangers and the properties of the gas have to be added.

4.2.6.1 Engine data

The values shown in the following table 4.8 describe the geometry, and the working conditions of the solar and biomass engine. The equations for the volumes are the same as in section 4.1.4 and are not shown here again.

		Biomass	Solar
		Set of constant values	
φ	[°]	90	
V_{se}	[m³]	5,65E-4	
V_{sc}	[m³]	4,51E-4	
V_{de}	[m³]	0,28E-4	
V_{dc}	[m³]	0,04E-4	
V_{r1}	[m³]	0,75E-4	
V_{r2}	[m³]	0,75E-4	
V_h	[m³]	5,44E-4	2,50E-4
V_k	[m³]	3,79E-4	
λ_c	[-]	0,257	
λ_e	[-]	0,288	
A_k	[m²]	1,03E-3	
A_{r1}	[m²]	2,50E-3	
A_{r2}	[m²]	2,50E-3	
A_h	[m²]	1,020E-3	0,905E-3
D_k	[m]	4,0E-3	
D_{r1}	[m]	3,0E-4	
D_{r2}	[m]	3,0E-4	
D_h	[m]	6,0E-3	6,0E-3
A_{wk}	[m²]	9,449E-2	
A_{wr1}	[m²]	1,523	
A_{wr2}	[m²]	1,523	
A_{wh}	[m²]	2,178E-2	0,139
dz	[°/s]	4200	2400
T_{wk}	[K]	328,00	331,00
T_{wh}	[K]	1173,00	628,00
C_{mr}	[J/K]	350	

Table 4.8: Engine data

4.2.6.2 Gas data

For the calculation several values for the gas (shown in table 4.9) are considered to be constant, as the process is far away from the critical point. In the calculation air is supposed to be the working gas of the engines.

R	[J/(kg*K)]	287,1	
κ	[-]	1,4	
c_v	[J/(kg*K)]	717,75	
c_p	[J/(kg*K)]	1004,85	
m_gas	[kg]	18,6E-3	11,7E-3

Table 4.9: Constant gas properties of air

The values for the thermal conductivity λ and the dynamic viscosity μ are highly dependent on the temperature and pressure. They are considered not to be constant and therefore different values are used for the cooler, heater and regenerator cells at its average temperature and pressure. Values are taken from the "VDI Wärmeatlas" [14] Db24 and Db26.

Biomass engine			
Cell	temperature T_m	pressure p_m	dynamic viscosity μ
	[K]	[bar]	[Pa·s]
k	350	15	20,97E-6
r1	500	15	27,13E-6
r2	800	15	37,45E-6
h	1100	15	46,19E-6
Solar engine			
k	350	10	20,91E-6
r1	450	10	25,65E-6
r2	550	10	27,56E-6
h	650	10	32,53E-6

Table 4.10: Dynamic viscosity of the working gas

Biomass engine			
Cell	temperature T_m	pressure p_m	therm. cond. λ
	[K]	[bar]	[W/(m·K)]
k	350	15	30,27E-3
r1	500	15	38,89E-3
r2	800	15	55,91E-3
h	1100	15	71,74E-3
Solar engine			
k	350	10	30,05E-3
r1	450	10	38,23E-3
r2	550	10	44,32E-3
h	650	10	50,16E-3

Table 4.11: Thermal conductivity of the working gas

Biomass engine			
cell	temperature T_m	pressure p_m	Prandtl Pr
	[K]	[bar]	[-]
k	350	15	0,7098
r1	500	15	0,7051
r2	800	15	0,7199
h	1100	15	0,7350
Solar engine			
k	350	10	0,7092
r1	450	10	0,7047
r2	550	10	0,7069
h	650	10	0,7118

Table 4.12: Prandtl number of the working gas

Biomass engine			
cell	temperature T_m	pressure p_m	c_p
	[K]	[bar]	[J/(kg·K)]]
k	350	15	1024,5
r1	500	15	1037,0
r2	800	15	1102,5
h	1100	15	1160,5
Solar engine			
k	350	10	1019,0
r1	450	10	1028,3
r2	550	10	1044,3
h	650	10	1065,5

Table 4.13: Specific isobar heat capacity of the working gas

4.2.6.3 Starting values

The starting or initial values are mainly taken from the results of section 4.1. The temperatures of the gas in the cells and the wall temperatures of the regenerator are given in the initial conditions (table 4.14). The first pressure values, masses and heat derivatives are then calculated with parts of the equation set (see appendix C3 and C4).

		Biomass	Solar
T_c	[K]	300	
T_k	[K]	$=T_c$	
T_e	[K]	800	500
T_h	[K]	$=T_e$	
T_{r1}	[K]	$=T_k+(T_h-T_c)/4$	
T_{r2}	[K]	$=T_{r1}+(T_h-T_c)/2$	
T_{wk}	[K]	295	
T_{wr1}	[K]	$=T_{r1}+3$	
T_{wr2}	[K]	$=T_{r1}+3$	
T_{wh}	[K]	1'180	635
h_{r1}	[W/(m²·K)]	800	
h_{r2}	[W/(m²·K)]	900	

Table 4.14: Initial values for the quasi steady analysis

4.2.7 Results for the experimental engines
4.2.7.1 Convergence behaviour

Figure 4-50 and 4-51 show the convergence behaviour of the compression space pressure and mass and the temperatures in the different spaces. It takes more than 2'000 iterations to reach cyclic steady state, because of the fact that the regenerator matrix takes many iterations to reach its final wall temperature. All the values are shown for the same crank angle (360°).
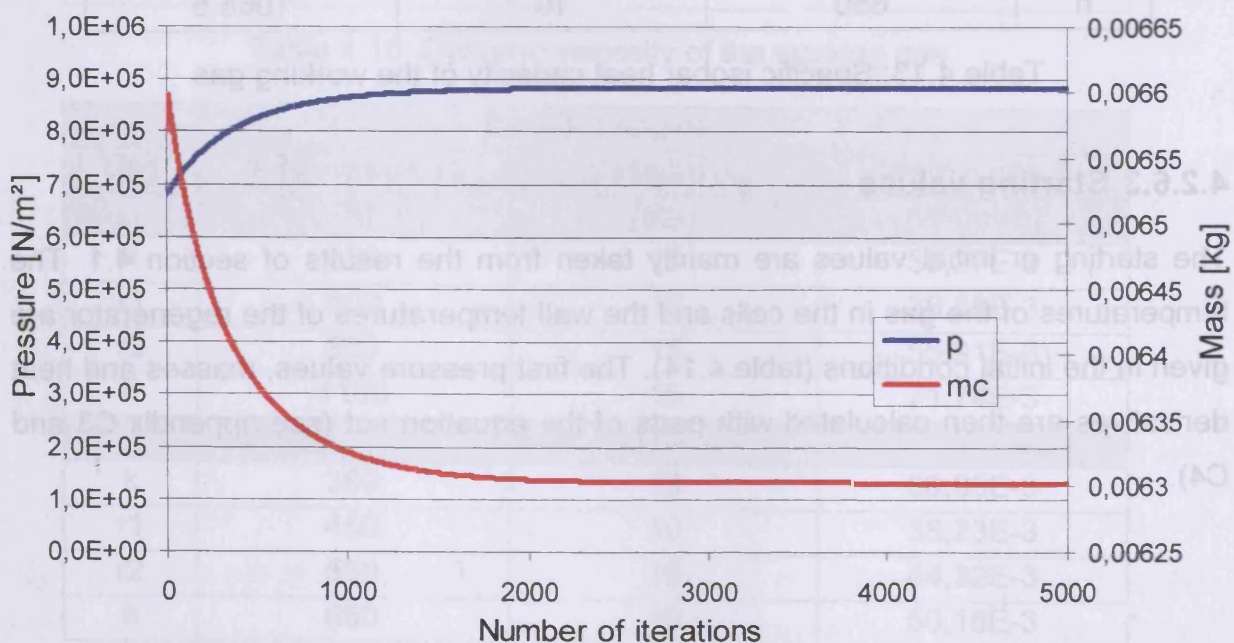
Figure 4-50: Convergence behaviour of pressure and compression space mass

162
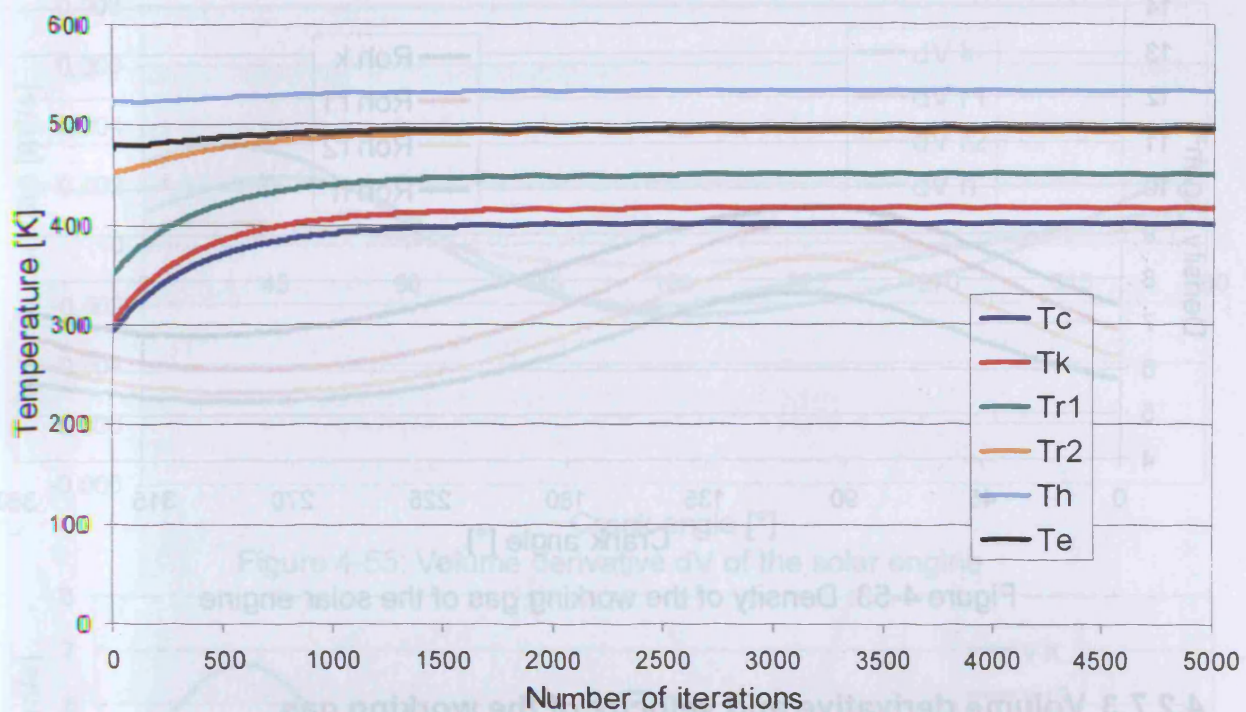
Figure 4-51: Convergence behaviour of the temperatures

In the following chapters the results of the quasi steady flow analysis are shown. They are presented for the biomass engine as well as for the solar engine to verify the results.

4.2.7.2 Density of the working gas

Figure 4-52 and 4-53 show the density of the working gas for the biomass and solar engine. The density is only calculated for the heat exchanger (k, r1, r2 and h) because here they are needed for the further calculation of the loss values.
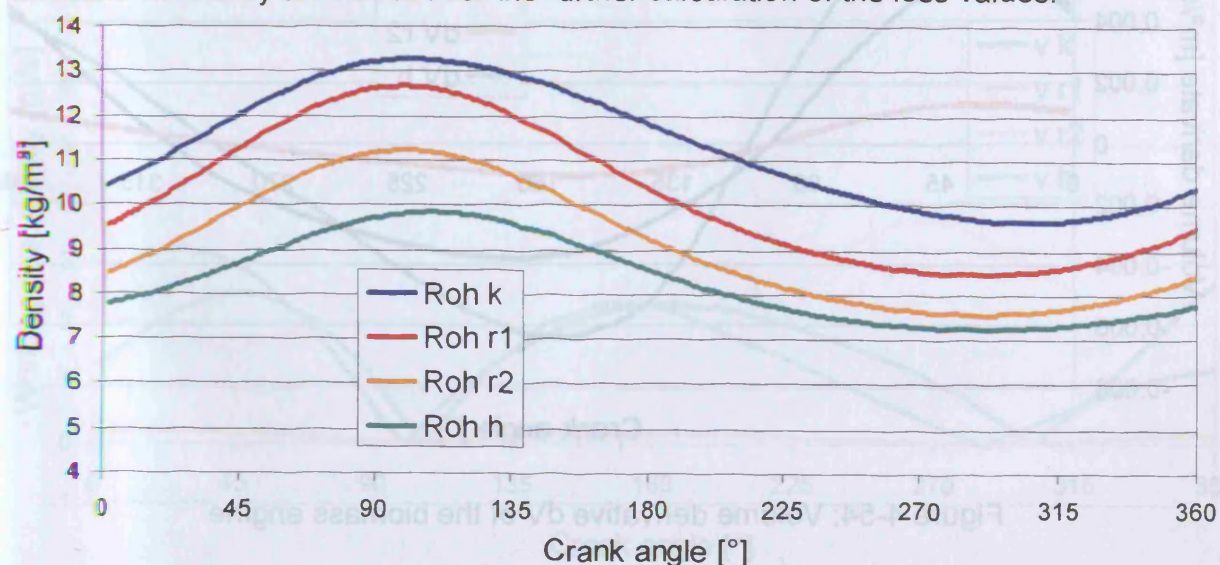
Figure 4-52: Density of the working gas of the biomass engine
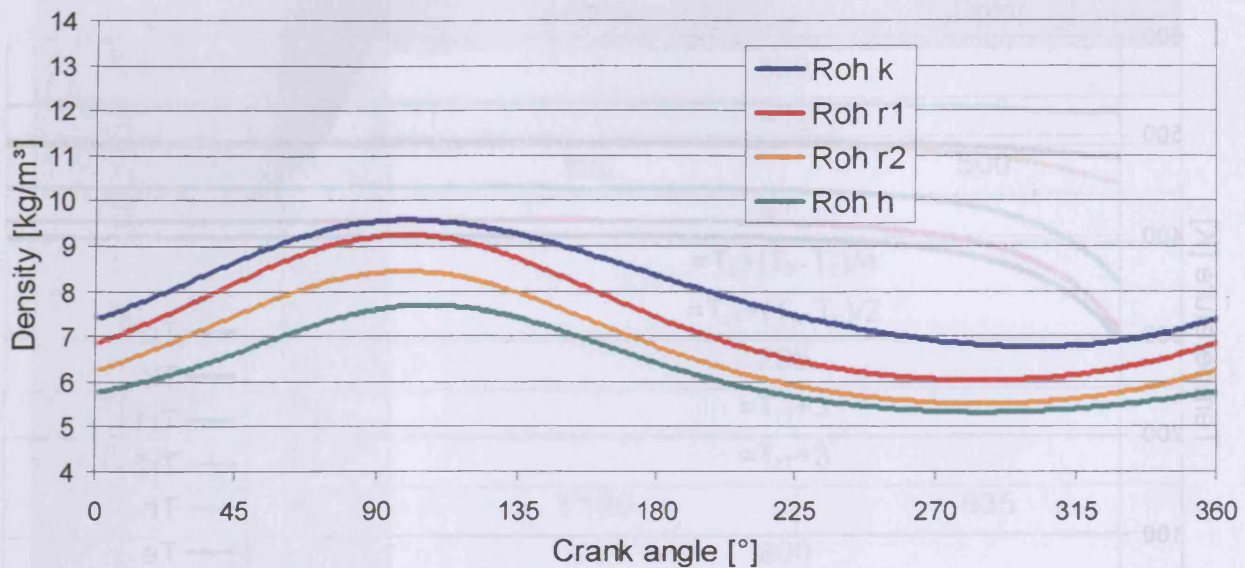
Figure 4-53: Density of the working gas of the solar engine

4.2.7.3 Volume derivative and velocity of the working gas

Figures 4-54 and 4-55 show the volume derivative dV of the working gas in the heat exchanger sections of the biomass and solar engine. The curves for the regenerator 1 and 2 are very close together, because of the same geometry and similar gas properties in these two cells. In the figures 4-56 and 4-57 the gas velocity in these cells is drawn. The velocity of the gas has a maximum value of 6,7 m/s for the biomass engine and 3,2 m/s for the solar engine.
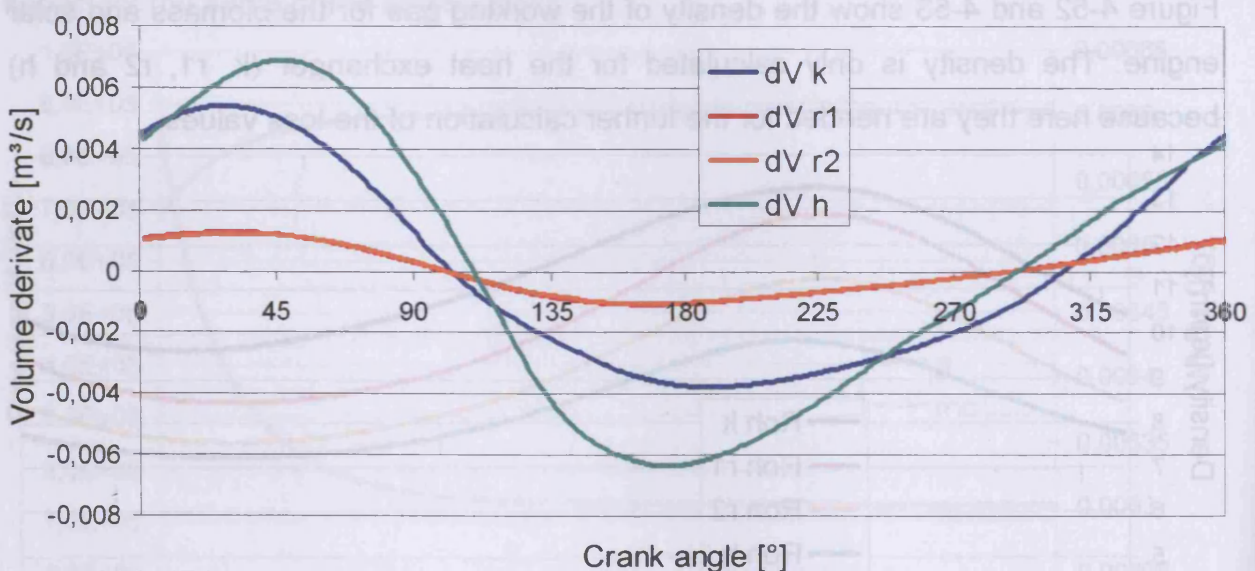
Figure 4-54: Volume derivative dV of the biomass engine
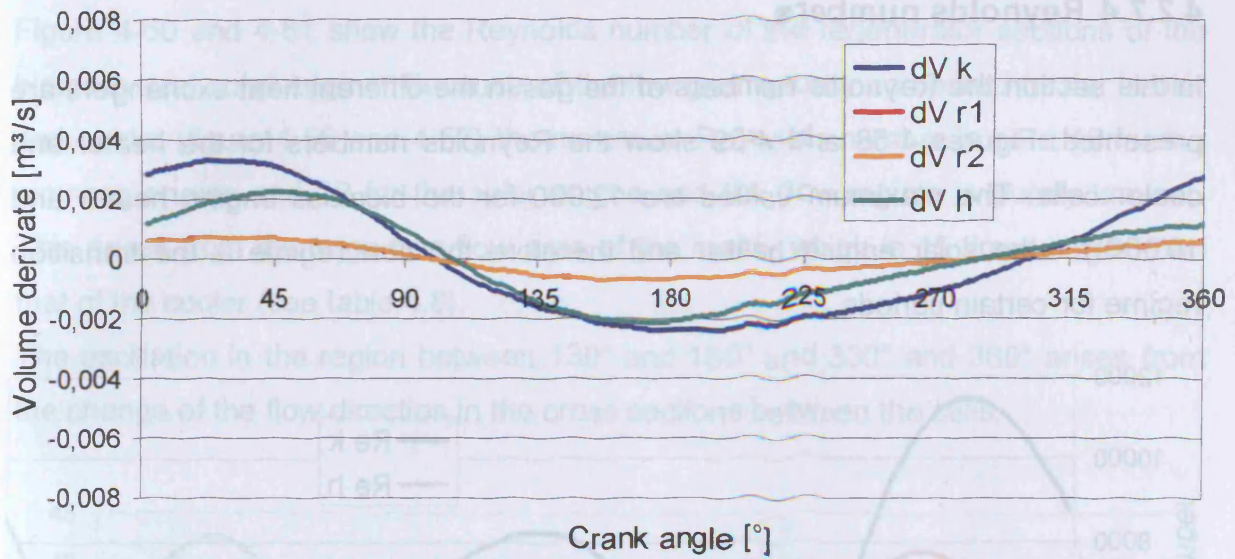
Figure 4-55: Volume derivative dV of the solar engine
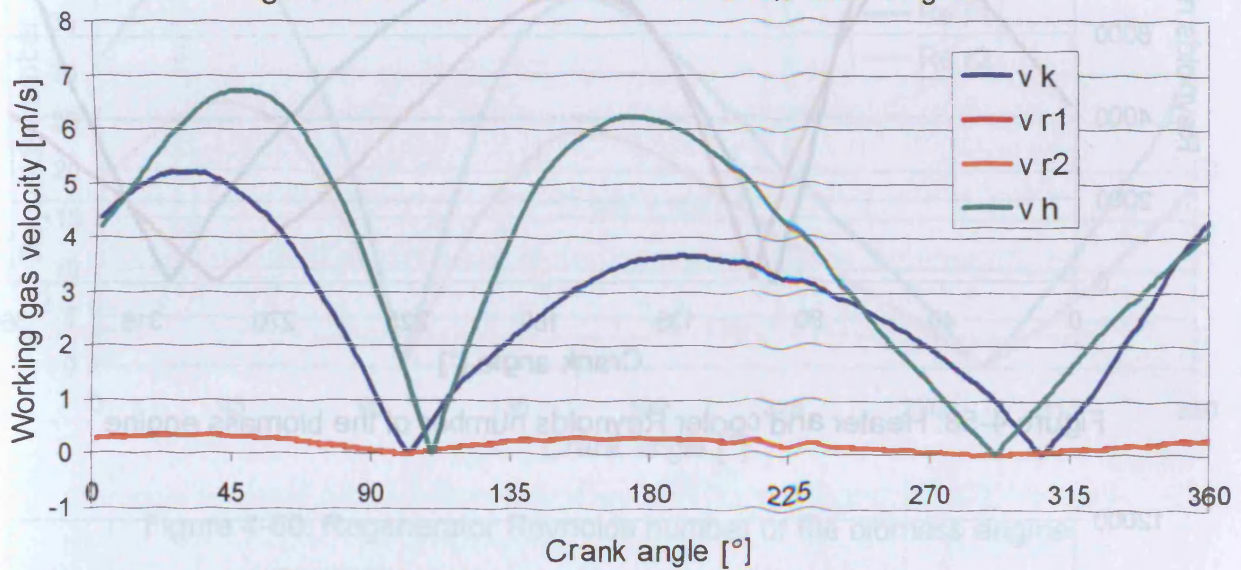
Figure 4-56: Gas velocity of the biomass engine

Figure 4-57: Gas velocity of the solar engine

4.2.7.4 Reynolds numbers

In this section the Reynolds numbers of the gas in the different heat exchangers are presented. Figures 4-58 and 4-59 show the Reynolds numbers for the heater and cooler cells. The maximum values are 12'000 for the biomass engine heater and 10'000 for the solar engine heater and therefore the flow regime is the transition regime for certain periods.
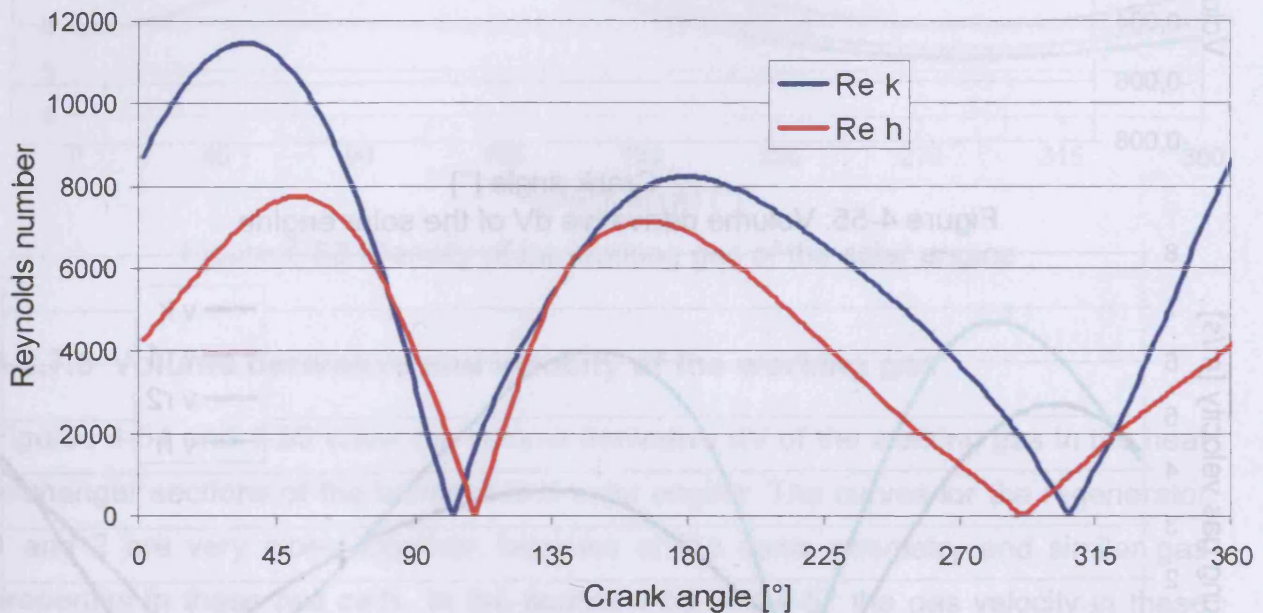
Figure 4-58: Heater and cooler Reynolds number of the biomass engine
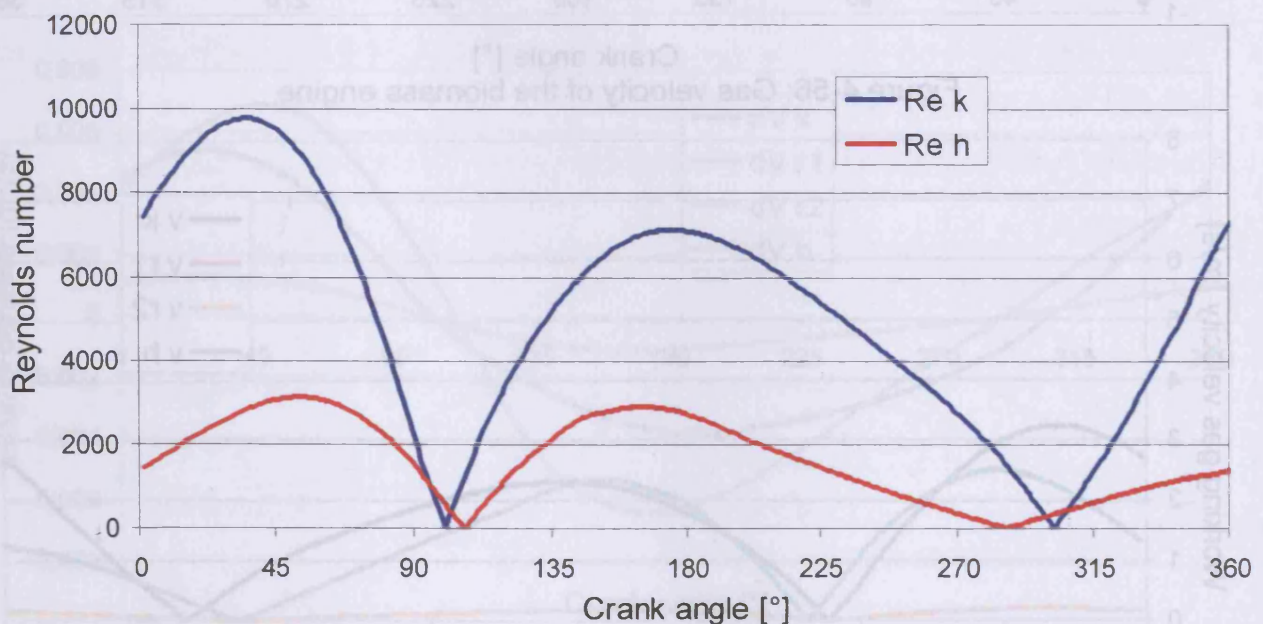
Figure 4-59: Heater and cooler Reynolds number of the solar engine

Figure 4-60 and 4-61 show the Reynolds number of the regenerator sections of the biomass and solar engine. Because of the low gas velocity compared to the heater and cooler (figure 4-56 and 4-57) the maximum Reynolds number is here 45 for the biomass engine and 20 for the solar engine and the flow regime is purely laminar. This arises from the huge free flow area of the matrix which is 15 times larger than that of the cooler (see table 4.8).

The oscillation in the region between 130° and 150° and 330° and 360° arises from the change of the flow direction in the cross sections between the cells.
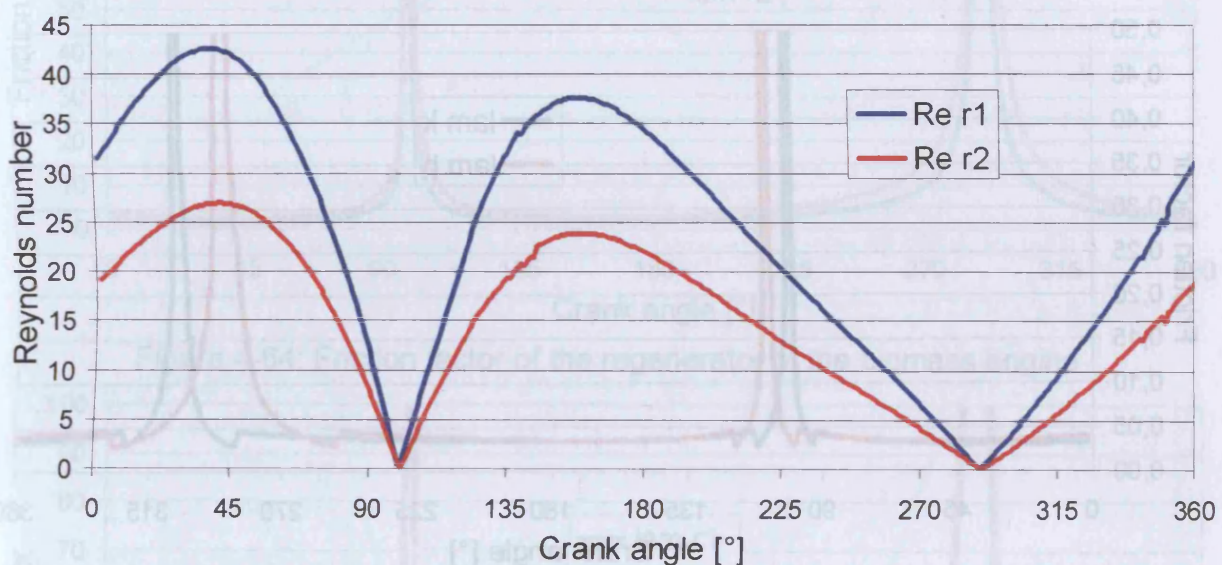
Figure 4-60: Regenerator Reynolds number of the biomass engine
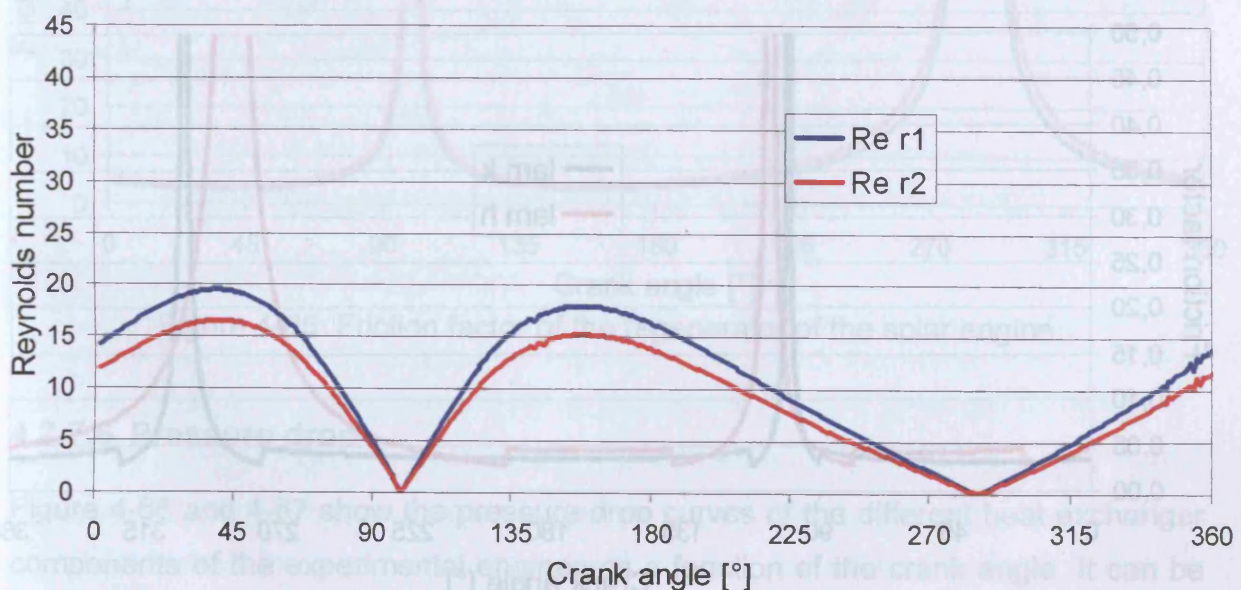
Figure 4-61: Regenerator Reynolds number of the solar engine

4.2.7.5 Friction factor

In figure 4-62 and 4-63 the curve of the friction factor for the cooler and heater of the two engines is displayed. The unsteadiness in the curves arise from the different equations for laminar and transition flow (4.131) – (4.133). It can be clearly seen, that the process of the solar engine proceeds longer under laminar flow conditions. This arises from the lower pressure and reduced speed of the solar system.

When the gas velocity reaches 0, the Reynolds number becomes also 0 and the friction factor could not be defined. Because of this the maximum value for the friction factor is defined to be 640.
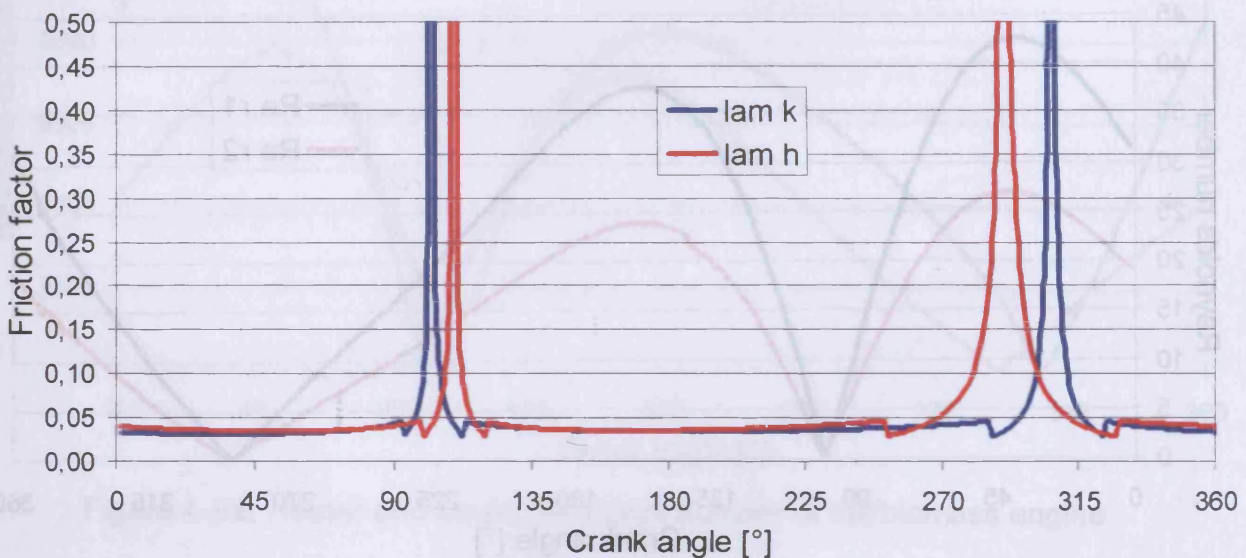
Figure 4-62: Friction factor of the heater and cooler of the biomass engine
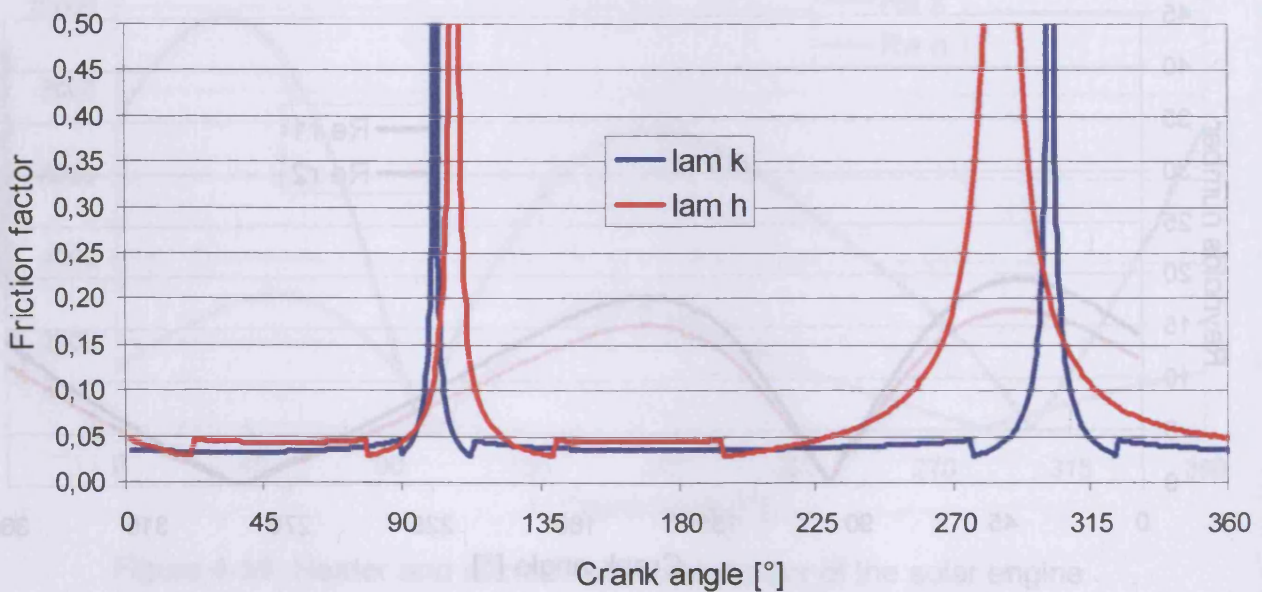
Figure 4-63: Friction factor of the heater and cooler of the solar engine

168

Figure 4-64 and 4-65 show the friction factors for the regenerator sections of both engines. The flow regime is laminar all the time and so the curves are steady over the complete cycle in contrast to the ones of the heater and the cooler (figure 4-62 and 4-63).
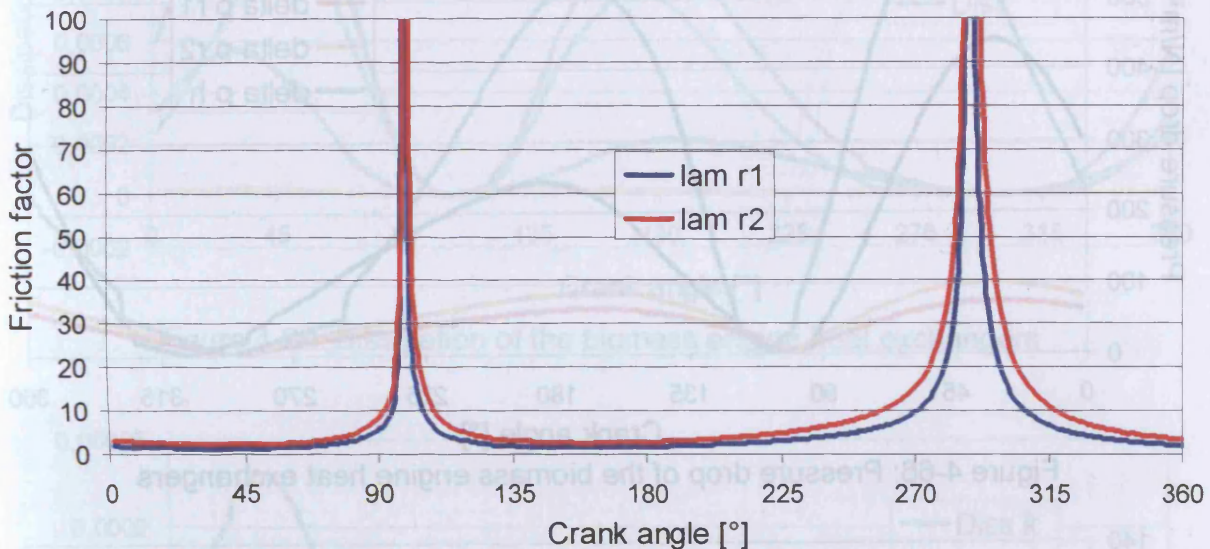
Figure 4-64: Friction factor of the regenerator of the biomass engine
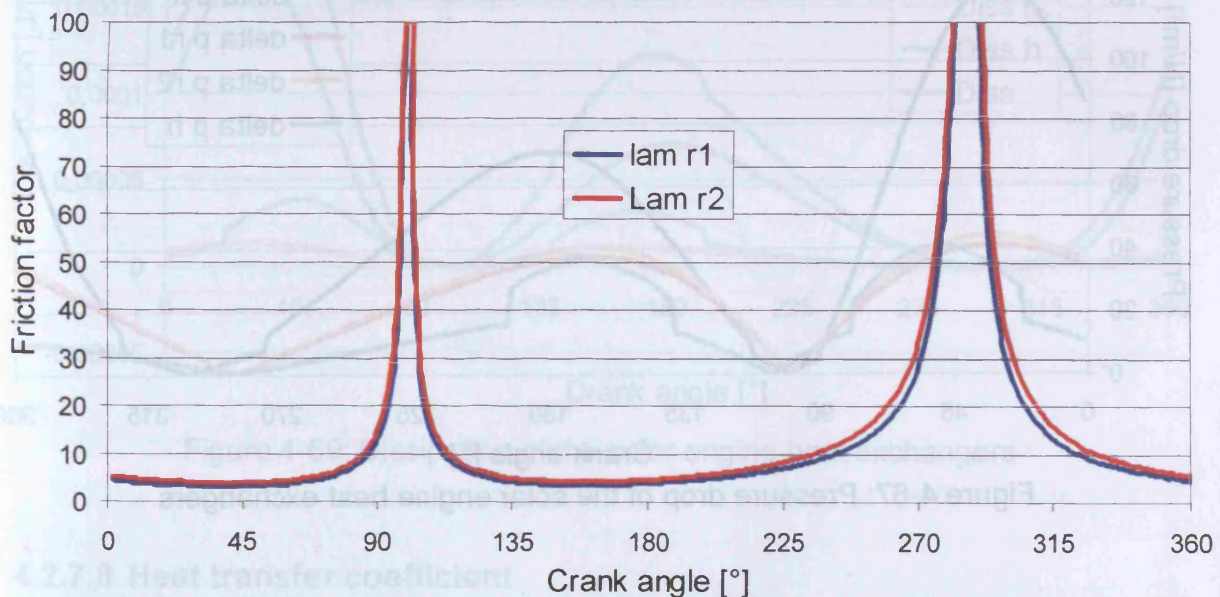
Figure 4-65: Friction factor of the regenerator of the solar engine

4.2.7.6 Pressure drop

Figure 4-66 and 4-67 show the pressure drop curves of the different heat exchanger components of the experimental engines as a function of the crank angle. It can be seen that the highest pressure drops of about 600 N/m² for the biomass engine and 130 N/m² for the solar engine are produced by the heater with its long pipes and the

highest gas velocity. The pressure drop of the regenerator is very low between 100 and 40 N/m². These values arise from the high free flow area and the low gas velocity of the regenerator.
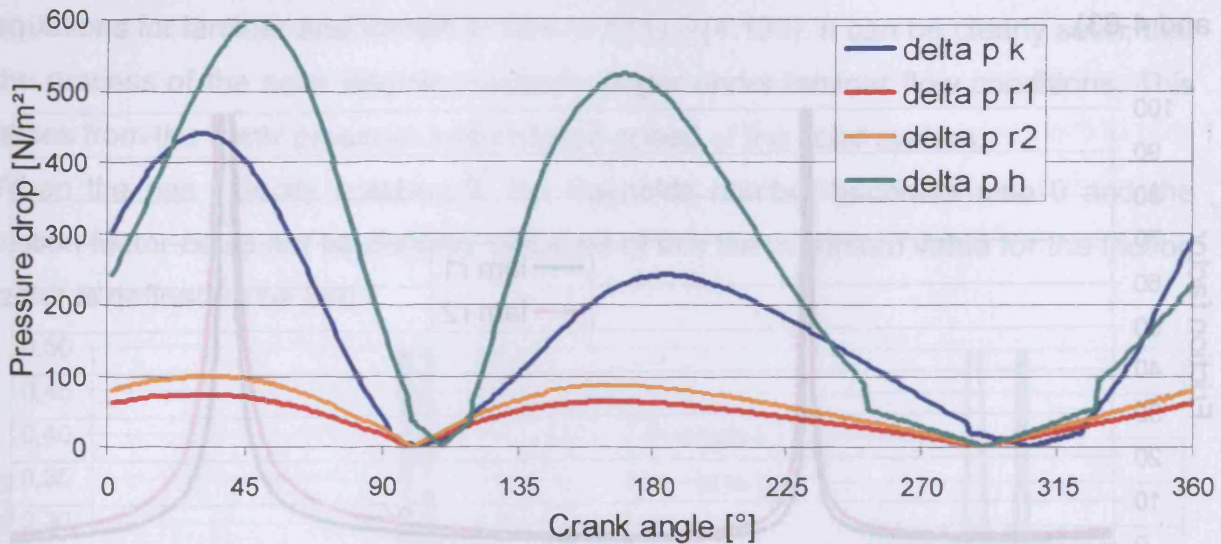
Figure 4-66: Pressure drop of the biomass engine heat exchangers
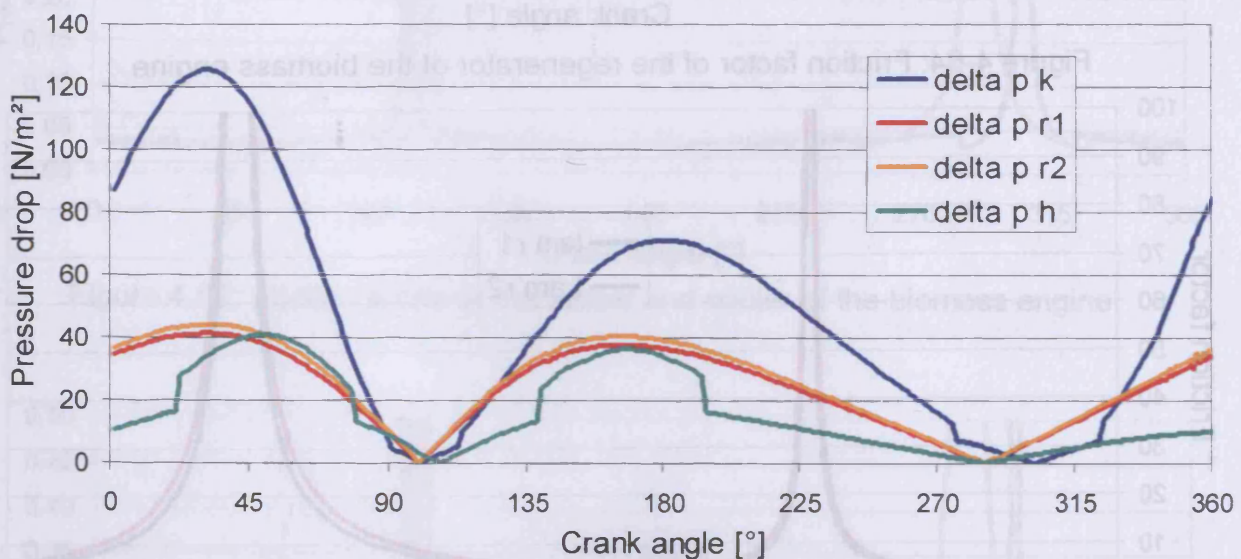
Figure 4-67: Pressure drop of the solar engine heat exchangers

4.2.7.7 Dissipation

The dissipation values of the biomass and solar engine can be seen in figures 4-68 and 4-69. The dissipation caused by the pressure drops has a very low value compared to the heat transferred by the heat exchangers. These losses are negligible small and cause only small differences from the ideal adiabatic model. The high losses are the heat transfer losses in the heater and cooler.
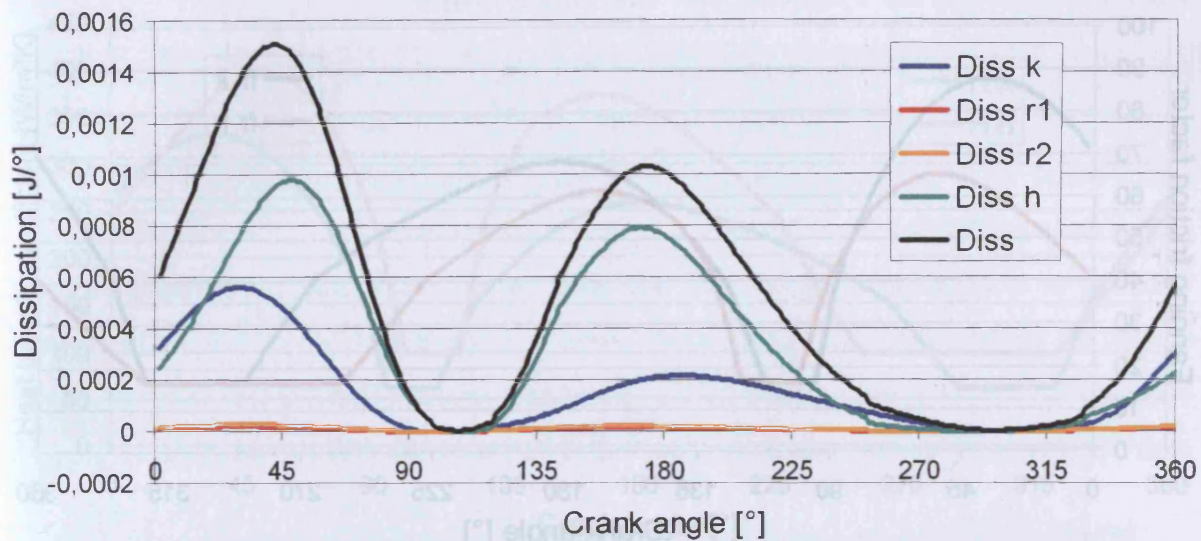
Figure 4-68: Dissipation of the biomass engine heat exchangers
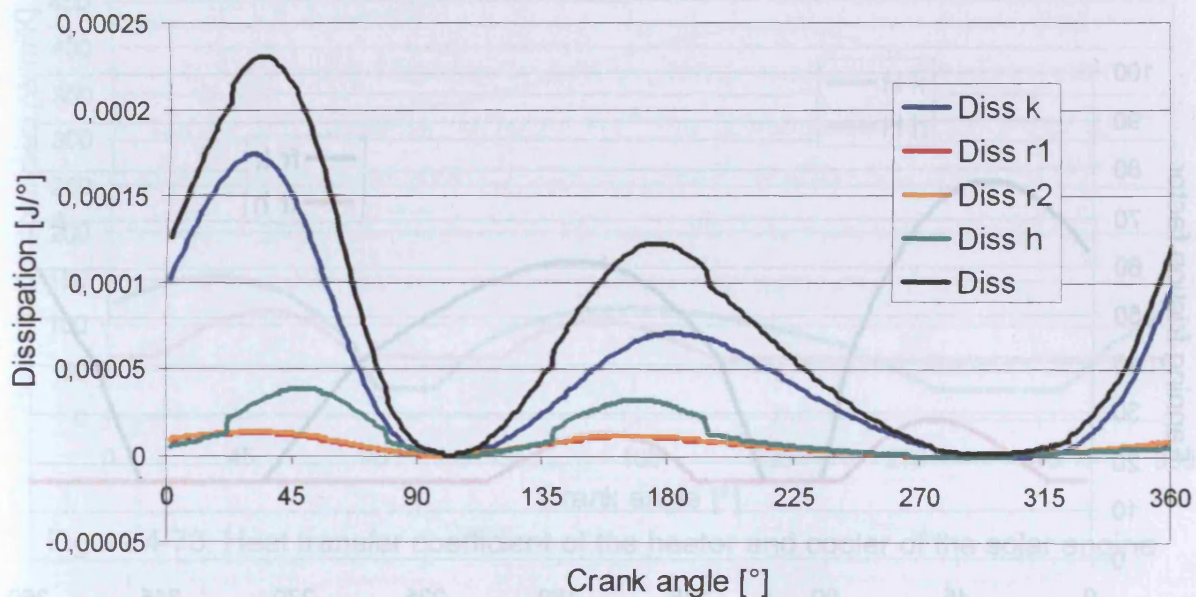
Figure 4-69: Dissipation of the solar engine heat exchangers

4.2.7.8 Heat transfer coefficient

Figures 4-70 and 4-71 show the Fanning friction factors of the heater and the cooler of the biomass and solar engine. The straight line in these figures shows where the Reynolds number is less than 2'000. For the regenerator section the Fanning friction factor is set to the constant value of 16 because of the low Reynolds numbers.
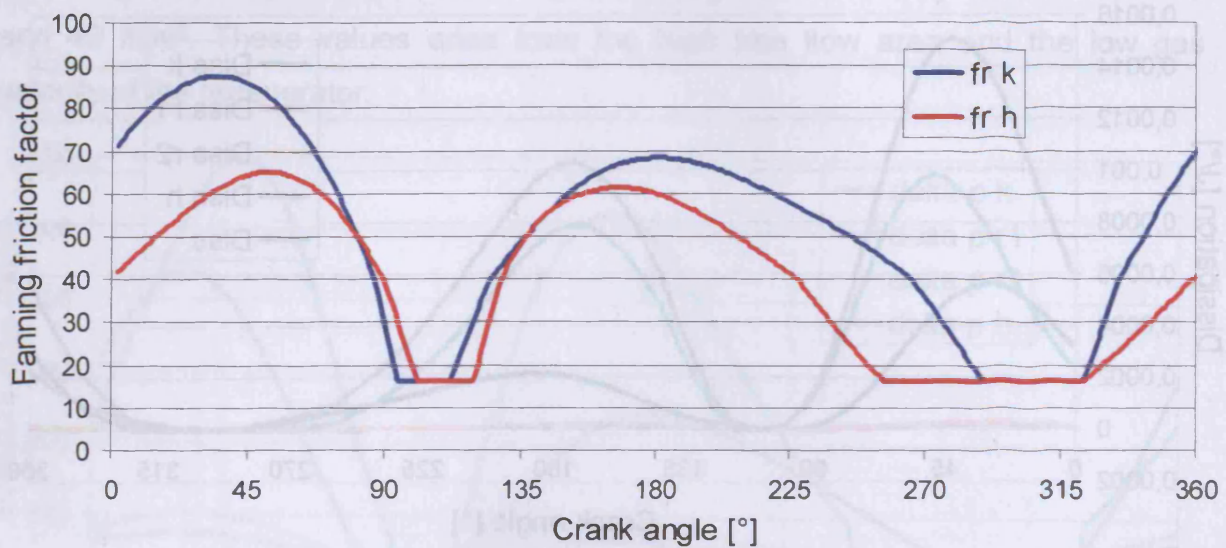
Figure 4-70: Fanning friction factor of the heater and cooler of the biomass engine
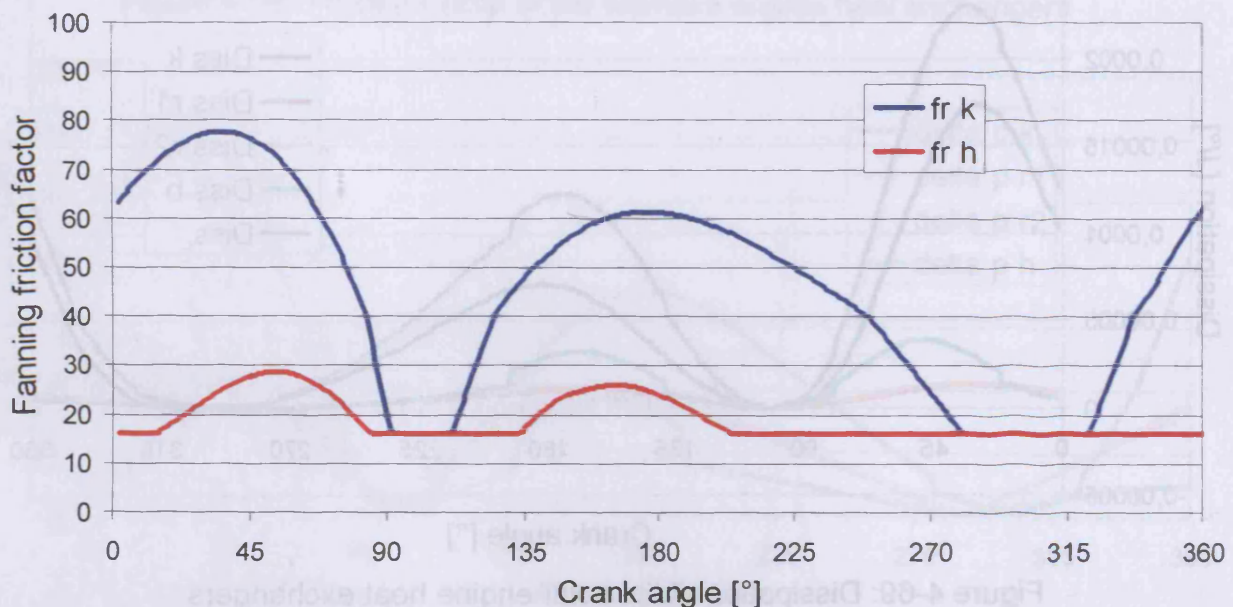
Figure 4-71: Fanning friction factor of the heater and cooler of the solar engine

Figures 4-72, 4-73 and 4-74 show the heat transfer coefficients of the heat exchangers of both engines. The regenerator values are constant because of the constant Fanning friction factor. The high heat transfer coefficients of the two regenerator cells arise from the low free flow diameter and the resulting Reynolds numbers.
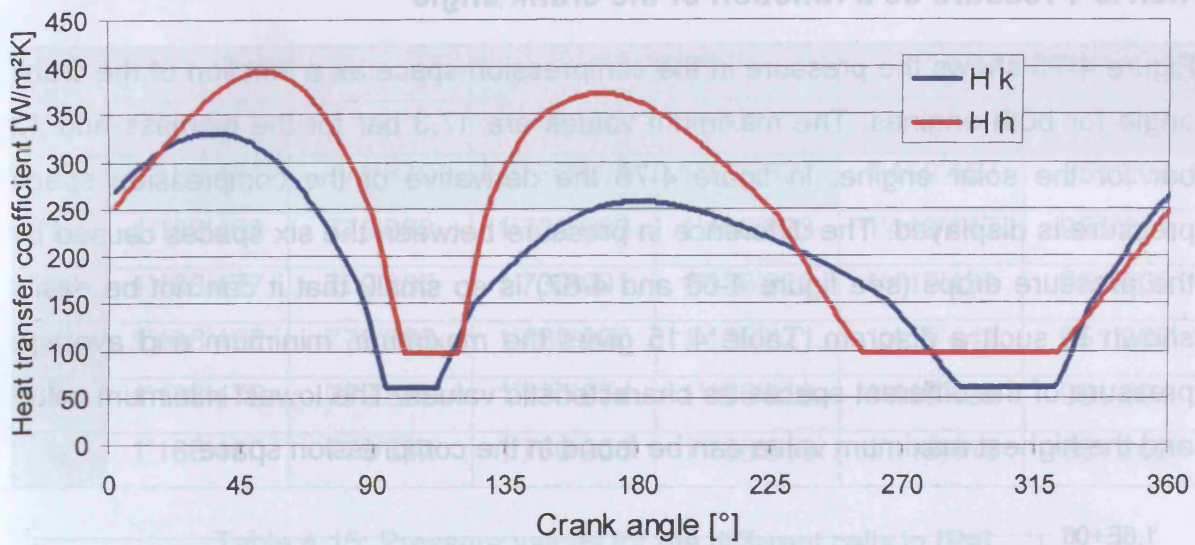
Figure 4-72: Heat transfer coefficient of the heater and cooler of the biomass engine
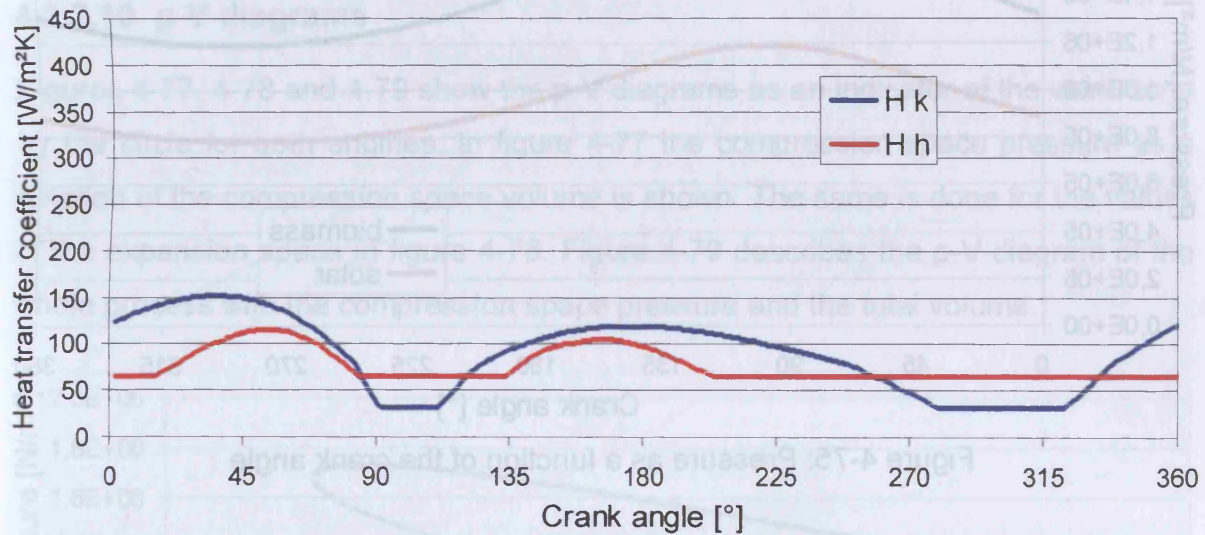
Figure 4-73: Heat transfer coefficient of the heater and cooler of the solar engine
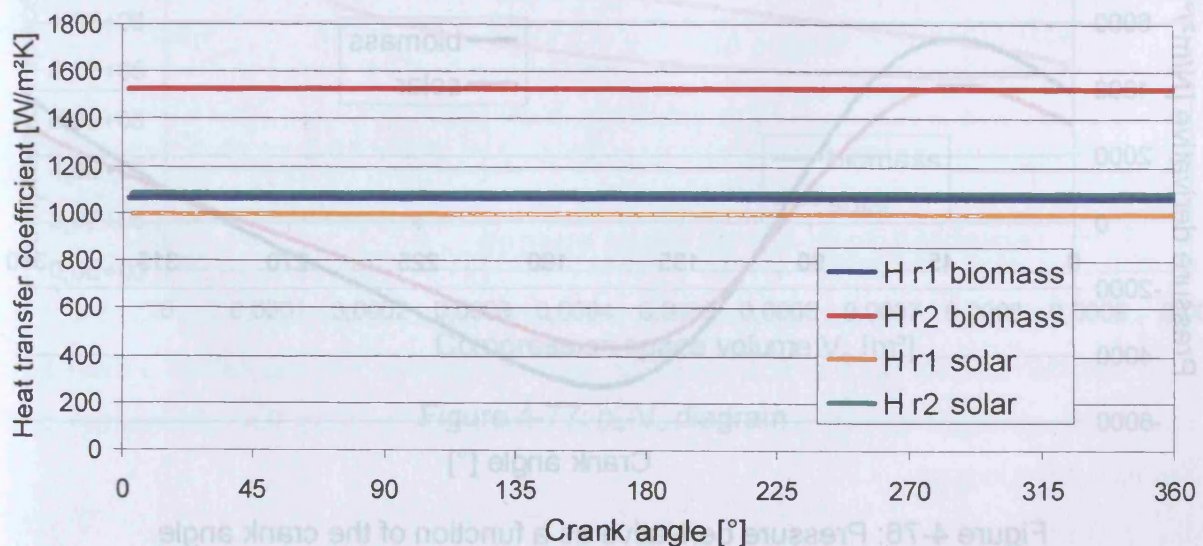
Figure 4-74: Heat transfer coefficient of the regenerator sections

4.2.7.9 Pressure as a function of the crank angle

Figure 4-75 shows the pressure in the compression space as a function of the crank angle for both engines. The maximum values are 17,3 bar for the biomass and 12 bar for the solar engine. In figure 4-76 the derivative of the compression space pressure is displayed. The difference in pressure between the six spaces caused by the pressure drops (see figure 4-66 and 4-67) is so small, that it can not be easily shown in such a diagram. Table 4.15 gives the maximum, minimum and average pressure of the different spaces as characteristic values. The lowest minimum value and the highest maximum value can be found in the compression space.
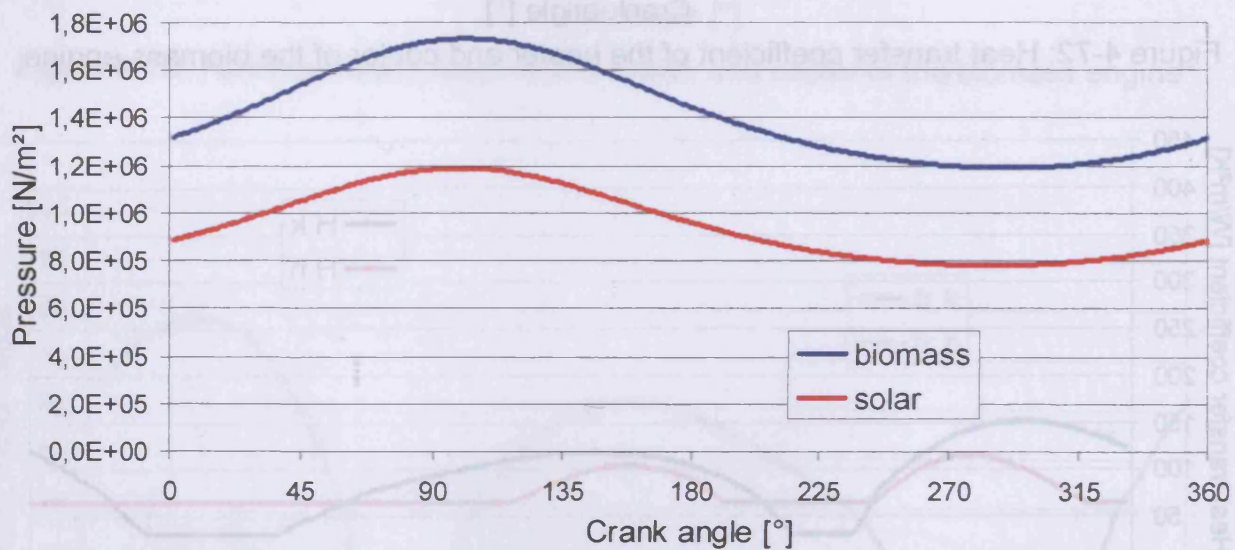
Figure 4-75: Pressure as a function of the crank angle
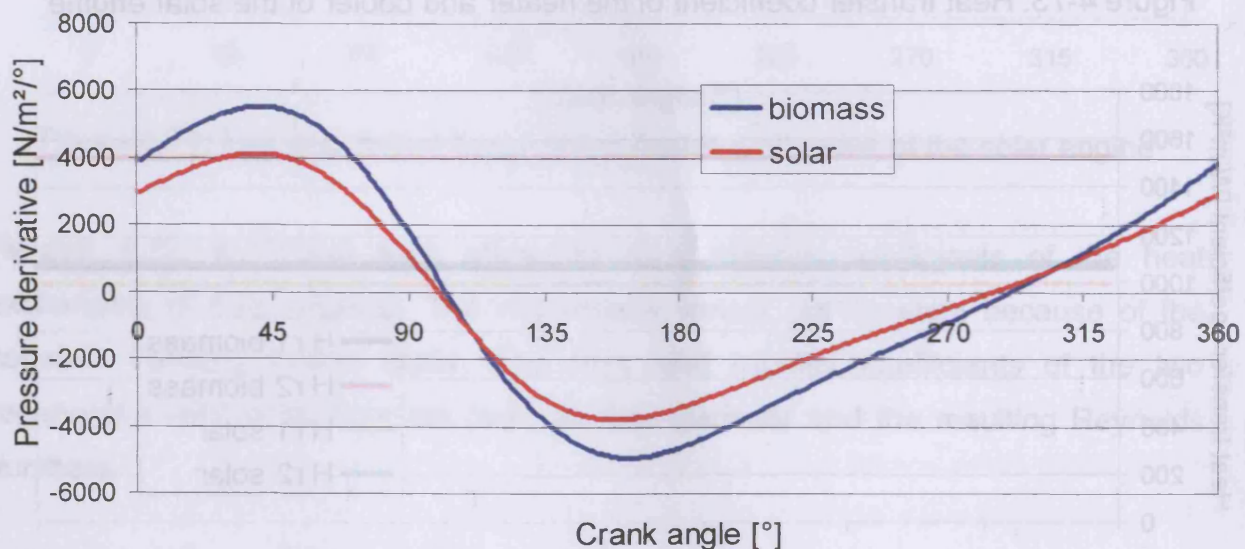
Figure 4-76: Pressure derivative as a function of the crank angle

cell	minimum		maximum		average	
	b	s	b	s	b	s
c	1'188'461	779'879	1'730'994	1'186'824	1'419'457	951'204
k	1'188'469	779'882	1'730'993	1'186'823	1'419'447	951'201
r1	1'188'477	779'885	1'730'991	1'186'822	1'419'439	951'200
r2	1'188'478	779'886	1'730'990	1'186'821	1'419'442	951'202
h	1'188'479	779'887	1'730'974	1'186'818	1'419'438	951'201
e	1'188'480	779'887	1'730'956	1'186'816	1'419'418	951'200

Table 4.15: Pressure values for the different cells in [Pa]

4.2.7.10 p-V diagrams

Figures 4-77, 4-78 and 4-79 show the p-V diagrams as an indicator of the work done by the circle for both engines. In figure 4-77 the compression space pressure as a function of the compression space volume is shown. The same is done for the values of the expansion space in figure 4-78. Figure 4-79 describes the p-V diagram of the whole process with the compression space pressure and the total volume.
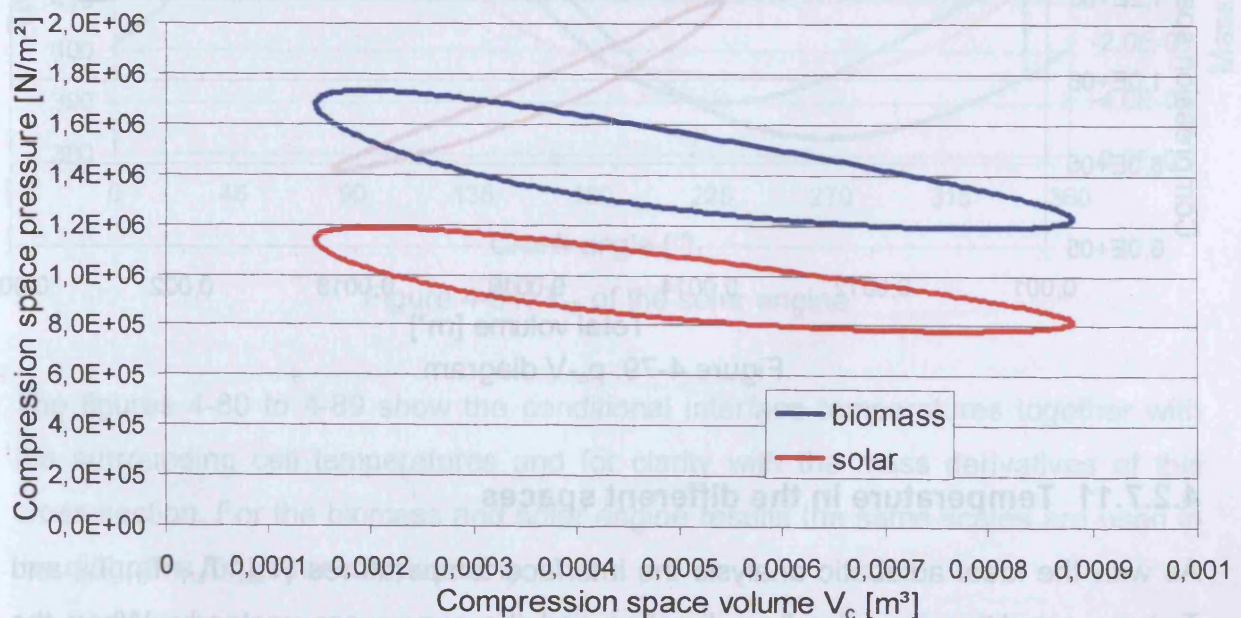
Figure 4-77: p_c-V_c diagram
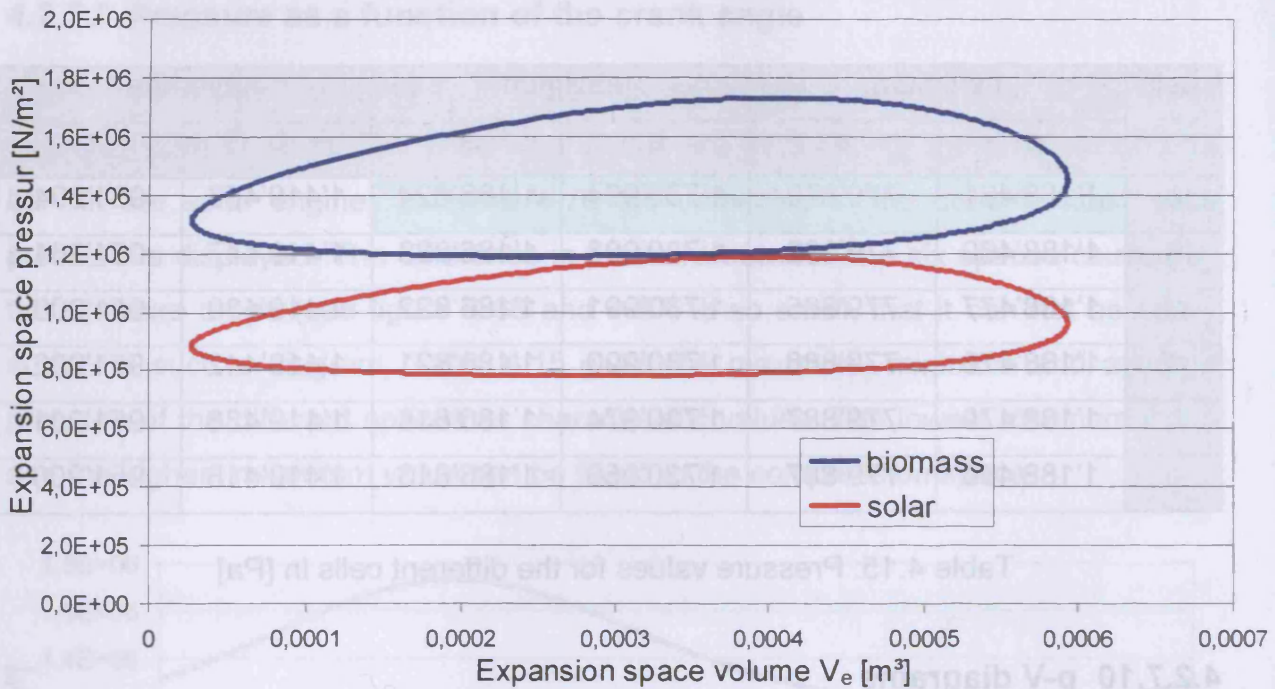
Figure 4-78: p$_e$-V$_e$ diagram
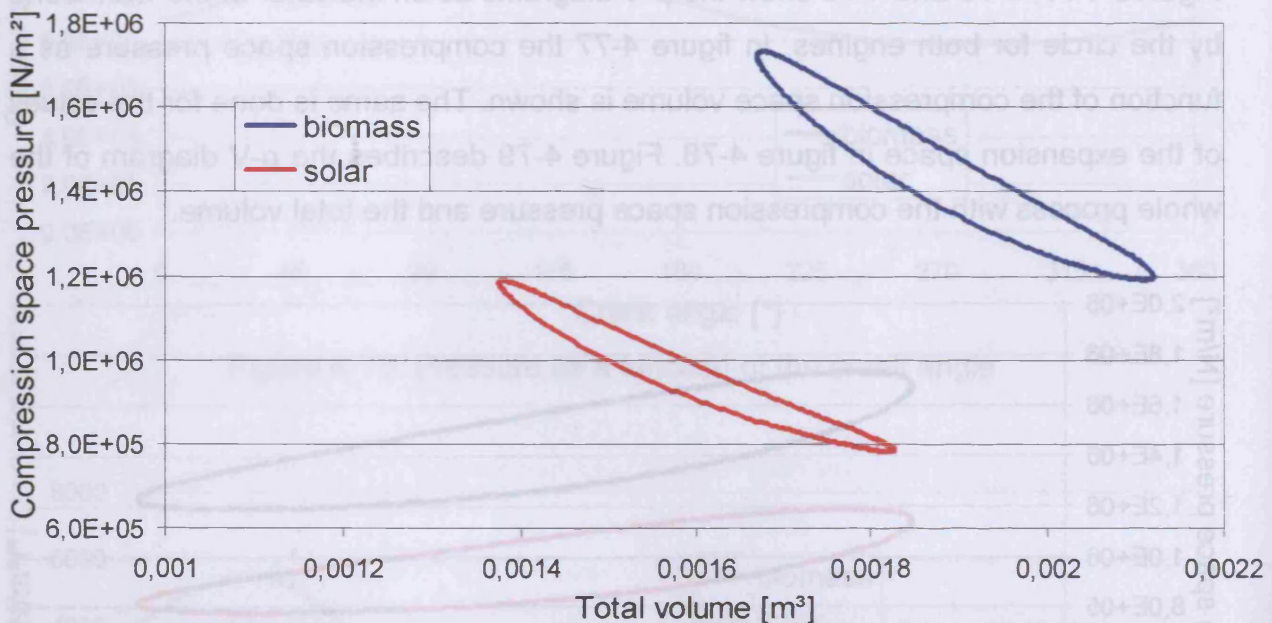
Figure 4-79: p$_c$-V diagram

4.2.7.11 Temperature in the different spaces

As with the ideal adiabatic analysis the interface temperatures (T$_{ck}$, T$_{kr}$, T$_{rr}$, T$_{rh}$ and T$_{he}$) are conditional on the flow direction and the curves are unsteady. When the mass flow changes its direction, the interface temperature takes the value of the cell the gas flows out of.
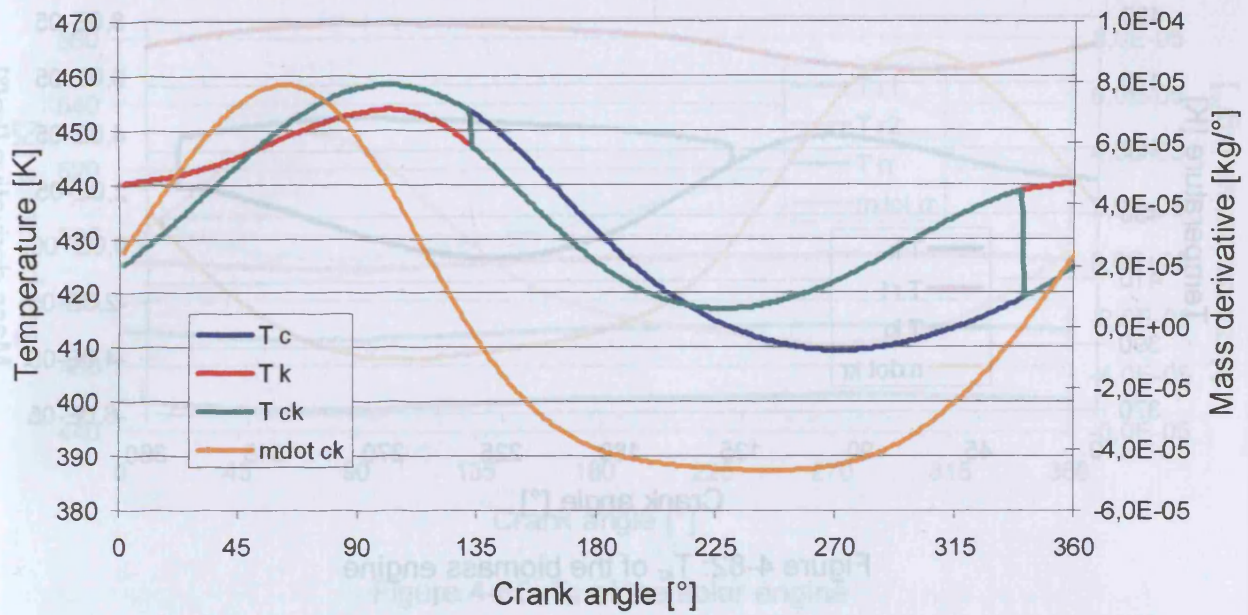
Figure 4-80: T_{ck} of the biomass engine
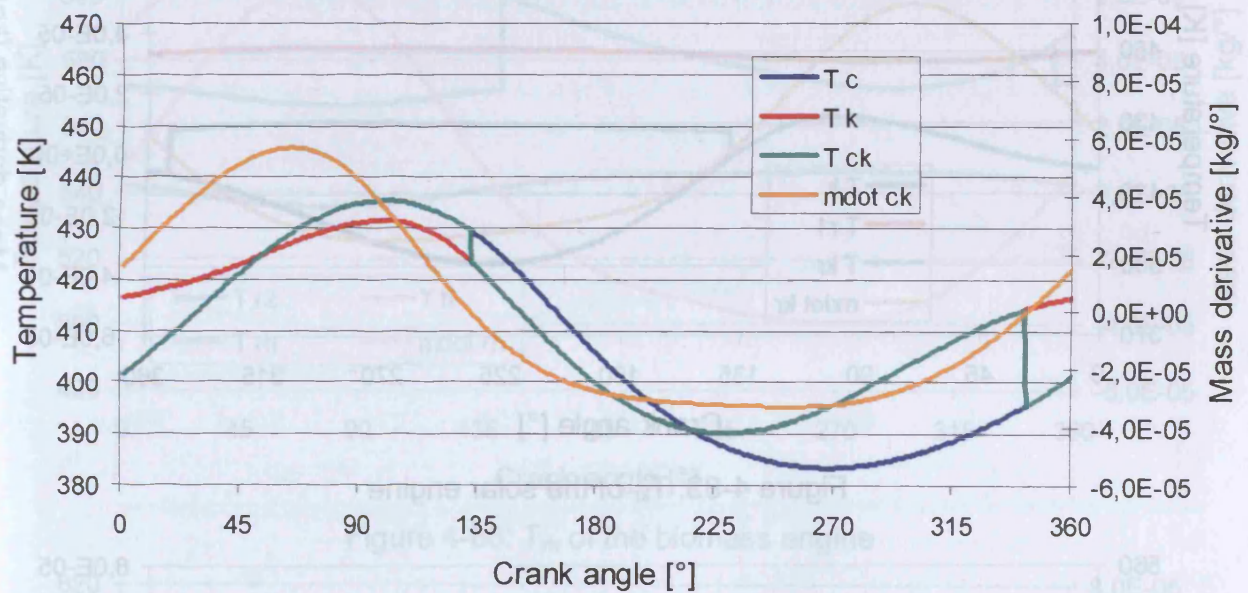
Figure 4-81: T_{ck} of the solar engine

The figures 4-80 to 4-89 show the conditional interface temperatures together with the surrounding cell temperatures and for clarity with the mass derivatives of this cross section. For the biomass and solar engine results the same scales are used in the diagrams for better comparability.
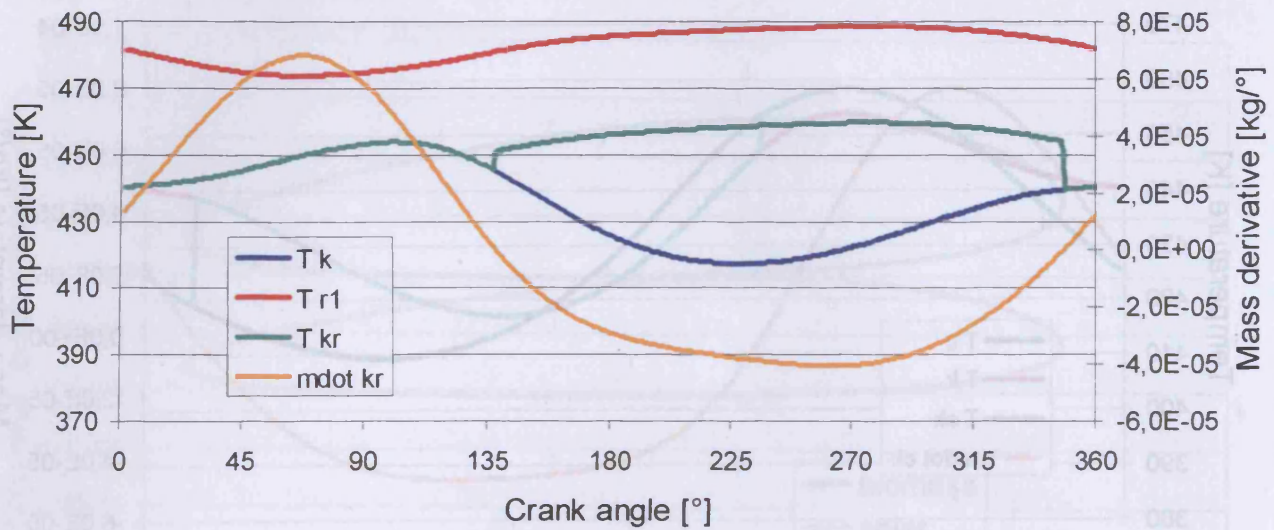
Figure 4-82: T_{kr} of the biomass engine
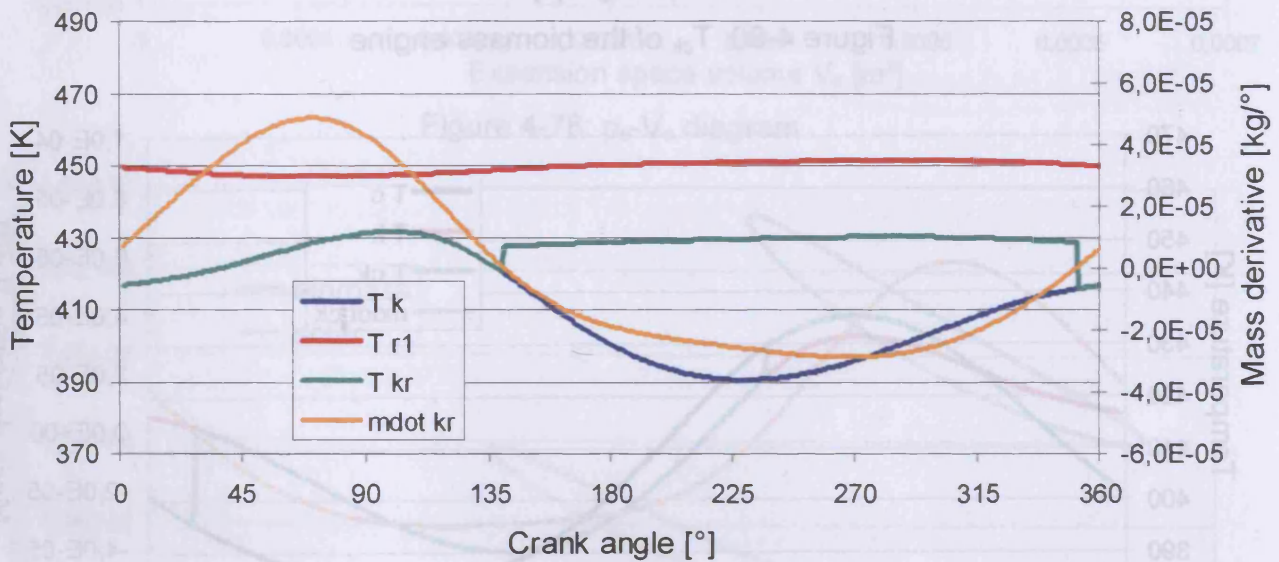
Figure 4-83: T_{kr} of the solar engine
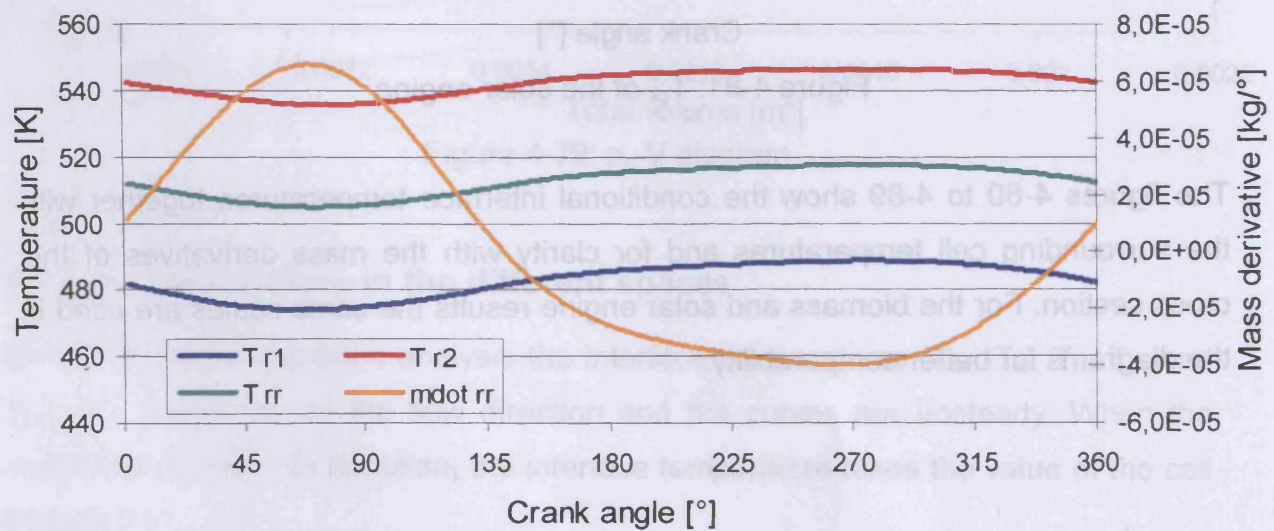
Figure 4-84: T_{rr} of the biomass engine
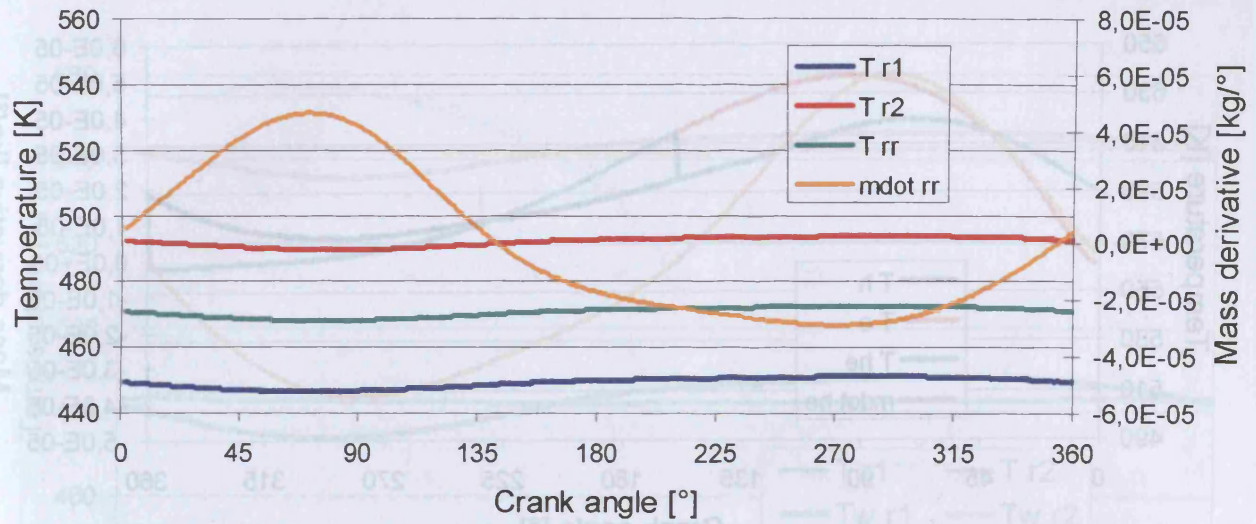
Figure 4-85: T$_{rr}$ of the solar engine
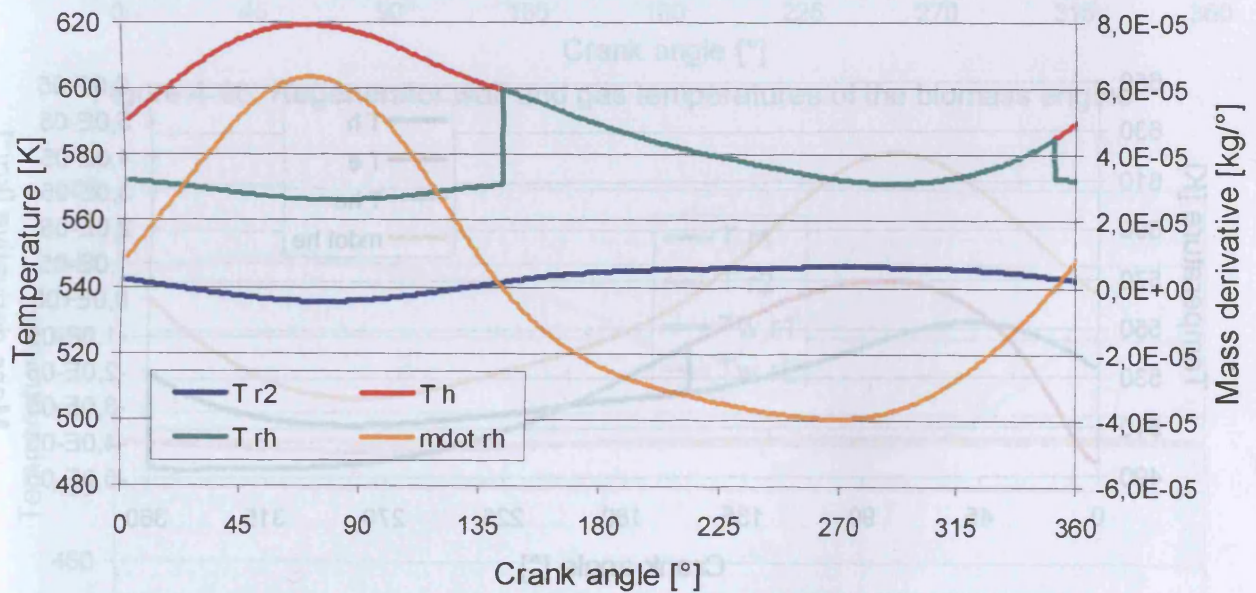
Figure 4-86: T$_{rh}$ of the biomass engine
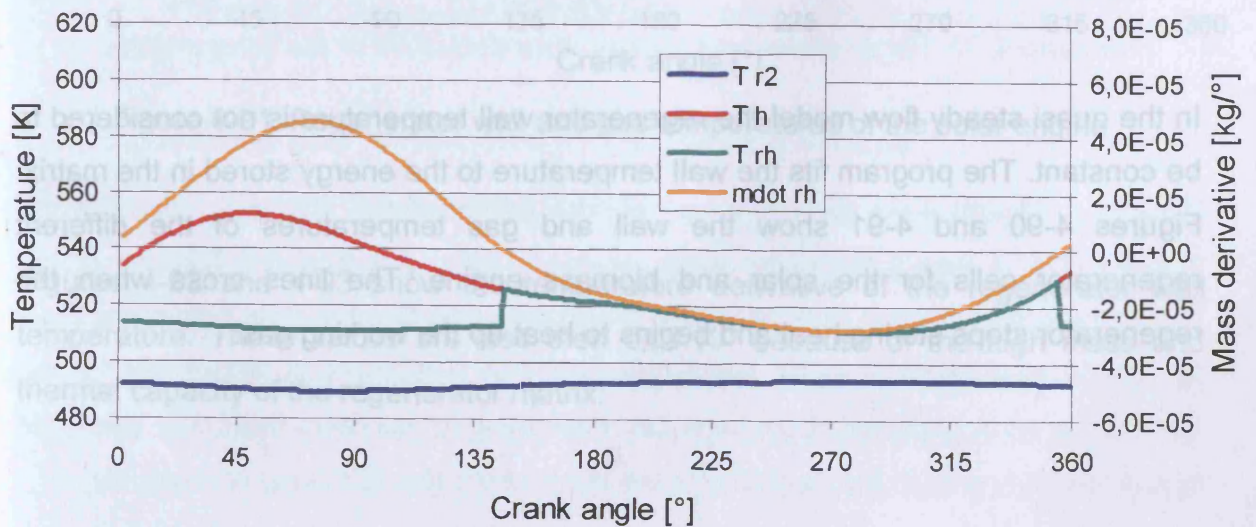
Figure 4-87: T$_{rh}$ of the solar engine
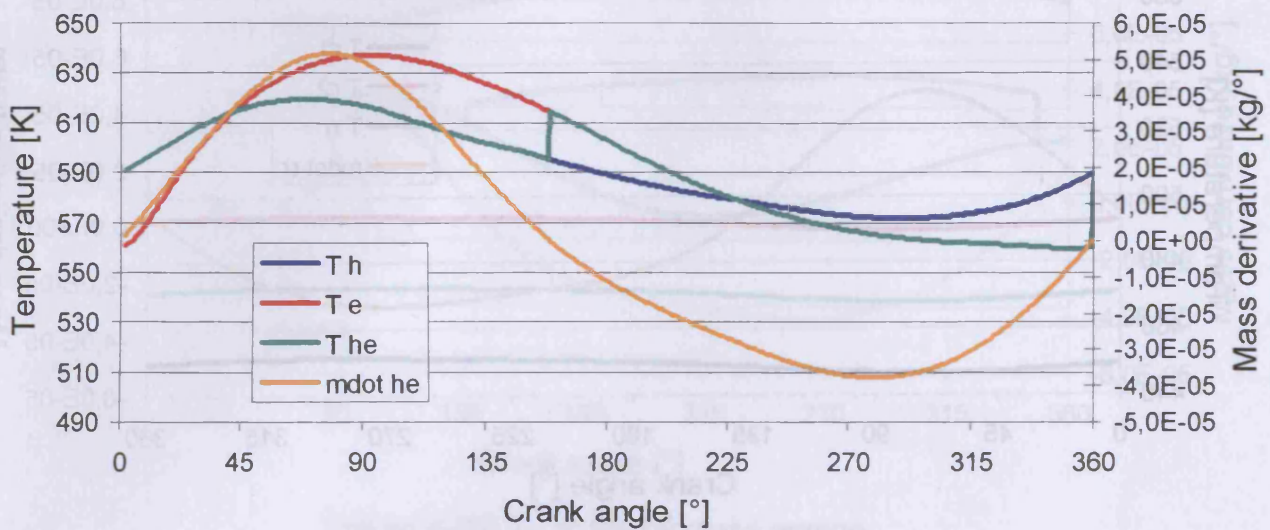
Figure 4-88: T$_{he}$ of the biomass engine
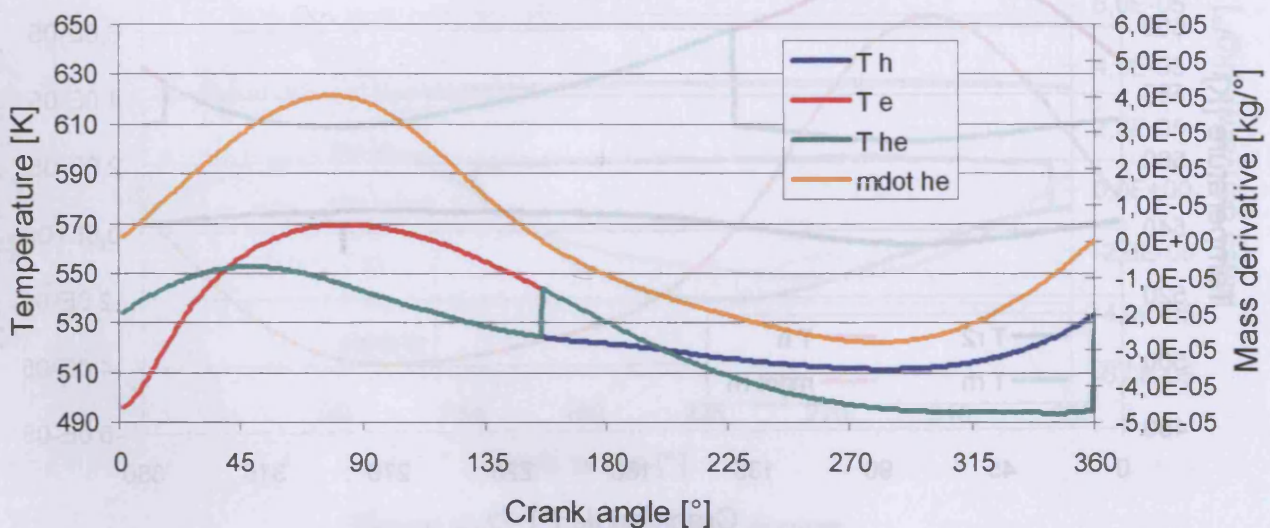
Figure 4-89: T$_{he}$ of the solar engine

In the quasi steady flow model the regenerator wall temperature is not considered to be constant. The program fits the wall temperature to the energy stored in the matrix. Figures 4-90 and 4-91 show the wall and gas temperatures of the different regenerator cells for the solar and biomass engine. The lines cross when the regenerator stops storing heat and begins to heat up the working gas.
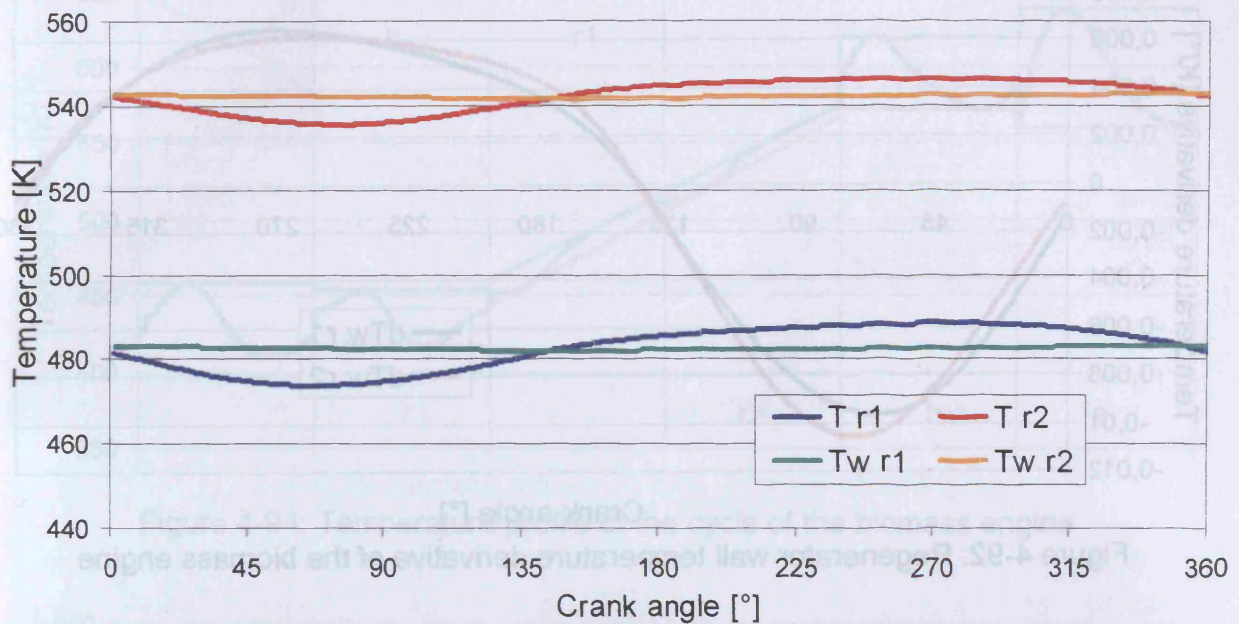
Figure 4-90: Regenerator wall and gas temperatures of the biomass engine
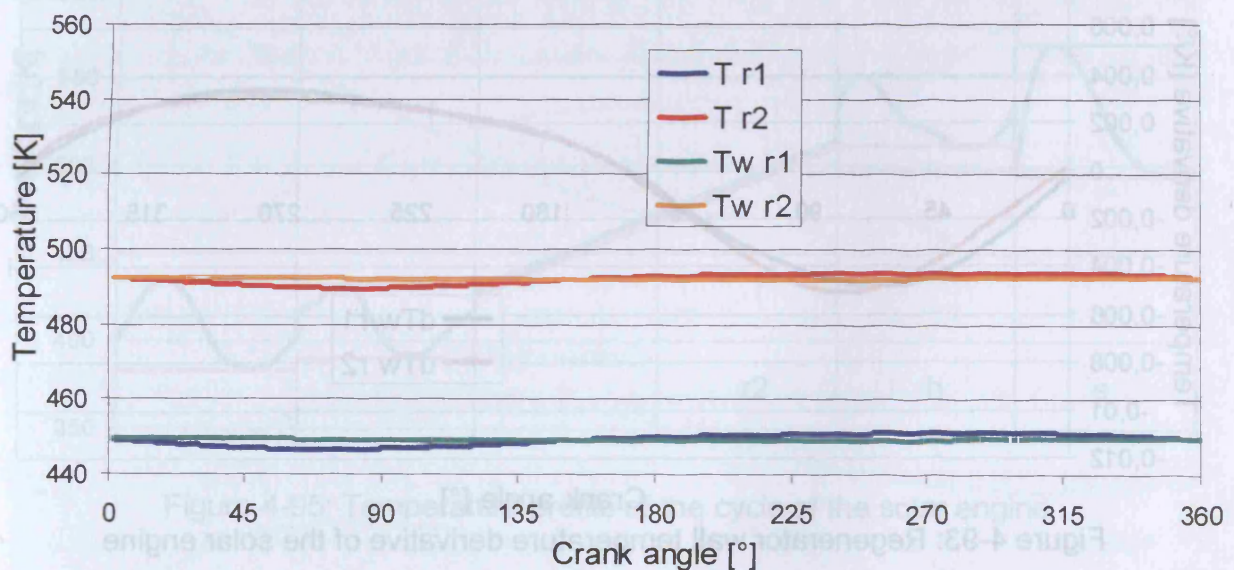
Figure 4-91: Regenerator wall and gas temperatures of the solar engine

Figures 4-92 and 4-93 show the temperature derivative of the regenerator wall temperature. These values are less then 0,01 K/° because of the high mass and thermal capacity of the regenerator matrix.
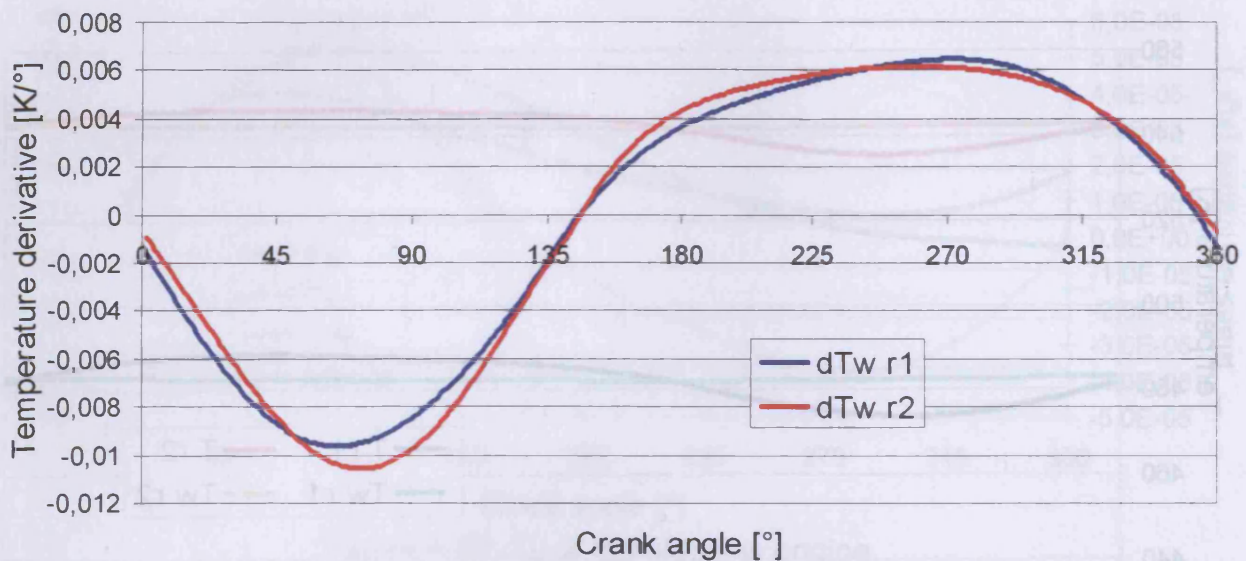
Figure 4-92: Regenerator wall temperature derivative of the biomass engine
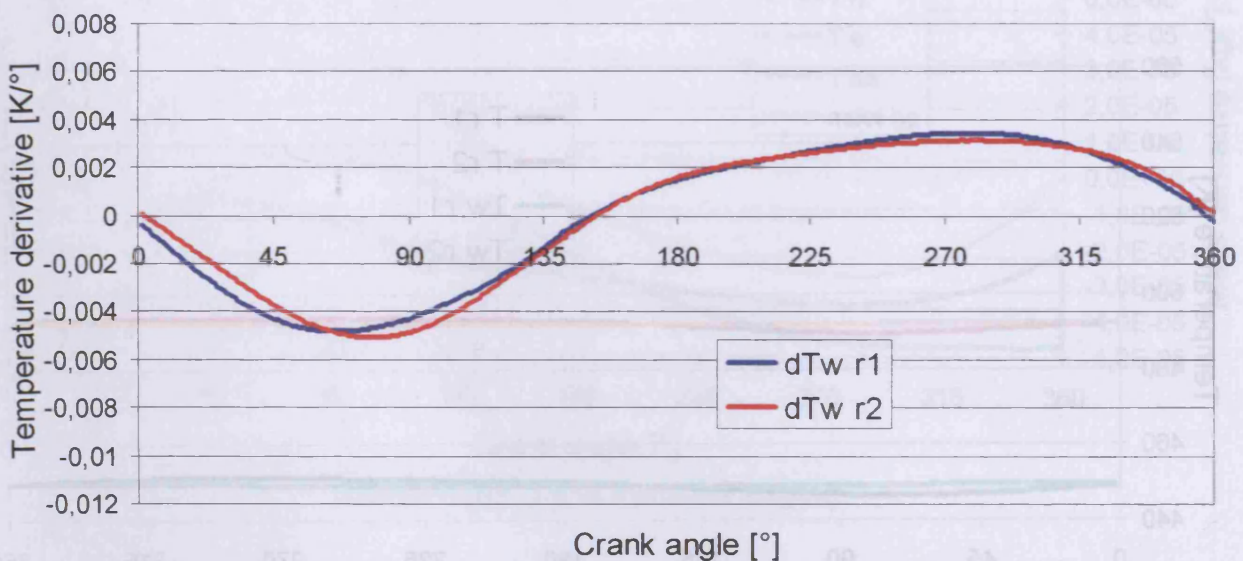
Figure 4-93: Regenerator wall temperature derivative of the solar engine

Figures 4-94 and 4-95 show the temperature profile of the different cells over the whole cycle in one diagram for each engine. The green and red lines mark the minimum and maximum temperatures. It can be seen that the gas temperatures of the cooler and heater are far away from the wall temperatures, especially for the biomass engine because of the high gas velocities. This shows that there are huge heat transfer losses in the heater sections diminishing the efficiency enormously.
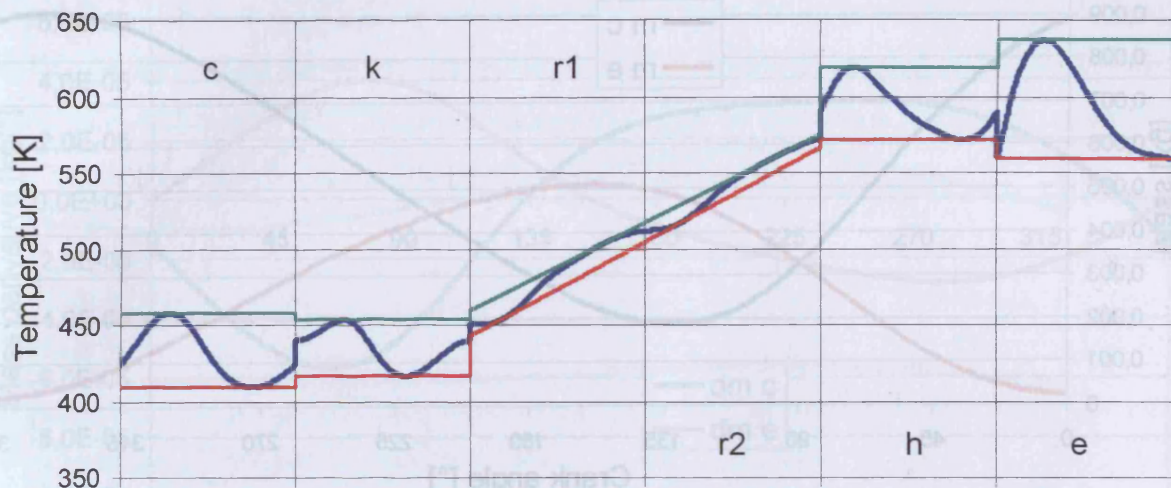
Figure 4-94: Temperature profile of the cycle of the biomass engine
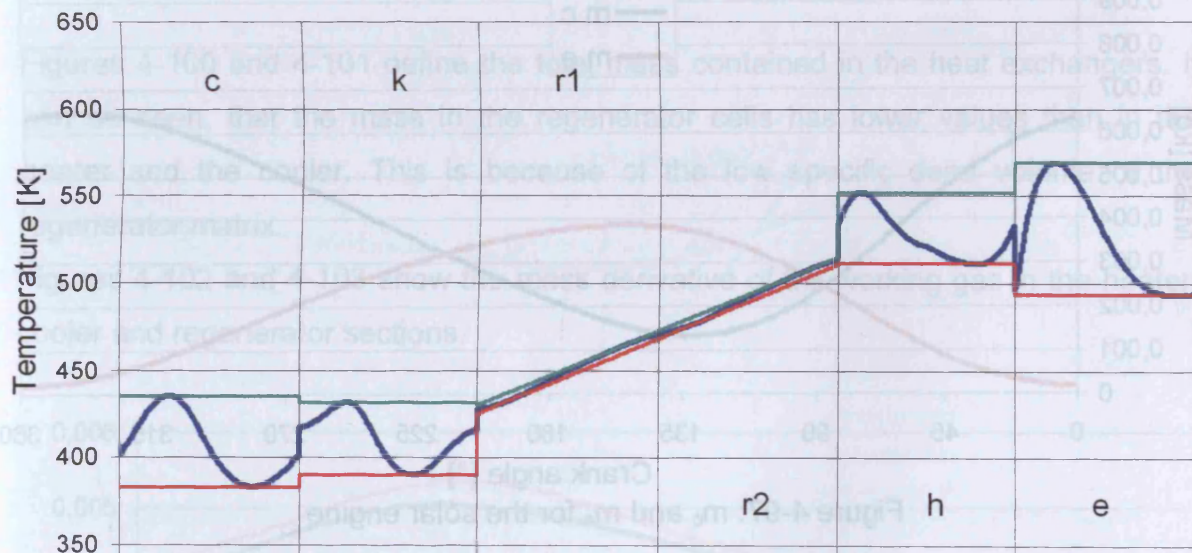
Figure 4-95: Temperature profile of the cycle of the solar engine

4.2.7.12 Masses and mass flows in the different spaces

Figures 4-96 and 4-97 show the total mass of working gas that is in the expansion and compression space of the biomass and solar engine. The figures for the engines are similar in their curves and can only be differentiated by the amplitudes. This is caused by the higher pressure of the biomass engine. Figures 4-98 and 4-99 display the mass derivative of the working gas in the compression and expansion space. The curves have a plateau between 170° and 270° caused by the non sinusoidal piston movement introduced in this calculation.

Figure 4-96: m_c and m_e for the biomass engine

Figure 4-97: m_c and m_e for the solar engine

Figure 4-98: dm_c and dm_e for the biomass engine

184
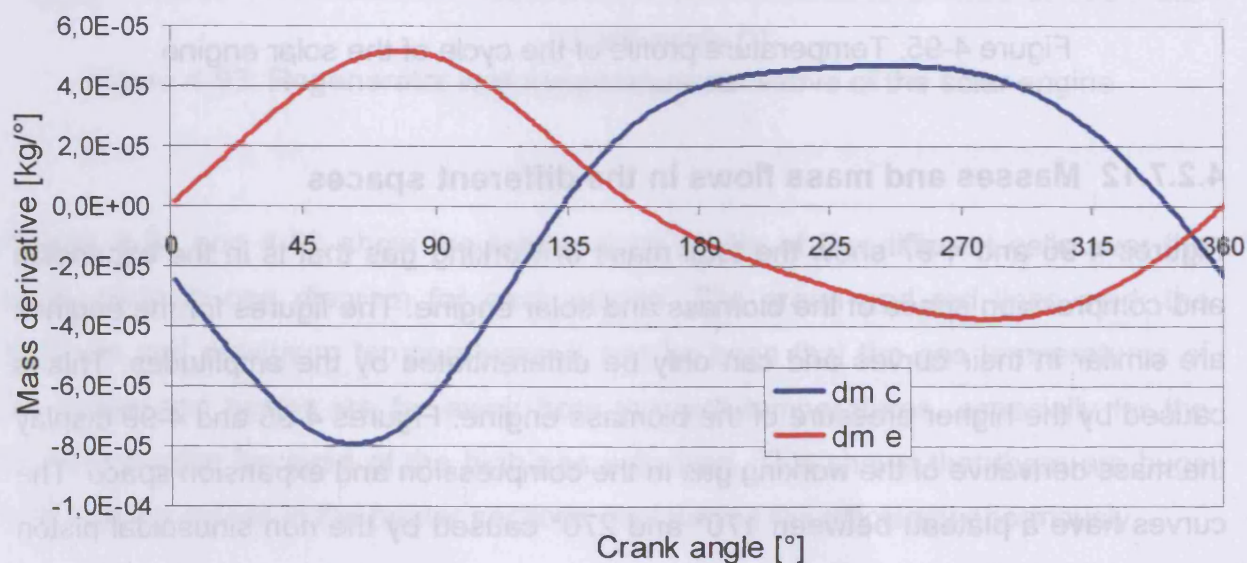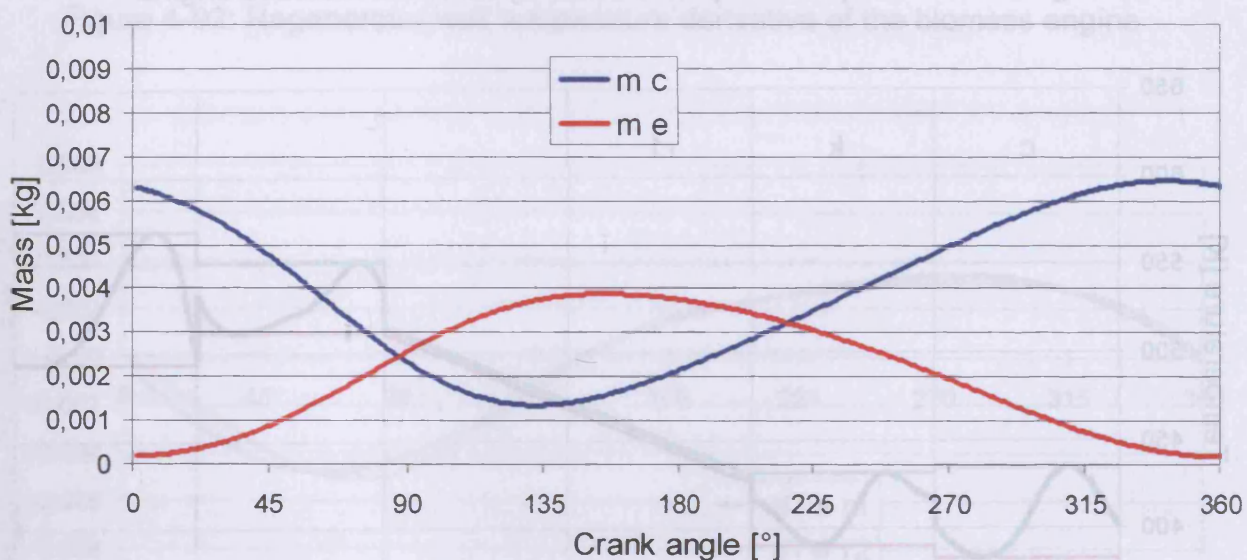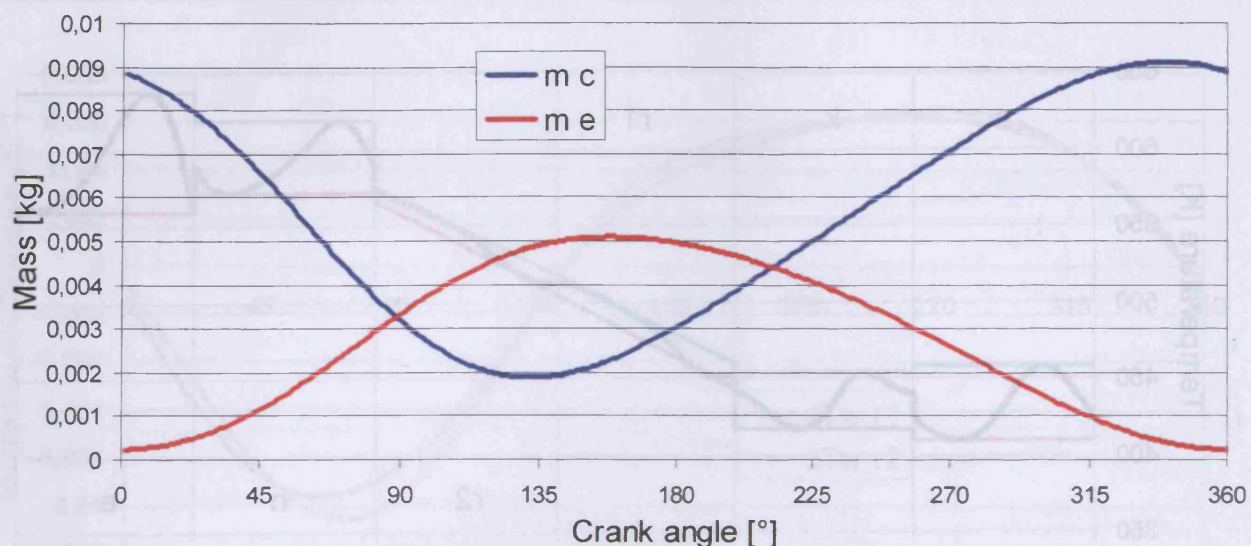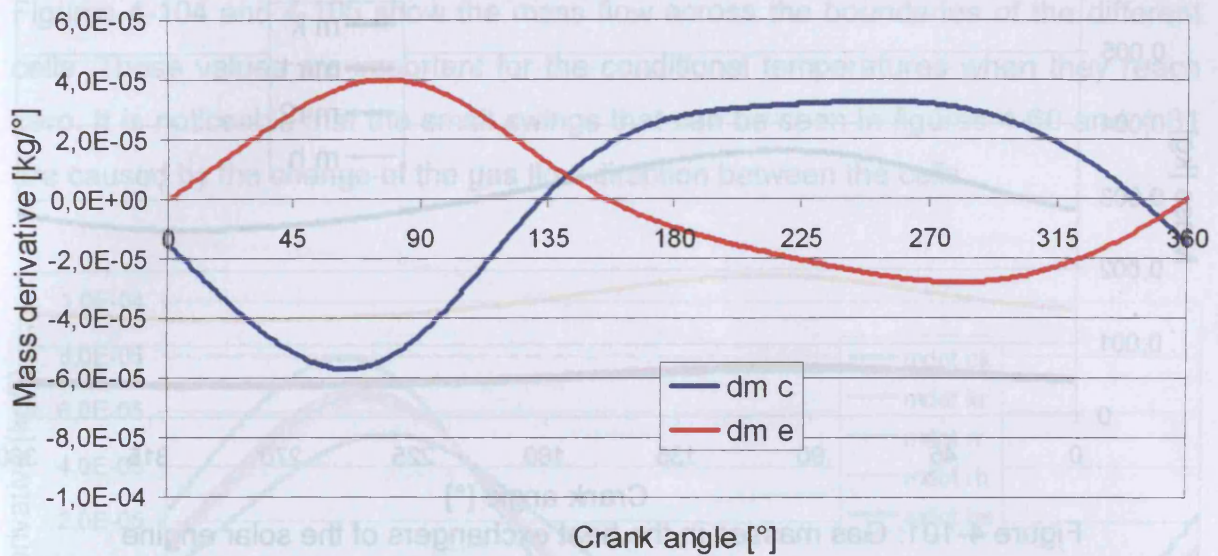
Figure 4-99: dm$_c$ and dm$_e$ for the solar engine

Figures 4-100 and 4-101 define the total mass contained in the heat exchangers. It can be seen, that the mass in the regenerator cells has lower values than in the heater and the cooler. This is because of the low specific dead volume of the regenerator matrix.

Figures 4-102 and 4-103 show the mass derivative of the working gas in the heater, cooler and regenerator sections.
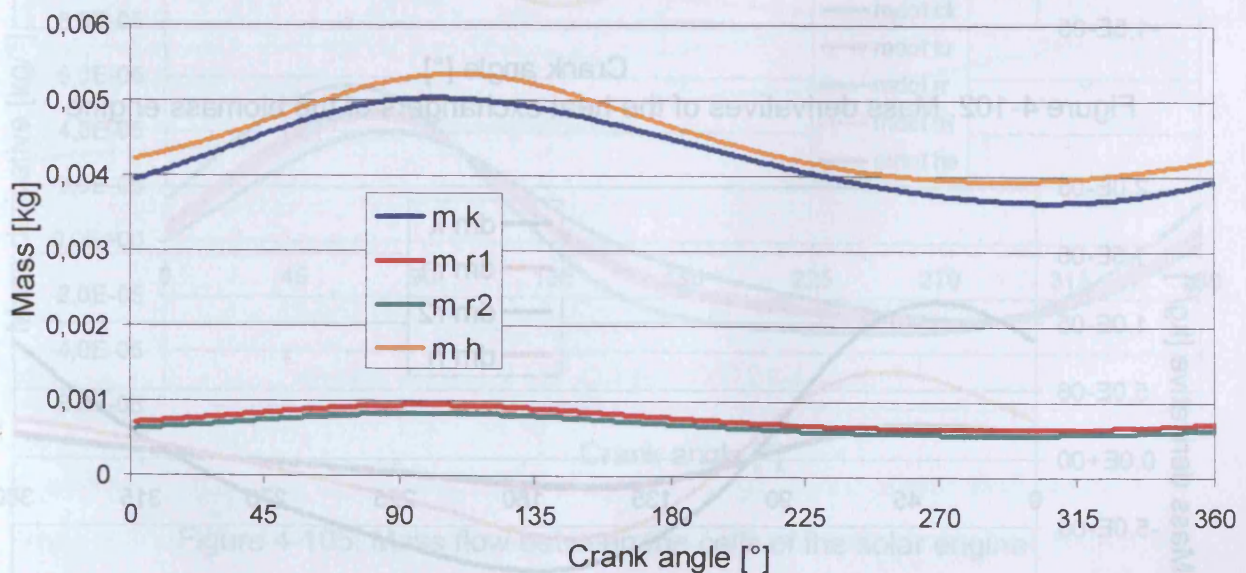
Figure 4-100: Gas masses in the heat exchangers of the biomass engine
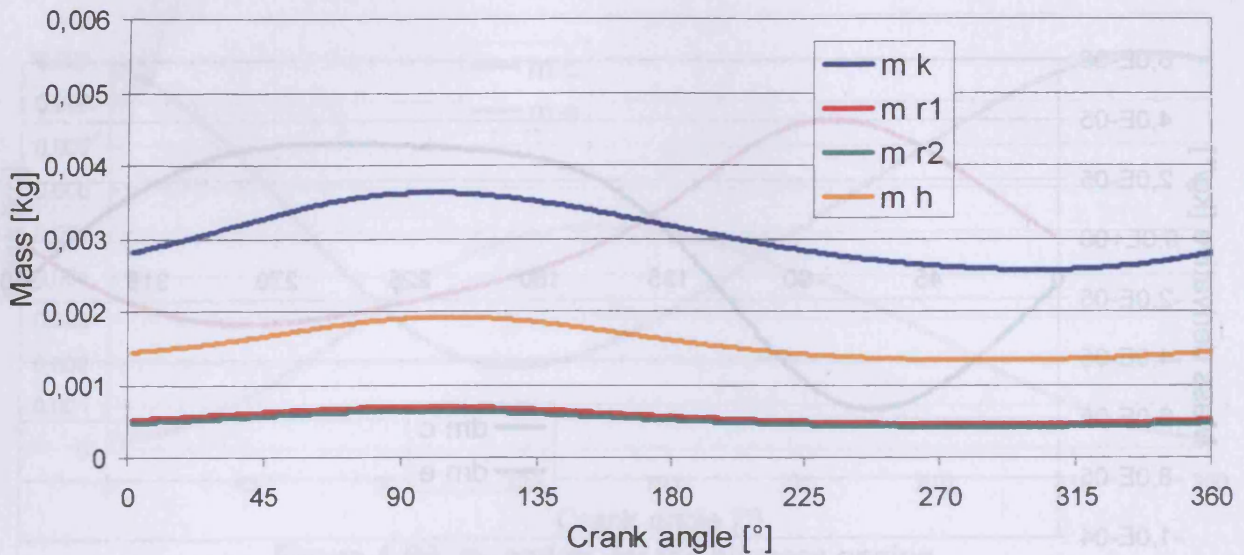
Figure 4-101: Gas masses in the heat exchangers of the solar engine
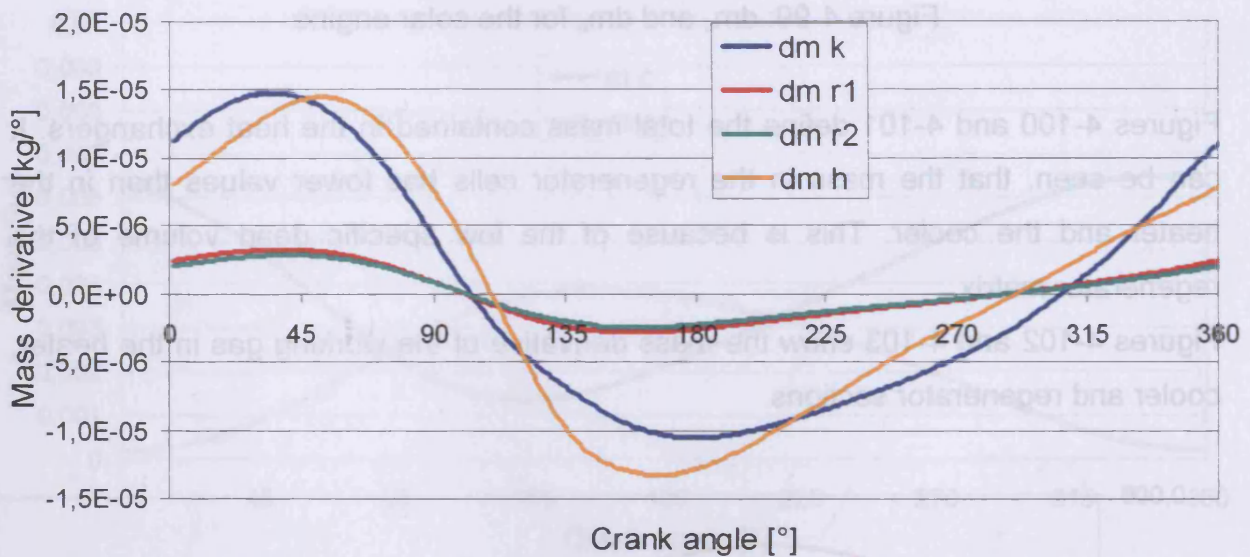
Figure 4-102: Mass derivatives of the heat exchangers of the biomass engine
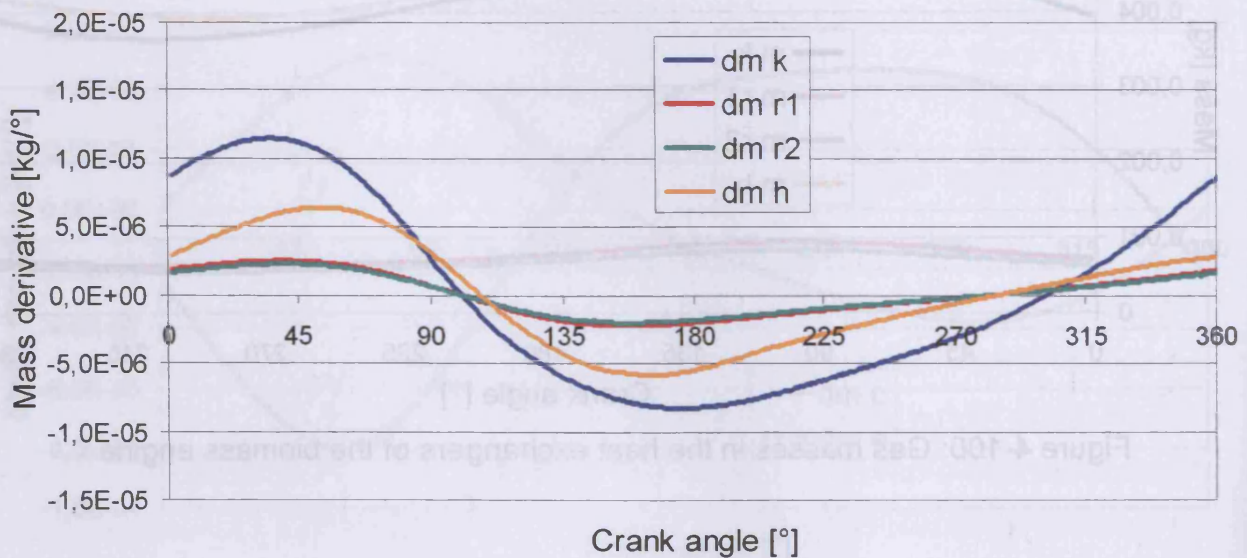
Figure 4-103: Mass derivatives of the heat exchangers of the solar engine

186

Figures 4-104 and 4-105 show the mass flow across the boundaries of the different cells. These values are important for the conditional temperatures when they reach zero. It is noticeable that the small swings that can be seen in figures 4-60 and 4-61 are caused by the change of the gas flow direction between the cells.
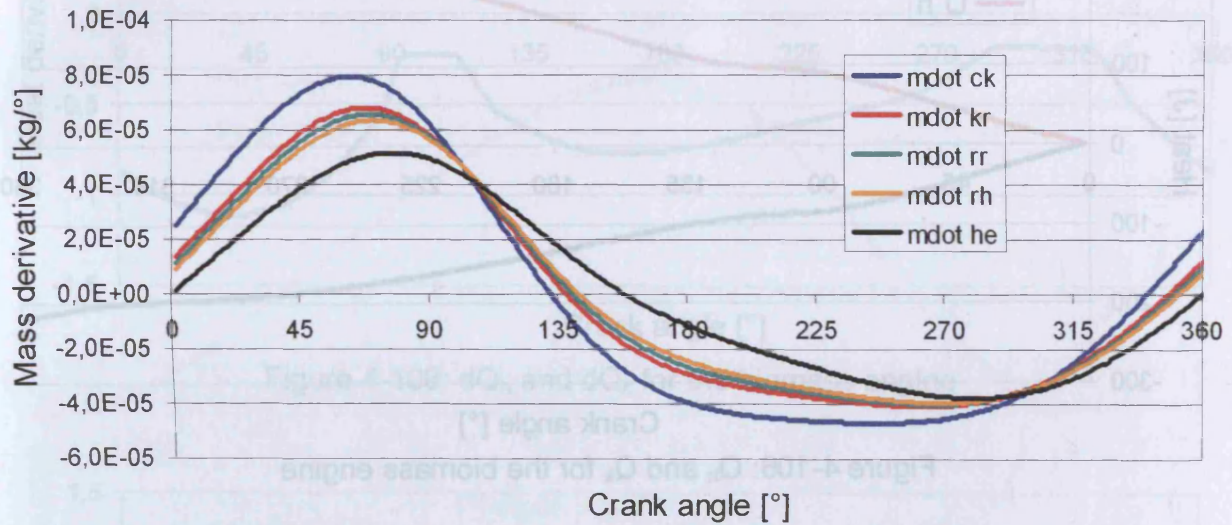
Figure 4-104: Mass flow between the cells of the biomass engine
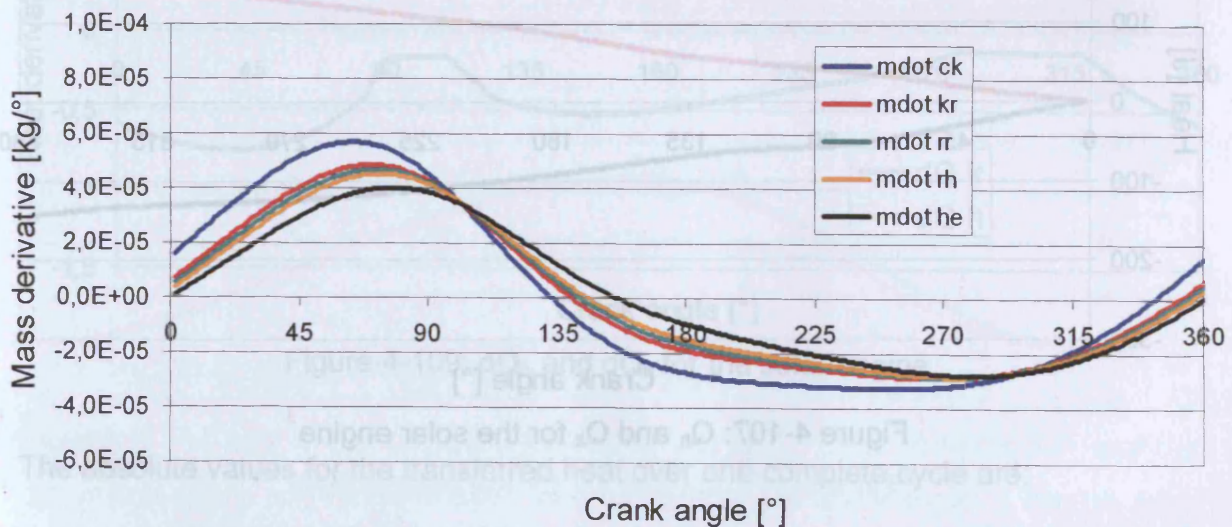
Figure 4-105: Mass flow between the cells of the solar engine

4.2.7.13 Heat transferred in the heater, cooler and regenerator

Figures 4-106 and 4-107 show the heat transferred in the cooler and heater sections of the biomass and solar engine.
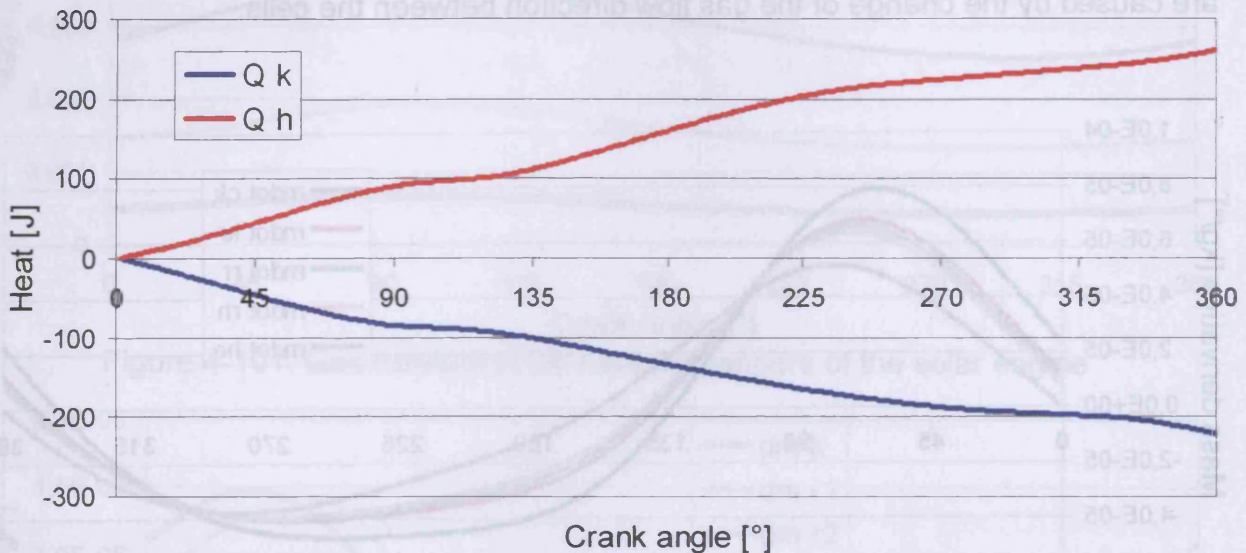
Figure 4-106: Q_h and Q_k for the biomass engine
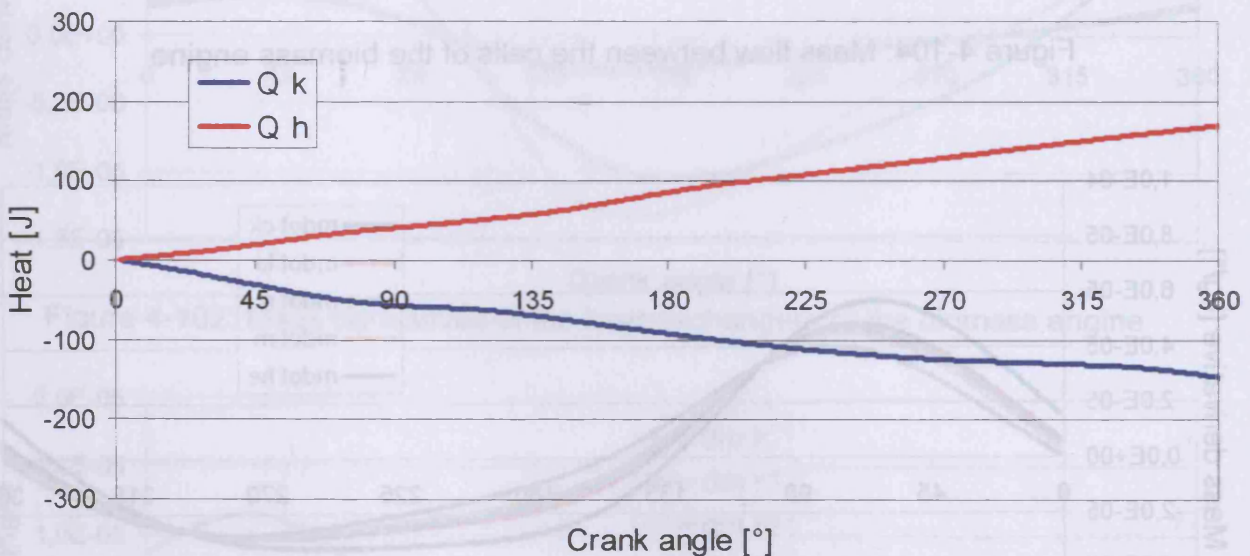
Figure 4-107: Q_h and Q_k for the solar engine

To analyse how these curves arise, in figure 4-108 and 4-109 the heat derivative of the cooler and heater is shown. The plateau values of the unsteady curves come from the heat transfer coefficients (shown in figures 4-70 and 4.71) that show similar functions with constant values for laminar flow regime.
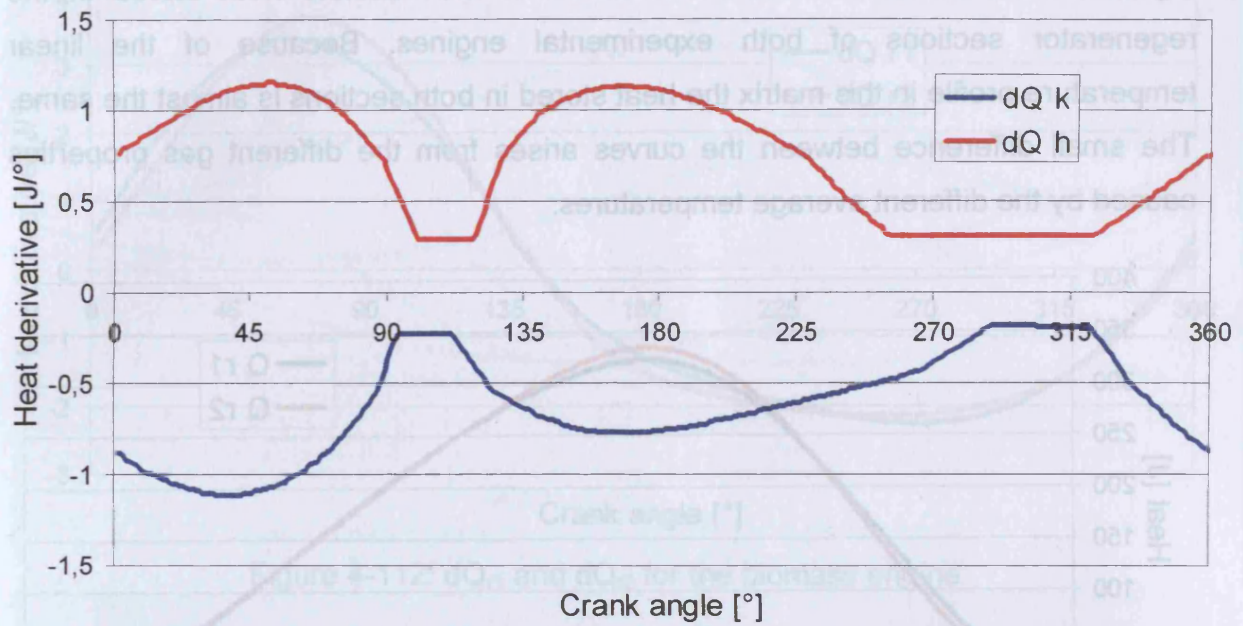
Figure 4-108: dQ$_h$ and dQ$_k$ for the biomass engine
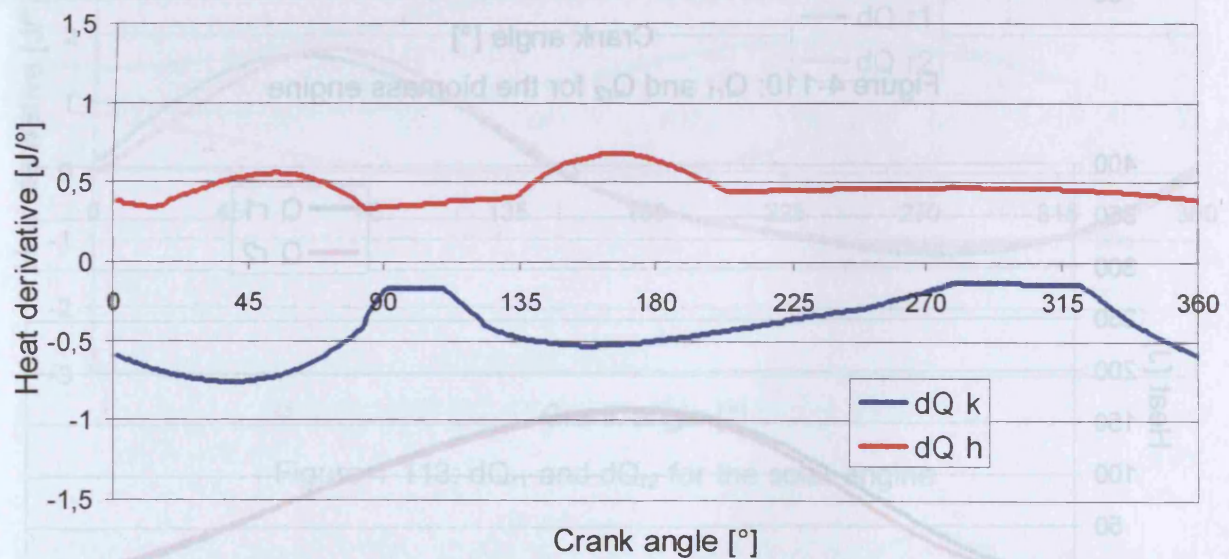
Figure 4-109: dQ$_h$ and dQ$_k$ for the solar engine

The absolute values for the transferred heat over one complete cycle are:

$$Q_{h,s} = 168,53 \, J \tag{4.140}$$

$$Q_{h,b} = 260,42 \, J \tag{4.141}$$

$$Q_{k,s} = -147,39 \, J \tag{4.142}$$

$$Q_{k,b} = -222,29 \, J \tag{4.143}$$

Figures 4-110 and 4-111 show the values of the absolute heat stored in the regenerator sections of both experimental engines. Because of the linear temperature profile in this matrix the heat stored in both sections is almost the same. The small difference between the curves arises from the different gas properties caused by the different average temperatures.
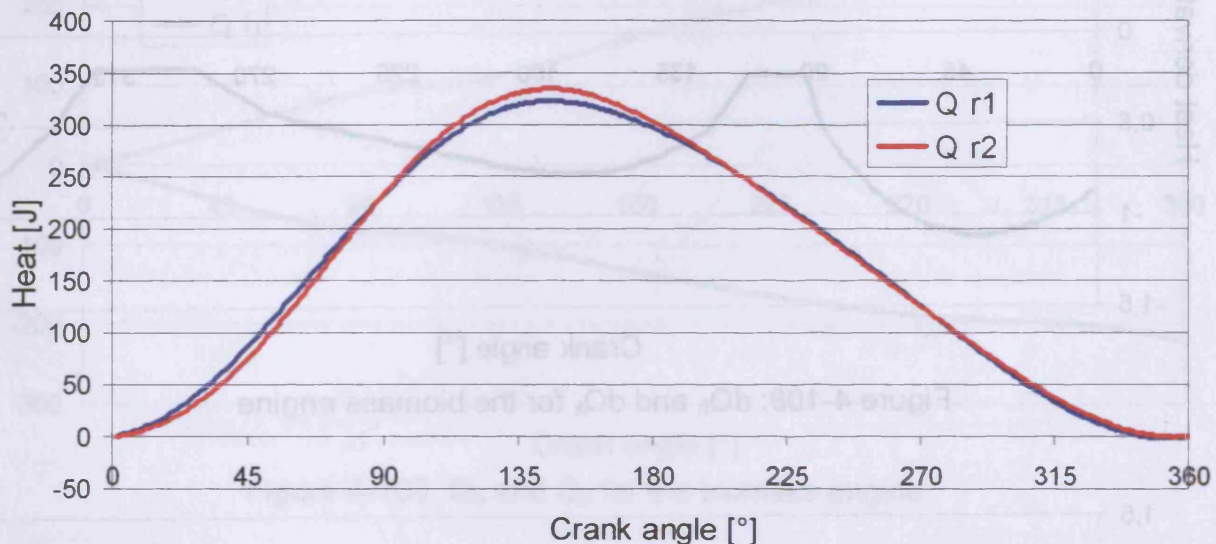
Figure 4-110: Q_{r1} and Q_{r2} for the biomass engine
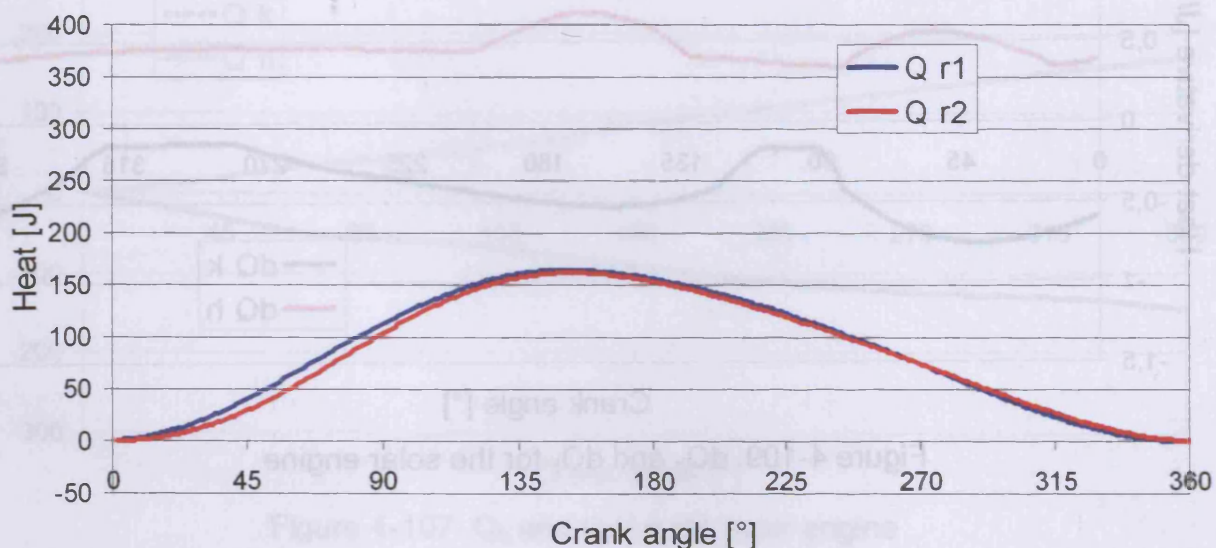
Figure 4-111: Q_{r1} and Q_{r2} for the solar engine

The convergence criterion is fulfilled with the absolute heat of the regenerator over a cycle being 0 (calculated 0,5E-6).

Figures 4-112 and 4-113 show the heat derivative of the regenerator over the complete cycle.

190
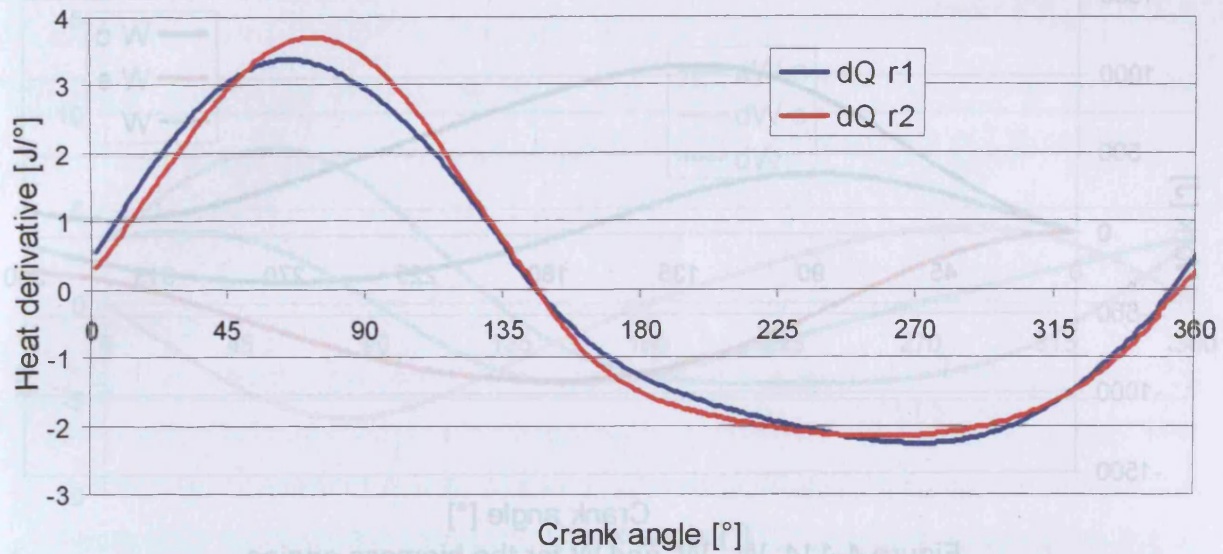
Figure 4-112: dQ_{r1} and dQ_{r2} for the biomass engine
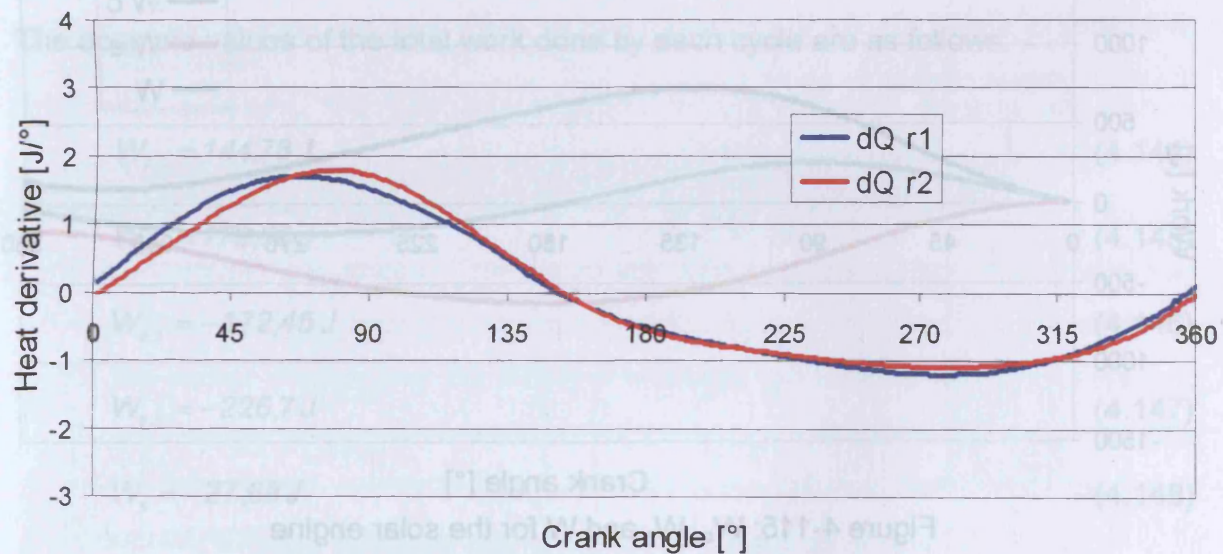
Figure 4-113: dQ_{r1} and dQ_{r2} for the solar engine

4.2.7.14 Work and performance

Figures 4-114 and 4-115 show the curves of the work of the compression and the expansion space and the total work as a function of the crank angle. It can be seen that the total work W at the end of the cycle is very low, because of the high heat transfer losses caused by the non ideal heat exchangers. Figures 4-116 and 4-117 show the corresponding curves of the work derivative.
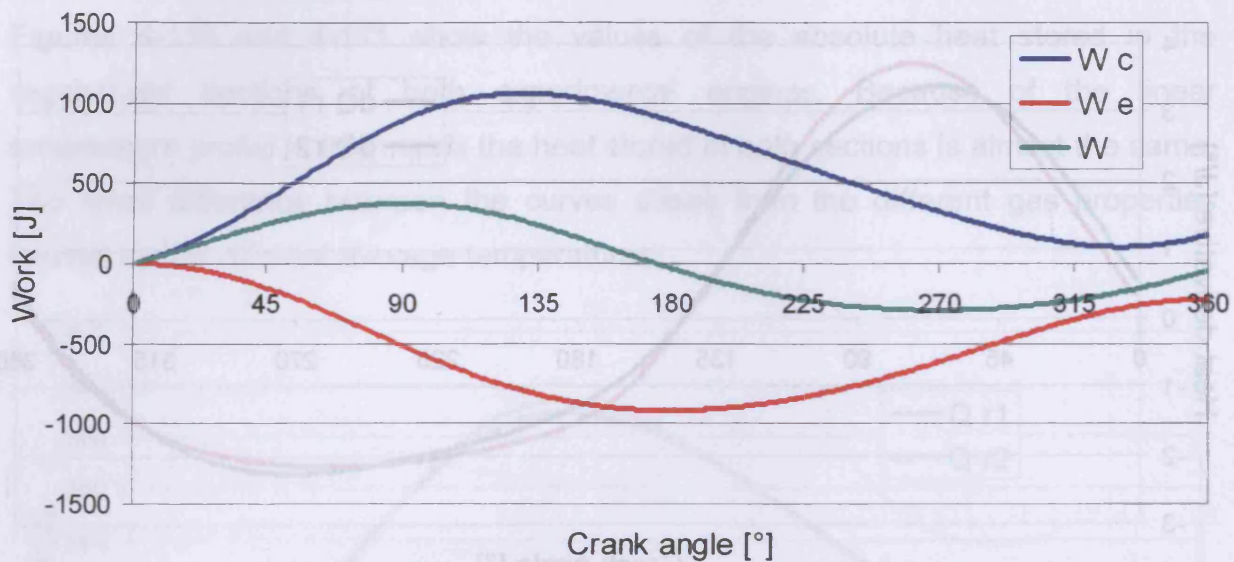
Figure 4-114: W_c, W_e and W for the biomass engine
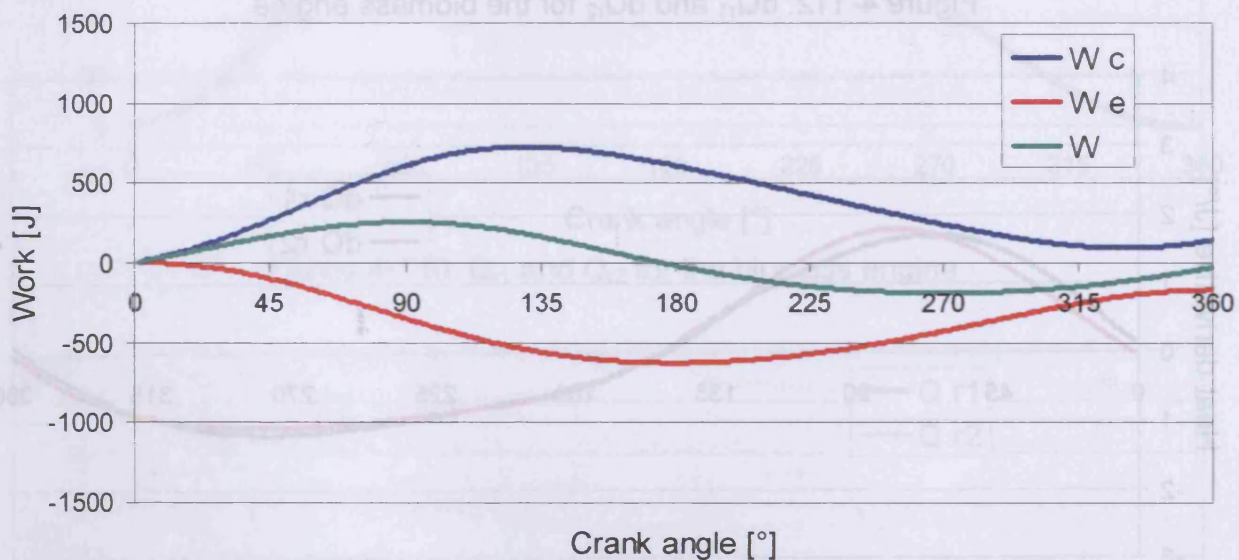
Figure 4-115: W_c, W_e and W for the solar engine
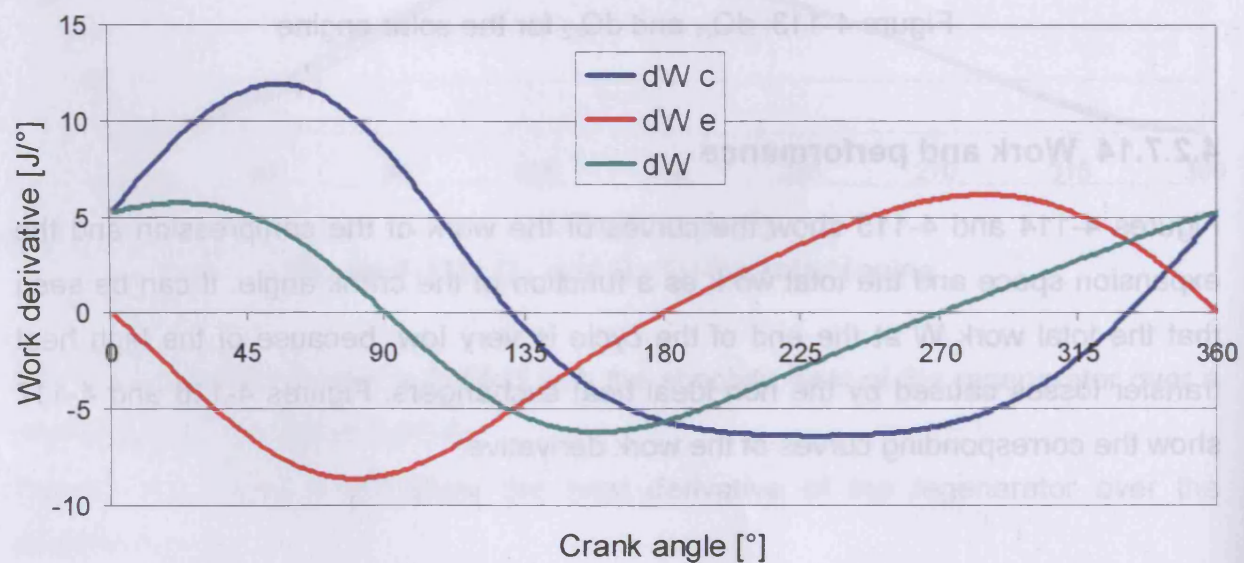
Figure 4-116: dW_c, dW_e and dW for the biomass engine
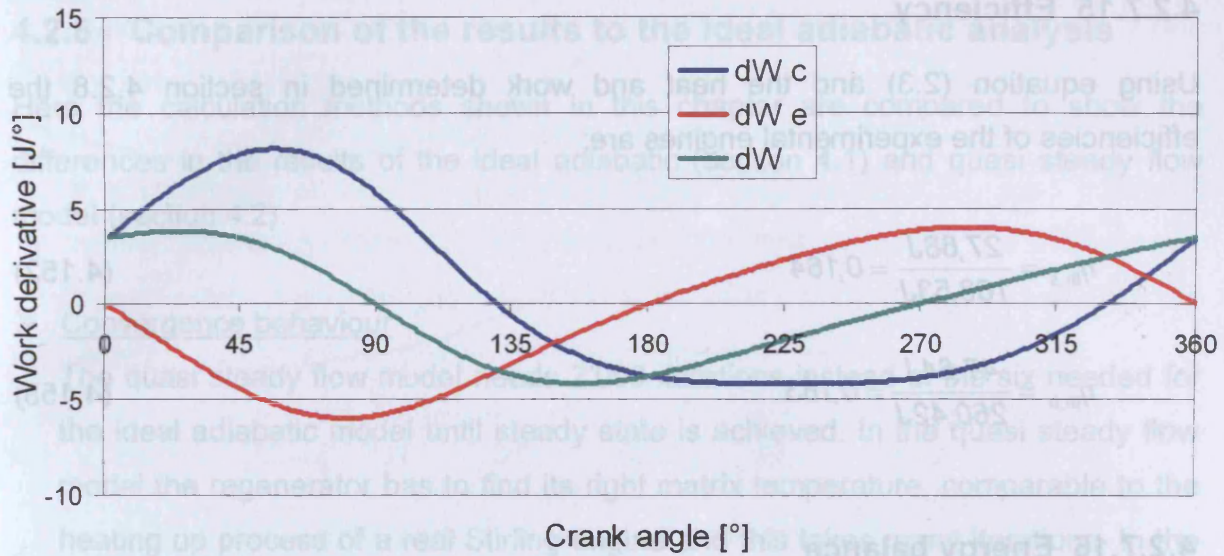
Figure 4-117: dW$_c$, dW$_e$ and dW for the solar engine

The absolute values of the total work done by each cycle are as follows:

$$W_{c,s} = 144{,}78\,J \tag{4.144}$$

$$W_{c,b} = 179{,}06\,J \tag{4.145}$$

$$W_{e,s} = -172{,}45\,J \tag{4.146}$$

$$W_{e,b} = -226{,}7\,J \tag{4.147}$$

$$W_s = -27{,}68\,J \tag{4.148}$$

$$W_b = -47{,}64\,J \tag{4.149}$$

Combining equations (2.74), (2.75) and (2.76) with the total work W done by the engines, the performance has values of:

$$P_s = 400\,\frac{1}{60s} \cdot 27{,}68\,J = 184{,}53\,W \tag{4.150}$$

$$P_b = 700\,\frac{1}{60s} \cdot 47{,}64\,J = 555{,}80\,W \tag{4.151}$$

4.2.7.15 Efficiency

Using equation (2.3) and the heat and work determined in section 4.2.8 the efficiencies of the experimental engines are:

$$\eta_{th,s} = \frac{27,68J}{168,53J} = 0,164 \tag{4.152}$$

$$\eta_{th,b} = \frac{47,64J}{260,42J} = 0,183 \tag{4.153}$$

4.2.7.16 Energy balance

As with the ideal adiabatic analysis the energy balance (see table 4.16) has a difference of about 10 J for the biomass engine and 7 J for the solar engine when the iteration step is chosen to be 1°.

1°	Biomass engine	Solar engine
Q_k	-222,29 J	-147,39 J
Q_h	260,42 J	168,53 J
W	-47,64 J	-27,68 J
η	18,3 %	16,4 %
Δ	9,51 J	6,54 J

Table 4.16: Energy balance for 360 steps per cycle

Choosing 36'000 steps per iteration the difference is as shown in table 4.17. It can be seen that with the heat and the work also the efficiency changes.

0,01°	Biomass engine	Solar engine
Q_k	-230,05 J	-164,19 J
Q_h	262,66 J	180,64 J
W	-33,74 J	-16,72 J
η	12,8 %	9,43 %
Δ	1,13 J	0,27 J

Table 4.17: Energy balance for 36'000 steps per cycle

4.2.8 Comparison of the results to the ideal adiabatic analysis

Here the calculation methods shown in this chapter are compared to show the differences in the results of the ideal adiabatic (section 4.1) and quasi steady flow model (section 4.2).

➤ Convergence behaviour

The quasi steady flow model needs 2'000 iterations instead of the six needed for the ideal adiabatic model until steady state is achieved. In the quasi steady flow model the regenerator has to find its right matrix temperature, comparable to the heating up process of a real Stirling engine and this takes many iterations. In the ideal adiabatic model the regenerator matrix temperature is fixed.

➤ Temperatures

In the following the gas temperatures in the different spaces are shown comparing the results of the quasi steady flow model and the ones of the ideal adiabatic analysis. Figures 4-118 and 4-119 describe the temperature of the gas in the compression space. The curves are quite similar but the values are higher because of the non ideal cooler. Figures 4-120 and 4-121 show the temperatures for the cooler considering the different analysis methods. In the ideal adiabatic model the gas temperature is assumed to be constant. The quasi steady flow model uses these constant values as wall temperatures and calculates a gas temperature that is higher than the wall temperature.
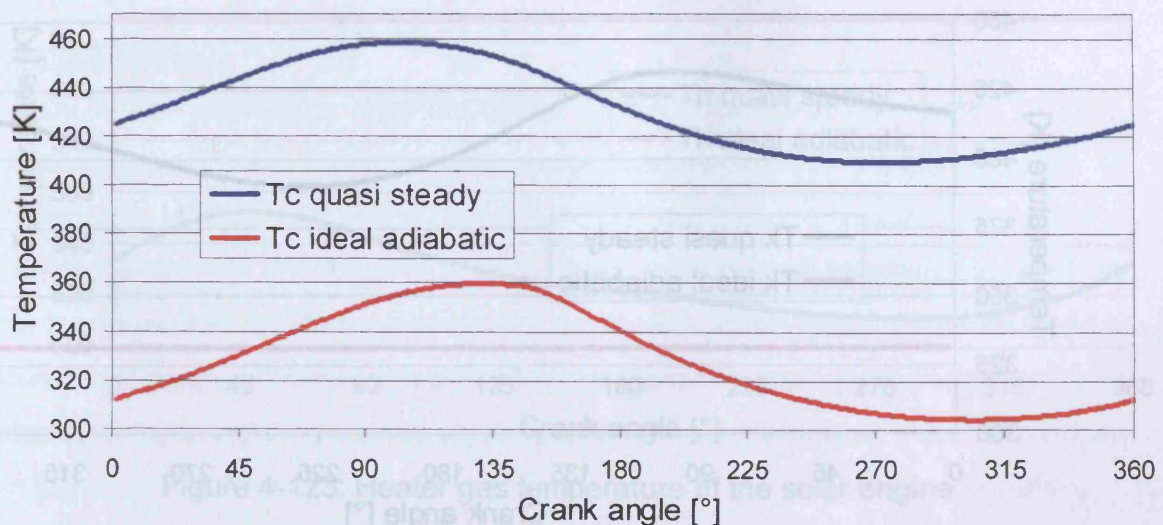
Figure 4-118: Compression space temperature of the biomass engine
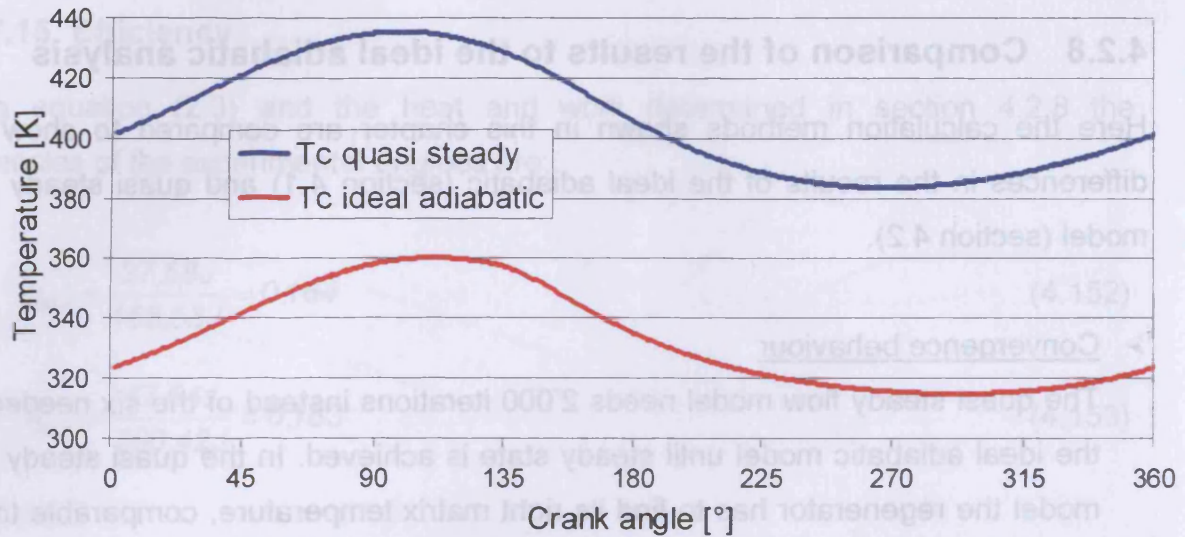
Figure 4-119: Compression space temperature of the solar engine
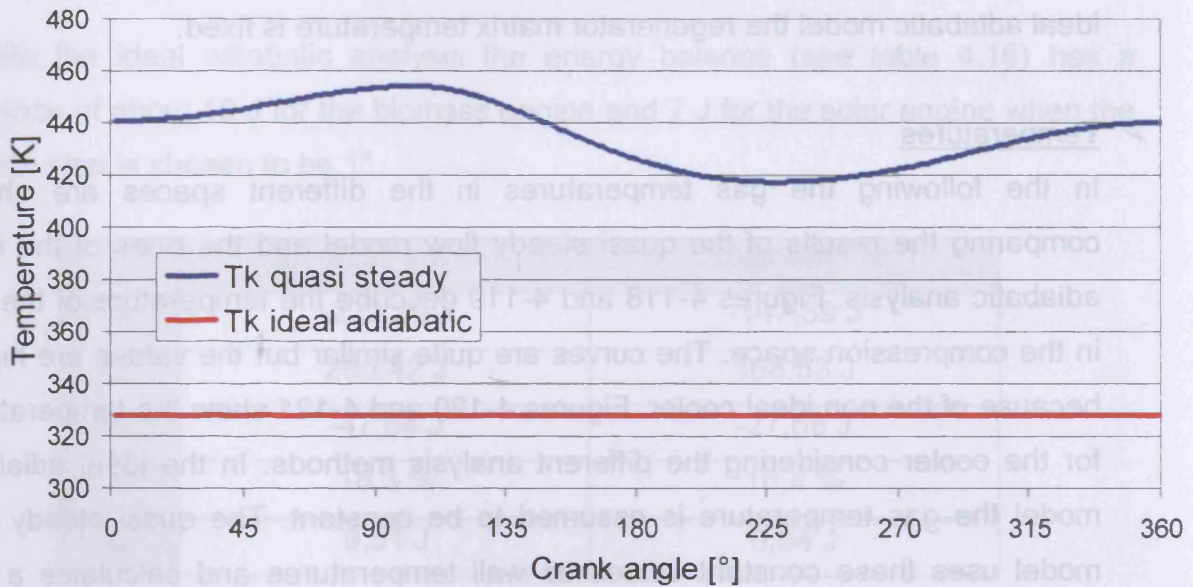
Figure 4-120: Cooler gas temperature of the biomass engine
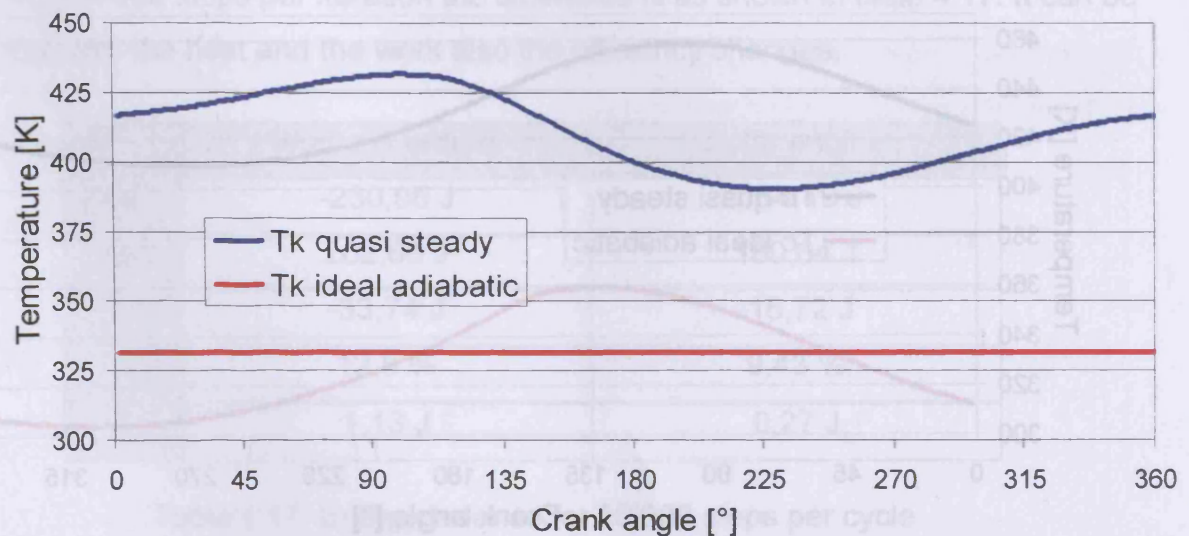
Figure 4-121: Cooler gas temperature of the solar engine

196

Figures 4-122 and 4-123 compare the results for the heater section of the experimental engines. It can be seen, that the heater of the biomass engine has a low efficiency at the high speed of the engine (700 1/min). This causes the large difference between the wall temperature (gas temperature of the ideal adiabatic model) and the gas temperature of the quasi steady flow model. The solar heater is more efficient and the gas velocity is lower (400 1/min). Those facts cause the lower temperature differences in the solar engine.
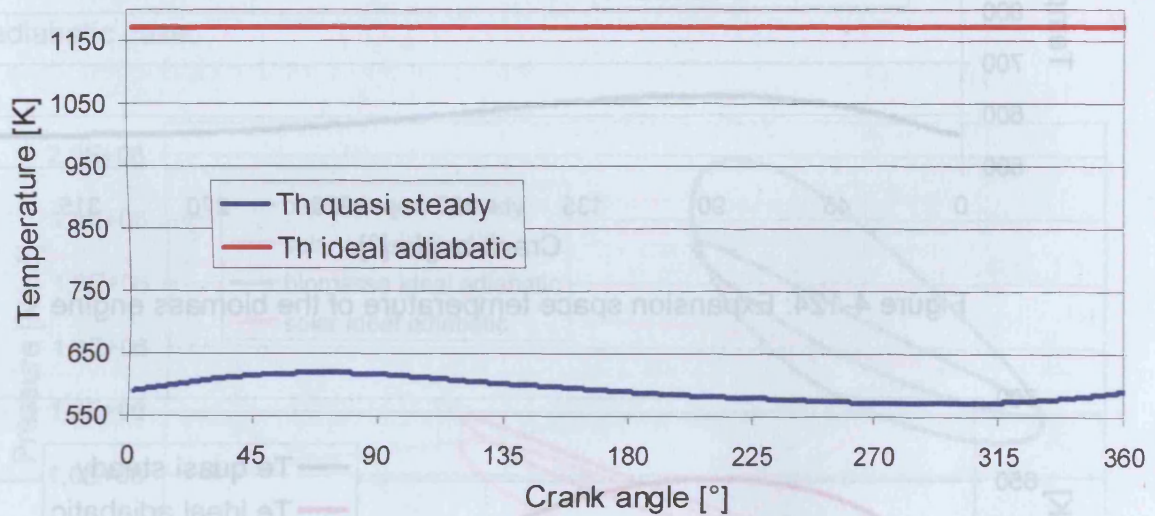
Figure 4-122: Heater gas temperature of the biomass engine
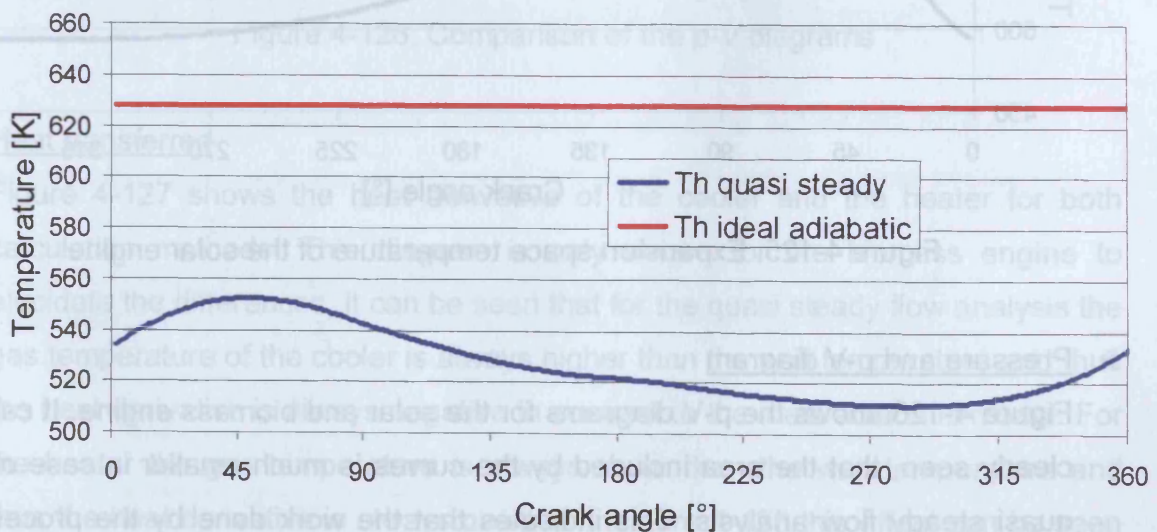
Figure 4-123: Heater gas temperature of the solar engine

Figures 4-124 and 4-125 show the gas temperature of the expansion space. The temperature there is much lower for the quasi steady flow model. This gives rise to the lower work done by the process and the lower efficiency.
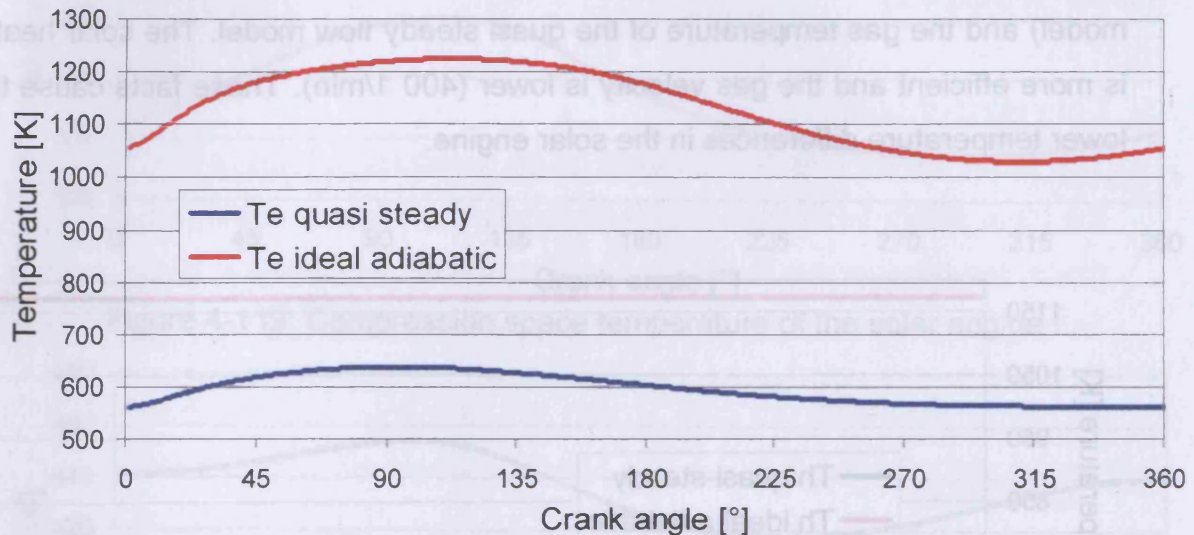
Figure 4-124: Expansion space temperature of the biomass engine
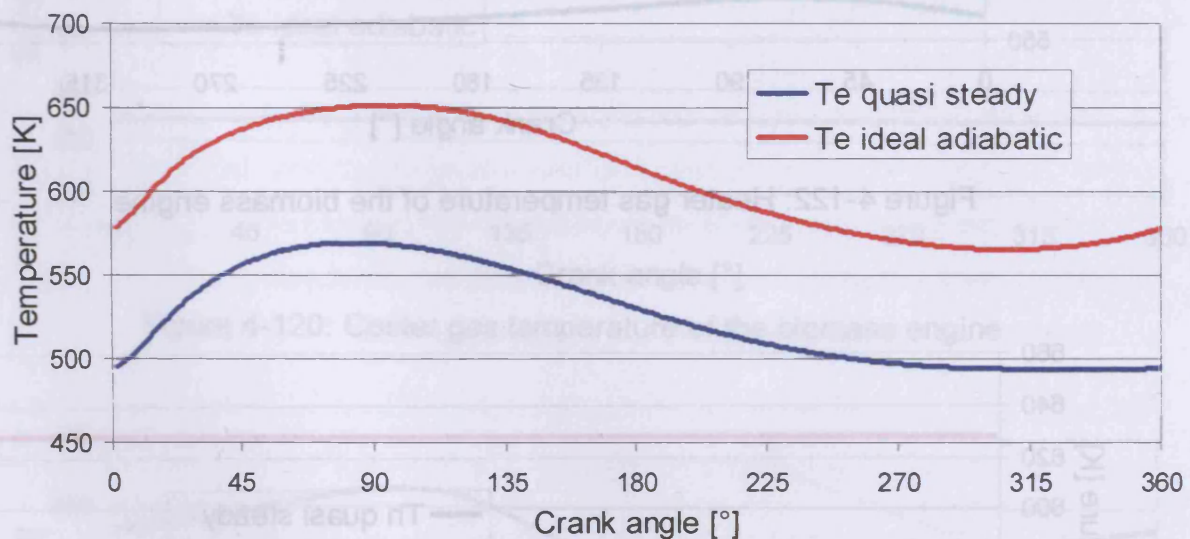
Figure 4-125: Expansion space temperature of the solar engine

➤ Pressure and p-V diagram

Figure 4-126 shows the p-V diagrams for the solar and biomass engine. It can be clearly seen, that the area included by the curves is much smaller in case of the quasi steady flow analysis. This indicates that the work done by the process is reduced.

198

The pressure swing between minimum and maximum pressure has smaller amplitude in case of the quasi steady model. The maximum pressure of the biomass engine is reduced because the working gas can not adapt to the high temperature of the heater section. This is because the speed of the engine and hence the velocity of the working gas is high. In the case of the solar engine the speed is lower and the gas temperature is closer to the wall temperature of the heater. The gas temperature in the cooler is higher than the wall temperature and because of these facts the maximum and minimum pressure of the solar engine are higher for the quasi steady analysis, being closer to those of the ideal adiabatic case.
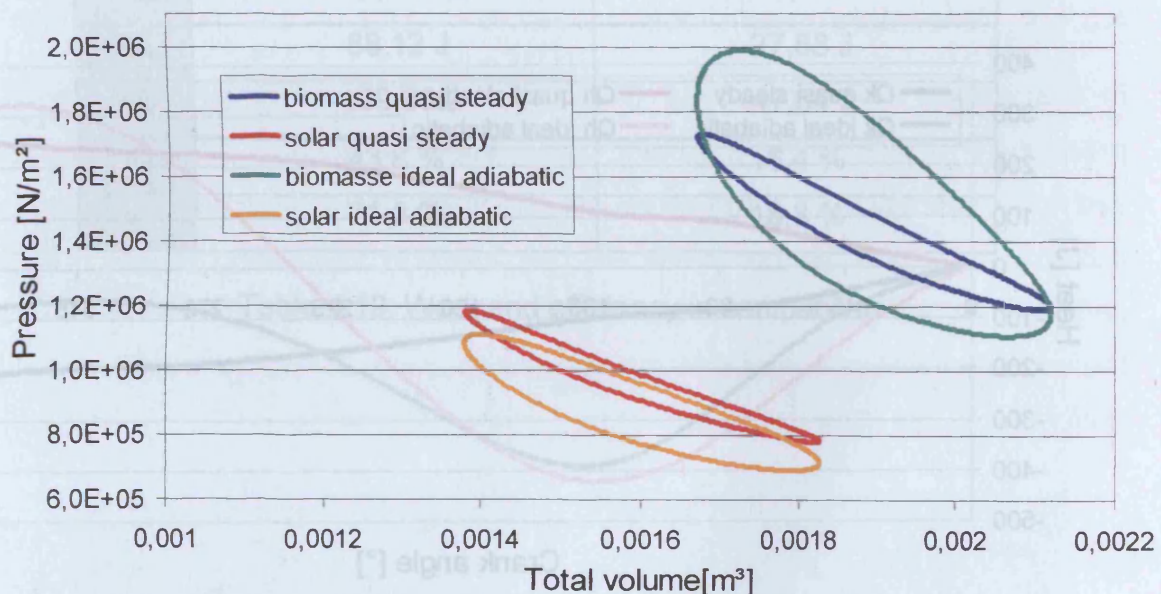
Figure 4-126: Comparison of the p-V diagrams

➤ Heat transferred

Figure 4-127 shows the heat derivative of the cooler and the heater for both calculation methods. This diagram is only shown for the biomass engine to elucidate the differences. It can be seen that for the quasi steady flow analysis the gas temperature of the cooler is always higher than the wall temperature and thus the heat derivative is always negative in contrast to the ideal adiabatic model. For the heater the gas temperature is always lower than the wall temperature and thus the heat derivative is always positive. In figure 4-128 this effect can be seen on the total heat for the biomass engine.

The figure for the regenerator is not drawn because the curves are similar.
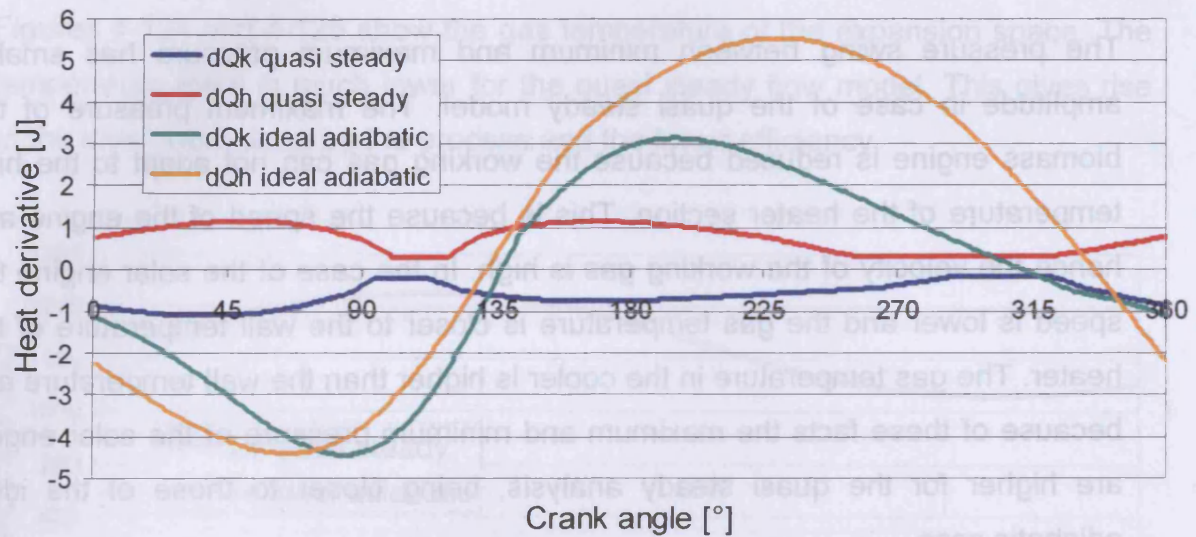
Figure 4-127: Comparison of the heat derivatives for the biomass engine
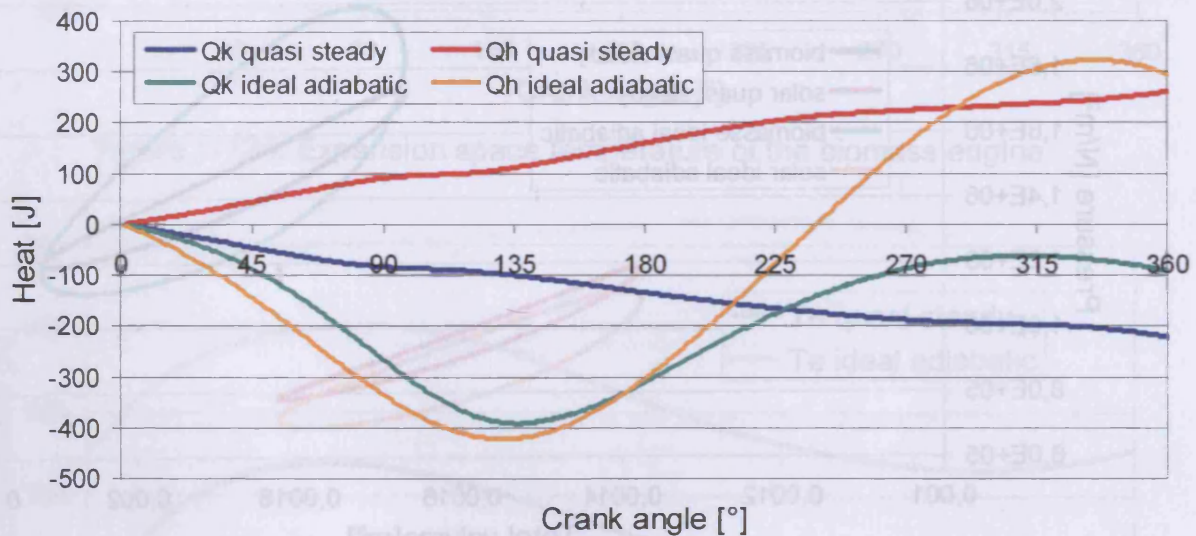
Figure 4-128: Comparison of the heat for the biomass engine

Table 4.18 shows the absolute values of the heat transferred by the cooler and the heater over the whole cycle for the quasi steady and ideal adiabatic model.

	Ideal adiabatic	Quasi steady
$Q_{k,s}$	-82,44 J	-147,39 J
$Q_{k,b}$	-92,65 J	-222,29 J
$Q_{h,s}$	155,58 J	168,53 J
$Q_{h,b}$	293,53 J	260,42 J

Table 4.18: Absolute values of the heat transferred in comparison

> ➢ Work and efficiency

Because of the non ideal heat exchangers and the pressure drops the work done by the process and the efficiency have to be less for the quasi steady flow model like it is indicated in the p-V diagram (4-126). Table 4.19 gives these values in comparison for the biomass and solar engine.

	Ideal adiabatic	Quasi steady
$W_{e,s}$	-158,66 J	-172,45 J
$W_{e,b}$	-294,26 J	-226,70 J
$W_{c,s}$	90,52 J	144,78 J
$W_{e,b}$	94,30 J	179,06 J
W_s	-68,12 J	-27,68 J
W_b	-199,96 J	-47,64 J
η_s	43,8 %	16,4 %
η_b	71,3 %	18,3 %

Table 4.19: Work and efficiency in comparison

4.3 Parameter variation with the quasi steady flow model

In the sections 4.3.1 to 4.3.8 the modifications are done one by one to show which modification has what kind of influence on the cycle and in which degree. There only the relevant characteristic values are shown as results. These results are the basis for later measurements where the parameters of the experimental engines are changed.

In section 4.3.9 an optimized engine is built up step by step to show how far the performance and efficiency of the experimental engines can be modified.

4.3.1 Influence of the working gas
4.3.1.1 Boundary conditions

In this section different working gases are used to show their influence on the process. Air is assumed in the basic calculation in section 4.2. Here H_2, He, N_2, Ne and Ar are introduced in the program with the following constant gas properties (table 4.20). In the boundary conditions the gas mass in the Stirling engine has to be defined. The biomass engine is loaded with 7,5 bar, the solar engine with 5,5 bar and the mass of each working gas is calculated with equation (2.65). The density is given under normal conditions (293 K, 1'013,3 hPa).

	R	κ	$m_{gas,b}$	$m_{gas,s}$	ρ_N
	[J/(kg·K)]	[-]	[kg]	[kg]	[kg/m³]
Air	287	1,40	18,60E-3	11,70E-3	1,29
H_2	4'124	1,40	1,30E-3	0,81E-3	0,09
He	2'077	1,66	2,58E-3	1,62E-3	0,18
N_2	297	1,40	18,03E-3	11,30E-3	1,25
Ne	412	1,66	12,99E-3	8,16E-3	0,90
Ar	208	1,66	25,72E-3	16,15E-3	1,78

Table 4.20: Constant gas properties for the different working gases

The thermal conductivity, dynamic viscosity, Prandtl number and the specific heat capacity at constant pressure are shown in tables 4.21 to 4.24. They are taken form the "VDI Wärmeatlas" [14] chapter Dc and interpolated to the same temperatures shown in table 4.9 for the different heat exchanger cells of the Stirling engines.

	k	r1	r2	h
Biomass engine				
Air	20,97E-6	27,13E-6	37,45E-6	46,19E-6
H$_2$	9,66E-6	12,62E-6	16,90E-6	21,41E-6
He	21,20E-6	27,68E-6	37,50E-6	46,92E-6
N$_2$	19,35E-6	25,58E-6	34,20E-6	41,82E-6
Ne	33,85E-6	44,18E-6	58,10E-6	71,18E-6
Ar	24,70E-6	33,25E-6	44,90E-6	55,76E-6
Solar engine				
Air	20,91E-6	25,65E-6	27,56E-6	32,53E-6
H$_2$	9,66E-6	11,75E-6	13,48E-6	15,03E-6
He	21,20E-6	25,73E-6	29,63E-6	33,23E-6
N$_2$	19,35E-6	23,75E-6	27,33E-6	30,60E-6
Ne	33,85E-6	41,08E-6	47,33E-6	52,13E-6
Ar	24,70E-6	30,78E-6	35,55E-6	39,93E-6

Table 4.21: Dynamic viscosity μ in [Pa·s] of the different working gases

	k	r1	r2	h
Biomass engine				
Air	0,03027	0,03889	0,05591	0,07174
H$_2$	0,19500	0,26500	0,37000	0,48100
He	0,16600	0,21450	0,29300	0,38300
N$_2$	0,02850	0,03850	0,05500	0,07660
Ne	0,05300	0,06950	0,09300	0,11720
Ar	0,01950	0,02675	0,03600	0,04450
Solar engine				
Air	0,03005	0,03823	0,04432	0,05016
H$_2$	0,19500	0,24400	0,28500	0,32100
He	0,16600	0,19950	0,22950	0,25900
N$_2$	0,02850	0,03550	0,04150	0,04750
Ne	0,05300	0,06450	0,07450	0,08300
Ar	0,01950	0,02475	0,02825	0,03200

Table 4.22: Thermal conductivity λ in [W/(m·K)] of the different working gases

	k	r1	r2	h
Biomass engine				
Air	0,7098	0,7051	0,7199	0,7350
H₂	0,7124	0,6862	0,6646	0,6756
He	0,6641	0,6710	0,6655	0,6370
N₂	0,7061	0,6976	0,6964	0,6442
Ne	0,6578	0,6548	0,6435	0,6256
Ar	0,6587	0,6464	0,6486	0,6516
Solar engine				
Air	0,7092	0,7047	0,7069	0,7118
H₂	0,7124	0,6939	0,6816	0,6747
He	0,6641	0,6707	0,6714	0,6672
N₂	0,7061	0,7024	0,7047	0,7022
Ne	0,6578	0,6560	0,6544	0,6470
Ar	0,6587	0,6467	0,6544	0,6489

Table 4.23: Prandtl number Pr in [-] for the different working gases

	k	r1	r2	h
Biomass engine				
Air	1'024,5	1'037,0	1'102,5	1'160,5
H₂	14'380,0	14'410,0	14'550,0	15'178,0
He	5'200,0	5'200,0	5'200,0	5'200,0
N₂	1'040,0	1'050,0	1'120,0	1'180,0
Ne	1'030,0	1'030,0	1'030,0	1'030,0
Ar	520,0	520,0	520,0	520,0
Solar engine				
Air	1'019,0	1'028,3	1'044,3	1'065,5
H₂	14'380,0	14'410,0	14'410,0	14'410,0
He	5'200,0	5'200,0	5'200,0	5'200,0
N₂	1'040,0	1'050,0	1'070,0	1'090,0
Ne	1'030,0	1'030,0	1'030,0	1'030,0
Ar	520,0	520,0	520,0	520,0

Table 4.24: Specific isobar heat capacity in [J/(kg·K)] for the different working gases

The Prandtl numbers in table 4.23 are calculated with

$$Pr = \frac{\eta \cdot c_p}{\lambda}$$
(4.154)

To make clear how different the properties of the gases described in table 4.20 to 4.24 are, the values for the cooler are shown in comparison in the following figures. Figure 4-129 gives the values of the dynamic viscosity. Neon and argon have a high viscosity compared to hydrogen and nitrogen which is a disadvantage for the Stirling process.
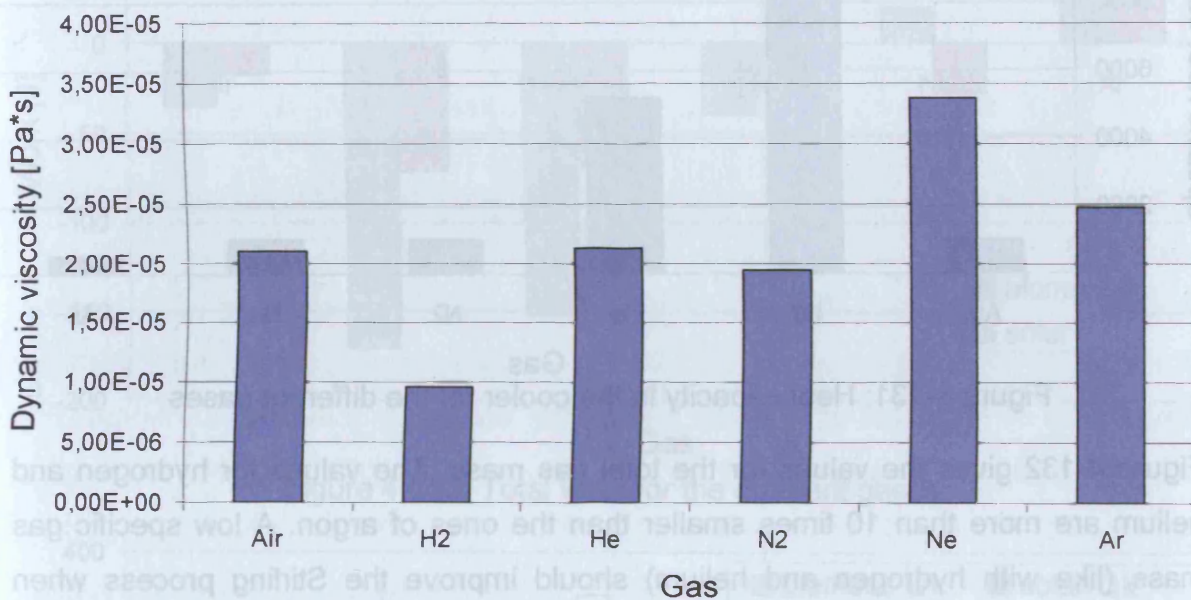
Figure 4-129: Dynamic viscosity in the cooler for the different gases
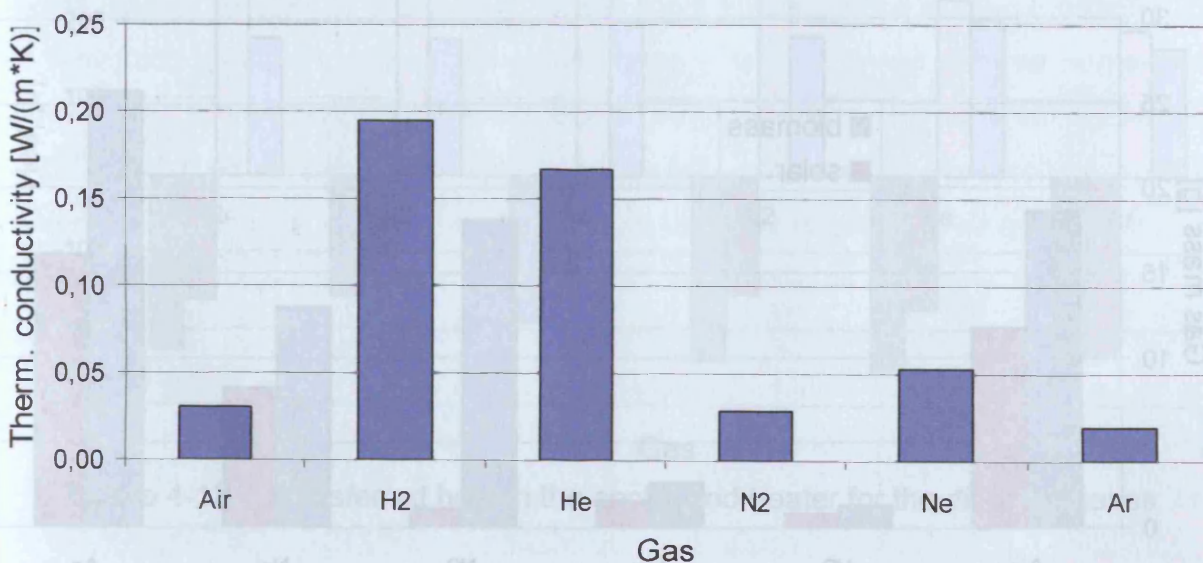
Figure 4-130: Thermal conductivity in the cooler for the different gases

Another important figure is the thermal conductivity shown in figure 4-130. The highest values are reached by hydrogen and helium. It is the same for the specific heat capacity shown in figure 4-131. The Prandt numbers calculated in table 4.23 are not shown, because the differences between the gases are very low.
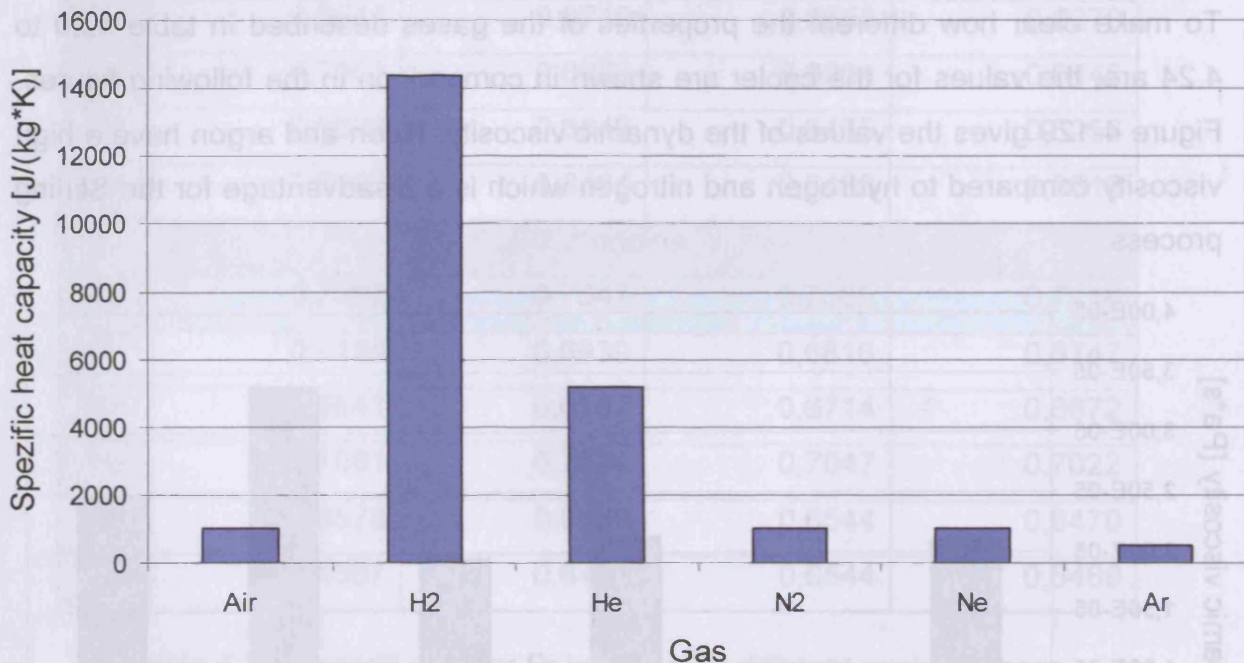
Figure 4-131: Heat capacity in the cooler for the different gases

Figure 4-132 gives the values for the total gas mass. The values for hydrogen and helium are more than 10 times smaller than the ones of argon. A low specific gas mass (like with hydrogen and helium) should improve the Stirling process when combined with high heat capacity, because less gas has to be heated and cooled.
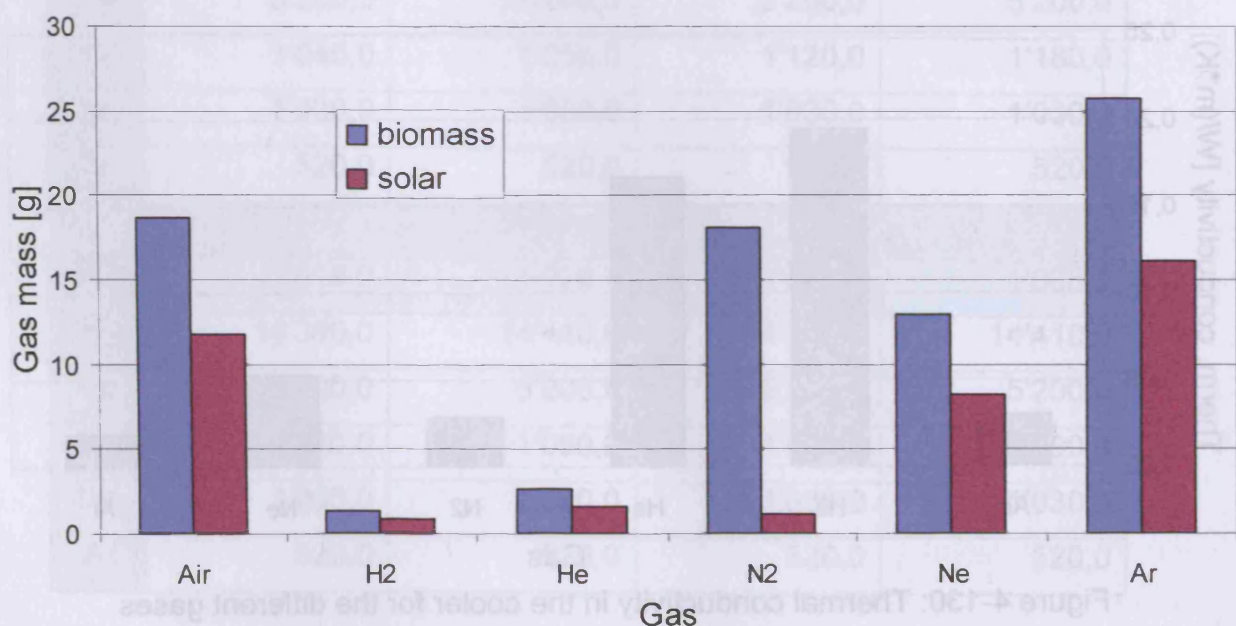
Figure 4-132: Total gas mass for the different gases

4.3.1.2   Results

To achieve good results for the different gases the program is modified with their different properties. The number of steps per cycle has to be modified from 360 to 3'600 to be able to solve the equation set for hydrogen. Therefore for all the gases 3'600 steps per cycle were used to make the values comparable. Figures 4-133, 4-134 and 4-135 show the characteristic values of the process for the different gases.
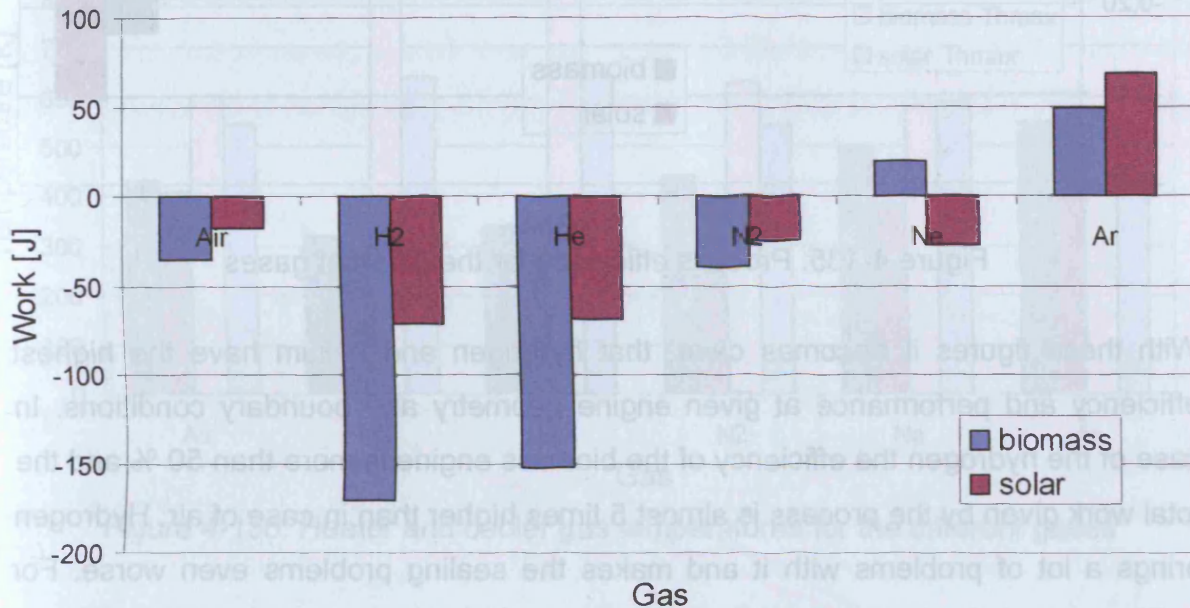
Figure 4-133: Total work for the different gases
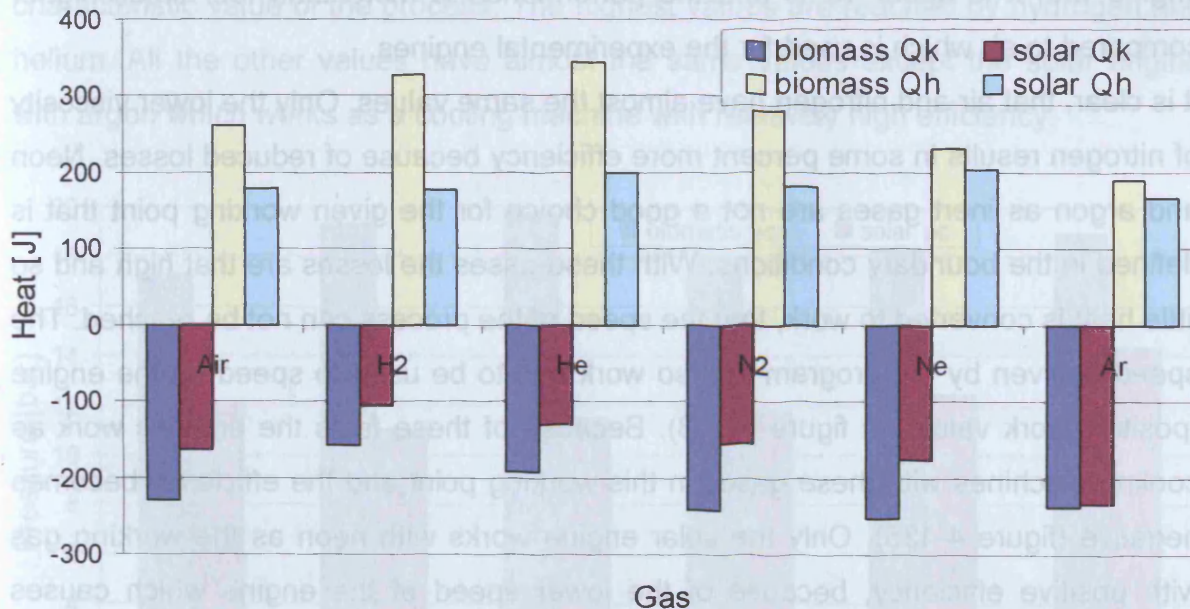
Figure 4-134: Transferred heat in the cooler and heater for the different gases

207
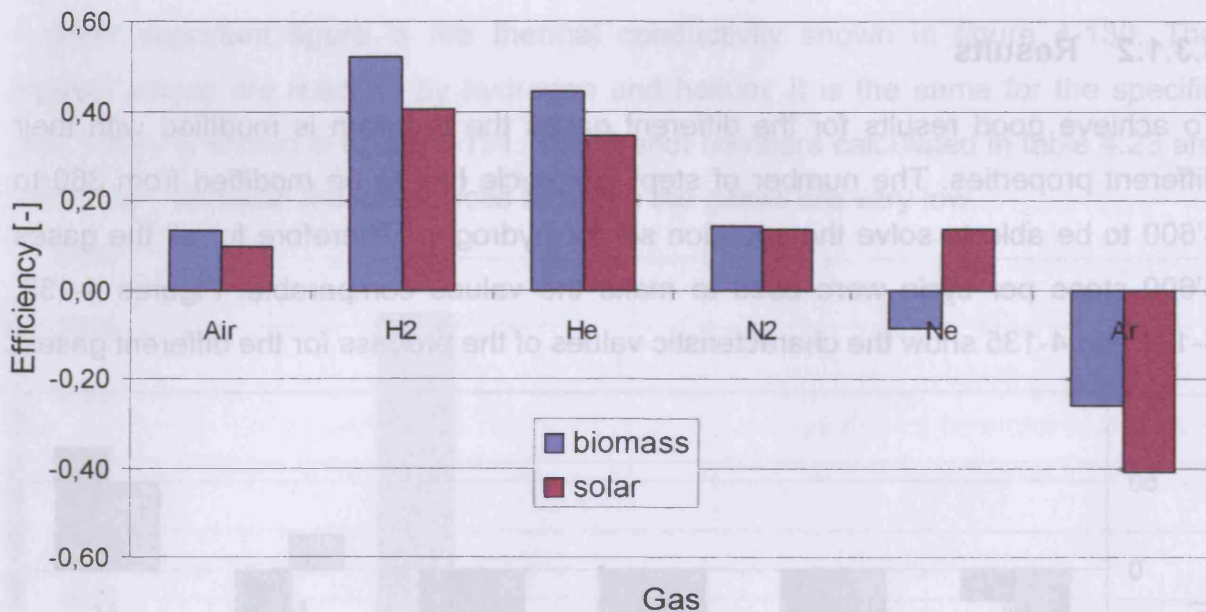
Figure 4-135: Process efficiency for the different gases

With these figures it becomes clear, that hydrogen and helium have the highest efficiency and performance at given engine geometry and boundary conditions. In case of the hydrogen the efficiency of the biomass engine is more than 50 % and the total work given by the process is almost 5 times higher than in case of air. Hydrogen brings a lot of problems with it and makes the sealing problems even worse. For safety and sealing reasons helium should be used. The efficiency of the biomass engine with it is about 45 % and the performance is more than four times higher compared to air which is used for the experimental engines.

It is clear, that air and nitrogen have almost the same values. Only the lower viscosity of nitrogen results in some percent more efficiency because of reduced losses. Neon and argon as inert gases are not a good choice for the given working point that is defined in the boundary conditions. With these gases the losses are that high and so little heat is converted to work, that the speed of the process can not be reached. The speed is given by the program and so work has to be used to speed up the engine (positive work values in figure 4-133). Because of these facts the engines work as cooling machines with these gases in this working point and the efficiency becomes negative (figure 4-135). Only the solar engine works with neon as the working gas with positive efficiency, because of the lower speed of the engine which causes reduced losses.

Figure 4-136 shows that with hydrogen and helium the gas temperatures are much closer to the wall temperatures than with the other gases. The temperature difference between T_{kmin} and T_{kmax} results in the efficiencies shown before. For neon and argon almost no temperature difference occurs because of reduced heat transfer.
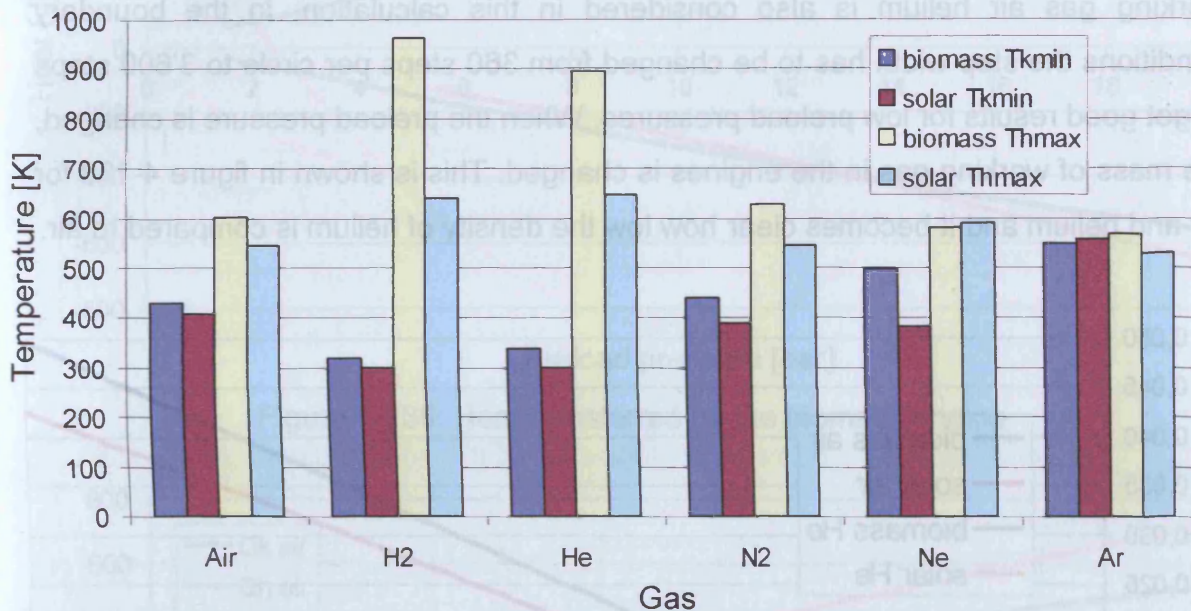
Figure 4-136: Heater and cooler gas temperatures for the different gases

Figure 4-137 shows the maximum pressure in the compression space as a characteristic value of the process. The highest values are reached by hydrogen and helium. All the other values have almost the same values except the solar engine with argon which works as a cooling machine with relatively high efficiency.
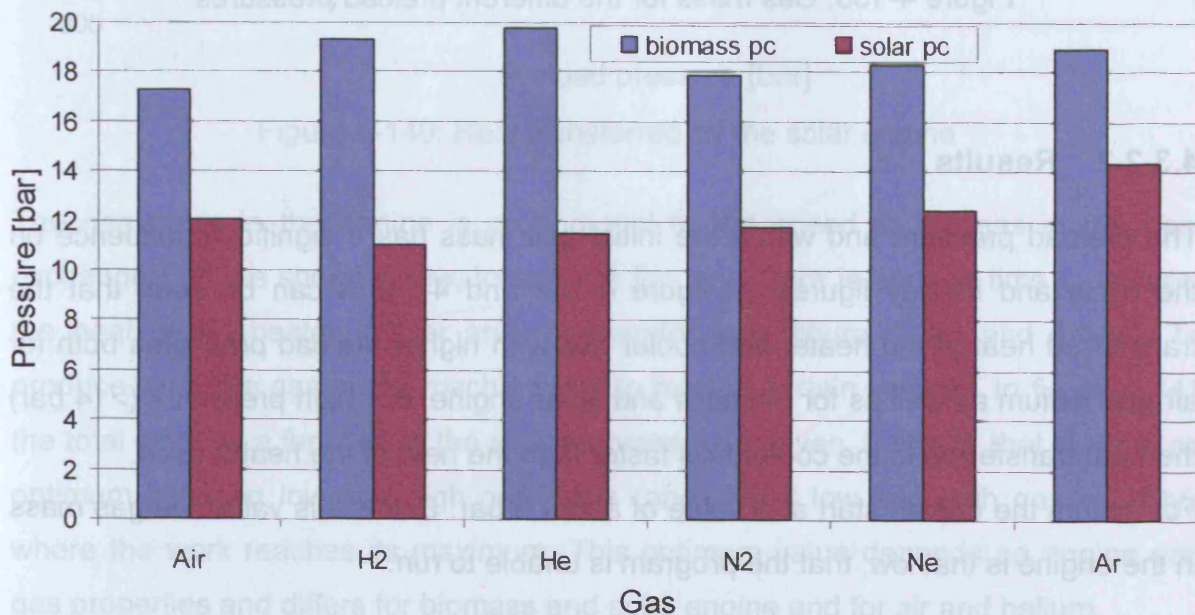
Figure 4-137: Compression space pressure for the different gases

4.3.2 Influence of the preload pressure
4.3.2.1 Boundary conditions

In this section the influence of the preload pressure of the biomass and solar engine on the performance and efficiency is shown. To have comparative values for the working gas air helium is also considered in this calculation. In the boundary conditions the step width has to be changed from 360 steps per circle to 3'600 steps to get good results for low preload pressures. When the preload pressure is changed, the mass of working gas in the engines is changed. This is shown in figure 4-138 for air and helium and it becomes clear how low the density of helium is compared to air.
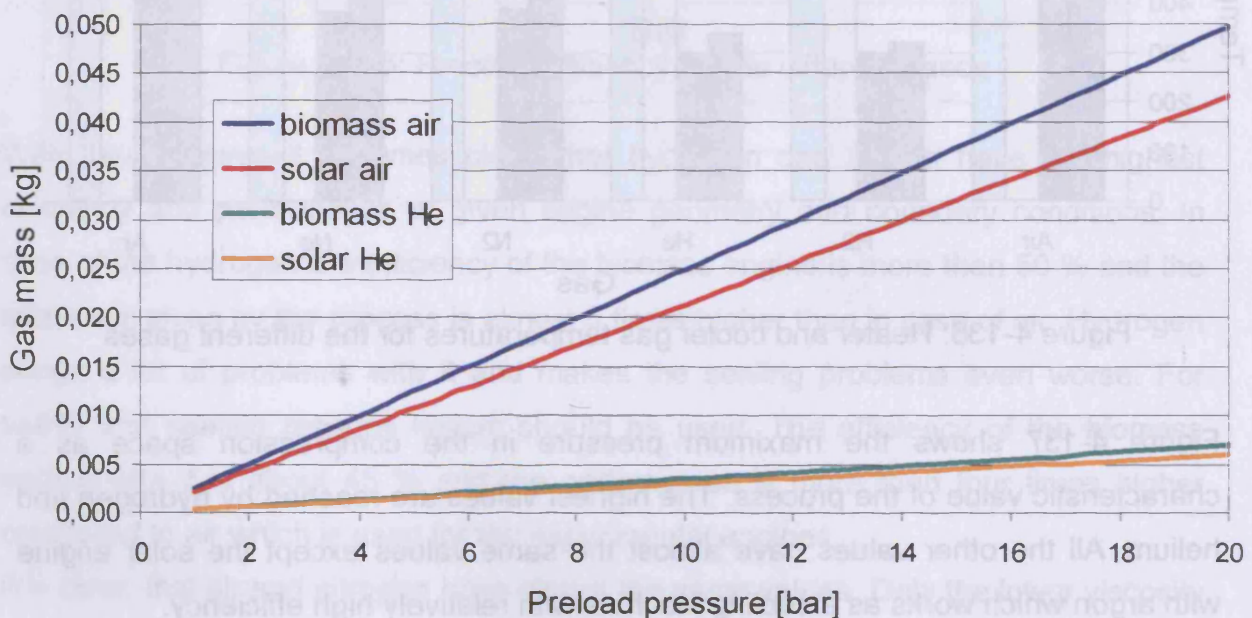
Figure 4-138: Gas mass for the different preload pressures

4.3.2.2 Results

The preload pressure and with it the initial gas mass has a significant influence on the cycle and its key figures. In figure 4-139 and 4-140 it can be seen that the transferred heat of the heater and cooler rise with higher preload pressures both for air and helium as well as for biomass and solar engine. For high pressures (>14 bar) the heat transferred in the cooler falls faster than the heat of the heater rises.

For helium the curves start at a value of about 5 bar. Below this value the gas mass in the engine is that low, that the program is unable to run.
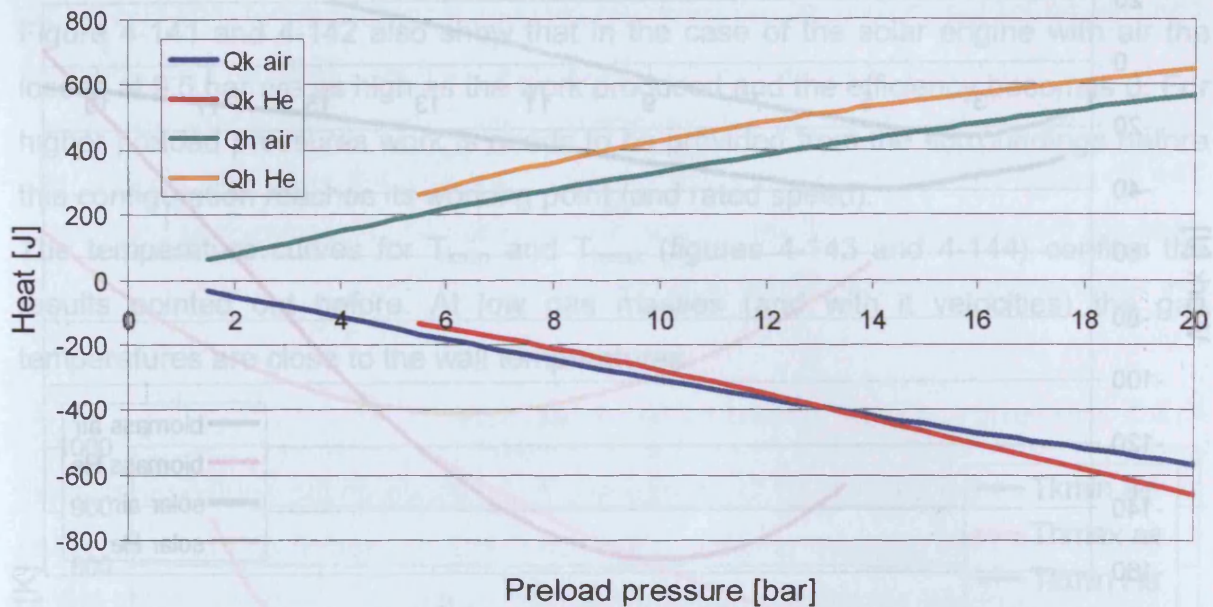
Figure 4-139: Heat transferred by the biomass engine
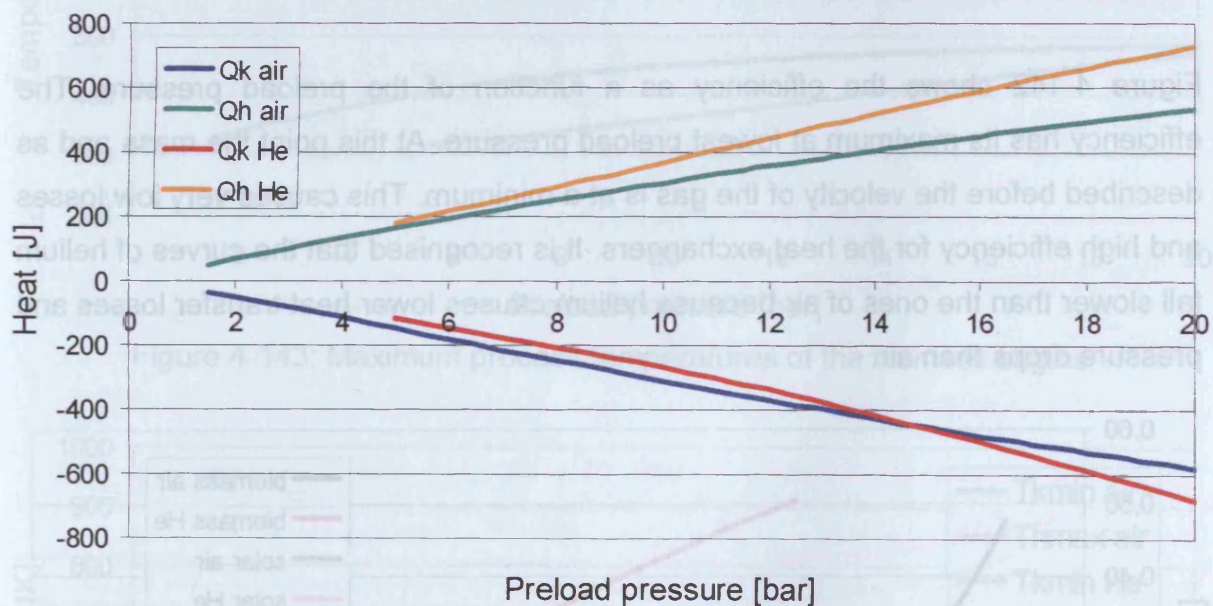
Figure 4-140: Heat transferred by the solar engine

The gas mass in the engine is proportional to the speed of the gas in the heat exchangers. If the speed is low, losses are low and there is enough time to transfer the heat in the heater, cooler and regenerator (see figure 4-143 and 4-144). To produce work the gas in the machine has to have a certain velocity. In figure 4-141 the total work as a function of the preload pressure is given. It shows that there is an optimum between low and high gas mass (and with it low and high gas velocity), where the work reaches its maximum. This optimum value depends on engine and gas properties and differs for biomass and solar engine and for air and helium.
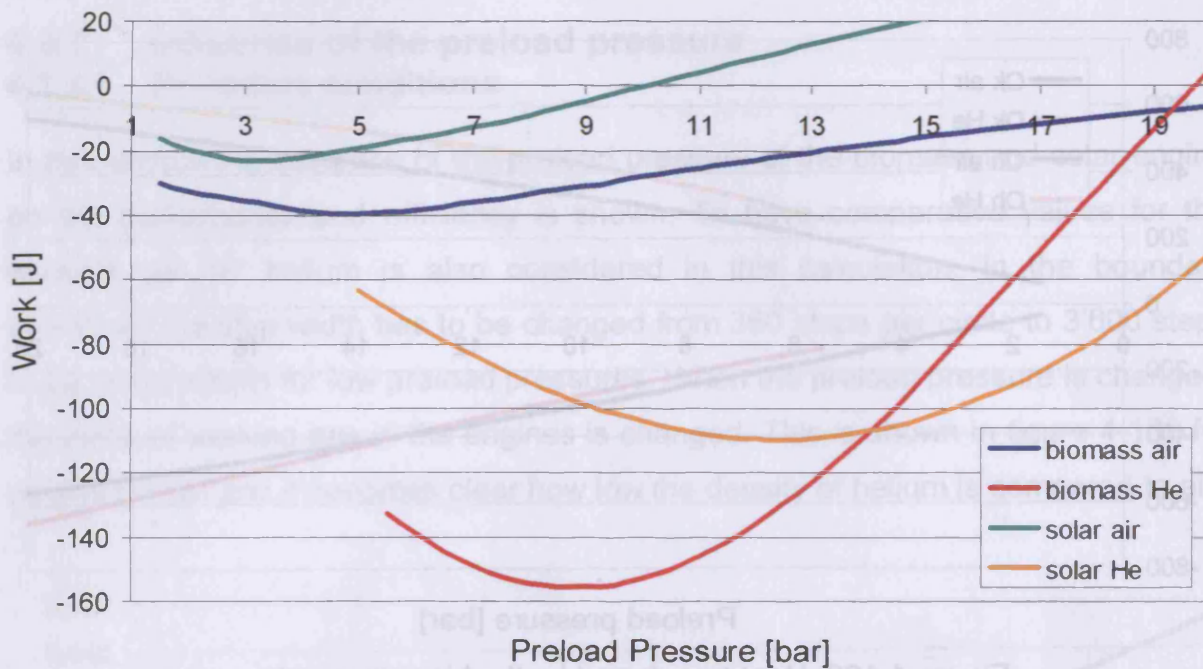
Figure 4-141: Total work as a function of the preload pressure

Figure 4-142 shows the efficiency as a function of the preload pressure. The efficiency has its maximum at lowest preload pressure. At this point the mass and as described before the velocity of the gas is at a minimum. This causes very low losses and high efficiency for the heat exchangers. It is recognised that the curves of helium fall slower than the ones of air because helium causes lower heat transfer losses and pressure drops than air.
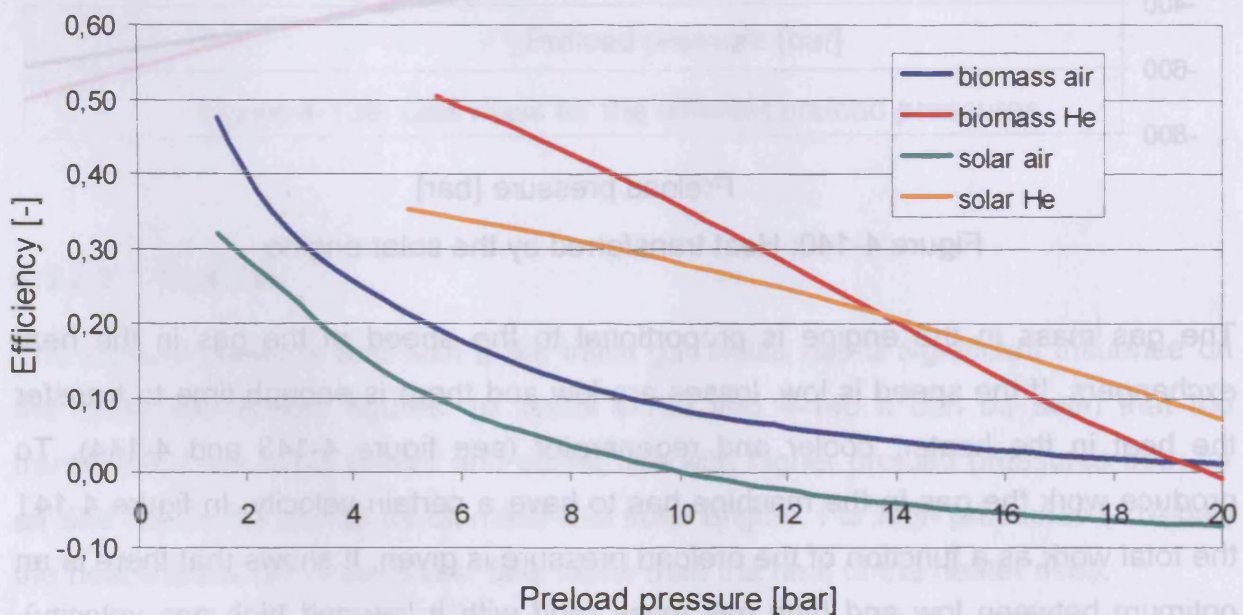
Figure 4-142: Efficiency of both engines for air and helium

Figure 4-141 and 4-142 also show that in the case of the solar engine with air the losses at 9,5 bar are as high as the work produced and the efficiency becomes 0. For higher preload pressures work is needs to be provided from the surroundings before this configuration reaches its working point (and rated speed).

The temperature curves for T_{kmin} and T_{hmax} (figures 4-143 and 4-144) confirm the results pointed out before. At low gas masses (and with it velocities) the gas temperatures are close to the wall temperatures.
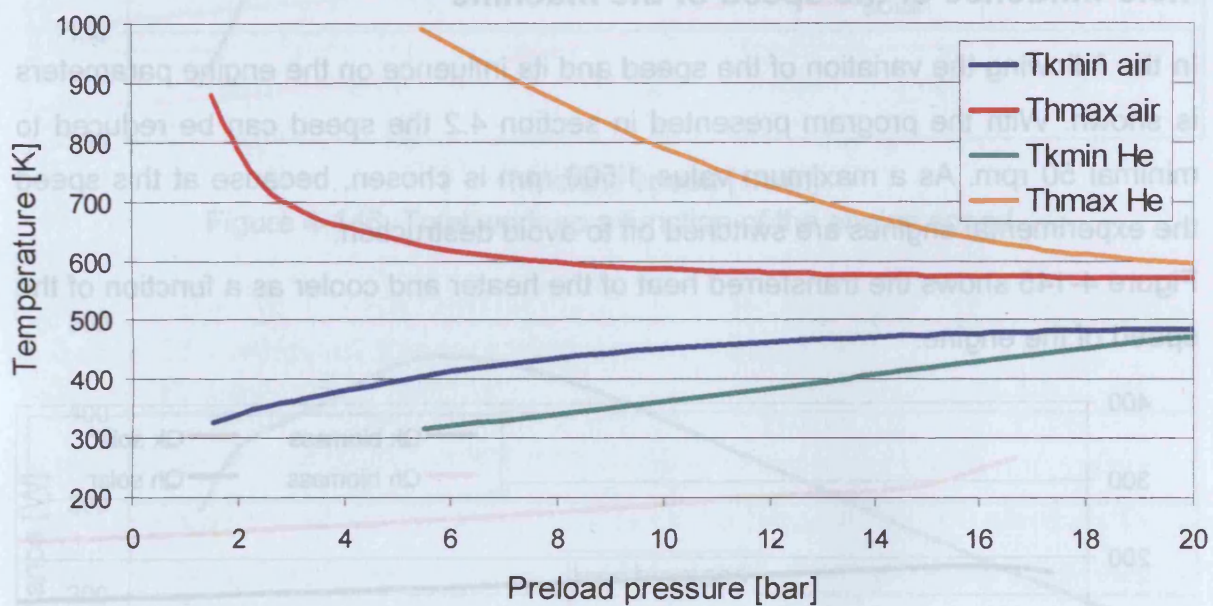
Figure 4-143: Maximum process temperatures of the biomass engine
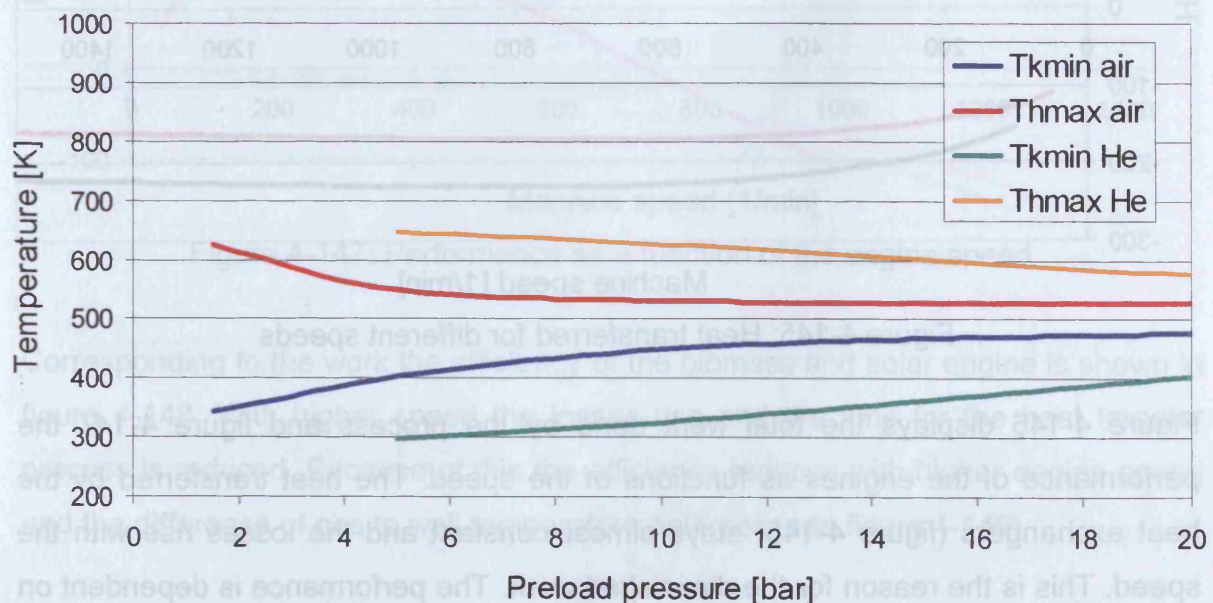
Figure 4-144: Maximum process temperatures of the solar engine

213

The figures for the maximum and minimum process temperatures (4-143 and 4-144) also show the much higher efficiency of engines filled with helium. The difference between heater and cooler gas temperature is three times higher than the one of air. The maximum process pressure, as an important key figure, is not shown here because the functions are all very similar straight lines and close together because of the same preload pressure and wall temperatures.

4.3.3 Influence of the speed of the machine

In the following the variation of the speed and its influence on the engine parameters is shown. With the program presented in section 4.2 the speed can be reduced to minimal 50 rpm. As a maximum value 1'500 rpm is chosen, because at this speed the experimental engines are switched off to avoid destruction.

Figure 4-145 shows the transferred heat of the heater and cooler as a function of the speed of the engine.
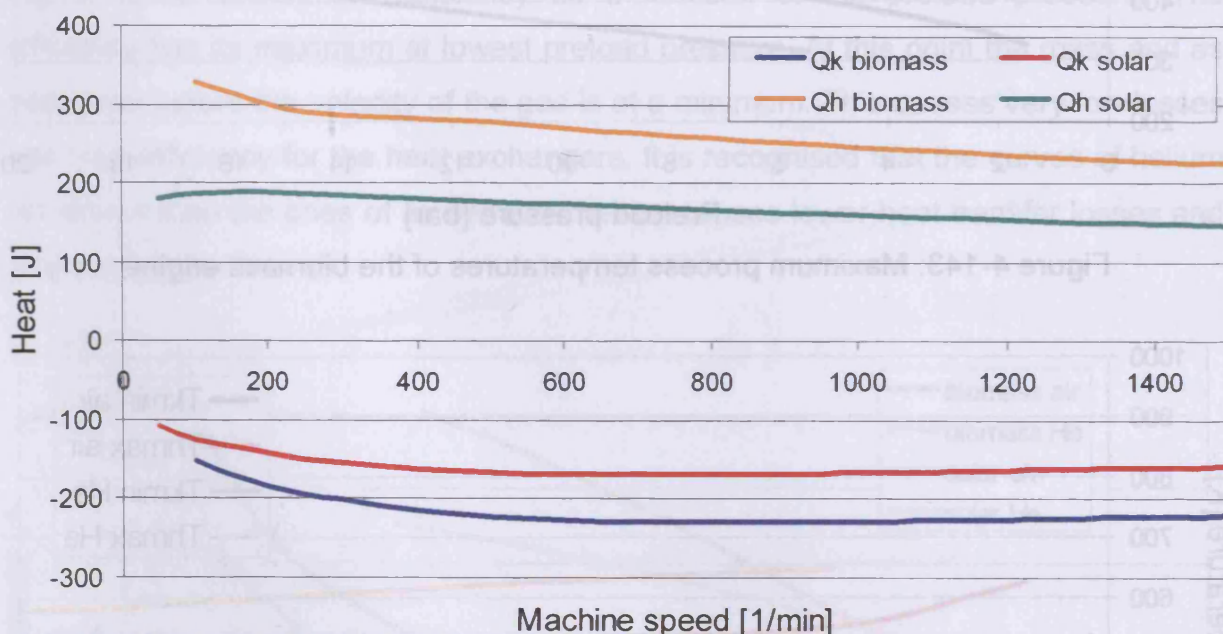
Figure 4-145: Heat transferred for different speeds

Figure 4-146 displays the total work done by the process and figure 4-147 the performance of the engines as functions of the speed. The heat transferred by the heat exchangers (figure 4-145) stays almost constant and the losses rise with the speed. This is the reason for the diminished work. The performance is dependent on the work and the speed as well and because of this fact a maximum can be found.

214
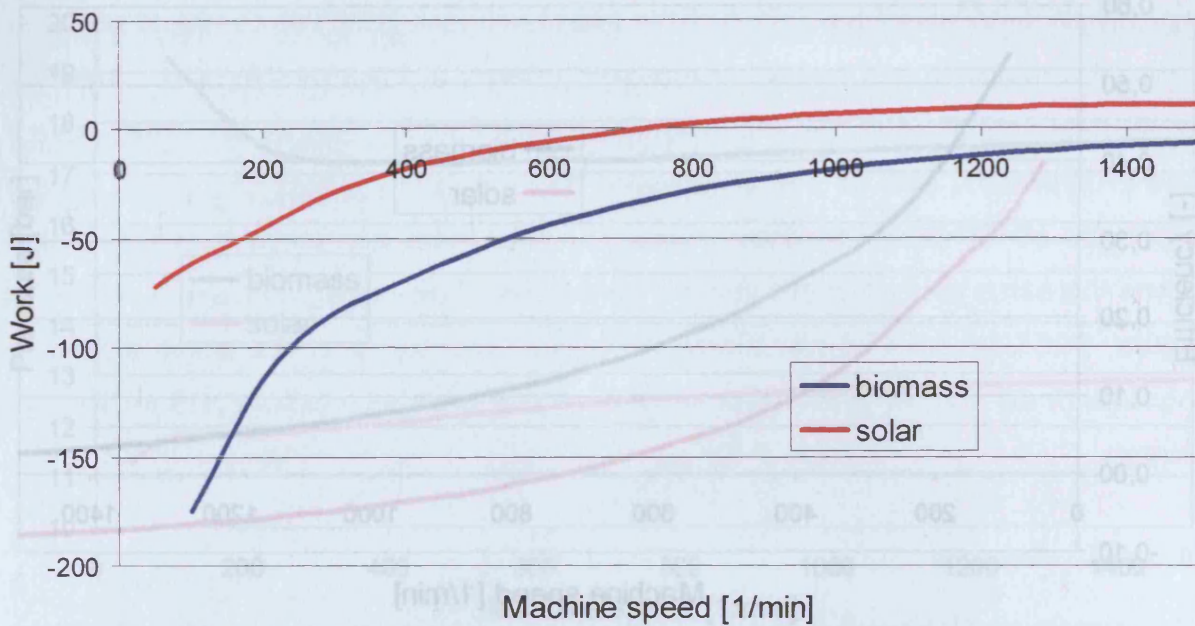
Figure 4-146: Total work as a function of the engine speed
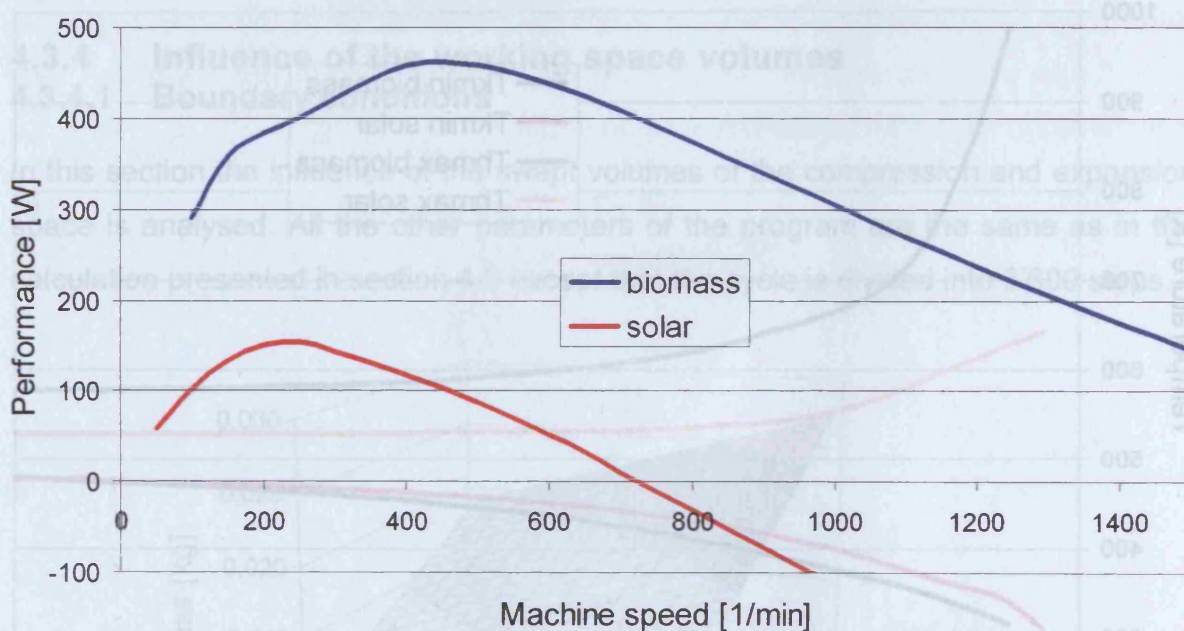
Figure 4-147: Performance as a function of the engine speed

Corresponding to the work the efficiency of the biomass and solar engine is shown in figure 4-148. With higher speed the losses rise and the time for the heat transfer process is reduced. Because of this the efficiency reduces with higher engine speed and the difference of gas to wall temperature enlarges (see figure 4-149)
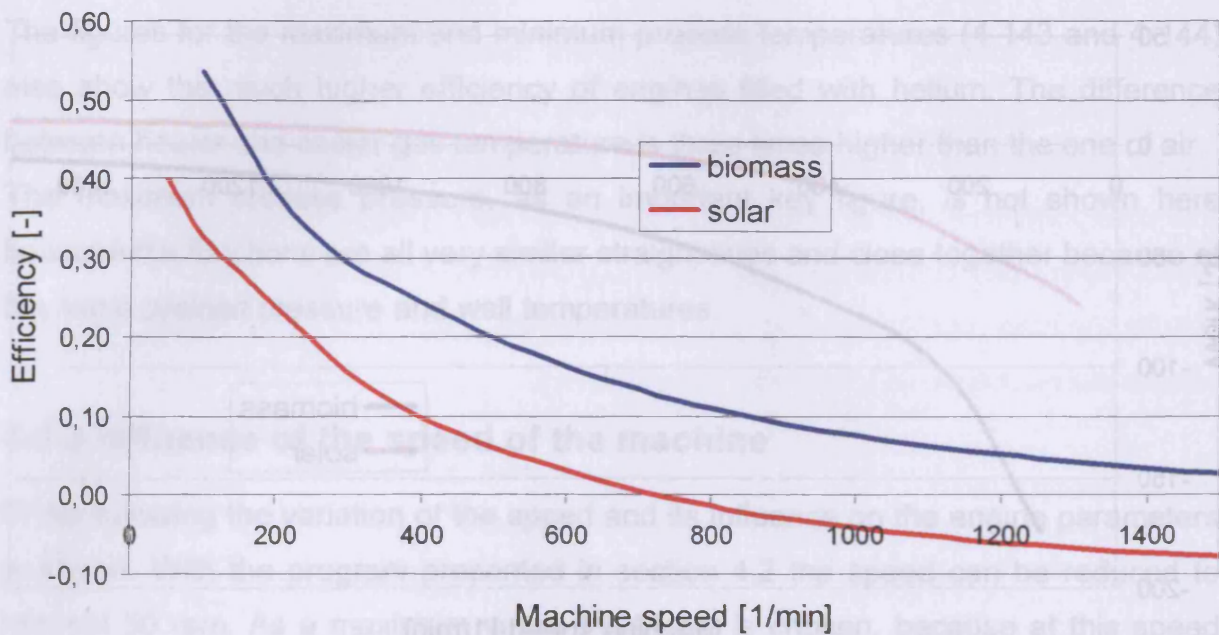
Figure 4-148: Efficiency for different speeds
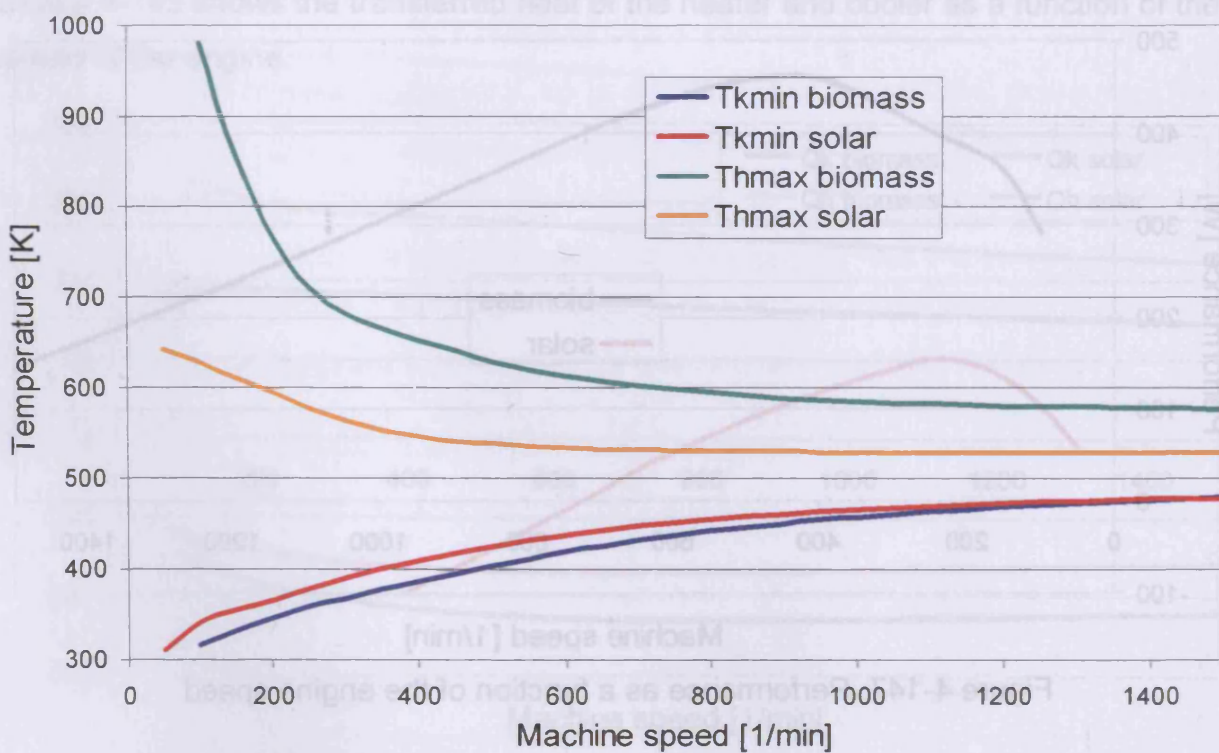
Figure 4-149: Maximum and minimum gas temperatures for different speeds

Figure 4-150 shows the maximum working gas pressure both for the biomass and solar engine as a function of the engine speed.
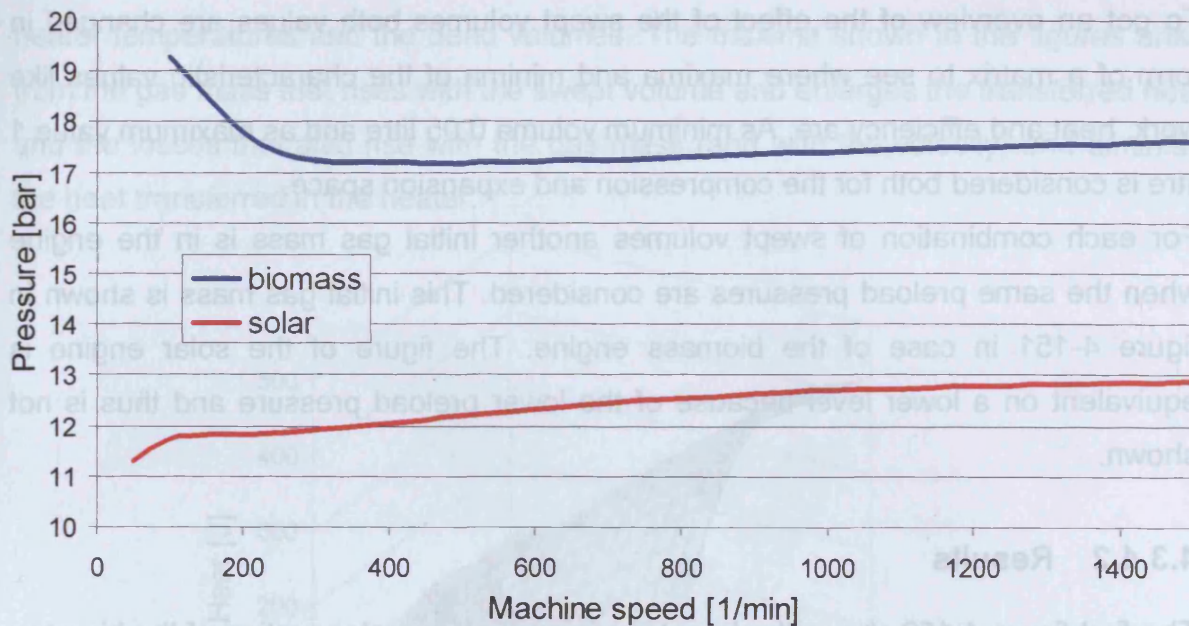
Figure 4-150: Maximum working gas pressure as a function of the speed

4.3.4 Influence of the working space volumes
4.3.4.1 Boundary conditions

In this section the influence of the swept volumes of the compression and expansion space is analysed. All the other parameters of the program are the same as in the calculation presented in section 4.2 except that the cycle is divided into 3'600 steps.
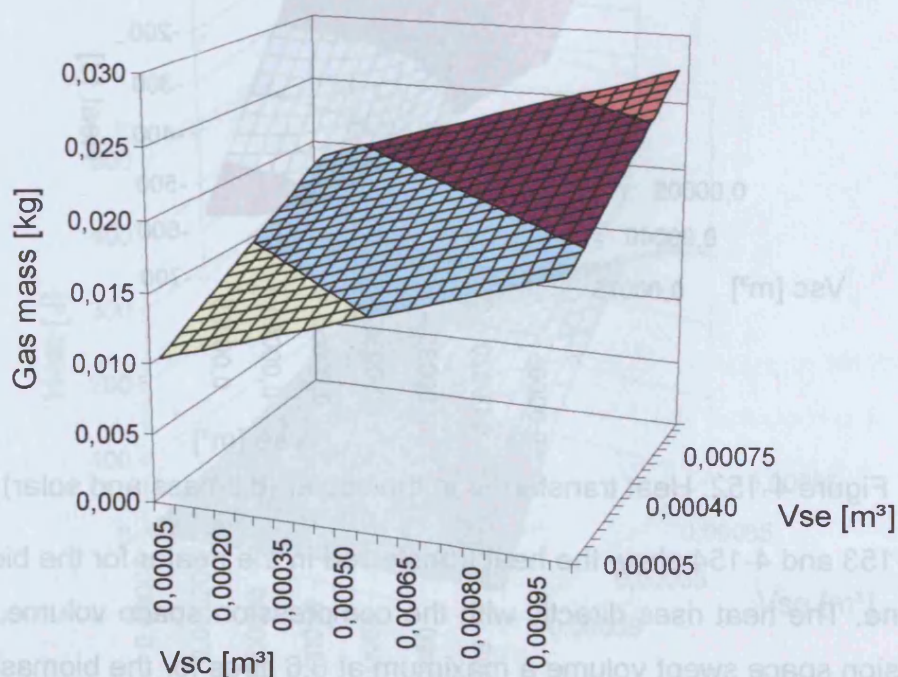
Figure 4-151: Initial gas mass for different swept volume combinations (for the biomass engine)

To get an overview of the effect of the swept volumes both values are changed in form of a matrix to see where maxima and minima of the characteristic values like work, heat and efficiency are. As minimum volume 0,05 litre and as maximum value 1 litre is considered both for the compression and expansion space.

For each combination of swept volumes another initial gas mass is in the engine when the same preload pressures are considered. This initial gas mass is shown in figure 4-151 in case of the biomass engine. The figure of the solar engine is equivalent on a lower level because of the lower preload pressure and thus is not shown.

4.3.4.2 Results

The first figure 4-152 shows the heat transferred in the cooler section of the biomass engine. Because the cooler section of both engines is very similar and the temperature of the cooler wall is the same this figure represents the solar engine as well. It can be seen, that with rising volumes and with it rising gas mass the heat transferred in the cooler section rises up to 570 J.
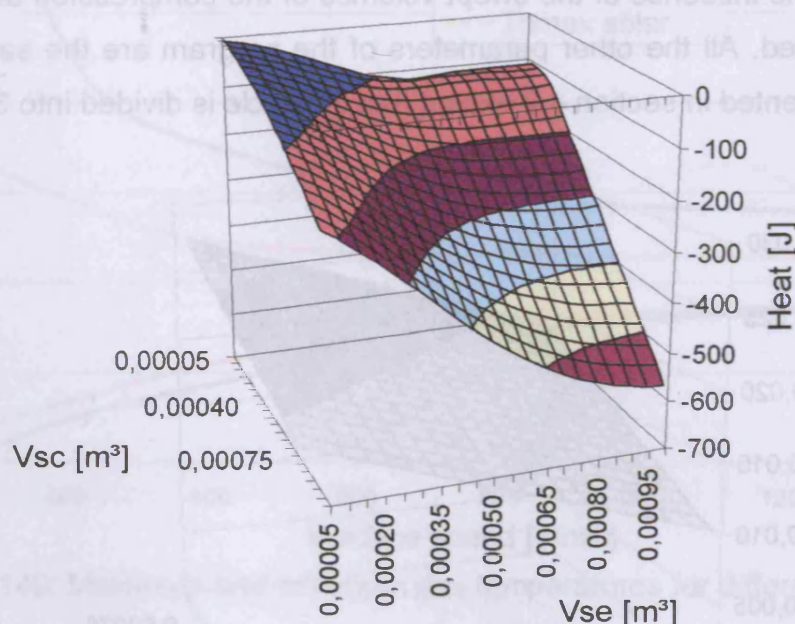
Figure 4-152: Heat transferred in the cooler (biomass and solar)

Figures 4-153 and 4-154 show the heat transferred in the heater for the biomass and solar engine. The heat rises directly with the compression space volume. Modifying the expansion space swept volume a maximum at 0,6 litres for the biomass and 0,65 litres for the solar engine can be found along the figures. This difference and the difference in the maximum values of the transferred heat come from the distinct

heater temperatures and the dead volumes. The maxima shown in the figures arise from the gas mass that rises with the swept volume and enlarges the transferred heat and the losses that also rise with the gas mass (and with the velocity) and diminish the heat transferred in the heater.
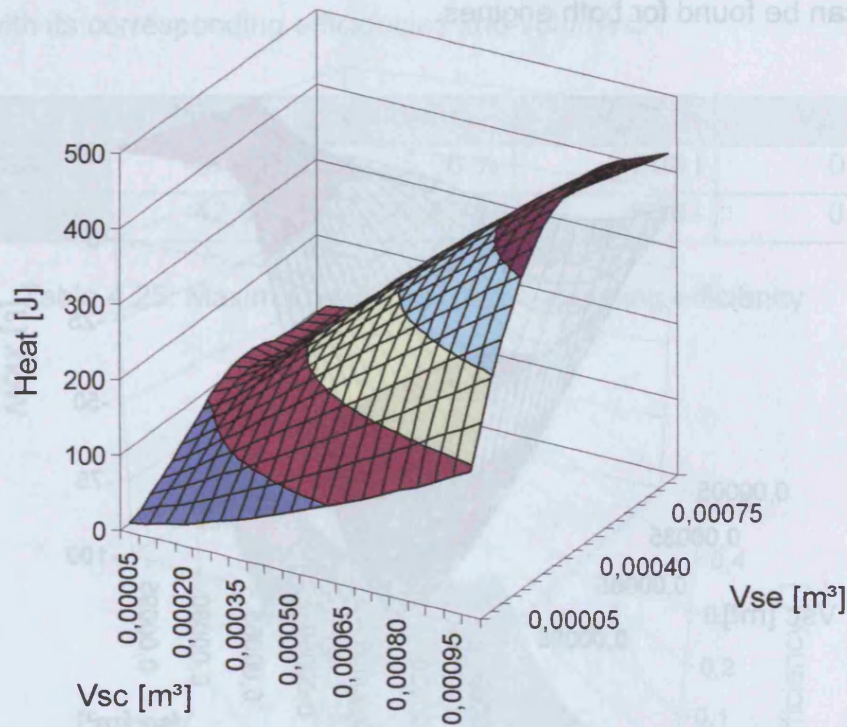
Figure 4-153: Heat transferred in the heater of the biomass engine
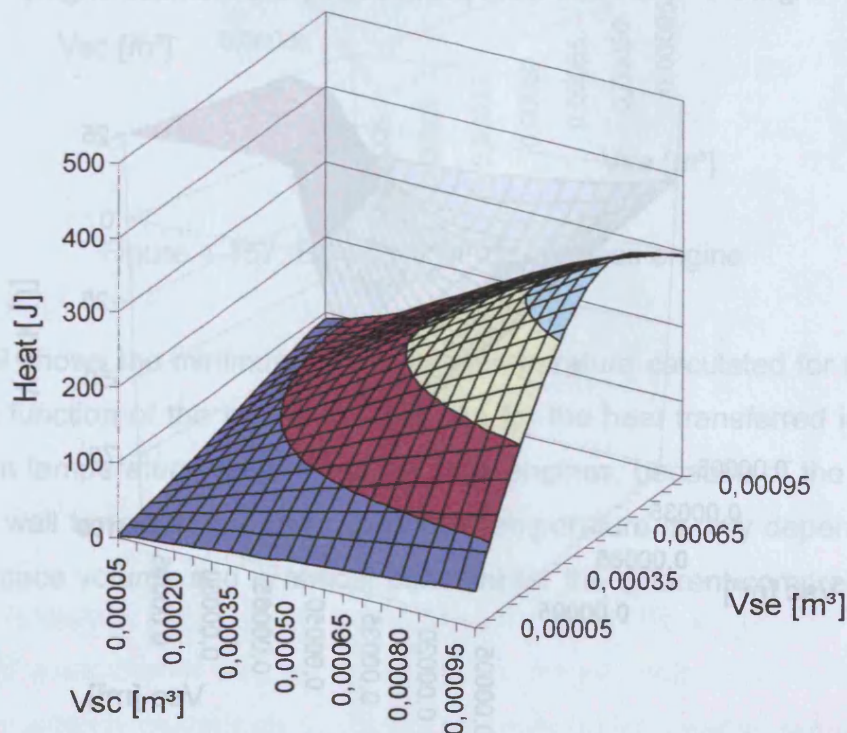
Figure 4-154: Heat transferred in the heater of the solar engine

In figure 4-155 and 4-156 the total work of the process is shown as a function of the swept volumes for both engines. It can be seen that the right choice of swept volumes has an enormous influence on the work. With some combinations of swept volumes the engine would not even work (in the areas where the work is positive). A maximum can be found for both engines.
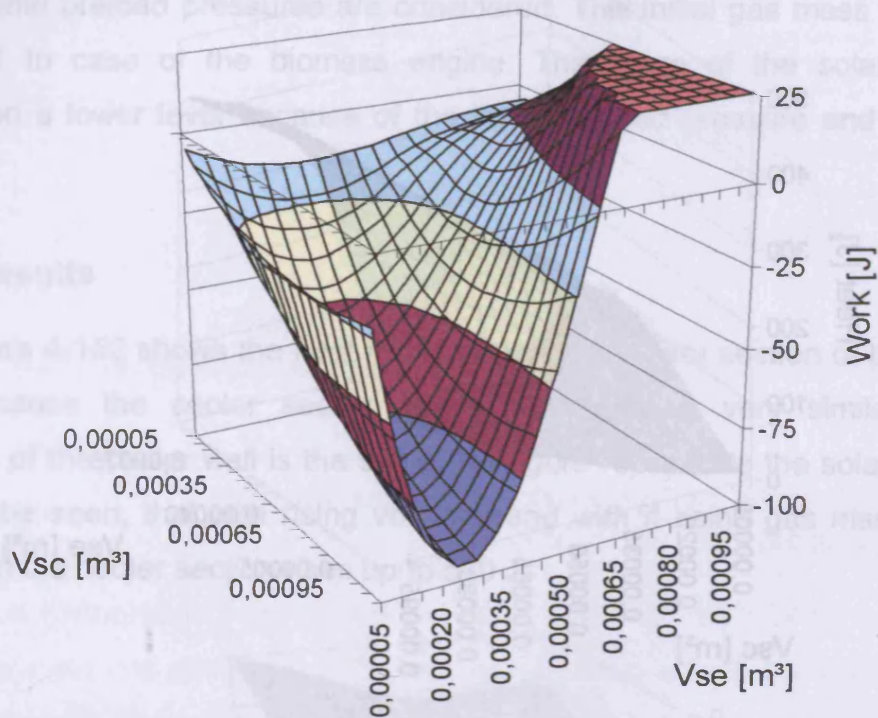
Figure 4-155: Total work produced by the biomass engine
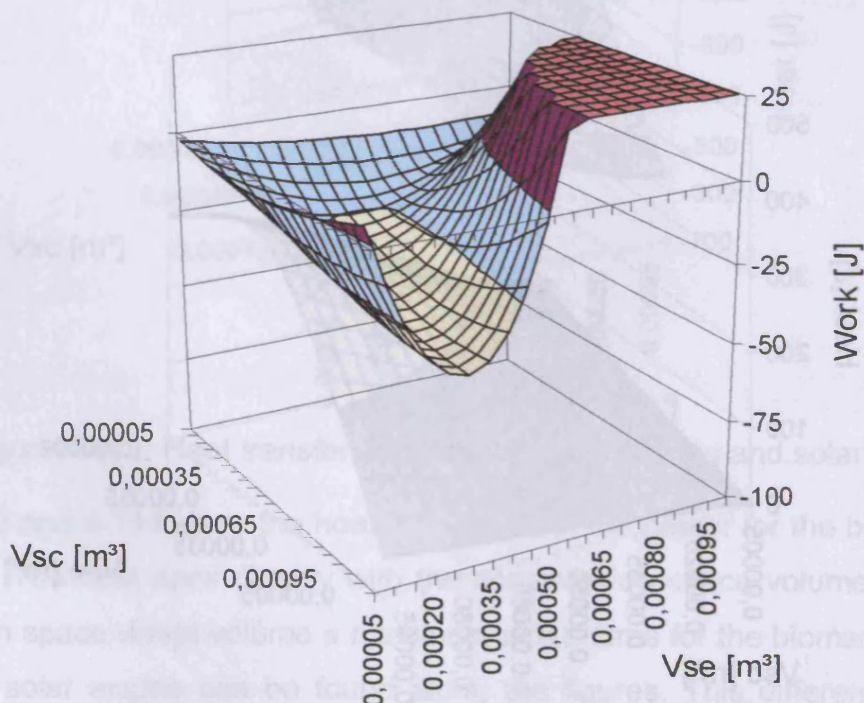
Figure 4-156: Total work produced by the solar engine

220

Figures 4-157 and 4-158 show the efficiency of both engines for the different swept volumes. At the points of maximum work the efficiency is not at its maximum. The highest efficiencies can be found at very low volumes. At this point the gas mass is at its minimum and the losses are neglectable. Table 4.25 shows the maximum values of the work with its corresponding efficiencies and volumes.

	Work	Efficiency	V_{sc}	V_{se}
Biomass	-97,10 J	25,96 %	1,00 l	0,25 l
Solar	-42,63 J	18,41 %	1,00 l	0,30 l

Table 4.25: Maximum work and corresponding efficiency
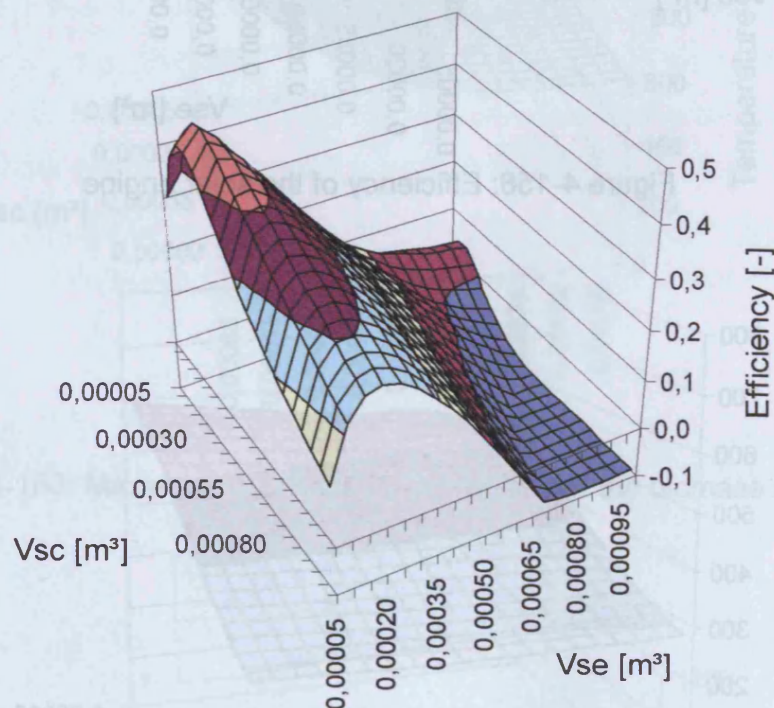
Figure 4-157: Efficiency of the biomass engine

Figure 4-159 shows the minimum cooler gas temperature calculated for the biomass engine as a function of the swept volumes. As for the heat transferred in the cooler this minimum temperature is the same for both engines, because of the same dead volume and wall temperature. The cooler gas temperature is only dependent on the expansion space volume and is almost constant for the different compression space volumes.
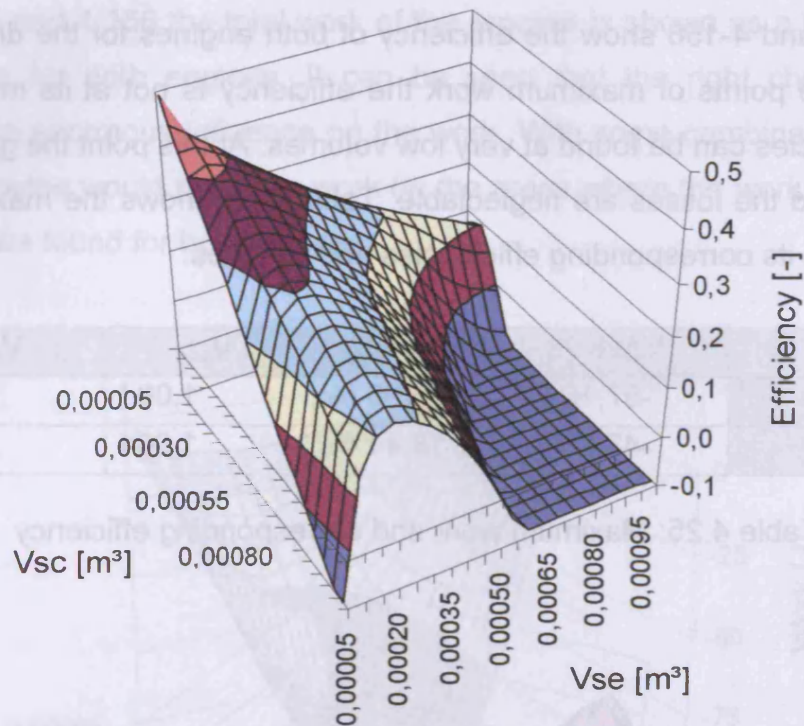
Figure 4-158: Efficiency of the solar engine
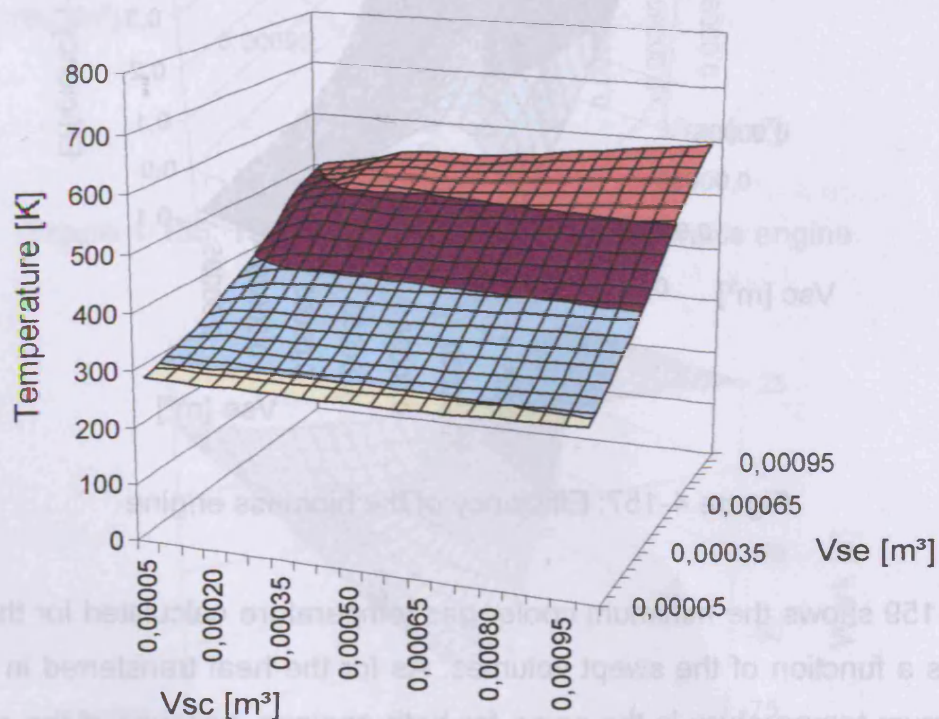
Figure 4-159: Minimum cooler gas temperature for the biomass and solar engine

Figures 4-160 and 4-161 show the maximum heater gas temperatures for the biomass and solar engine. As the minimum cooler gas temperature the maximum heater gas temperature only depends on the expansion space volume. For changing compression space swept volumes this temperature stays almost constant. It can be

clearly seen that in case of the biomass engine the heater gas temperature depends much more on the swept volumes. For low expansion space volumes the gas temperature in the heater is much closer to the high wall temperature. The solar Stirling has a lower wall temperature and the gas reaches this wall temperature better because of the lower speed and the higher heater efficiency for the complete range of swept volumes.
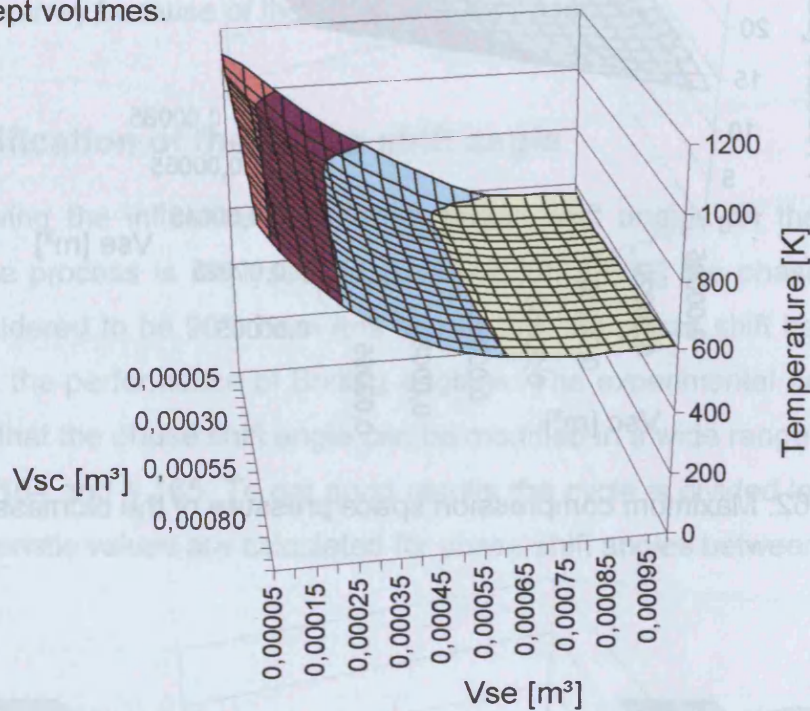
Figure 4-160: Maximum heater gas temperature of the biomass engine
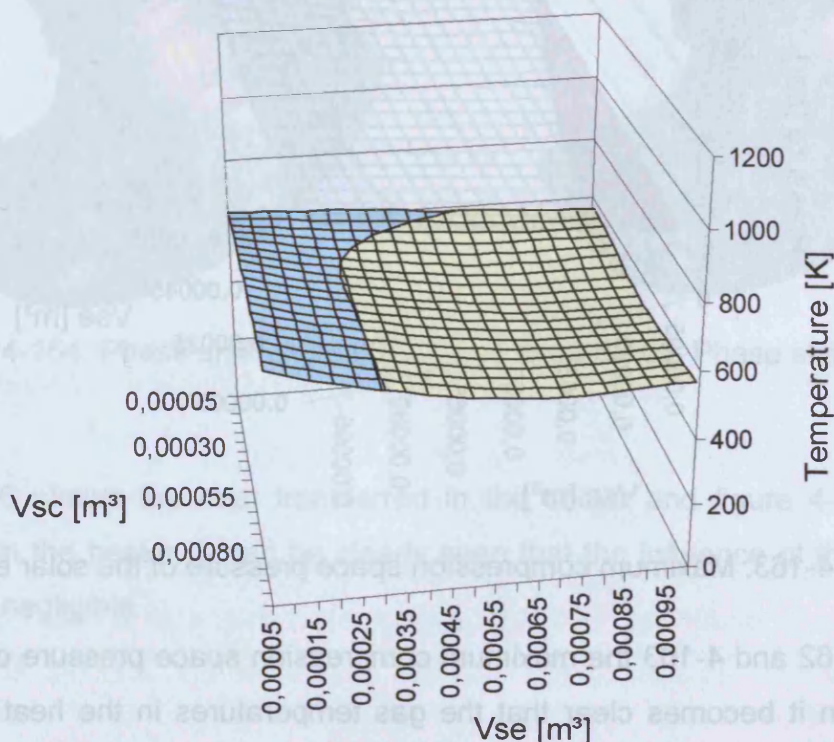
Figure 4-161: Maximum heater gas temperature of the solar engine
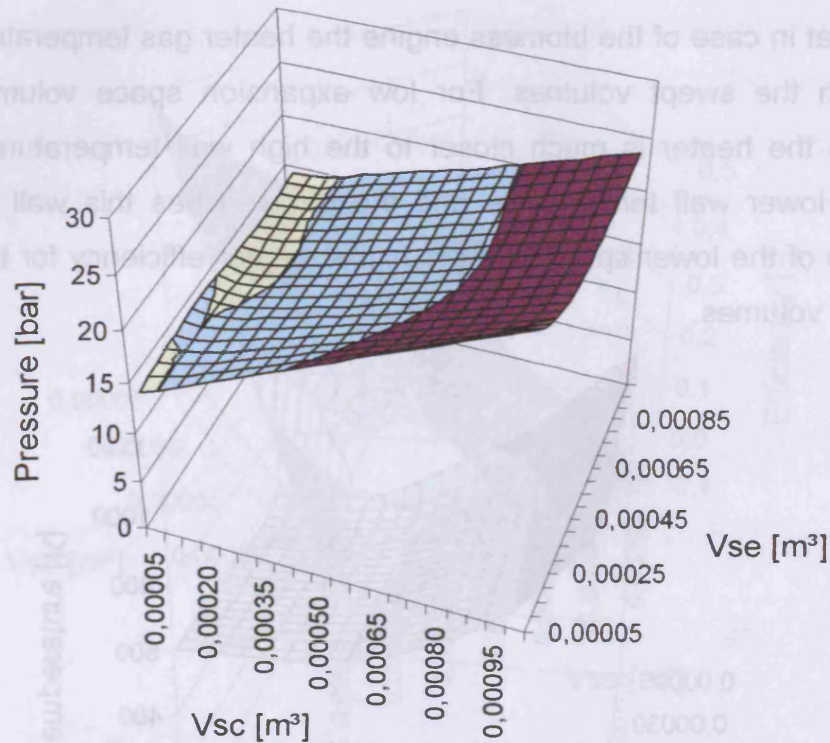
Figure 4-162: Maximum compression space pressure of the biomass engine
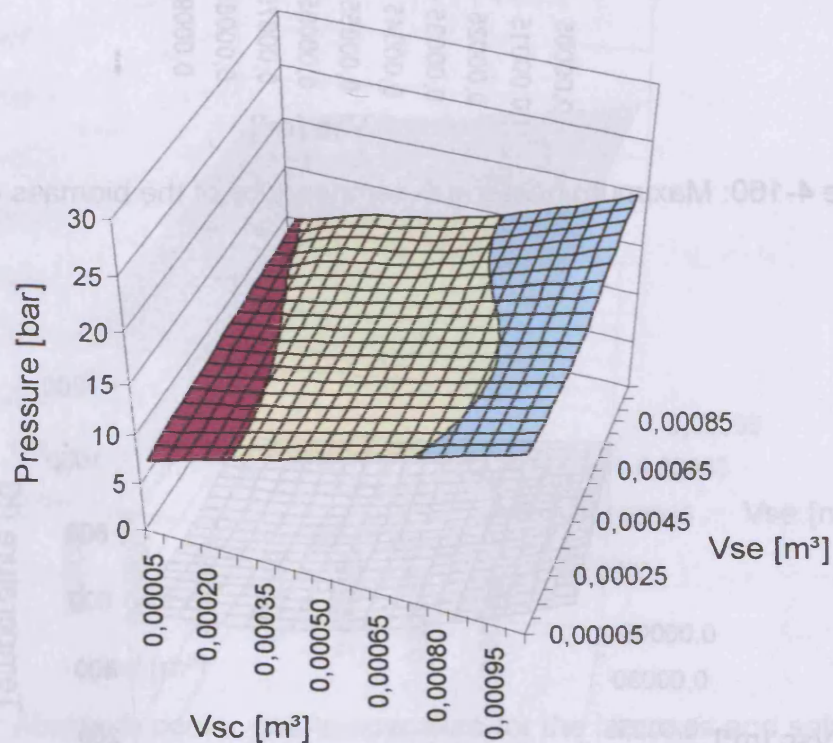
Figure 4-163: Maximum compression space pressure of the solar engine

In figures 4-162 and 4-163 the maximum compression space pressure can be seen. In this section it becomes clear that the gas temperatures in the heat exchangers only depend on the expansion space volumes. The pressure in the engines only

224

depends on the compression space swept volume. This is obvious because in the case of the expansion space of a gamma type Stirling engine only a displacer is moving. The proportion of the compression space swept volume to the dead volume and displacer volume defines the compression ratio and with it the maximum pressure in the engine. In case of the solar engine the maximum pressure is lower in the complete array because of the lower initial gas load.

4.3.5 Modification of the phase shift angle

In the following the influence of different phase shift angles on the characteristic values of the process is analysed. In literature [3], [6], [9] the phase shift angle is always considered to be 90°. Here it is shown that the phase shift has an important influence on the performance of Stirling engines. The experimental engines are built up in a way that the phase shift angle can be modified in a wide range like it is shown in figures 4-164 and 4-165. To get good results the cycle is divided into 3'600 steps. The characteristic values are calculated for phase shift angles between 70° and 150°.
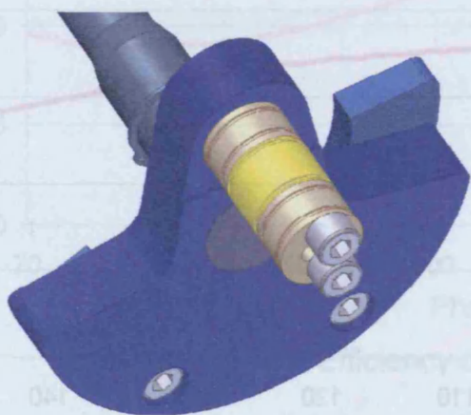
Figure 4-164: Phase shift angle 90°   Figure 6-165: Phase shift angle 105°
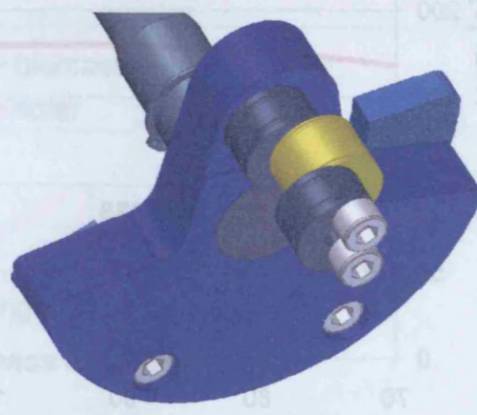
Figure 4-166 shows the heat transferred in the cooler and figure 4-167 the heat transferred in the heater. It can be clearly seen that the influence of the phase shift angle is not negligible.

separately from each other. They all depend on the heat exchanger geometry. To analyse their influence, various geometries with different wetted areas, free flow areas and dead volumes are built up. Figure 4-179 shows the original cross section of the cooler as used in the solar and biomass engine as well.
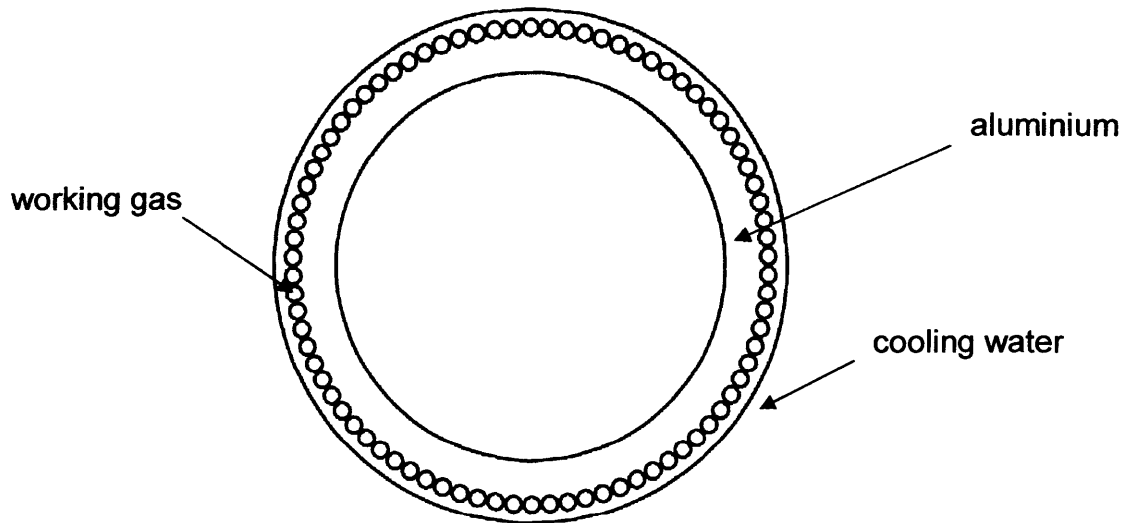
Figure 4-179: Original cross section of the solar and biomass cooler

Six versions of the cooler are analysed in the following. Version 1 and 2 (see figure 4-180 and 4-181) have the same diameter of the drillings where the working gas flows. Only the number of drillings is raised. Version 3 (figure 4-182) has the same number of pipes as version 2 but a reduced drilling diameter. Version 4 (figure 4-183) has the same drilling diameter like version 3 but a raised number of drillings. Version 5 and 6 (figure 4-184 and 4-185) have the same reduced number of drillings and only the diameter varies.
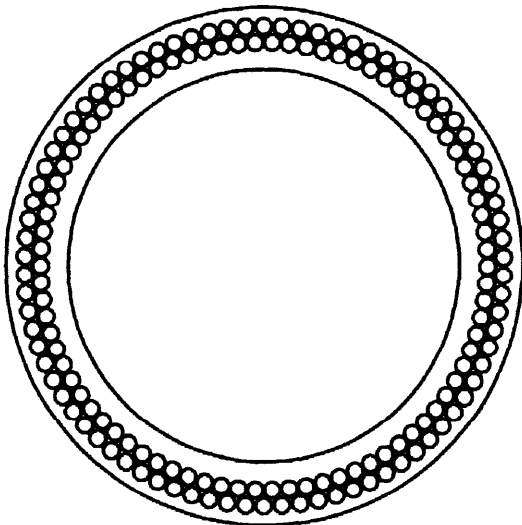
Figure 4-180: Version 1
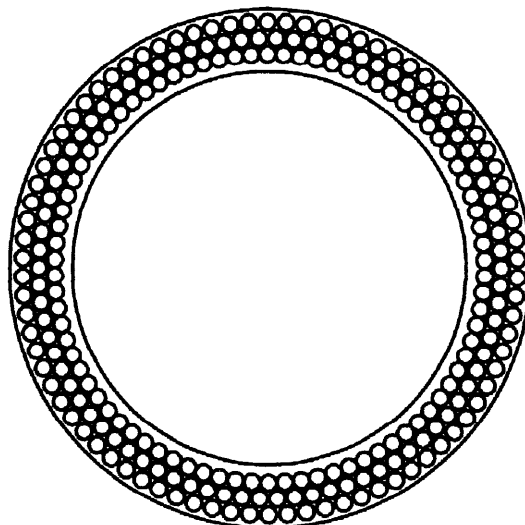
Figure 4-181: Version 2
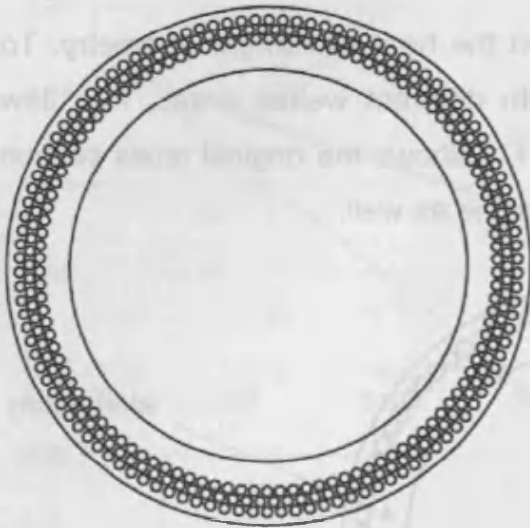
Figure 4-182: Version 3

Figure 4-183: Version 4
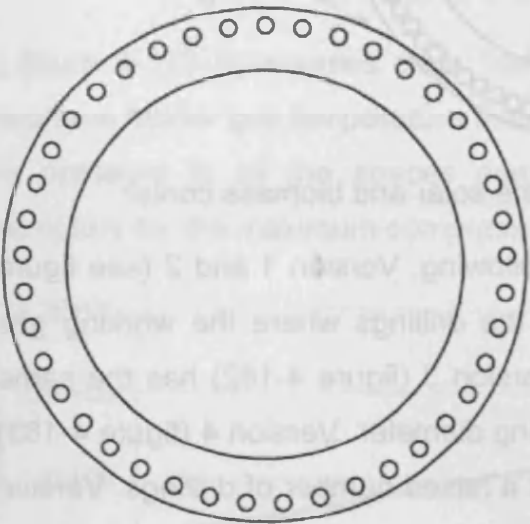
Figure 4-184: Version 5
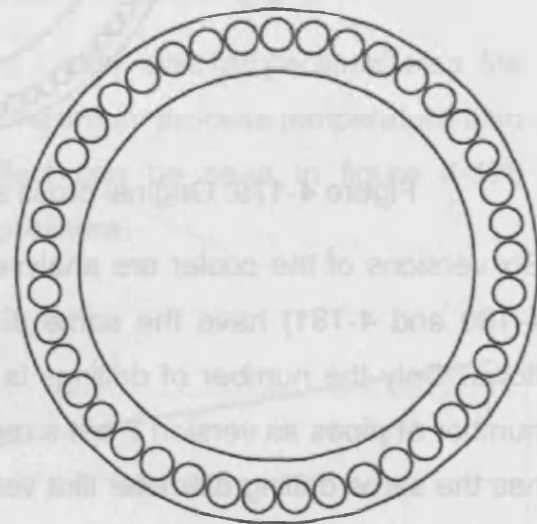
Figure 4-185: Version 6

Table 4.27 shows the parameters of the different versions of the cooler in comparison. n stands for the number of drillings, d for the diameter, A for the free flow area, V for the dead volume and A_w for the wall surface of all the drillings.

	n	d	A_k	V_k	A_{wk}	m_{g-b}	m_{g-s}
	[-]	[mm]	[m²]	[m³]	[m²]	[kg]	[kg]
Original	82	4	1,03E-03	3,79E-04	9,45E-02	0,0186	0,0117
V - 1	164	4	2,06E-03	5,85E-04	1,89E-01	0,0205	0,0131
V - 2	246	4	3,09E-03	8,94E-04	2,83E-01	0,0232	0,0151
V - 3	330	2,5	1,62E-03	4,38E-04	2,38E-01	0,0192	0,0121
V - 4	550	2,5	2,70E-03	5,46E-04	3,96E-01	0,0201	0,0128
V - 5	41	4	5,15E-04	3,27E-04	4,72E-02	0,0182	0,0114
V - 6	41	8	2,06E-03	4,82E-04	9,45E-02	0,0196	0,0124

Table 4.27: Parameters of the different versions of the cooler

> Changing the working gas

Section 4.3.1 showed that with hydrogen the highest efficiencies are possible. Because of the difficulties in handling and the dangers of H_2 here He is considered as working gas. Table 4.32 shows the effect on the characteristic values of filling the biomass engine with He. The minimum and maximum gas temperatures are pushed further to the corresponding wall temperatures and the pressure rises. As a result the efficiency is raised by more than 330 % and the output is 1,8 kW instead of 400 W.

$T_{k\,min}$	336,68	[K]
$T_{h\,max}$	894,46	[K]
$p_{c\,max}$	19,753	[bar]
Q_k	-193,35	[J]
Q_h	344,43	[J]
W	152,47	[J]
P	1'778,82	[W]
eta	-0,443	[-]

Table 4.32: Characteristic values of the biomass engine filled with He

> Changing the preload pressure

In the case of the biomass engine the preload pressure is 7,5 bar. Changing the pressure to a value of 9 bar improves the work of the process by 3 J to a maximum but also diminish the efficiency by 4 % (see figures 4-141 and 4-142). Because of this the preload pressure is not changed.

> Changing the speed of the machine

In section 4.3.3 the influence of the machine speed is described for the working gas air. For helium these values are different. Figure 4-208 shows the efficiency and the performance as a function of the machine speed for helium. The actual speed of the biomass engine is 700 rpm (marked with the green line in figure 4-208). It can be seen that this speed is good compromise between performance and efficiency and will be adopted for further calculations.

that is felt to be unique. A comparison of the nominal performance values from the specifications in tables 2.2 and 2.3 with the calculated ones using the ideal adiabatic and the quasi steady flow method can be found in table 4.38.

	Solar engine	Biomass engine
Nominal value	200 W	600 W
Ideal adiabatic	454,1 W	2'359,5 W
Quasi steady flow	184,5 W	555,8 W

Table 4.38: Comparison of calculated and nominal performance values

The performance values of the ideal adiabatic method show a difference by factors to the nominal ones like the Schmidt analysis does, because the heat exchangers are still based on an isothermal assumption. The values of the quasi steady flow model fit very well. A comparison of the results of the ideal adiabatic and the quasi steady flow model is given in section 4.2.8.

With the quasi steady flow analysis a method is found that can predict the performance with a higher accuracy than any other method before. Hence it is taken as a basis for a parameter variation that deals with different geometric parameters and boundary conditions to see its effect on the performance and efficiency of the Stirling engine. Analysing different working gases it could be seen that He is the best choice for this kind of engine as the performance and the efficiency as well can be tripled. The correct choice of the preload pressure and with it of the initial gas mass is also eminent to get good results. Even the best working point (speed) for the biomass and the solar experimental engine could be calculated. With this value the right generator unit (number of poles and with it the mean speed) can be chosen in advance. Another important parameter in the design stage is the choice of the expansion and compression space swept volume. Within the parameter variation it can be shown that for a compression space volume of 1 litre and an expansion space volume of 0,3 litre best results in efficiency and performance can be found. Furthermore the phase shift angle and different heat exchanger parameters like wetted areas, free flow areas and wall temperatures are analysed.

With all these parameter variations a biomass engine configuration could be found that has theoretically more than 4-times higher performance and efficiency as well (see table 4.37). The process data for this engine is calculated and compared to the original one in section 4.3.9.2.

5   4th order multidimensional analysis with CFD

In contrast to the other analysis methods shown before it is not the main task of a CFD simulation to determine p-V-diagrams, process performances or efficiencies. Computational Fluid Dynamics (CFD) is used to show the flow behaviour of the fluid in certain geometries. It is capable of determining flow losses and pressure drops and it is able to show exactly how the gas is heated up and cooled down and helps to make heat exchangers more efficient by optimising flow conditions, pressure drops and heat transfer.

A forerunner of 4th order multidimensional analysis is the 3rd order nodal analysis defined by Finkelstein in his work "Computer analysis of Stirling engines" [10]. This kind of calculation was defined in 1979. Finkelstein wrote this thesis for TCA Stirling Engine Research and Development Company in Beverly Hills, California, USA. This Chapter shows what today's analysis tools like ANSYS CFX are capable of.

5.1   Numerical flow analysis

Using today's flow analysis programmes like Fluent, FlowSim or ANSYS CFX it is often forgotten what complex sets of equations this kind of software is based on. There are many laws like that of Bernoulli up to the latest knowledge of the flow with particles. Not only flow modelling specialists are needed but also mathematicians and computer specialists to build up such complex flow modelling systems.

Computational Fluid Dynamics (CFD) is a computer-based tool for simulating the behaviour of systems involving fluid flow, heat transfer and other related physical processes. It works by solving the equations of fluid flow in a special form over a region of interest with specified known boundary conditions of this region [15]. CFD is used by engineers and scientists in a wide range of fields. Typical applications include:

- Process industry: mixing vessels, chemical reactors
- Building services: ventilation of buildings, such as atria
- Health and safety: investigating the effects of fire and smoke
- Motor industry: combustion modelling, car aerodynamics

- Electronics: heat transfer within and around circuit boards
- Environmental: dispersion of pollutants in air or water
- Power and energy: optimisation of combustion processes
- Medical: blood flow through grafted blood vessels

5.1.1 History of CFD

Computers have been used to solve fluid flow problems for many years. Numerous programs have been written to solve either specific problems or specific classes of problems. From the mid 1970's the complex mathematics required to generalise the algorithms began to be understood and general purpose CFD solvers were developed. These began to appear in the early 1980's and required very powerful computers at this time as well as an in-depth knowledge of fluid dynamics and large amounts of time to set up simulations. Consequently CFD was a tool used almost exclusively in research programmes.

Recent advantages in computing power together with powerful graphics and interactive 3-D manipulation of models mean that the process of creating a CFD model and analysing the results is much less labour-intensive reducing the time and therefore the costs. Advanced solvers contain algorithms which enable steady solutions of the flow field to be obtained in reasonable time [16].

As a result of these factors, CFD is now an established industrial design tool helping to reduce design timescales and improve processes throughout the engineering world. CFD provides a cost-effective and accurate alternative to scale model testing. Variations on the simulation can be performed much more quickly which offers an obvious advantage [17].

5.1.2 Mathematics of CFD

The set of equations which describes the processes of momentum, heat and mass transfer is known as the Navier-Stokes equation set. These are partial differential equations which were derived in the early nineteenth century. They have no known general analytical solution but can be discretisised and solved numerically. The set of equations most CFD-programmes are basically built up on are the unsteady Navier-

At the opposite side of the control volume the mass flow has changed by

$$\frac{\partial(\rho \cdot \bar{u})}{\partial x} \cdot dx \qquad (5.2)$$

Changing equation (5.1) for the opposite side of the control volume:

$$\dot{m}_{out} = \left(\rho \cdot \bar{u} + \frac{\partial(\rho \cdot \bar{u})}{\partial x} \cdot dx \right) \cdot dy \cdot dz \qquad (5.3)$$

Analogue to equation (5.3) the mass flows in the directions y and z can be defined. Out of them the equation of continuity for compressible fluids can be designed in the conservative form.

$$\frac{\partial \rho}{\partial t} + \frac{\partial(\rho \cdot \bar{u})}{\partial x} + \frac{\partial(\rho \cdot \bar{v})}{\partial y} + \frac{\partial(\rho \cdot \bar{w})}{\partial z} = 0 \qquad (5.4)$$

> **Equation of impulse**

The second basic equation is the equation of impulse. It can be derived by the balance of the entering and the leaving impulse flows according to the control volume. The shear and normal force affecting the volume element are balanced as well as the gravity, magnetic and electric forces.

$$\underbrace{\frac{\partial(\rho \cdot \bar{u})}{\partial t} + \frac{\partial(\rho \cdot \bar{u}^2)}{\partial x} + \frac{\partial(\rho \cdot \bar{u} \cdot \bar{v})}{\partial y} + \frac{\partial(\rho \cdot \bar{u} \cdot \bar{w})}{\partial z}}_{\text{impulse flow in and out}} =$$

(5.5)

$$= \underbrace{F_x}_{\text{force}} - \underbrace{\frac{\partial \sigma_{xx}}{\partial x}}_{\substack{\text{normal} \\ \text{force}}} + \underbrace{\frac{\partial \tau_{xx}}{\partial x} + \frac{\partial \tau_{yx}}{\partial y} + \frac{\partial \tau_{xz}}{\partial z}}_{\text{shear force}}$$

By dividing the normal force part into one pressure and one friction part and by using the Stokes friction equation this equation can be modified to the Navier-Stokes-equation.

> ➤ Energy equation

Analogue to equation (5.5) the third basic equation can be derived by balancing the energy flow in and out of the control volume together with the pressure and the tensions. For incompressible fluids the equation is as follows:

$$\frac{\partial T}{\partial t} + \bar{u} \cdot \frac{\partial T}{\partial x} + \bar{v} \cdot \frac{\partial T}{\partial y} + \bar{w} \cdot \frac{\partial T}{\partial z} =$$

$$= \frac{1}{\rho \cdot c_v} \cdot \left[\frac{\partial}{\partial x} \cdot \left(\lambda \cdot \frac{\partial T}{\partial x} \right) + \frac{\partial}{\partial y} \cdot \left(\lambda \cdot \frac{\partial T}{\partial y} \right) + \frac{\partial}{\partial z} \cdot \left(\lambda \cdot \frac{\partial T}{\partial z} \right) + \eta \cdot \Phi \right]$$

(5.6)

Equations describing other processes, such as combustion, can also be solved in conjunction with the Navier-Stokes equations. Often an approximating model is used to derive additional equations; turbulence models are a particularly important example [19].

This is just a very small part of the equation set, on which CFD-programmes are based on, but it is to show that even behind complex simulations there are always basic equations. In practice the user is not confronted with these equations. The CFD programs choose the right kind of equations that fit the boundary conditions defined by the user.

5.1.3 CFD methodology

CFD may be used to determine the performance of a component at the design stage or it can be used to analyse difficulties with an existing component and lead to its improved design. For example, the pressure drop through a component may be considered extensively (figure 5-2). The geometry of the region of interest is then defined. If the geometry already exists in CAD it can be imported directly. The mesh

➢ Geometry / Mesh

This interactive process is the first pre-processing stage. Its aim is to produce a mesh for the input to the physics pre-processor. Before a mesh can be produced, a closed geometric 3D solid is required. The geometry and mesh can be created in one of a variety of geometry and mesh creation tools. The basic steps involve: [17]

- defining the geometry of the region of interest
- creating the regions of the fluid flow, solid regions and surface boundary names
- setting properties for the mesh

This pre-processing stage is becoming increasingly automated. In most CFD programmes the geometry can be imported from most major CAD packages using standardised formats. Then the mesh control volumes are created automatically (only possible for tetra meshes).

➢ Physics definition

This interactive process is the second pre-processing stage and is used to create the input for the solver. The mesh files are loaded into the physics pre-processor and then the following properties are defined: [17]

- the physical models which have to be included in the simulation are selected
- the properties of the fluid are specified
- the boundary conditions are specified
- the heat transfer (isothermal, thermal and total energy) and turbulence model (e.g. SST and k-ε) are defined. Also the time step and the convergence criteria have to be set.

➢ The solver

The solver is the component which solves the CFD problem, producing the required results in a non-interactive / batch process. It solves the CFD problem as follows: [17]

- The partial differential equations are integrated over all the control volumes in the region of interest. This is equivalent to applying a basic conservative law (e.g. for mass or momentum) to each control volume.

- These integral equations are converted to a system of algebraic equations by generating a set of approximations for the terms in the integral equations.

- These algebraic equations are solved iteratively.

An iterative approach is required because of the non-linear nature of the equations and as the solution approaches the exact solution it is said to converge. For each of the iteration steps an error or residual is reported as measure of the overall conservation of the flow properties. How close the final solution is to the exact solution depends on a number of factors, including the size and the shape of the control volumes and the size of the final residuals. Complex physical processes, such as combustion and turbulence are often modelled using empirical relationships and the approximations contained in these models also contribute to differences between the CFD solution and the real flow [20].

The solution process requires no user interaction and is therefore usually carried out as a batch process. The solver produces a file of results which is then passed to the post-processor.

➤ The post-processor

The post-processor is the component used to analyse, visualise and present the results interactively. Post-processing includes anything from obtaining point values to complex animated sequences. Examples of some important features of post-processors are:

- visualisation of the geometry and the control volumes

- vector plots showing the direction and magnitude of the flow

- visualisation of the variation of scalar variables (variables that have only magnitude and no direction, like temperature, pressure and speed) through the domain

- quantitative numerical calculations

- animation
- charts showing graphic plots of variables
- hardcopy outputs

5.1.4 Meshes

The basis for every kind of FEM simulation is to generate a grid. According to the application 2D or 3D grids are used for the simulation. A grid projects a structure with defined elements. The connecting points in a grid are the knots. The areas surrounded by the elements are called shells in 2D grids and elements in 3D grids. These elements produce a shell structure on the outside of the model, which projects the surface area of the object in the required manner. The inner structure can be modified by different parameters.

This section is used to describe the different kinds of meshes, elements and techniques (mainly taken from [17]) to build up meshes of a good quality. It is not a complete overview, but it is included to show the methods needed to build up the meshes for this thesis.

5.1.4.1 Mesh types

Basically two different kinds of mesh generation can be applied (figure 5-4). Structured meshes built up of hexahedrons are essentially complex in their construction. In a first step a block structure has to be built up, which projects the starting geometry. On this basis in a second step a surface 2D mesh is generated, out of which the 3D grid structure is assembled. At present developments run to automate this procedure. At structured meshes each knot is defined with the indices i, j and k. These indices stand for the Cartesian coordinates x, y and z.

A second easier way to get a 3D mesh is to generate non structured meshes with tetrahedrons. Here different parameters are set at the beginning and the model is filled up automatically with these elements. Unstructured meshes do not use the indices to save the knot information. The knots of an element are always connected to their neighbour knots. The mesh information is defined in the so called allocation

matrix. Because of this fact an unstructured mesh has a much higher memory capacity requirement than the structured mesh.

Another method is the combination out of structured and unstructured grids (see figure 5-4) to a hybrid mesh. This method is useful when an unstructured tetrahedron grid is used to build up the outer sections with structured elements in the inner region with flow close to walls to improve the performance of the solver.

structured mesh   unstructured mesh   hybrid mesh
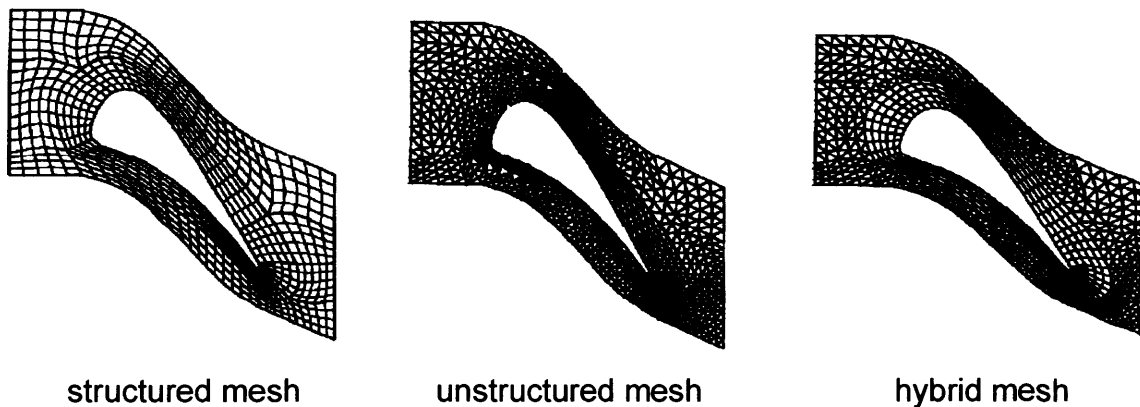
Figure 5-4: Different kinds of 3D grids [17]

The choice of the right kind of mesh depends on the one hand on the texture of the geometry and on the other on the physics of the simulated problem. In the used program ICEM CFD there are different algorithms for the grid generation and they are described in detail in section 5.1.4.3. The generation of the grid takes at least half of the time needed for the simulation. The grid has an enormous influence on the length of time and quality of the simulation in the solver.

5.1.4.2 Element types

The most important element types are the hexahedrons for structured meshes and the tetrahedrons for unstructured meshes. There are many other element types for special applications, but they are not described in this thesis.

5.1.4.2.1 Hexahedrons

In contrast to tetrahedron meshes, meshes consisting out of hexahedrons are more complex to be built up. They have significant advantages for small, round geometries

and moving meshes. For the same geometry four times less elements are needed in contrast to unstructured meshes to reach the same mesh quality. One method for the generation of hexahedrons is so called blocking. A block is modified in a way that it fits roughly the geometry. After that the edges of the block are divided and the resulting parts are connected to each other (see figure 5-5). The generated 2D mesh is then projected to the whole 3D geometry. The disadvantage of this method is that the meshing process takes a lot of time for complex geometries and cannot be automated yet.
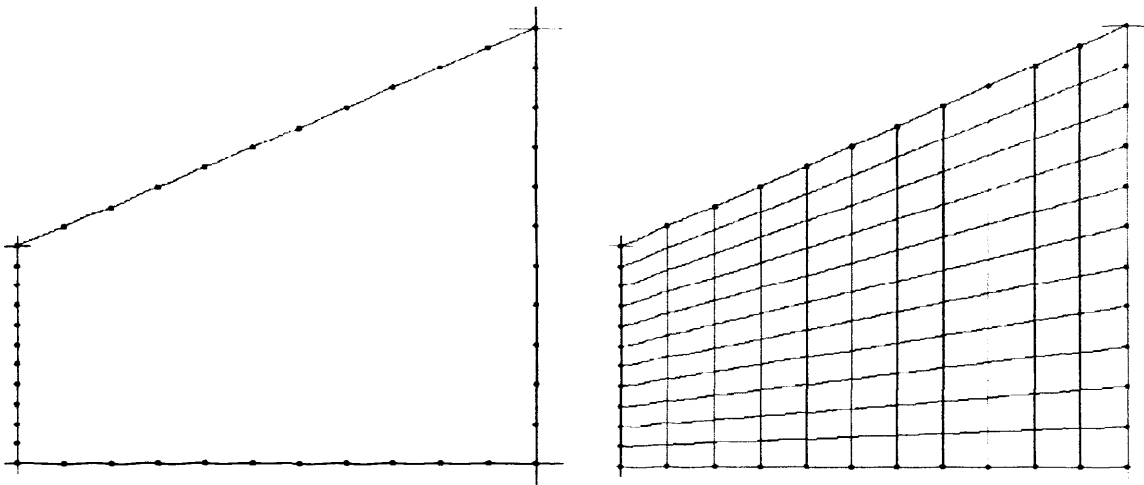
Figure 5-5: Blocking of a geometry

The quality criteria of hexahedron meshes are the determinants and the angles. The determinants define a value that tells the user how the opposite sides of a hexahedron are positioned to each other. If all the opposite sides are parallel to each other the determinant quality is 1,0. The optimal angle of a hexahedron mesh is 90°. Usually the determinants should have a value over 0,15 and the minimal angle should not be less than 12°. Meshes with lower values for the quality criteria can be used in the solver, but the results can be uncertain. Under special circumstances the proportion of the surfaces of the hexahedron is of interest, especially when the flow in small gaps with flat elements is analysed. Here the aspect ratio should have a value below 5'000 to give good results.

repair defective blocks. Incorrect blocks can be deleted and substituted by new ones. The inserting process is done by merging.

5.1.4.3.6 2D blocking

For geometries that have a constant dimension in one direction there is a very effective way to generate the blocking. In a first step a 2D blocking is built up and in the second one it is transformed to a 3D blocking. Figure 5-17 and 5-18 show this procedure for the regenerator of the Stirling engine.
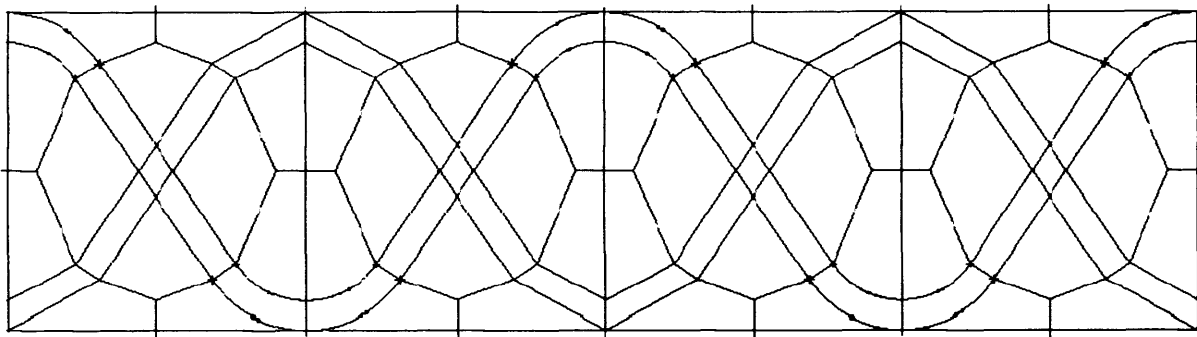
Figure 5-17: 2D blocking of the regenerator
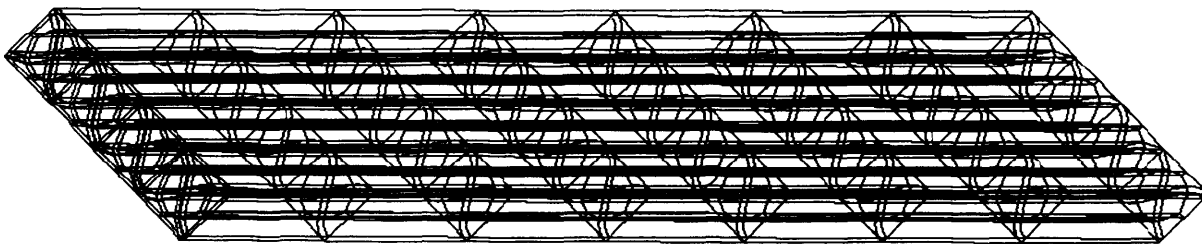
Figure 5-18: 3D blocking of the regenerator built up of the 2D blocking

The mesh generation process of the regenerator is shown in detail in section 5.4 and is named here only for completeness.

The blocking methods shown above are only a very small part of what is possible to be applied for complex geometries with structured hexahedron meshes with ICEM CFD. Further information can be taken from the tutorials of the program [17] and from internet on the ANSYS homepage for interactive learning [15].

5.1.5 Structure of the analysis of the Stirling engines

The CFD methodology described in the last pages is used to analyse the performance relevant parts of the biomass and solar Stirling engine system. In this chapter the following heat exchanging parts are analysed in detail:

➢ Heater:

In the heater analysis the working gas side of the solar and biomass engine is simulated to get values for the pressure drops and flow behaviour. In addition to this the combustion gas side of the biomass engine also is analysed. This is done to find dead zones in the flow and the pressure drops that arise.

➢ Cooler:

The most interesting aspect about the cooler is the efficiency of the cooling water side of the Stirling engines. This geometry is the same for the biomass and solar engine. The working gas side is not analysed because it is one of the main constituents of the parameter variations in chapter 4 and no new results can be expected.

➢ Regenerator:

The regenerator is analysed with one of the most complex simulation methods available – the fluid structure interaction (FSI) analysis. Here the interaction between the working gas and the metal matrix can be analysed. The linear temperature profile assumed for the lower order calculation methods is checked and pressure drops are calculated.

The flow in the complete Stirling system is not analysed in this chapter. It would take about 150 million elements to build up a complete model of the engine. No available computer could analyse such a system in an adequate time. It would break the boundaries of this thesis and therefore is neglected.

5.2   Analysis of the heater components
5.2.1   Analysis of the biomass heater

The heater of the engine has an immense influence on the efficiency of the whole Stirling system and is with its gas flow on both sides one of the most interesting parts. The heater is an ordinary heat exchanger, on the one side the working gas flows through, on the other side it is heated by the combustion gases. As a heat source for this system wooden pellets are combusted in the burner and the gas is led around the heater. Afterwards this, the combustion gas leaves the combustion chamber towards a hot water boiler (see figure 5-19).

Heater of the
Stirling engine

Inlet of the
burner

Outlet to hot
water boiler

Combustion
chamber
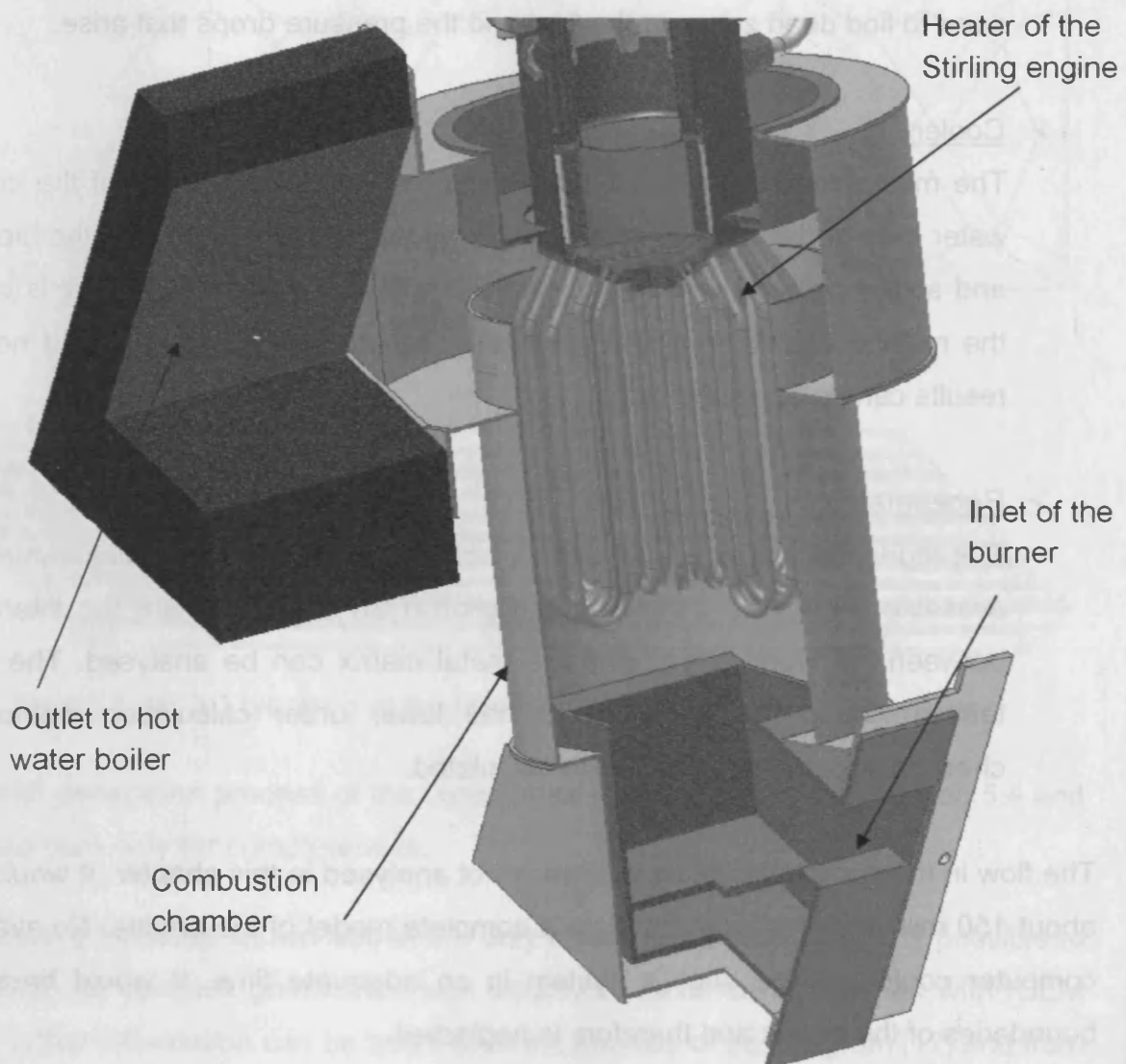
Figure 5-19: Cross section through the heater system of the biomass Stirling

$$\xi_O = \xi_O \cdot 1{,}08235 = 0{,}398 \qquad (5.10)$$

$$\xi_W = 0{,}080 \qquad (5.11)$$

$$\xi_A = \xi_A \cdot 1{,}08235 = 0{,}011 \qquad (5.12)$$

To see how much oxygen (in mol) for the combustion process is needed the chemical reaction equations are as follows [13]:

$$1g\,C \;+\; \frac{1}{12}\,mol\,O_2 \;\rightarrow\; \frac{1}{12}\,mol\,CO_2 \qquad (5.13)$$

$$1g\,H \;+\; \frac{1}{4}\,mol\,O_2 \;\rightarrow\; \frac{1}{2}\,mol\,H_2O \qquad (5.14)$$

$$1g\,S \;+\; \frac{1}{32}\,mol\,O_2 \;\rightarrow\; \frac{1}{32}\,mol\,SO_2 \qquad (5.15)$$
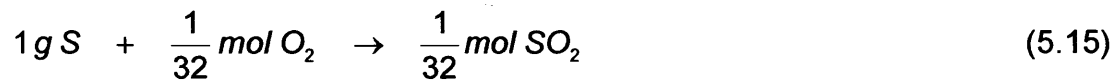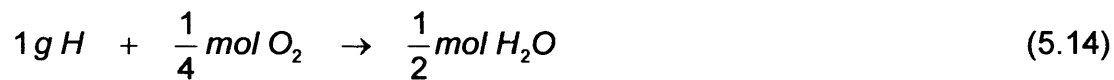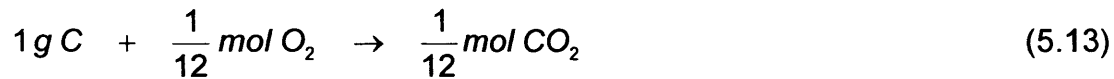
With equations (5.13) to (5.15) the minimum mass of oxygen O_{min} (in mol) needed per g combustible is:

$$O_{min} = \frac{1}{12}\cdot\xi_C + \frac{1}{4}\cdot\xi_H + \frac{1}{32}\cdot\xi_S - \frac{1}{32}\cdot\xi_O = 0{,}04\,\frac{mol}{g} \qquad (5.16)$$

With an air composition of 21 % oxygen and 79 % nitrogen and a measured value of 1,5 for lambda the minimum mass of air L_{min} needed and the mass of air L used can be calculated.

$$L_{min} = \frac{O_{min}}{\gamma_{O_2/A}} = 0{,}19\,\frac{mol}{g} \qquad (5.17)$$

$$L = \lambda \cdot L_{min} = 0{,}28\,\frac{mol}{g} \qquad (5.18)$$

5.3.1 Boundary conditions

Each surface group with different colour in figure 5-84 represents a different group of boundary conditions. The basic values for these surfaces are defined in table 5.10. Before the simulation can be started the physical time step has to be defined. The complete cooling system of the Stirling engine contains 0,8847 kg of water. The measured volume flow has a value of 0,0917 kg/s. As it is said the time step has to be chosen in a way that one particle entering the system needs ten times more time to pass the system than the value of the time step.

Global settings	
Reference pressure	1,5 bar
Fluid	water
Heat transfer model	Thermal Energy
Turbulence model	SST
Inlet	
Mass flow rate	0,0917 [kg/s]
Temperature	318 [K]
Turbulence	Middle (5 %)
Outer walls	
Boundary type	wall
Wall condition	no slip
Temperature	318 [K]
Working cylinder wall	
Boundary type	wall
Wall condition	no slip
Temperature	378 [K]
Cooler wall	
Boundary type	wall
Wall condition	no slip
Temperature	573 [K]
Crank case inner wall	
Boundary type	wall
Wall condition	no slip
Temperature	448 [K]

5.4.3.2 Solver settings

The setup of the solver can be seen in table 5.14. The convergence criterion with a value of $1 \cdot 10^{-4}$ is quite high. This is done, because there are only 10 iterations for each of the 120 time steps calculated. With only 10 iterations no higher convergence criterion can be reached. A higher number of iterations per time step is not useful because of the high demand of time to solve the model.

Advection scheme	high resolution
Transient scheme	2nd order backward Euler
Max. coeff. loops	10
Residual type	RMS
Residual target	0,0001

Table 5.14: Solver settings

5.4.3.3 Output control

In the CFX pre processor there is the option to define monitor points. These monitor points are defined variables like the inlet and outlet temperature or mean domain temperature that are chosen in the output control of the pre processing. As the calculation proceeds the user can analyse the defined values in real time. With this tool the quality of the calculation can be assessed in an early stage of the simulation. It is often used for transient calculation with lots of iteration steps where it is important not to waste much time.

For the simulation in this chapter two monitor points are defined. The first one is the pressure drop over the whole geometry and the second one is the gas velocity at the inlet. For the first point a function is defined that subtracts the mean pressure at the outlet and the inlet. The second point shows the mean inlet velocity.

5.4.4 Solver calculation

The function of the convergence behaviour can not be compared with the ones shown in previous chapters because here a transient calculation is processed. Every time step is calculated with ten iterations. The convergence behaviour for the

6 Experiments and modifications of the Stirling systems

In this chapter the work on the experimental engines (biomass Stirling, solar Stirling and Stirling engine test bench) is described and furthermore detailed descriptions of the systems and the results of the measurements are given. The measured values are additionally compared with the results of the different calculation methods.

6.1 Detailed description and modifications of the biomass Stirling system

In 2002 a new building of the department of mechanical engineering of the University of Applied Sciences in Regensburg was installed. New laboratories were equipped with modern machines and technologies. In the thermodynamics laboratory two new Stirling engine systems were built up – a biomass cogeneration system and a Dish / Stirling system. The handing over to the University of Applied Sciences occurred on the 09.03.2004. The biomass Stirling system with the following components (also partly named in chapter 2) was originally designed by the EPAS Company. The main components of the cogeneration biomass system are:

> ➢ blow pipe (hot air system)
> ➢ heater and hot water boiler
> ➢ Stirling engine BM 1000
> ➢ housing technology with the pumps
> ➢ electrical installation

The Stirling system delivered from this company caused a lot of problems from the beginning arising from leakages and disadvantageous material combinations. This was one of the reasons why this company became bankrupt in 2005 and does not exist any more. In this section the system is described in detail and all the modifycations made are pointed out.

6.1.1 Blow pipe and hot water boiler

Manufacturer of the blow pipe and the hot water boiler is Swedish Bioburner Systems (SBS) Janfire AB from Sweden. The German factory is located in Weilheim. SBS Janfire AB was founded in 1983 and is one of the oldest and experienced companies

6.1.6.2 Temperature sensors

For the analysis of the biomass CHP system four different temperatures have to be measured. The temperature at the inlet of the Stirling engine and the inlet to the hot water boiler and the common return temperature at the outlet are of special interest to find the temperature rise in the Stirling engine and the boiler to calculate the transferred heat. Values between 20 °C at the start of the system and 95 °C, which is the maximum return temperature of the boiler, can be expected. This task can be fulfilled with a standard temperature sensor Pt100. For the measurement with a Pt100 the rise of the resistance with rising temperature is used. The sensor is fed with constant current and the voltage drop at the resistor is measured which is a function of the temperature.

Also the combustion gas temperature close to the heater pipes has to be determined. In this area the maximum values can reach up to 1'300 °C and a Pt100 is not appropriate. Because of this a NiCr-Ni temperature sensor manufactured from two spot-welded wires of different metal alloys is chosen. For the measurement the so called thermo-electrical effect in the contact surface is used. This effect causes a small thermo voltage which is a function of the temperature difference between the test point and the terminal clamp.

6.1.6.3 Axial turbine flow meter

In the biomass system two different volume flows of the cooling water system have to be determined. One test point is at the inlet to the Stirling engine, the other one at the inlet to the hot water boiler. These values are needed for the energy balance. For the measurement two axial flow meters equipped with Hall Effect sensors are used.

At the inlet to the Stirling the flow meter type FVA 915VTHM from the Ahlborn company is installed. Its measuring span is between 2 and 40 l/min. With a flow of 0,3 l/min the sensor starts to produce a signal. This part is designed for a maximum permanent load of 20 l/min. The measurement accuracy is defined with a value of +/- 1 % of the measured value. For the recommended volume flow of 10 – 20 l/min for the Stirling engine this sensor is ideally adapted.

For the cooling water circuit of the hot water boiler a higher volume flow than in the Stirling engine has to be expected. Because of this the flow meter FVA 915VTH25M from the Ahlborn company is used. The measuring span is between 4 and 160 l/min

6.2   Measurements of the biomass Stirling system

In this section the measurement process of the biomass CHP system is described. The procedure and the results of one example set of measurement are shown in the following sub chapters. The results of it are additionally compared with those derived from the different calculation methods.

6.2.1   Procedure of the measurement

The measurement procedure can be divided into four phases: the start of the system, the heating up, the processing of the measurement and the shutdown of the system.

6.2.1.1 Start of the system

To start up the system clearance from the building process control unit is needed. Clearance is requested when the main switch of the electric control box is turned to the on position. The building process control unit checks different parameters like the air pressure and the function of the pumps and fans in the laboratory. If clearance is not given the blow pipe can not be started. When clearance is permitted the nominal values of the pressure and flow in the system have to be checked, before the blow pipe is started. The nominal values that have to be checked can be seen in table 6.10.

Pressure in the cooling water system	1,5	bar
Preload pressure in the Stirling engine	7,5	bar
Volume flow of cooling water		
through the Stirling engine	7	l/min
through the hot water boiler	8	l/min

Table 6.10: Control values before the system is started

If the parameters of the systems do not correspond to the ones from table 6.10 appropriate steps have to be taken. If the pressure in the cooling water systems is not right it can be corrected by filling up or releasing water. If the flow through the Stirling engine or the hot water boiler is not right the solenoid angle seat valves (see figure 6-17 positions 9 and 11) have to be readjusted or the whole circuit has to be bleed. For the starting of the blow pipe it should be set to level 4 (quick start).

transferred to the water (see table 6.14) is proportional to the combustible energy flow produced in the same time.

$$\eta_{hwb} = \frac{\dot{Q}_{hwb}}{P_{cef}}$$ (6.3)

For the two periods mentioned in the sections before the efficiency of the hot water boiler can be found in table 6.16. The average efficiency of the total period is higher than the one of the 3 kg period. This leads to the conclusion that the efficiency of the hot water boiler is higher for 800 °C combustion gas temperature than for 860 °C.

η_{hwb} in [%]	
Total period	3 kg period
34,98	29,50

Table 6.16: Efficiency of the hot water boiler for the two periods

6.2.3.3 Characteristics and efficiencies for the Stirling CHP part

For CHP systems producing electrical and thermal energy the following values can be calculated. In the following only the Stirling engine is analysed as a complete CHP system. The hot water boiler is neglected in this section.

> Current characteristic

The current characteristic is the direct measure for the dimensions of a CHP system if the demand of heat is known. This value defines the mass of avoided CO_2 emissions. The performance of the pump is neglected for this value. Equation (6.4) shows how this value can be calculated.

$$\sigma = \frac{P_s}{\dot{Q}_s}$$ (6.4)

Table 6.17 defines the values of the current characteristic for the total and 3 kg period in comparison.

σ in [-]	
Total period	3 kg period
0,044	0,052

Table 6.17: Current characteristic for the two periods

> ➤ Heat convection on the surface of the Stirling engine
> ➤ Losses by non insulated pipes
> ➤ Friction losses in the Stirling engine
> ➤ Generator losses

Most of these losses are difficult to determine with exact values. In the following sections the main parts, like the exhaust gas losses and the heat conduction losses of the combustion chamber are analysed in detail. Values of the other kinds of losses are estimated in section 6.2.5 where an energy balance is built up.

6.2.4.2 Heat conduction losses of the combustion chamber

One of the weak points of the system is the connection of the burner to the hot water boiler by the combustion chamber, where the Stirling engine is mounted. In the combustion chamber the major part of the total energy is lost by heat conduction. To get an estimation equation (6.9) is used to calculate the lost heat flow.

$$\dot{Q}_L = -\frac{1}{\dfrac{d_{iso}}{\lambda_{iso}}} \cdot \Delta T \cdot A_{iso} \qquad (6.9)$$

The used insulation material PROMAGLAF – HTI 1250 is defined with a thermal conductivity of 0,20 W/m·K at a temperature of 800 °C [27]. The surface of the inner side of the insulation is calculated with a value of 0,926 m² and the thickness of the insulation material is 0,06 m. The temperature difference between the inner and outer side is measured with a value of - 735 K (40 °C to 775 °C). Using these values the conducted heat can be calculated.

$$\dot{Q}_L = 2{,}15\,kW \qquad (6.10)$$

At the combustion chamber 2,15 kW of the combustible energy flow are lost. This is a percentage of 10,6 % of the average combustible energy flow.

6.2.4.3 Exhaust gas losses

The exhaust gas losses are measured from the experiment on the 25.08.2005. The measured and calculated values can be seen in table 6.24. The gas composition and the performance is calculated as in section 5.2.1.1.1 and not shown here in detail.

The mirror is formed in a way that the irradiation is not concentrated to one point, but to an area that looks like a flower (see figure 5-64). Its diameter on the absorber plate is about 0,15 m. With this value and the diameter of the aperture surface the concentration proportion can be calculated.

$$C = \frac{A_{aperture}}{A_{absorber}} = 215 \tag{6.11}$$

With the concentration proportion the theoretical maximum absorber temperature T_{max} can be calculated [36]. To do this the temperature of the sun surface T_{sun} with a value of 5'762 K and the maximum concentration proportion C_{max} with a value of 4'6211 is needed. The theoretical maximum absorber temperature for the Dish / Stirling system presented in this thesis has a value of

$$T_{max} = T_{sun} \cdot \left(\frac{C}{C_{max}}\right)^{1/4} = 5762K \cdot \left(\frac{215}{46211}\right)^{1/4} = 1504,9K . \tag{6.12}$$

6.3.2 Cooling system

The cooling system of the Dish / Stirling unit has to avoid an overheating of the Stirling engine and to transfer the produced heat to the surroundings. The system is built up of a cooling water pump, a convective cooler and an overpressure valve.

> Cooling water pump

The pump supplied by the EPAS company is an encapsulated 230 V circulating pump for heating systems. As the Dish / Stirling system is based on direct current the choice of an alternating current pump is not useful. For the first experiments this pump is still used. It has an input power of 70 W and a mean volume flow of 10 – 15 l/min.

> Cooler

The cooler, used for the heat transfer to the surroundings, is mounted on the front side of the frame (see figure 6-46). Thus the complete cooling system with the pump is continuously moved with the parabolic mirror according to the sun's position. This simultaneous motion has the advantage that the Stirling engine and the cooler are a static unit where the hoses are not in danger of rubbing on other elements. This assembly has the big disadvantage that the

drive the frame towards the ideal position to the sun. The EASY 412-DC-RC PLC from Moeller company is used.

6.3.4 Electronic system

In the existing state the electrical system of the unit is very simple. For the starting of the Stirling engine (12 V), for the power supply of the electrical motors of the tracking system (12 V) and the PLC (24 V) two 12 V plumb accumulators with 36 Ah are delivered with the unit. These accumulators have to be recharged externally and are not connected to the generator (0-110 V) of the Stirling engine. The pump is connected to the 230 V alternating current grid. It becomes clear that there are different voltages in use all over the system. The concept of an insular system has not been met in any way. For the pump and the battery charger a 230 V grid is needed, which is not available in many regions where this unit would be useful. At this state the Stirling engine has to be started by pushing a button when the heater temperature has reached 400 °C and clearance from the system is given.

6.3.5 Measurement equipment

The measurement equipment needed to analyse the Dish / Stirling system is shown in this section. Apart from the components mentioned in the following an Almemo V55 data logger presented in section 6.1.6.1 is used. For the determination of the cooling water flow the axial turbine flow meter FVA 915VTHM presented in section 6.1.6.3 is utilized. The measurement of the solar irradiation is shown in section 6.3.6 where the conversion of the values occurs.

6.3.5.1 Performance controller

Within the scope of a diploma thesis [30] for the Dish / Stirling system a performance control unit has been designed. This part is constructed in a way that the maximum electrical output performance of the Stirling engine (400 W) can be converted to heat by the use of resistors. With its help the engine can be controlled by parameters as speed, current, voltage and output performance. In the electronic control unit a nominal value of these parameters can be set. A PID controller compares the nominal with the measured values and adjusts the Stirling engine to run with the desired values. This is done to get reliable measurement results.

436

required direction on a mast. It is located in immediate proximity to the Dish / Stirling system in full irradiation. The mast is dimensioned in a way that the sensor sees the horizon all around and no walls, houses or trees influence the measurement.

6.3.6.3 Conversion of the values on declined surfaces

The SDE 9.1 sensor used has the disadvantage that it is fixed in a horizontal plane and consequently can only measure the horizontal irradiation. For the determination of the efficiency of the Dish / Stirling system the direct irradiation vertical to the aperture of the concentrator is needed, because it is tracking the sun's position continuously along two axes.

$$S_D = S_{D,hor} \cdot \frac{cos\,\Phi}{sin\,\gamma_s} \qquad (6.14)$$

In equation (6.14) γ_s stands for the angle between the horizon and the sun. Furthermore it is assumed that the irradiation always meets the aperture vertically ($\Phi=0$; $cos\Phi=1$). This simplifies the conversion of the measured direct irradiation to the irradiation on the declined surface. [36]

$$S_D = \frac{S_{D,hor}}{sin\,\gamma_s} = \frac{S_{D,hor}}{sin\big(90^\circ - \Phi_{hor}\big)} \qquad (6.15)$$

Figure 5-56 shows the correlation between the angles and the irradiation as an explanation of equation (6.15).
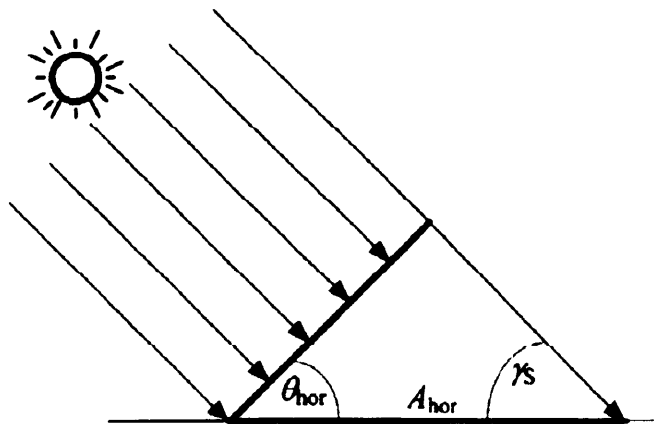
Figure 6-56: Correlation of the angles [1]

From equation (6.15) and figure 6-56 it can be derived that the irradiation on a vertical to the irradiation declined surface always has a higher value compared to that of a horizontal surface.

6.3.6.4 Calculation of the sun's position

For the described conversion of the measured irradiation to a declined surface the knowledge of the exact sun's position is needed. For each point on this planet the actual position can be defined by two angles. One is the elevation γ_S and the other one is the azimuthal angle α_S. In DIN 5034 the elevation is described as the angle between the line from the suns centre to the observer and the observer's horizontal plane. Here 0° stands for the sunrise and the sunset. The maximum value for the elevation is 90°, when the sun is directly above the observer. The suns azimuthal angle describes the angle between the geographic northern direction and the line between the suns centre and the observer projected on the horizontal plane. Here 0° (also 360°) stands for northern direction, 90° for east, 180° for south and 270° for west.

The elevation and the azimuthal angle are dependent on the observer's location as well as on the date and the time. The declination δ, the angle between the equator and the line between the suns and earths centre, plays the biggest role in this content. It shows values between + 23,45° and − 23,45°. Furthermore the duration of the sunshine per day is dependent on the season. [1]

For a Dish / Stirling system the azimuthal angle α_S does not play a role, if it is tracked automatically. Because of this only the algorithm for the calculation of the declination δ and the elevation γ_S for the northern hemisphere is shown in the following.

$$sin\,\gamma_S = sin\,\delta \cdot sin\,L - cos\,\delta \cdot cos\,L \cdot cos(\omega \cdot t)$$ (6.16)

In equation (6.16) L is the latitude (for Regensburg L = 49°01'), ω is the angular velocity of the earth with 15 °/h and t is the daytime in hours. The declination δ can be calculated with equation (6.17) where J stands for the number of days (1 to 365).

$$\delta = -23,45° \cdot cos\left(\frac{360}{365,25} \cdot (J + 10)\right)$$ (6.17)

needed. The 38 pole alternating current generator of the Stirling engine produces, depending on the irradiation, a three phase alternating current in a range of 0 – 110 V at a speed of 0 – 600 1/min. This alternating current is transformed to a direct current with a low ripple in the 3 phase bridge rectifier and a 1'000 µF electrolyte capacitor. A 300 W switched mode power supply unit stabilizes the variable generator voltage from a value of 60 V at 300 1/min to a constant value of 48 V. With this 48 V a regulator unit from a photovoltaic system with an overload under voltage switch is operated. From this unit the accumulators are charged and a constant 24 V power supply for the pump and the tracking system generated.

6.3.7.2 Automatic starting of the Dish / Stirling system

The starting up procedure of the Dish / Stirling system has been automated to make it a stand alone system [44]. A circuit has been built that controls and performs the following processes. Underneath only a short overview of the functions is given as this is not the main part of the thesis.

> ➢ An automated tracking procedure starts when the irradiation reaches a value where the Stirling engine can produce power.

> ➢ If a heater temperature of over 500 °C is reached the engine is started. This is done in a no load situation so that the engine can be started easily.

> ➢ The load is engaged when the voltage reaches 60 V. The produced power is then used to load the accumulators and run the surrounding systems. The load is turned off again when the voltage is lower than 55 V because of lower irradiation.

> ➢ With this circuit also the cooling water pump is controlled. It is turned on before the engine is started and runs on after the engine is turned off until a certain cooling water temperature is reached.

> ➢ If the irradiation is too low to run the system the complete unit is driven to the initial position.

Various security systems to avoid damage to the system because of high temperatures, currents or non working components are also introduced. The main part of the system is the MOELLER EASY 619-DC-RC control unit that is programmed with the software tool MOELLER EASY-SOFT.

447

6.4.1 Procedure of the measurement

As in section 6.2.1 for the biomass engine the measurement procedure for the Dish / Stirling system can be divided into four phases.

6.4.1.1 Start of the system

To start the system the accumulator charge needs to be checked. When the voltage level reaches 24 V the logic unit can be started. The volume flow and pressure level of the cooling water and the pressure level of the Stirling engine have to be controlled. The nominal values can be seen in table 6.37.

Pressure in the cooling water system	1,5	bar
Preload pressure in the Stirling engine	5	bar
Volume flow of cooling water	2,3	l/min

Table 6.37: Control values before the system is started

If the parameters of the system are not in accord with those in table 6.37 appropriate steps have to be taken as in section 6.2.1.1. Before the logic unit is set to the automatic mode the motors of the tracking system and the starter motor of the Stirling engine need to pass an operation check.

6.4.1.2 Tracking and starting process

When the sun dancer sensors recognize enough irradiation the system starts the tracking process. When the focus reaches the absorber plate it has to be checked if it is right in the middle and does not touch the housing. The temperature sensor mounted on the absorber gives the values to the logic unit which starts the Stirling engine when the temperature has reached 500 °C.

6.4.1.3 Measurement

After the heating up period the measurement can be started. In the Almemo data logger the values shown in table 6.38 are recorded. When the engine is started it runs without load until the speed and with it the voltage increase (300 1/min and 60 V). The engine is coupled with the load until the speed becomes too low (100 1/min and 20 V). Then a no load period follows until the speed increases to the

In the last section only the most important results of the measurements are discussed. For the calculation all the measured values are required. In appendix D averaged measured values for the most important experiments can be found for all the sensors used. For comparison the date and the preload pressure can be used to find the right table in the appendix.

6.4.2.6 Reference values for comparison

In order to define the efficiency of the system and to build up an energy balance it is necessary to define a reference set of values upon which the calculations are based. The values are also used for the comparison of the different calculation methods.

As a reference the measurement from the 12.06.2006 is chosen. The interesting part is the period when the peak performance of the Stirling engine is reached at 225 1/min. The experiment with this speed started at 12:42 and ended at 12:57. Table 6.40 shows the average values for this period. The preload pressure is 6 bar and the engine has already reached steady state conditions as the measurement starts. The average irradiated performance on the parabolic mirror is calculated with the mirror diameter of 2,2 m and the direct irradiation measured.

12.06.2006	6 bar
Average voltage [V]	41,61
Average current [A]	1,69
Average performance [W]	70,19
Speed (Hall) [1/min]	228,49
Average global irradiation [W/m²]	724,97
Average direct irradiation [W/m²]	581,73
Average diffuse irradiation [W/m²]	143,25
Average irradiated performance [W]	2'211,35
Average absorber temperature [°C]	930,14
Average cooling water return [°C]	41,28
Average cooling water flow [°C]	47,11
Volume flow of cooling water [l/min]	2,30
Heat flow by the cooling water [W]	937,33

Table 6.40: Values for the reference measurement

The heat flow transferred by the cooler can be calculated with the volume flow of cooling water and the difference between the return and the flow temperature.

6.4.3 Determination of the efficiency and the energy balance

In this section the different efficiencies of the system are calculated, it is determined where the losses of the system arise, which values they have and additionally an energy balance is built up.

6.4.3.1 Performance

The performance values determined in section 6.4.2 are measured values at the performance control unit right after the bridge rectifier. For this part an efficiency of 90 % is assumed. With it the electrical performance of the solar Stirling engine can be calculated.

$$P_{el} = \frac{70,2W}{0,90} = 78W \tag{6.19}$$

To determine the mechanical performance of the Stirling engine figure 6-14 is used. For 70 W and a speed of 225 1/min the efficiency of the generator reaches a value of

$$\eta_{gs} = 0,90 \tag{6.20}$$

$$P_M = \frac{78W}{0,90} = 86,6W \tag{6.21}$$

The process performance including the mechanical losses is defined in equation (6.23). For the biomass engine a value of 100 W is assumed for the mechanical losses. This value is much too high for the solar engine. Because of this a mechanical efficiency is assumed that corresponds to that of the biomass engine.

$$\eta_M = 0,70 \tag{6.22}$$

$$P = \frac{86,6W}{0,70} = 123,74W \tag{6.23}$$

6.4.3.2 Efficiency of the system

The efficiency of the whole Dish / Stirling system can be calculated as a function of benefit and energy input. The benefit is the electrical performance produced by the system and the energy input comes from the irradiation. To calculate the efficiency

the electrical performance defined in equation (6.19) has to be reduced to allow energy inputs for the system's electronic equipment. The energy needed to keep the system running arises from the following components:

- ➤ The pump of the cooling water system runs all the time and needs 15 W.
- ➤ The easy control unit needs 3,5 W.
- ➤ The two sun dancer sensors are supplied with power all the time and need 0,5 W each
- ➤ The transducers between the sun dancer sensors and the control unit need 2 W each.
- ➤ The energy input to the starter motor is less than 0,1 W because the Stirling engine is only started once every 7 till 8 hours. Hence this is neglected.
- ➤ The energy input to the two tracking motors is assumed to be 2,5 W each (50 W Motor operated three seconds per minute).

Summing up these values the power consumption of the system auxiliary units is

$$P_{ap} = 26W \,. \tag{6.24}$$

With this value, the electrical performance and the irradiated performance calculated in table 6.40 the efficiency shows a value of

$$\eta = \frac{P_{el} - P_{ap}}{\dot{Q}_{irr}} = \frac{78W - 26W}{2211,35W} = 2,37\% \,. \tag{6.25}$$

6.4.3.3 Energy balance

To analyse this further the energy balance for the Dish / Stirling system is given for the relevant measurements from section 6.4.2.5.

The system boundaries start at the mirrors and end with the cables leading out of the system. Figure 6-70 shows a full scale energy balance of the complete system.

The measurement shaft is connected via RS 232 to the measuring amplifier Scout 55, that is also produced by the Hottinger Baldwin Messtechnik GmbH. To be able to record the measured data to a computer the BNC analogue output of the Scout 55 is connected to the Cäsar Mops system described in the section before. The output channel of the Scout 55 gives a signal of ± 10 V.

6.5 Measurements of the Stirling engine test bench

With the γ-type Stirling engine test bench described in the section before different parameter variations are investigated. The preload pressure is varied in the range between 2 and 6 bar. The heater temperature is the second parameter which is varied between 400 °C and 650 °C. The combination of these two variations results in 24 experiments. These experiments are processed for three different phase shift angles 78,6°, 90° and 101,4°. For all these experiments the mechanical and electrical performance values are calculated and the p-V diagrams are plotted. From the area surrounded by the curves the process performance can be calculated. The boundary conditions of these experiments are used to calculate the process performance with the quasi steady flow analysis program developed in section 4.2. At the end of this section the measured values are compared with the calculated ones.

6.6.1 Measurement procedure

In the following the measurement procedure for the Stirling engine test bench is described in detail.

6.6.1.1 Adjustment of the parameters and start up

As was said before three parameters have to be adjusted before the measurement is started. The heater temperature can be adjusted with the temperature control unit described in section 6.5.1.2. A laptop computer is connected to the Siemens LOGO! and the temperature of the heating elements can be adjusted. The modification of the phase shift angle is described in section 4.3.5 and shown in figures 4-164 and 4-165. To change the phase shift angle the crank case has to be opened and the push rods of the displacer and the working piston have to be disconnected.
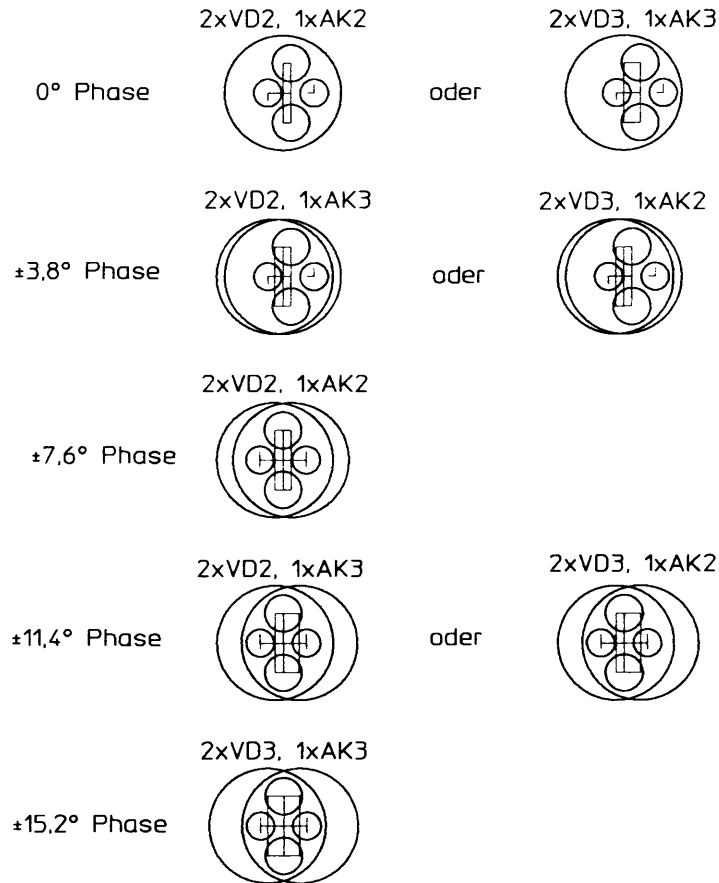
Figure 6-88: Phase shift angles

Figure 6-88 shows that with two different connection parts between crank shaft and displacer push rod (VD2 and VD3) and two connection parts between crank shaft and working piston push rod (AK2 and AK3) nine different phase shift angles can be realised. In this work three phase shift angles 78,6° (=90°-11,4°), 90° and 101,4° (=90°+11,4°) are used for the parameter variation as VD3 is not available. The preload pressure can be easily adjusted by filling in or letting out working gas using the valve installed.

After the parameters are set to their correct value and all the measurement and control equipment is started the pressure and volume flow of the cooling water through the test bench assembly has to be checked. The corresponding control values can be found in table 6.10.

6.6.1.2 Heating up process

In the second step the temperature control unit with the heating elements is started. At a temperature of 350 to 400 °C, depending on the preload pressure, the Stirling engine can be started. At this stage the resistor unit is switched off. When the speed

level the pressure drops from the heat exchangers between the expansion and compression space are low even for the 5 bar experiment.

Another interesting value is the pressure in the crank case. It can be seen that the pressure level is always higher than the preload pressure. This results from the heating up of the working gas in the crank case caused by the warm crank case and from leakages caused by the sealing of the working piston and of the push rod of the displacer which is led through the crank case wall from the working gas side. The phase of the pressure in the crank case is shifted by about 180° towards the working gas pressures, because the working piston is at its upper dead point when the volume at the working gas side is minimal and the pressure reaches its maximum whilst the gas volume in the crank case reaches a maximum and the pressure comes to its minimum value.

With the pressures as a function of the crank angle and the volumes as a function of the crank angle p-V diagrams can be built up. As there is no possibility on this test bench to determine the position of the crank shaft exactly when the motor is running the synchronisation of the volumes and the pressure is processed with the help of the results of the quasi steady flow analysis. For a certain preload pressure, phase shift angle and heater temperature the pressure reaches its minimum and maximum values always at the same crank angle. Because of this the minimum pressure of the measurement is set to the same crank angle value where the minimum pressure can be found in the theoretical analysis. This assumption has uncertainties. In order to make the results more reliable, an absolute value encoder should be mounted on the crank shaft to measure the crank angle together with every pressure value in real time. As the Caesar measurement device has no port for such an encoder this point remains for further developments. A new expensive measurement amplifier has to be bought and the encoder has to be adjusted. This is not part of the work shown in this thesis and hence the p-V diagrams are generated with the assumptions made above.

The p-V diagrams are generated for the expansion (figure 6-91 and 6-92) and compression space (figure 6-93 and 6-94) with its particular pressures and for the total volume (expansion space, compression space and all dead volumes) with the pressure of the compression space (figure 6-95 and 6-96). As previously stated, the area under the p-V curve is equivalent to the work performed. To calculate the parameters characterising the curve it has to be divided into two functions at the minimum and maximum volumes in order to generate a trend line with a polynomial

Figure 6-99 and 6-100 show the torque and synchronised pressure as a function of the crank angle for the 2 and 5 bar measurement. The peaks mentioned before can be clearly seen right after the pressure maximum has been reached. The swings of the torque curve in the lower region can be explained by clearance effects of the fixture of the measurement shaft and by so called cogging effects caused by the magnets of the synchronous generator.

Using the average torques for the whole measurement period and the speeds from table 6.53 the mechanical performance can be calculated as follows.

$$P_{mech,2} = M \cdot \frac{n}{60} \cdot 2\pi = 1,898\,Nm \cdot \frac{360}{60} \cdot 2\pi = 71,55\,W \tag{6.33}$$

$$P_{mech,5} = M \cdot \frac{n}{60} \cdot 2\pi = 2,913\,Nm \cdot \frac{800}{60} \cdot 2\pi = 244,04\,W \tag{6.34}$$

With the thermal and mechanical performances the mechanical efficiency for the two measurements can be defined.

$$\eta_{mech,2} = \frac{71,55\,W}{82,32\,W} = 86,92\,\% \tag{6.35}$$

$$\eta_{mech,5} = \frac{244,04\,W}{285,33\,W} = 85,53\,\% \tag{6.36}$$

It can be seen that about 15 % of the total produced performance is lost by friction in the sealing and bearing of the engine. Because of the higher speed at the 5 bar measurement the mechanical efficiency is about 1,5 % lower than at 2 bar.

On the generator side current and voltage are measured as mean values.

$$U_{av,2} = 80\,V \tag{6.37}$$

$$U_{av,5} = 174\,V \tag{6.38}$$

$$I_{av,2} = 0,45\,A \tag{6.39}$$

$$I_{av,5} = 0,55\,A \tag{6.40}$$

With these values the electrical performance and the electrical generator efficiency can be calculated.

steady flow parameter variation and the CFD analysis an improved engine geometry and a set of boundary conditions is found that can improve the engine performance and efficiency considerably. As a summary it can be stated that the quasi steady method is modified in a way that the performance values can be calculated better than ever before. In addition an prediction of the influence of many parameters is possible with the generated computer code. This can help to build high efficient Stirling engines and give this type of machine a chance on the market.

7.2 Future research

As a suggestion for further scientific activities the following aspects can be named. These points are planned to be put in practice in the future at the University of Applied Sciences in Regensburg to bring the Stirling engine closer to serial production readiness for the conversion of renewable energy sources into electrical power.

In order to predict the performance and the influence of the geometry data and the boundary conditions in a more precise way, the quasi steady flow analysis should be modified in order to use less simplifying assumptions. In the CFD analysis it can be seen, that the inlet and outlet losses of the heat exchangers play an important role for the total pressure drops. These losses should be introduced into the program code. In the measurement it can be seen that the average pressure level of the crank case is higher than the preload pressure. Because of this the leakage losses of the sealing for the pistons and the push rod of the displacer should be integrated into the calculation. These losses cause an even higher effect than the inlet and outlet losses of the heat exchangers and should not be neglected. Today's calculation methods allow a calculation of the leakage losses as a function of the sliding speed along the sealing and the pressure difference between both sides. Furthermore the gas data (dynamic viscosity, thermal conductivity, Prandtl number and the specific heat capacity) should not be assumed with constant values for the whole cycle, but be calculated for every step of the cycle. As the approach to introduce the Sutherland equations into the equation set failed because the program did not converge any more a method has to be found to solve this problem. If all these modifications are installed the program might give better results especially for the dependency on the phase shift angle, because here the behaviour of the working gas in the different spaces has an eminent influence.

8 Publications

In the following the most important publications and presentations produced during the writing of this thesis can be found. The papers published in the conference proceedings and the magazine articles are added to show the acceptance of the work among experts. If texts are written in German language additionally a short summary is given.

8.1 "Anwenderforum Innovative Energietechnik in Gebäuden"

On the 20.11.2004 a forum for the use of innovative energy techniques in houses took place at the University of Applied Sciences Amberg – Weiden in Germany. Within an one hour presentation the use of a biomass Stirling CHP system for heat and power supply in houses was discussed. In the conference proceedings the presentation was published.

At first the history of Stirling engines from the first engine of Rev. Dr. Robert Stirling to high tech engines invented by the NASA and the US army was shown. The process steps and criteria like advantages, disadvantages and possible fields for the use of this concept were discussed. The biomass CHP and the solar Dish Stirling system were described in detail with technical data. Additionally the reasons for the use of wooden pellets and the advantages of local small power CHP systems were shown. As a last issue the experiences of the observed system at the University of Applied Sciences and the further development planed was discussed. In a following 30 minute discussion questions about possible efficiencies and the availability of such systems were answered.

8.2 "12th International Stirling engine conference "

The 12th International Stirling engine conference and technology exhibition took place in the period form 07.09.2005 to 09.09.2005 at the school of engineering at Durham University in Great Britain [100]. In this conference a one hour presentation about first order calculation (Schmidt analysis) was delivered in the theoretical analysis part. The International Stirling Engine Conference (ISEC) takes place each other year and the 12th ISEC continues the highly successful series begun in 1982. This conference has received worldwide recognition as the major international forum devoted to the exchange of the most recent Stirling cycle machines research, development and demonstration (RD&D) results. The ISEC brings together experts and interested parties from the wide mechanical and power engineering R & D community and provides an excellent opportunity for interactions among delegates. The conference is intended to provide a stage for researchers and manufactures to exchange information and identify research and industrial needs in this emerging area. The focus of the conference is the fundamental aspects and practical applications of Stirling Cycle Machines in industry. [100]

The abstract and the presentation which was published in the conference proceedings can be found in the following pages.

8.3 Publication in "BWK"

The BWK is an energy related journal of the Springer VDI publishing company that releases professional articles about different topics in the field of the use of energy. Prevailing economical, political and technical issues of different energy supply concepts are discussed in detail. In edition 9 / 2005 on the pages 52 to 54 the article about γ-type Stirling engines shown in the following was printed.

The working principle with the ideal process steps and the different types of Stirling cycle machines with advantages and disadvantages were described in the introduction. In the following the theoretical and experimental investigations carried out for this thesis are described. In detail the results of the Schmidt analysis were shown in comparison to the ones of the ideal process calculation method with the help of p-V diagrams and pressure curves as a function of the crank angle. In the conclusion a forecast to higher order calculation methods in order to improve the Stirling engine efficiency was given.

8.4 "Energie Innovativ – Politik, Technik, Märkte"

At the "Energie Innovativ" energy symposium on the 01.06.2006 in Nuremberg in Germany two posters were shown in the exhibition. Additionally in a handout paper the activities in the field of Stirling engines were shown. The investigation of the experimental engines, the test bench and the different calculation methods was described in a short overview. On the posters some results of the CFD calculations were shown and an overview of the experiments and the calculation methods was given.

8.5 Publication in „Wissenschaft Bayern Innovativ"

In a magazine called "Wissenschaft Bayern Innovativ" a professional article was published in August 2006. "Bayern Innovativ" is an initiative for the transfer of scientific knowledge in Bavaria. This magazine was handed out at the world exhibition in Hanover in Germany. The article with the topic "Theoretical and experimental analysis of Stirling engines" was translated in English and can be found in the following (below the line). The English version was not published. The original German version published in the magazine can be found accordingly.

Within the context of a research and development project at the University of Applied Sciences in Regensburg measurements are performed on several experimental Stirling engines. The results of these measurements are compared with the ones of different kinds of calculation methods. The target of the work is an improvement of the efficiency of the experimental engines.

Technology transfer in the department of mechanical engineering

For several years sponsored research and development projects are successfully realized in the department of mechanical engineering at the University of Applied Sciences in Regensburg. With the new built laboratory building at the corporate campus of the University and the University of Applied Sciences the professors have the ideal conditions for research and development projects. These works proceed with major involvement of students, who get the possibility to use their theoretical knowledge for practical applications and gain first experiences. With this composition of learning and applying the learned the quality of university education is improved and the future of the science location Regensburg is assured. One of the main points of the technology transfer of the department of mechanical engineering is the field heat and power engineering, where several development projects were performed and successfully realized.

Main types of Stirling engines

Within the context of a several years research and development project sponsored by the Solarenergieförderverein Bayern e.V. at the University of Applied Sciences in Regensburg measurements are done on several experimental γ-type Stirling engines. The results of these measurements are compared with the ones of different kinds of calculation methods. Stirling engines are discussed again and again as machines to provide electrical energy. Thereby the main advantages of this concept especially the

high efficiency of the theoretical circle and the various capabilities of supplying the thermal energy are pointed out. At Stirling engines the energy supply can happen by the combustion of solid, liquid or gaseous fuel as well as by concentrated solar radiation. Because of these facts this principle offers various fields of applications and can help with the adequate choice of combustible to reduce the greenhouse gas CO_2. In the course of the development project the real circle of γ-type Stirling engines is analysed with different kinds of calculation methods and the influence of various operating parameters on performance and efficiency is pointed out. Furthermore extensive measurements are performed with the experimental engines and compared with the theoretical results. The outcome of the theoretical and practical analysis is used to design a new engine with appreciable higher efficiency and durability.

The over 25 different types of Stirling engines are divided by the arrangement of the working spaces into the three main groups α-, β- and γ-type. In figure 1 for these 3 concepts the main components working piston (P), displacer (D), heater (H), cooler (C), regenerator (R) und the swept volumes of the working space (CS) and displacer space (ES) are shown. In this classification the α-type is the simplest arrangement, because only the pistons have to be sealed against the surroundings, like it is done in conventional combustion engines. For β- and γ-type engines one piston and one connecting rod have to be sealed, which implies a complex crank drive, because the connecting rod may only move along one axis. The β-type Stirling engine realizes an optimum according to its efficiency. With its arrangement of the pistons an overlapping of the working spaces of both pistons can be managed which leads to an immense reduction of dead volume and high compression ratios. In this respect the γ-type engine acts disadvantageous, because the dead volumes are high and the compression ratio is low. Typically the cylinders of α- and β-type engines are arranged in a line while the ones of γ-types have an angle of 90°.

The experimental engines at the University of Applied Sciences in Regensburg

The practical examinations are performed on three Stirling engines with different performances. Two of these engines have an electrical output of 1 kW and are fired in combination with a hot water boiler with wooden pellets. This concept is of special interest for combined heat and power facilities for houses. Using such systems the energy contained in combustibles can be used in a much higher amount than it is possible with the separated generation of electricity in power stations and thermal

energy in heating systems, because the waste heat produced by the Stirling engine can be used for heating. The two experimental biomass engines differ in the design of the connection to the generator. While at one engine the generator is allocated outside of the crank housing, at the other engine the generator is integrated into the housing to reduce the well known sealing problems to a minimum. In figure 2 the third engine in its so called Dish-Stirling-System is shown. It is driven by concentrated solar radiation and has a maximum performance of about 300 W. This technology can be used for the electrification of sunny regions far away from general electrical supply to water land or drive all kinds of machines. With the automatic tracking in two axes the system runs completely self-reliant.

For the characterisation of the process in the experimental engines various values have to be recorded. To get a p-V-diagram the pressure and the speed – to calculate the current working spaces – have to be measured. For the calculation of the transferred heat and performance flow meters and temperature sensors are installed in the working spaces as well as in the cooling system. With these values efficiencies and characteristic curves of this engine type can be displayed and compared with the calculated results. Figure 3 shows exemplary the direct solar radiation, the produced electrical power and the absorber temperature for 12th June 2006 for the solar Stirling engine.

Theoretical examinations of the Stirling process

The basis for the Stirling process as well as for the Otto- and Diesel-process is to compress cold gas and to expand the hot gas. The ideal circle happens under the condition that the whole mass of working gas is located in the actual working space for the compression and expansion phase. So the assumption is made that the heat conduction takes place in infinite short time and no working gas is in the dead volume of the heat conductors. In the ideal process no losses are taken into consideration. Because of those facts the ideal calculation gives much higher values for the performance and efficiency. In this case the calculated performance of the experimental engines is twelve times higher than the measured one.

For the theoretical analysis of the Stirling process various calculation methods with different complexity are used. With the simplest model, the Schmidt-analysis, the working spaces are assumed as isothermal whereas because of the sinusoidal changes of volumes the heat conduction between cylinder wall and working gas is processed in finite time. The complete equation set is derived for the used γ-type

engine. The main advantage of this analysis method is that all equations can be solved in close form without the use of iterations whereas heat conduction and flow friction losses are not considered. In figure 4 the real and ideal p-V-diagrams for two of the examined engines are shown in comparison. The difference between the areas included by the curves, which is a measure for the engines performance, is clearly recognisable.

Another alternative to analyse the real Stirling process is the 2nd order calculation method. In contrast to the 1st order calculation method the processes in the compression and expansion space are not considered to be isothermal but adiabatic. A main advantage of this method is that the heat transferred in the heater, cooler and regenerator can be clearly defined. Furthermore the 2nd order analysis allows the introduction of heat convection and flow friction losses. For the calculation the engine is divided into the five spaces compression and expansion space, heater, cooler and regenerator. In this analysis for the processes of the five regarded spaces the energy balance, the mass balance and the equation of state are used. The equation set has to be solved with numerical help and with the use of starting values. In figure 5 exemplary the compression space pressure as a function of the crank angle for the biomass and solar Stirling engine are shown. Beneath the pressures of all spaces other values like temperatures, mass flows, gas velocities and densities as well as the convected heat and produced work as a function of the crank angle can be displayed. Because of those facts this calculation method is the right tool for parameter variations and optimisation calculations.

Summary

The results of the 1st and 2nd order calculation presented here simulate the Stirling process much better than the ideal process could do. These methods allow a determination of temperature and pressure behaviours as well as of the mass distribution of the working gas over the different working spaces as a comparison for the measured values of the experimental engines. Using the 1st and 2nd order calculation methods for parameter variations of the real circle the influence of various process parameters on performance and efficiency can be pointed out. As a result of these optimisation calculations boundary conditions and geometry modifications can be found to exploit the potential of the theoretically very high efficiency of the Stirling process much better than it is done till now.

8.6   Seminar series "Erneuerbare Energien"

In the year 2006 the Centre of Competence for Renewable Energies arranged a seminar series in Straubing in Germany. On the 11.12.2006 a 1,5 hour presentation with a subsequent discussion about the use of Stirling engines for combined heat and power supply was given in this context. The presentation that can be found in the following was published in the internet [102] and the seminar proceedings. More than 200 people came to hear the presentation which made it the best visited of the complete series. The local daily newspaper wrote an article about this event. Because of the general approval this presentation was repeated in a shorter version at the 15th CARMEN symposium for the use of renewable energies. It was held on the 02.06.2007 and the presentation was printed in the conference proceedings.

8.7 "25th CIMAC World Congress"

The International Council on Combustion Engines (Conseil International des Machines a Combustion — CIMAC) was founded in Paris in 1951. It is a worldwide non-profit association consisting of National Member Associations, National Member Groups and Corporate Members in 24 countries in America, Asia and Europe. It brings together manufacturers of diesel engines and gas turbines, users, utilities and rail operators and also suppliers, oil companies, classification societies and scientists. In 2007 the 25th CIMAC world congress took place in Vienna in Austria in the period from 21. – 24.05.2007. [103]

In this context a presentation about non ideal adiabatic analysis of Stirling engines was given in cooperation with the University of Sakarya in Turkey. The paper published in the conference proceedings can be found in the following.

8.8 "13th International Stirling engine conference"

As said in section 8.2 at the 12th international Stirling engine conference in Durham, Great Britain a presentation about 1st order calculation was held in 2005. The 13th international Stirling engine conference in Tokyo, Japan took place in the period form 23.09. – 26.09.2007 at the Waseda University [101]. There the 2nd order non ideal adiabatic analysis method was presented and the results of the parameter variation were discussed. The abstract and the paper for the conference proceedings can be found in the following.

9 References

[1] Prof. Dr. Elsner – *private communication*
Regenerative Energienutzung
Lecture notes University of Applied Sciences Regensburg, 2003

[2] Walker, Graham
Stirling Cycle machines
Clarendon Press, Oxford, 1973

[3] Walker, Graham
Stirling Engines
Clarendon Press, Oxford, 1980

[4] Finkelstein, Organ
Air Engines
Professional Engineering Publishing Ltd., London, 2001

[5] Kolin, Ivo
Historische Stirlingmotoren 1815 - 1990
Munich, Germany, 1992

[6] Schleder, Frank
Stirlingmotoren
Vogelverlag, Würzburg, 2002

[7] Martini W. R.
Stirling Engine Design Manual Vol.2
NASA Report, 1983 (CR – 168088)

[8] Werdich, Kübler
Stirling Maschinen
Freiburg, 1999

[9] Urieli, Berchowitz
Stirling Cycle Engine Analysis
Adam Hilger Ltd., Bristol, 1984

[10] Finkelstein
Computer Analysis of Stirling Engines
TCA Stirling Engine Research and Development Company (Report No. 759140), Beverly Hills, California, 1975

[11] Martini W. R.
Stirling Engine Design Manual Vol.1
NASA Report, 1978 (CR – 135382)

[12] Prof. Sandner – *private communication*
Verbrennungsmotoren
Lecture notes University of Applied Sciences Regensburg, 2002

[13] Prof. Dr. Elsner – *private communication*
Thermodynamik
Lecture notes University of Applied Sciences Regensburg, 2002

[42] Sier, Robert
      A History of Hot Air and Caloric Engines
      UK by L.A Mair, 1987

[43] Sier, Robert
      Rev. Robert Stirling, Inventor of the Heat Economiser and Stirling Cycle Engine
      UK by L.A Mair, 1995

[44] Sier, Robert
      HOT AIR CALORIC and STIRLING ENGINES. Volume One: A History
      UK by L.A Mair, 2000

[45] Meijer
      The Philips Stirling Thermal Engine
      Technical University, Delft, November 1960

[46] Hargreaves, C. M.
      The Philips Stirling Engine
      Elsevier Publishers, GB, 1991

[47] Ross, Andy
      Stirling Cycle Engines
      Columbus, Ohio, USA, 1981

[48] Ross, Andy
      Making Stirling Engines
      Columbus, Ohio, USA, 1993

[49] Senft, James R.
      An Introduction to Stirling Engines
      Moriya Press, GB, 1993

[50] Vieweg, Theodor
      Heissluftmotoren I. Funktionsmodelle
      Neckar Verlag, Germany, 1991

[51] Vieweg, Theodor
      Heissluftmotoren II. Schiffsmodell-Antriebe
      Neckar Verlag, Germany, 1990

[52] Vieweg, Theodor
      Heissluftmotoren III. Bau von Betriebsmodellen
      Neckar Verlag, Germany, 1993

[53] Viebach, Dieter
      Der Stirlingmotor
      Ökobuchverlag, Germany, 1998

[54] Steimle, Fritz
      Stirling- Maschinen- Technik
      C. F. Müller Verlag, Germany, 1996

[55] Prof. Dr. Kauke – *private communication*
      Störmungsmaschinen
      Lecture notes University of Applied Sciences Regensburg, 2002

[56] Lehmann, Hendirk
Untersuchungen zum Betriebsverhalten einer Stirlingmaschine des Gamma-Typs auf dem Teststand
Diploma thesis, University of Applied Sciences Dresden, 2002

[57] Hermsdorf, Jörn
Untersuchung und Optimierung eines Versuchs - Stirlingmotors vom Gamma-Typ unter besonderer Berücksichtigung der Phasenverschiebung zwischen Verdränger und Arbeitskolben
Diploma thesis, University of Applied Sciences Zwickau, 2003

[58] Borde, Tobias
Aufbau, Inbetriebnahme und Erprobung einer Dish/Stirling Einheit für den Einsatz in Inselnetzen
Diploma thesis, University of Applied Sciences Amberg/Weiden, 2003

[59] Wellein, Stefan
Inbetriebnahme eines mit Holzpellets befeuerten Heizkessels mit integriertem Stirlingmotor
Diploma thesis, University of Applied Sciences in Regensburg, 2004

[60] Herzog, Christoph
Betreuung eines Gamma-Typ Stirling Motors mit Messungen
Diploma thesis, University of Applied Sciences in Regensburg, 2005

[61] Miller, Daniel − *private communication*
Berechnungsverfahren zweiter Ordnung für Stirlingmotoren des Gamma-Typs
Diploma thesis, University of Applied Sciences in Amberg/Weiden, 2005

[62] Jockel, Florian
Konstruktive Integration eines Anlassers in das Stirlinggehäuse
Diploma thesis, University of Applied Sciences in Regensburg, 2005

[63] Fuchs, Stefan
Student research project: Integration eines Stirlingmotors in einen Pelletheizkessel
Diploma thesis, University of Applied Sciences in Regensburg, 2006

[64] Kronpass, Manuel
Stundent research project: Verbesserung der Aufhängung und Nachführung eines Dish/Stirling Systems
Diploma thesis, University of Applied Sciences in Regensburg, 2006

[65] Lang, Patrik
Technische Modifikation und weiterführende Messung am Gamma-Typ Stirlingmotor
Diploma thesis, University of Applied Sciences in Regensburg, 2006

[66] Geltinger, Gaby
Messungen und weiterführende Berechnungen an einem Gamma-Typ Stirlingmotor
Diploma thesis, University of Applied Sciences in Regensburg, 2006

[67] Dragoi, Daniel
      Magnetisch gekoppelter Stirlingmotor
      Diploma thesis, University of Applied Sciences in Regensburg, 2006

[68] Baumann, Andreas
      Leistungsspezifikation eines solarbetriebenen Stilingmotors
      Diploma thesis, University of Applied Sciences in Regensburg, 2006

[69] Zierer, Klaus
      Verbesserung und Weiterentwicklung von vorhandenen Gamma-Typ Stirlingmotoren
      Diploma thesis, University of Applied Sciences in Regensburg, 2006

[70] Baier, Michael
      Integration eines Gamma-Typ Stirlingmotors in einen Holzpelletofen
      Diploma thesis, University of Applied Sciences in Regensburg, 2007

[71] Mühl, Roland
      Weiterentwicklung eines Gamma-Typ Stirlingmotorenprüfstands mit Messungen
      Diploma thesis, University of Applied Sciences in Regensburg, 2007

[72] Hubert Oertel jr. Eckart Laurien
      Numerische Strömungsmechanik Lösungsmethoden – Softwarebeispiele
      Vieweg Verlag, Germany, 2003

[73] Montageanleitung Messkopf SDE 9.1,
      Ahlborn company

[74] QUASCHNING, V.
      Regenerative Energiesysteme
      Hanser Verlag, 3. Auflage 2003

[75] http://mathe-online.at/mathint/fun2/i.html
      state 05.08.2006

[76] http://www.beldrive.com/deutsch/wir.html
      Beldrive company
      state 01.2005

[77] http://www.dwd.de
      state 10.2004

[78] http://www.sesusa.org/history.1816.htm
      state 22.10.2004

[79] http://www.stirlingengine.com
      http://www.stirlingengine.com/download/lockwood_chpt6.pdf
      state 12.12.2004

[80] http://www.k-wz.de/vmotor/stirling.html
      state 23.08.2005

[81] http://www.stirlingengines.org.uk/
      by Robert Sier
      state 12.07.2007